NASA CR-72952

EVALUATION OF LIQUID METHANE STORAGE AND TRANSFER PROBLEMS IN SUPERSONIC AIRCRAFT

by

J. L. McGrew, D. L. Buskirk
H. F. Brady and M. W. Leeds

MARTIN MARIETTA CORPORATION

Prepared for
NATIONAL AERONAUTICS AND SPACE ADMINISTRATION

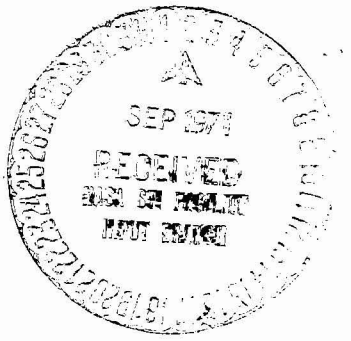

NASA Lewis Research Center
Contract NAS3-12411
Joseph M. Ladd, Project Manager

NOTICE

This report was prepared as an account of Government-sponsored work. Neither the United States, nor the National Aeronautics and Space Administration (NASA), nor any person acting on behalf of NASA:

A.) Makes any warranty or representation, expressed or implied, with respect to the accuracy, completeness, or usefulness of the information contained in this report, or that the use of any information, apparatus, method, or process disclosed in this report may not infringe privately-owned rights; or

B.) Assumes any liabilities with respect to the use of, or for damages resulting from the use of, any information, apparatus, method or process disclosed in this report.

As used above, "person acting on behalf of NASA" includes any employee or contractor of NASA, or employee of such contractor, to the extent that such employee or contractor of NASA or employee of such contractor prepares, disseminates, or provides access to any information pursuant to his employment or contract with NASA, or his employment with such contractor.

Requests for copies of this report should be referred to

National Aeronautics and Space Administration
Scientific and Technical Information Facility
P. O. Box 33
College Park, Md. 20740

NASA CR-72952

FINAL REPORT

EVALUATION OF LIQUID METHANE STORAGE AND TRANSFER PROBLEMS IN SUPERSONIC AIRCRAFT

by

J. L. McGrew, D. L, Buskirk
H. F. Brady and M. W. Leeds

MARTIN MARIETTA CORPORATION
P. O. Box 179
Denver, Colorado 80201

prepared for

NATIONAL AERONAUTICS AND SPACE ADMINISTRATION

August 6, 1971

CONTRACT NAS3-12411

NASA Lewis Research Center
Cleveland, Ohio
Joseph M. Ladd, Project Manager
Air-breathing Engines Division

FOREWORD

The work described herein was done at the Denver Division of the Martin Marietta Corporation, under NASA Contract NAS3-12411 with Mr. Joseph M. Ladd, Air-breathing Engines Division, NASA-Lewis Research Center, as Project Manager, and Mr. Rene Chambellan, Air-breathing Engines Division, NASA-Lewis Research Center, as Research Advisor.

TABLE OF CONTENTS

LIST OF ILLUSTRATIONS

LIST OF ILLUSTRATIONS (continued)

LIST OF ILLUSTRATIONS (continued)

LIST OF ILLUSTRATIONS (continued)

LIST OF ILLUSTRATIONS (continued)

LIST OF ILLUSTRATIONS (continued)

LIST OF ILLUSTRATIONS (continued)

LIST OF ILLUSTRATIONS (continued)

LIST OF ILLUSTRATIONS (continued)

LIST OF ILLUSTRATIONS (continued)

LIST OF ILLUSTRATIONS (continued)

LIST OF TABLES

ABSTRACT

The objective of this program was to evaluate the problems involved in using liquid methane in a supersonic cruise-type aircraft. The analyses included pressurization and fuel transfer in systems using liquid methane in a saturated state, in the subcooled state, or partly as a saturated liquid and partly as a subcooled liquid. The program included designing and fabricating a test rig, conducting 49 tests, and reducing and analyzing some 100 channels of data. Three separate low-pressure tank configurations and one high-pressure tank were tested. The tests demonstrated that subcooled methane can be loaded and held for reasonable lengths of time under simulated aircraft conditions using methane vapors to maintain the pressurization.

EVALUATION OF LIQUID METHANE STORAGE AND TRANSFER PROBLEMS IN SUPERSONIC AIRCRAFT

BY

J. L. McGREW, D. L. BUSKIRK
H. F. BRADY AND M. W. LEEDS

I. SUMMARY

The objective of this program is to evaluate problems of liquid methane storage in a supersonic cruise type aircraft, including pressurization and fuel transfer in systems using liquid methane in the saturated state, in the sub-cooled state, or in a system where part of the fuel is stored as a saturated liquid and part of it is stored as a subcooled liquid.

To accomplish this objective a "thermal" wing test bed was designed to test four full-sized tanks of different configurations. The test rig had provisions for providing simulated slosh and aero-heating. Each of the four tanks could be filled, drained, pressurized and vented individually. Provisions were made in the latter portion of the test program for simulated series filling of the low pressure tank. The test rig and tanks were extensively instrumented.

Three low-pressure tank designs were chosen, each with its own unique feature to store subcooled methane and minimize condensation of the pressurixing methane gas. These designs consisted of the standpipe configuration (a main tank with connecting lines to a separate pressurization chamber); the baffled tank, containing five partitioned compartments; and a tank filled with polyurethane foam. All tanks, even to the high-pressure tank, were 2 ft (0.61 m) in diameter, had an overall length of 7 ft (2.13 m), and had domed ends. The insulation was thick enough to permit a steady-state heat flux of approximately 120 BTU/ft^2-hr (378 W/m^2) under the worst test conditions.

The tests simulated all phases of an actual aircraft flight--ground fill and hold, taxi, ascent, cruise, fuel outflow, descent, and drain. To avoid the need for an altitude test chamber when simulating flight, the temperature of the liquid methane and the test pressures were changed to achieve conditions comparable to those experienced by an actual aircraft using a local barometric pressure as a base.

A computer program was written to read the raw millivolt data from digital tapes, smooth the values, average them, convert them to engineering units, and plot the data in finished form. This model also calculated the vent and pressurization flowrates from the respective venturi pressure and temperature data, and integrated the flowrates over specified time intervals.

Loading tests proved the feasibility of loading and maintaining subcooled methane, pressurized with its own vapors. The degree of subcooling, however, was sensitive to pressure control in the source dewar. Several degrees of subcooling were lost during each test while the liquid was flowing from the supply dewar to the tank inlet. Possible solutions might be to use insulated or externally cooled fill lines to reduce this loss of subcooling or increase the initial subcooling.

Only one tank, which had no special slosh apparatus, experienced any pressure fluctuations when a sub-cooled liquid was sloshed. These pressure fluctuations were relatively small and it is anticipated that a very simple pressure system could be designed to rectify the problem for this type of tank.

Heat transfer tests were run on three tank configurations. These tests indicated that the effective thermal performance of the tank can be maintained at nearly the level of the basic insulation material. It was also shown that sloshing had little effect on thermal performance.

The liquid pumping tests did not uncover any significant problems in the pumping of cryogenic methane. It was verified that a significant increase in tank pressure is required to maintain NPSH at the pump if it is an appreciable distance from the tank. This was primarily due to heat leak in the line.

The flight simulation tests successfully demonstrated that the liquid methane could be kept pressurized during the ascent and descent portions of a flight, that the liquid boiloff losses during ascent could be controlled by loading subcooled liquid, and that the pressurization system adequately maintained tank pressure above ambient during the descent.

Nitrogen was tried on three tests as the pressurant and solubility samples were taken. Nitorgen appears to be worthy of further investigation as a pressurant for liquid methane, based on maximum solubility values of 4.5% within 1 1/2 in. (3.8 cm) of the surface of the liquid.

II. INTRODUCTION

Cryogenic fuels pose a number of significant problems not encountered with conventional aircraft fuels. The performance advantages of a cryogenic fuel such as liquid methane (or liquid natural gas) are substantial as compared to light petroleum distillates, but ultimate application in either commercial or government uses will depend upon satisfactory solutions of significant engineering problems.

The objective of this program was to study and investigate the most significant of the anticipated problems with liquid methane and to develop practical and useful solutions to them. It is anticipated that the results of this program will materially assist in future aircraft cryogenic fuel system designs. It is obviously not possible in a program of this type to answer completely all fuel system problems for a diverse variety of future applications. Consequently, in this program a number of more basic questions were examined and a broad base of fundamental engineering data was developed. Specific fuel system elements and problems which were investigated experimentally are:

(1) Various fuel tank loading techniques.

(2) Several tank pressure control techniques.

(3) Liquid pumping and transfer.

(4) The effect of heat flow on pressure control and liquid net positive suction head--maintaining a proper fuel tank thermal balance.

(5) The effect of sloshing during various phases of aircraft operation on pressure control.

A more detailed discussion of the specific problem areas and the test program designed to examine them is presented in Section III. Section IV presents a detailed description of the test hardware. Test procedures and a complete summary of the test data are given in Section V. Typical data for each type of testare also presented in this section. A complete compilation of data is presented in Volumes I and II of the Comprehensive Data Report. The conclusions and recommendations for future investigations are discussed in Section VI. Appendix A contains a thermal analysis of the heat transfer from the simulated wing to the test tanks as well as internal tank energy balances performed during various test periods.

III. DISCUSSION

During the operation of an aircraft, the fuel system is subjected to a number of environments and must predictably and reliably continue to store and feed fuel in accordance with propulsive requirements. The fuel system operating environments for a high altitude supersonic vehicle are more severe, but otherwise are similar to the environments for more conventional craft. That is, the supersonic fuel storage system must have additional thermal insulation in order to regulate heat flow from the aerodynamically heated surrounding structure, and must operate over a wider range of ambient pressures. A typical supersonic aircraft operating profile is shown below.

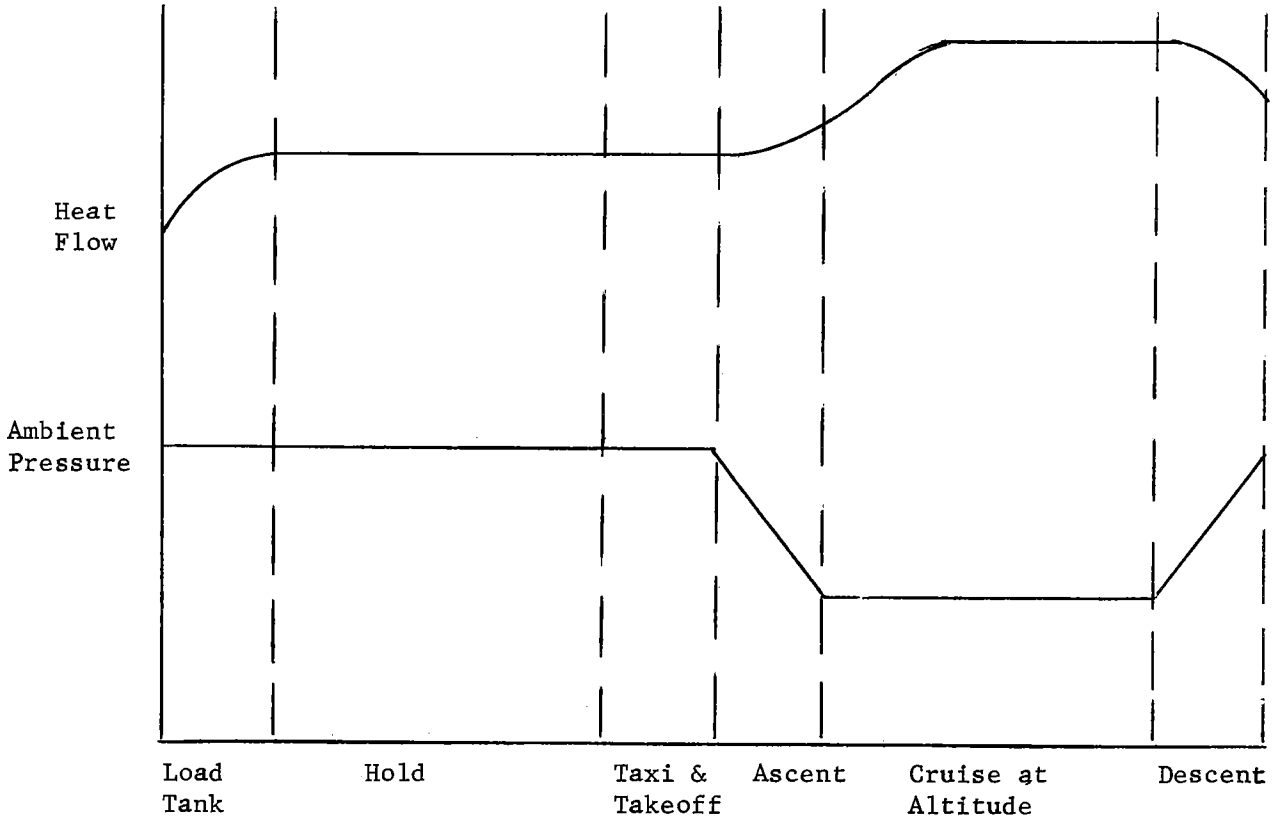

The most significant fuel system problem associated with cryogenically fueled supersonic aircraft is maintaining fuel tank pressure within acceptable limits during all phases of operation. This problem and a discussion of the test program designed to investigate it are discussed in the following sections.

A. CRYOGENIC FUEL STORAGE AND CONTROL PROBLEMS

Fuel tank pressurization is required to provide sufficient engine pump net positive suction head (NPSH) for reliable engine operation throughout all phases of the aircraft mission. Because the bulk of the fuel may be carried in the wings, fuel tanks of almost rectangular cross section may be employed to gain maximum volumetric efficiency. Generally, this tank configuration is quite weight sensitive to internal tank pressure. To build a fuel tank of required volume within reasonable weight allowances, the tank operating pressure must be held to a minimum. This low tank pressure requirement is the heart of what is probably the most significant engineering problem in applying liquid methane to commercial aircraft.

Along with the required liquid subcooling which introduces fuel loading difficulties, this low pressure criterion requires regulation of tank conditions during ascent and descent, and requires NPSH maintenance during fuel sloshing as a result of turbulent conditions encountered during aircraft operation.

1. Fuel Slosh

A serious problem in the operation of the liquid methane propellant system may occur when a period of rest or smooth flight is followed by sudden disturbances, causing sudden accelerations of the fuel tank. The undistrubed period may be long enough to result in a thermal stratification of the gas layer above the cryogenic propellant: gas temperatures near the skin may be several hundred degrees Fahrenheit in excess of the liquid temperature. Sudden acceleration of the tank may result in liquid slosh and considerable cooling of the gas. The resulting pressure change may adversely affect the operation of the fuel system, or the integrity of the tank/wing structure.

Typically, the following conditions may cause sudden tank accelerations following a period of rest or smooth flight:

1) Takeoff, when the normal accelerations imposed on the aircraft by unevenness of the runway surface follow a period of parking;

2) Maneuvering conditions, which may impose large steadystate or transient acceleration on the aircraft structure;

3) Atmospheric turbulence (gust penetration).

The fuel tank pressure control problem can be resolved by reducing thermal mixing to a minimum and concurrently utilizing a sufficiently reactive and sensitive gas flow control system.

2. Fuel Loading

As mentioned previously, the inherent difficulties in handling cryogenic liquids can conceivably become major obstacles to the use of liquid methane as a fuel for a commercial aircraft. One of the first considerations is the loading of the fuel into the tanks. Loading a cryogenic liquid with a vapor pressure equal to or greater than the required total pressure in the fuel tank can be easily accomplished if care is taken during the initial tank cooldown and if proper venting control is provided; however, if the vapor pressure of the cryogenic liquid is considerably lower than the required tank total pressure and a major fraction of the tank total pressure results from gasses which are condensible at the cryogenic liquid temperature (the liquid's own vapor) considerable difficulties can arise. The reason for the difficulty encountered is fundamental from a thermodynamic point of view. To maintain a subcooled liquid pressurized with its own vapor, for example: a temperature stratification in the liquid must occur, because for all practical purposes the liquid/vapor interface is at the saturation temperature for the tank pressure. But while the tank is being filled the liquid is agitated and temperature stratification is difficult. Experience has shown that the condensation rate is extremely high and the rate of gas flow into the tank becomes the limiting factor in determining tank pressure. The high condensation rate and liquid mixing result in rapid liquid heating during this process.

Obviously the condensation and heating are detrimental to the proper operation of the fuel system and some method of overcoming the problem must be found. One approach is to stop liquid mixing druing fill to permit the development of temperature stratification.

Another method of preventing the rapid condensation is to fill the tank with a mixture of condensible and noncondensible gas. As the liquid flows into the tank, the condensible gas fractions adjacent to the liquid/vapor surface condense leaving a layer of noncondensible gas. This layer greatly reduces the condensation rate. The two-component concept is attractive because only a small percentage of noncondensible gas is required.

3. Depressurization During Ascent to Altitude

During aircraft ascent to altitude ambient pressure decreases and it is desirable to correspondingly decrease the pressure in the fuel tank in order to minimize the structural loading requirements of the fuel tank. If the vapor pressure of the fuel is high relative to total tank pressure at the beginning of aircraft ascent, liquid boiling will occur as tank pressure is lowered. An unacceptable loss of fuel can thus occur unless preventive steps are taken. This excessive fuel loss during ascent can be minimized or eliminated by loading subcooled liquid. If the liquid is subcooled to the point that its vapor pressure is equal to or less than the ambient pressure at altitude, the fuel loss would be completely eliminated.

4. Fuel Pumping and Transfer

High-volume pumping of near boiling liquids has been of considerable concern in many cryogenic liquid applications. The fundamental problem is that of maintaining a static pressure at least equal to the vapor pressure of the liquid at all points in the flow systems to prevent boiling. The problem usually is more critical at the inlet side of a pump or at other points in the flow system where liquid is being accelerated. The solution to the problem is to pressurize the liquid to a level somewhat higher than the vapor pressure of the liquid. The exact net positive suction head (NPSH, defined as total pressure minus vapor pressure) required to prevent local boiling (cavitation) depends primarily on the design of the pump inlet.

In the application of liquid methane as a fuel for supersonic aircraft, the increased heat flow to the liquid due to aerodynamic heating, and the requirement to minimize tank operating pressure amplify the problems associated with maintaining adequate flow NPSH.

The characteristics of the aircraft pressurization system will be strongly influenced by fuel transfer requirements.

5. Repressurization During Descent From Altitude

As the aircraft descends from altitude ambient pressure increases occur, and since the fuel tank will probably not be capable of withstanding crushing pressure, the tank must be repressurized. Some advantages occur if methane vapor is used as a pressurant; however, some problems in maintaining stable pressure might result. If considerable vapor condensation occurs excessive use of methane gas might be required.

The use of more expensive pressurants such as helium would easily resolve any technical problems but are economically unattractive because of the large volume required. Nitrogen pressurization might be used if concentrations of disolved nitrogen less than equilibrium values could be achieved. Combustion efficiency of the equilibrium methane/nitrogen mixtures is poor.

B. EXPERIMENTAL PROGRAM OUTLINE

The various problems associated with the storage and control of cryogenic fluid discussed previously can only be resolved through a comprehensive experimental program. The significant features of our experimental program designed to resolve the major problems are outlined here, while a detailed presentation of the test apparatus and test results follow in later sections of this report.

The general approach used in our study was to construct a full scale segment of a wing mounted fuel storage and control system and to subject it to test conditions which are closely representative of actual operational conditions. The test article consisted of a thermally simulated wing segment, four insulated wing mounted fuel tanks, and a liquid and gas control system. The wing segment

was mounted on a shaker capable of high amplitude oscillations over a wide variety of frequencies such that representative fuel slosh modes could be obtained. A large radiant heat source was developed to simulate aerodynamic heating on the wing segment surfaces. An instrumentation system was developed to record all significant test results.

Specific test objectives and associated experimental apparatus features are outlined below while a detailed description of the test apparatus and each test conducted is presented in a later section of this report.

1. Fuel Loading

The objective of the fuel loading was to investigate the feasibility of loading subcooled liquid methane while maintaining an adequate tank pressure.

All loading tests were conducted using the standpipe tank which is described in detail later. This tank is of open unbaffled internal construction and thus represents the most difficult tank to load since liquid mixing is unhampered and liquid temperature stratification tendencies are minimized. Loading with subcooled liquid methane was attempted using methane gas as a pressurant with the tank initially at room temperature and also with the tank precooled to liquid methane temperature. Conceivably the precooled tank might reduce liquid heating and thus increase the degree of liquid subcooling at the termination of loading. Tests were also run to compare parallel and series tank loading. The effects of series loading should be similar to precooling the tanks.

In addition to the room temperature and precooled loading tests with methane gas pressurant, additional tests were conducted in which subcooled liquid methane was loaded using a helium/methane gas mixture as a pressurant.

Loading tests were also conducted with liquid nitrogen using a nitrogen gas pressurant. These tests included both series and parallel tank loading.

2. Ground Hold and Taxi Tests

The objective of these tests was to determine whether pressure control could be maintained when the tanks were allowed to reach thermal equilibrium after fill and then were sloshed as might be expected during the taxi portion of a flight. It is possible that both liquid and gas temperature stratification might take place during ground hold, and sloshing incurred during subsequent runway taxi could result in pressure oscillations. These pressure fluctuations would be directly attributable to thermal mixing of the liquid and/or gas and, therefore, could be sensitive to tank configuration. To investigate these problems, ground hold and taxi tests were run on all four tank configurations with near zero ullage and with about 95% ullage. During the tests various degrees of slosh were induced.

3. Heat Transfer Tests

In this series of tests the overall heat transfer rates into the liquid were determined, including the effects of tank insulations, supports, and penetrations. These data help establish the validity of the rest of the test program and in addition are useful in verifying a thermal design which is applicable in future actual flight system designs.

4. Fuel Transfer Tests

The objective of these tests was to study the problems associated with high flow rate pumping of liquid methane under the environment encountered in actual flight. The pump used in these tests was a centrifugal pump requiring a low NPSH in liquid methane. A complete discription of this pump is given in a later section.

The problems of pump cooldown and pumping under a variety of inlet conditions were investigated.

5. Simulated Aircraft Flight Tests

A series of tests was conducted in which various phases of aircraft operations were simulated and the effects of these conditions on fuel tank pressure were observed. Operating phases which were simulated are: ground hold and taxi, ascent to altitude, cruise at altitude with liquid outflow, and descent to land. Specific details of each test conducted are given later. In these tests four different tank configurations were used under a variety of test conditions. Three of the test tanks incorporated different designs to prevent mixing between the liquid methane and the pressurizing gas, thus reducing the tank pressure fluctuations caused by such mixing. The fourth tank configuration was a high pressure storage system in which it was anticipated that any pressure oscillations occurring during operation would be small compared to the total tank pressure and could thus be neglected.

IV. TEST HARDWARE

A. DESIGN

To adequately investigate the problems associated with the storage and pressurization of liquid methane in supersonic aircraft it was necessary to fabricate a full scale section of a wing for use as a test bed. The simulated wing section did not have the same structural characteristics as an actual wing; however, from a thermal standpoint the simulation was completely adequate.

The objectives of the tests dictate that the methane thermodynamic conditions must be completely duplicated. This specifically meant that liquid subcooling and ascent/descent environment conditions must be simulated. Since it was impractical to run a test of this magnitude in a vacuum chamber, it was decided to simulate the ascent/descent profiles by pressurizing the tanks. The actual aircraft operating conditions are shown in figure 1. The fuel is loaded at atmospheric pressure and is subcooled to the saturation temperature at altitude. This prevents boiloff due to decreasing pressure during ascent. The important parameter to be duplicated for the test is the enthalpy change Δh. in going from saturated liquid at 14.7 psia to saturated liquid at 3.3 psia.

In the test the 3.3 psia at ascent was simulated by atmospheric pressure at Denver which is about 12 psia. The liquid to be loaded was also saturated at 12 psia. The tank loading pressure was then determined so that the enthalpy change h_2 between saturated liquid at loading pressure and saturated liquid at 12 psia was equal to the actual flight enthalpy change, Δh. The pressure which achieves this enthalpy change is 36 psia. The simulated flight pressure and temperature profile is shown in figure 2. As can be seen from figure 2, the saturation temperature difference is the same in both actual and simulated conditions. However, the pressure change in the simulated case is considerably larger than the actual conditions. This is due to the steeper saturation pressure curve at the higher pressures. The aircraft and equivalent test conditions are summarized in table 1.

TABLE 1.- COMPARISON OF AIRCRAFT AND TEST CONDITIONS

	Aircraft conditions				Test conditions			
	Pressure		Saturation temperature		Pressure		Saturation temperature	
	psia	N/cm^2	^oF	^oC	psia	N/cm^2	^oF	^oC
At cruise altitude	3.3	2.3	-285	-176	12	8.3	-263	-164
On the ground	14.7	10.1	-259	-162	36	24.8	-237	-149
Pressurized tanks	29.7	20.5	-243	-153	62	42.7	-221	-141

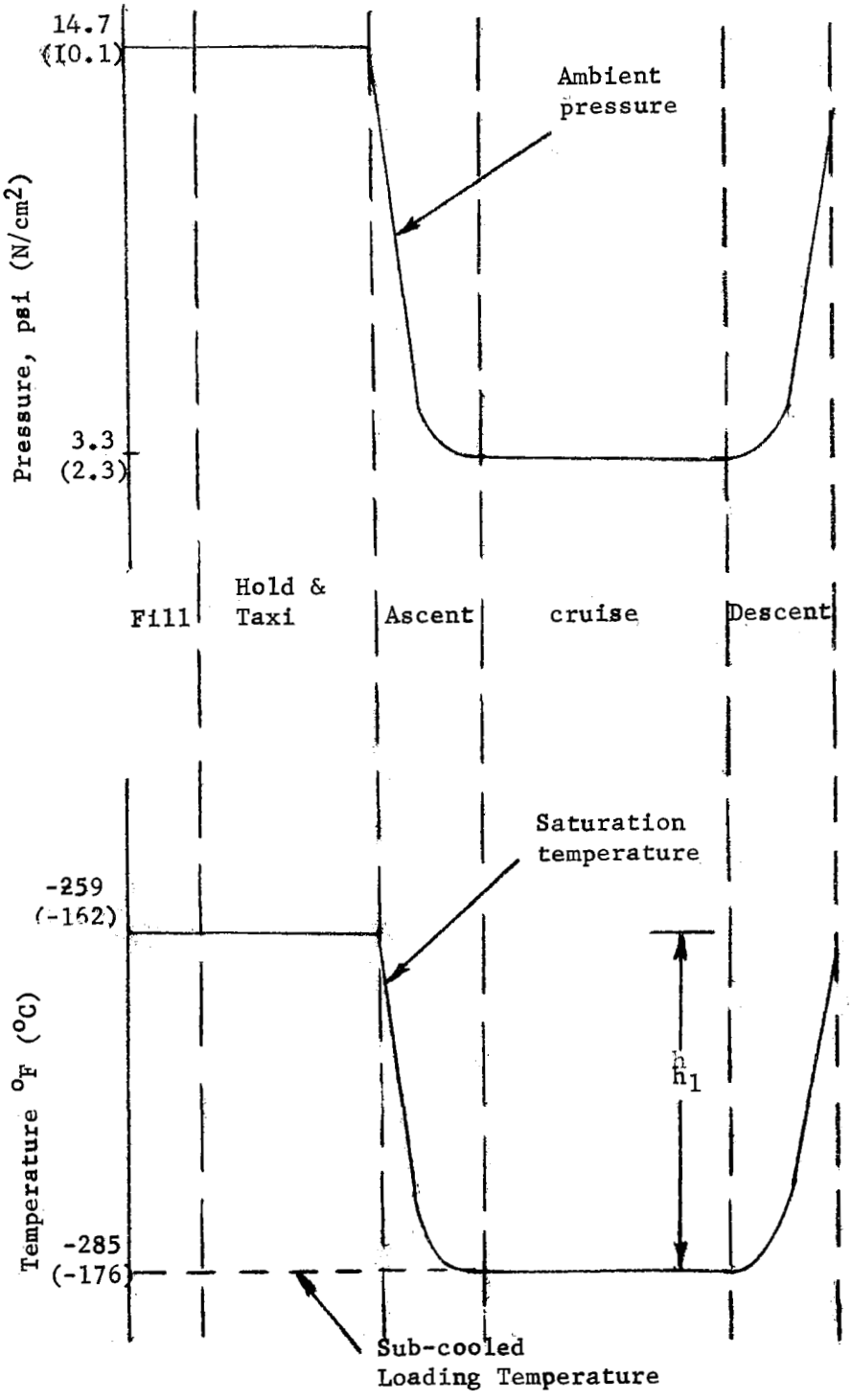

Figure I.- Typical Aircraft Flight Profile

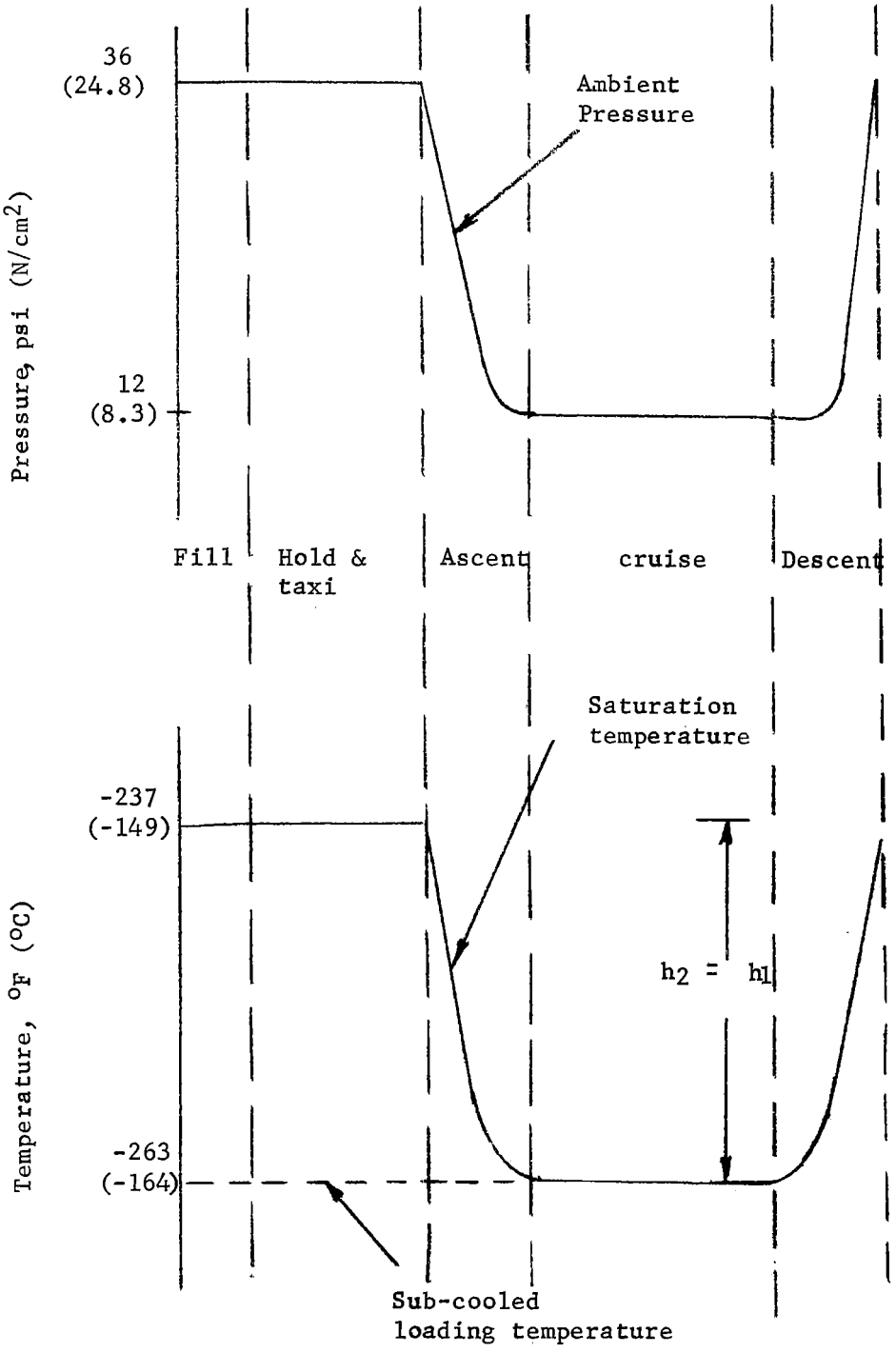

Figure 2.- Simulated Aircraft Flight Profile

The thermal wing was designed to accomodate four flight-sized tanks which were cylinderical with domed ends. The two center tanks would always be the test tanks, while the two outer tanks would serve as guard tanks to eliminate thermal end effects. The wing design was such that the tanks would be easily interchanged allowing all four tank configurations to be fully tested.

The associated subsystems included a liquid methane supply system, a regulated vent system, a gaseous pressurization system, an aerodynamic heating system, and a simulated slosh system. A schematic of the system is shown in Figures 3 and 4. Figure 3 represents the system used during the first 37 tests which used parallel tank loading. Figure 4 represents the system used during the last 12 tests which featured series tank loading through the standpipe tank.

The design of these various components and subsystems are described in the following sections.

1. Test Tanks

The tank system consisted of four tanks, each of a different configuration. Three of the tanks were low pressure configurations and were interchanged during the test series. The fourth tank was designed for high pressure use. During each portion of the test series, one of the low-pressure tank configurations was mounted in one center bay section of the wing box. The high-pressure tank was mounted in the other center bay section and the remaining two tanks were mounted in the outer bay sections. Both center bay tanks were extensively instrumented. In each case, the outer bay tanks acted as guard tanks to eliminate span-wise heat transfer effects. Each tank configuration was designed to minimize the problems inherent in using a cryogenic fuel in a supersonic aircraft.

a. Low-pressure tank, standpipe configuration.- This tank had two major elements: the main tank and the standpipe. The main tank was 24 in. (61 cm) in diameter, 84 in. (213 cm) long, and had hemispherical ends. It was made from 21-6-9 stainless steel and hydrostated at 1 1/2 times the expected operating pressure of 25 psig (17.2 N/cm^2). The wall thickness was 0.035 in. (0.089 cm).

Figure 5 shows design details of the tank. The skin sections were separated by rings 0.187 in. (0.47 cm) thick, which were, in turn, attached to three longerons located at 120-deg intervals around the outside of the tank. The longerons provided tank-to-wing mounting points and a load path for the slosh and gravity loads.

The tank penetrations included a 2.5-in. (6.35-cm) diameter fill line and a 1-in. (2.54-cm) vent line. A vent cup provided entrance to the vent line within the tank. Within the vent cup, a number of baffles with offset holes acted as a liquid-vapor separator during attempts at zero-ullage fills. Both the fill and the vent lines penetrated the tank skins at the tank centerline through the apex of the dome. The fill line was curved down to within 0.5 in.

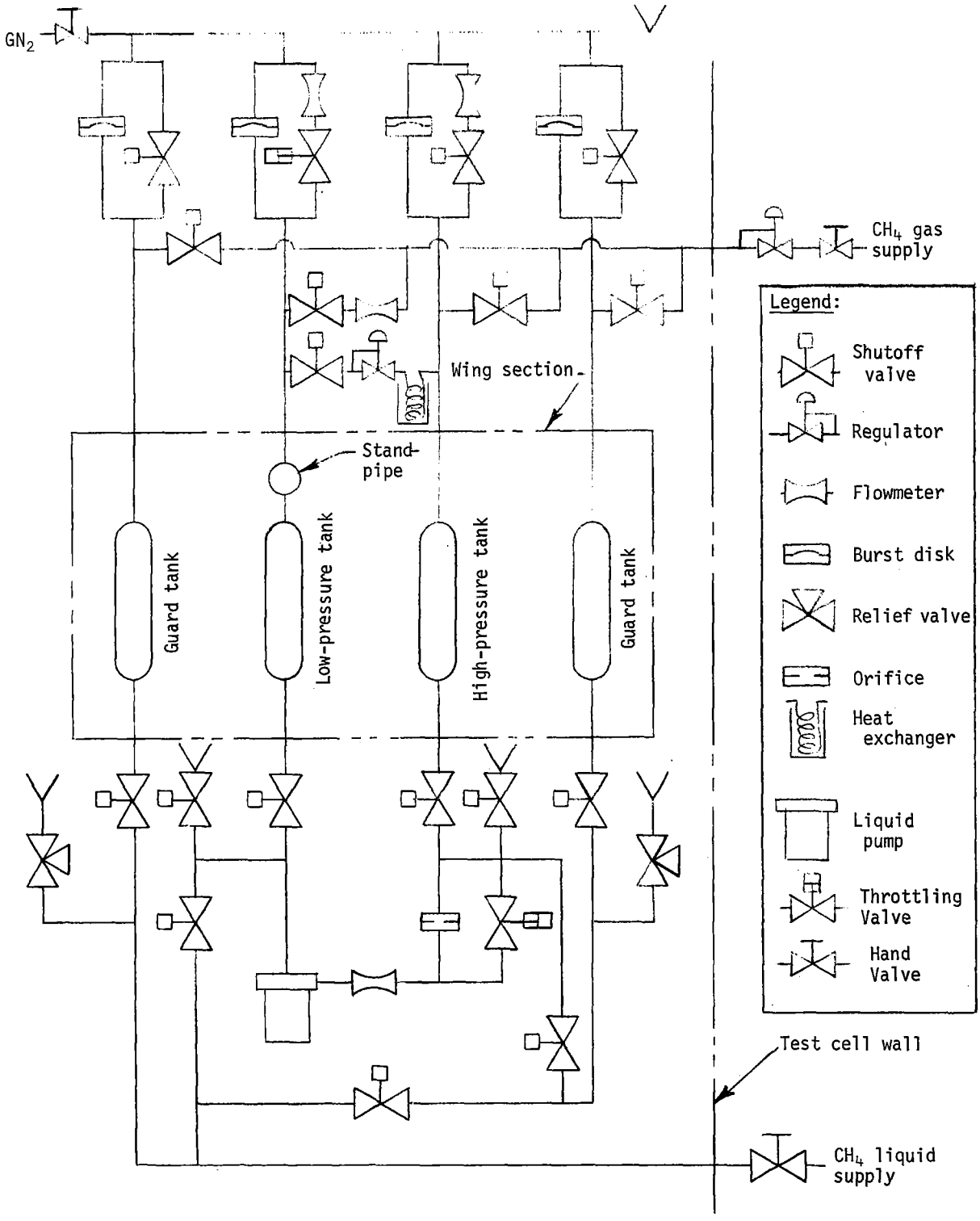

Figure 3.- Test Schematic for Tests I through 37

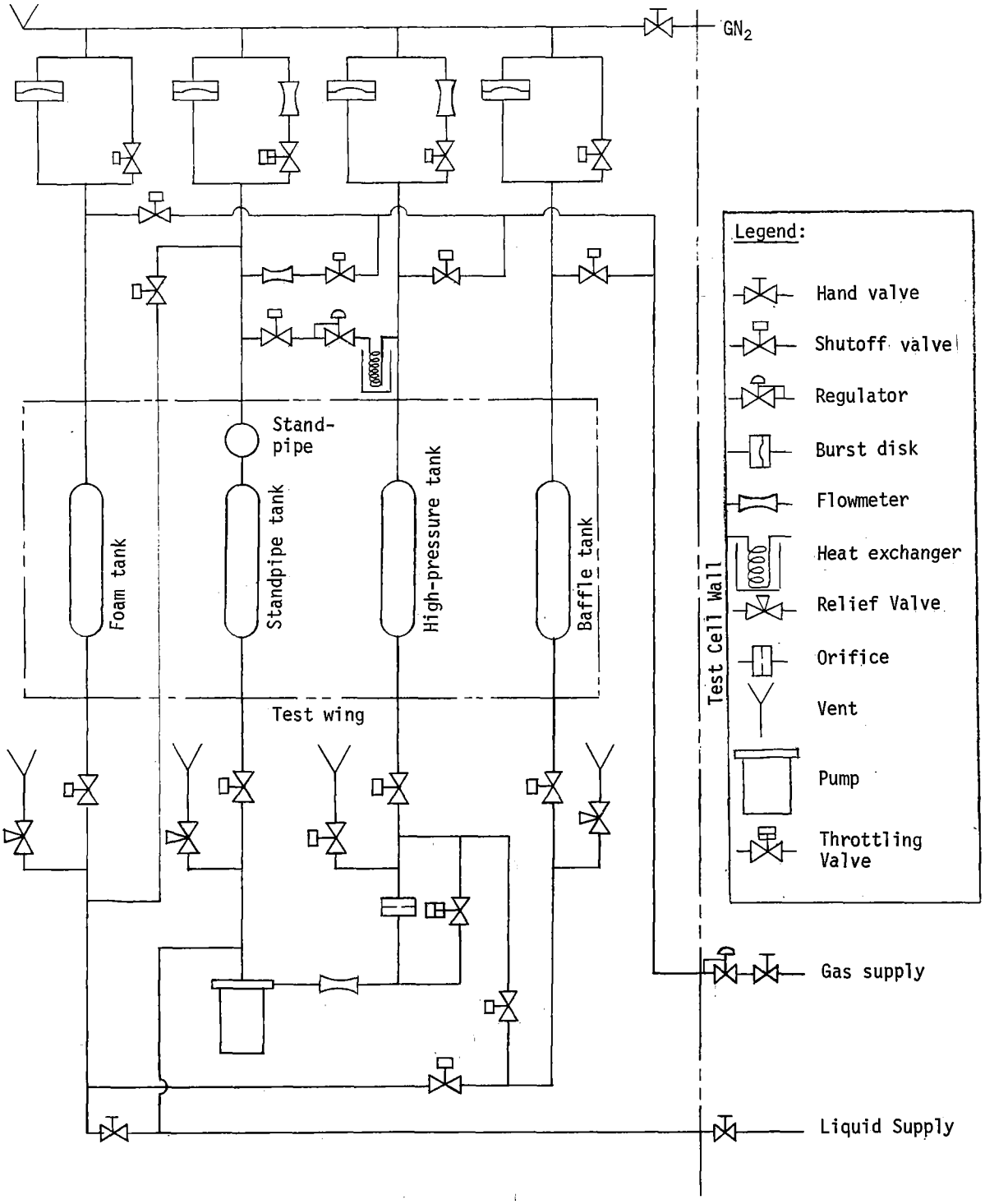

Figure 4.- Test Schematic for Tests 38 through 49

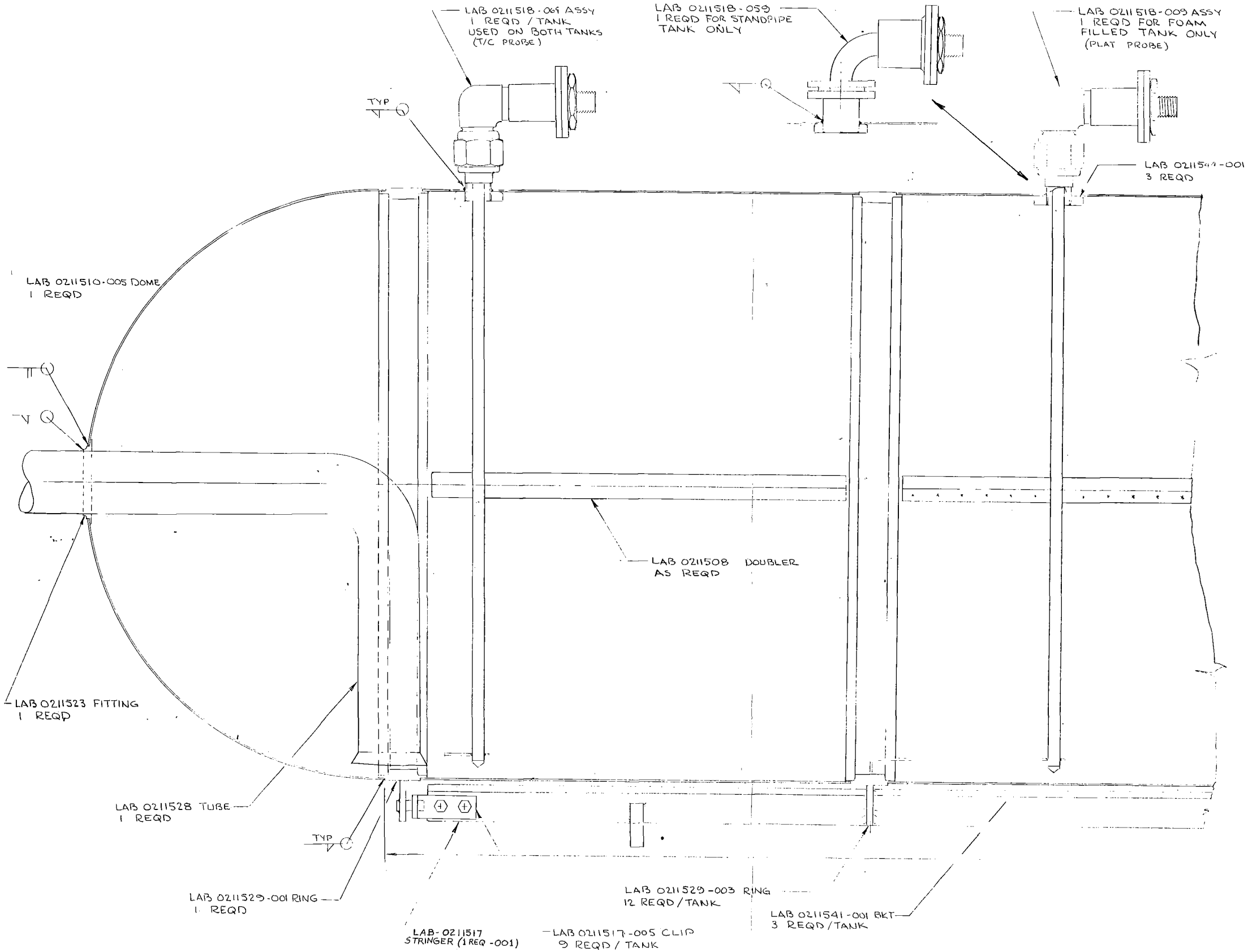

Figure 5. - Tank Construction Details

(1.27 cm) of the bottom of the tank to limit turbulence during filling. The vent line curved up into a vent cup that extended outside the basic inside skin line of the tank. Three instrumentation probe penetrations were located along the top centerline of the tank. Two of the penetrations were through 1-in. (2.54-cm) AN tubing bosses welded to the tank skin. The third was through a port that was flanged larger in diameter to provide clearance for the slosh sensors. A typical instrumentation probe installation is shown in figure 6. Note the vent line extending into the vent cup in the upper portion of the tank.

The tank had 1.25 in. (e.18 cm) of Cerafelt insulation. There were four layers each 0.25 in. (.635 cm) thick and two layers each 0.125 in. (0.318 cm) thick. Each layer was separated by a layer of aluminum foil, and the outer covering of foil was painted black. The black surface served a twofold purpose: it increased absorptivity and thus decreased the power requirement to the IR lamps, and provided a surface with stable thermal characteristics from test to test. Figure 7 shows the tank insulation being applied and figure 8 shows the insulated tank after painting.

The standpipe (fig. 9) was a spherical stainless steel vessel 14 in. (36.6 cm) in diameter. It was supported by circular sheets of Micarta and mounted on a framework that fit within the simulated wing section. The line from the main tank was connected to the bottom of the sphere and the flanged outlet on the top was used for a vent gas outlet and an instrumentation port.

The connecting line had two flexible line sections and three elbows with a total length of 5 feet. Liquid temperature instrumentation ports were provided in each elbow. The insulation of the line was similar to that used on the tanks.

b. Low-pressure tank, baffled configuration.- This tank was similar in design and construction to the main tank with the standpipe configuration, but a standpipe was not used and internal baffles were incorporated (fig. 10). A baffle 0.035 in. (o.89 cm) thick was welded into the tank within each ring section and penetrated by a standpipe-type connecting line for communication between compartments. Figure 11 shows a ring section with baffle and line installed. The lines used to fill and vent the tank were identical to those used on the standpipe configuration.

Instrumentation penetrations were located in each compartment, and the mounting was as shown by figure 11. The tank insulation was identical to that used on the standpipe configuration.

c. Low-pressure tank, foam-filled configuration.- This tank was also similar in design and construction to the main tank portion of the standpipe configuration. The primary difference involved the filling of the tank with open-celled polyurethane foam, a material that is completely compatible with liquid methane. Ciruclar foam disks were cut from 1-in. (2.54-cm) thick material and packed into the cylindrical portion of the tank. The foam sections used to fill the dome are shown in figure 12. A slice approximately 1 in. (2.54 cm) deep was

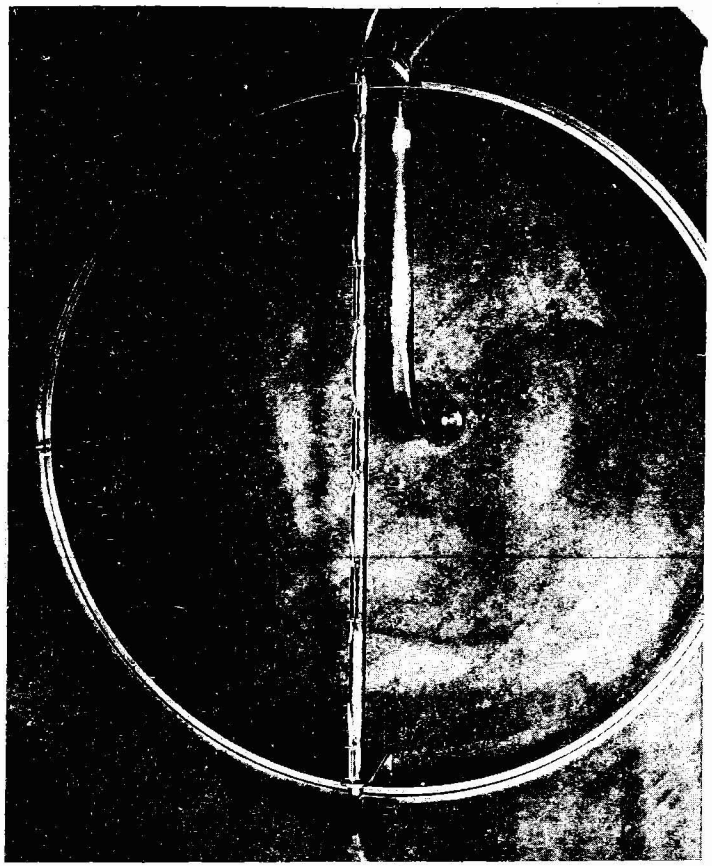

Figure 6.- Typical Instrumentation Probe Installation

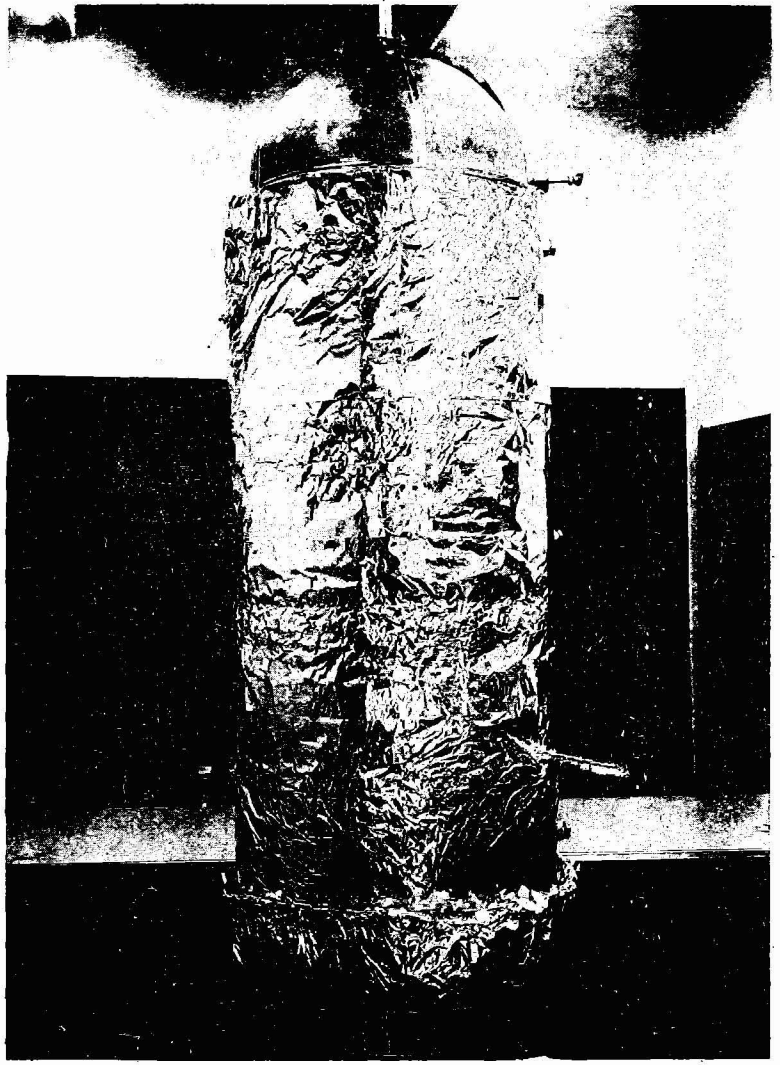

Figure 7.- Tank Insulation Being Applied

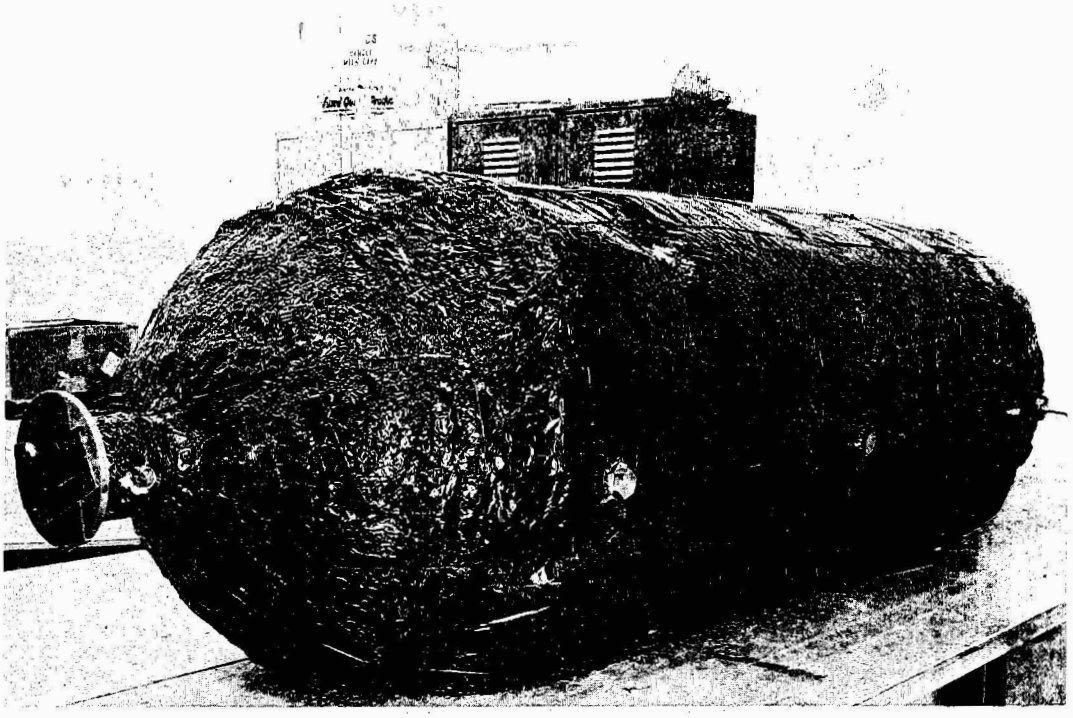

Figure 8.- Insulated Tank After Painting

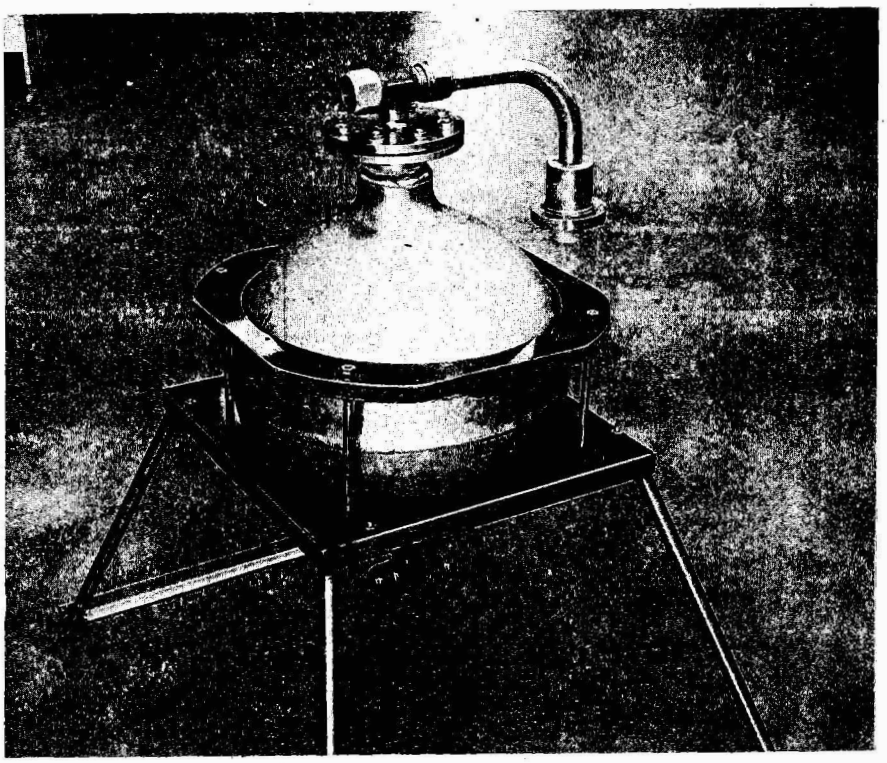

Figure 9.- Standpipe

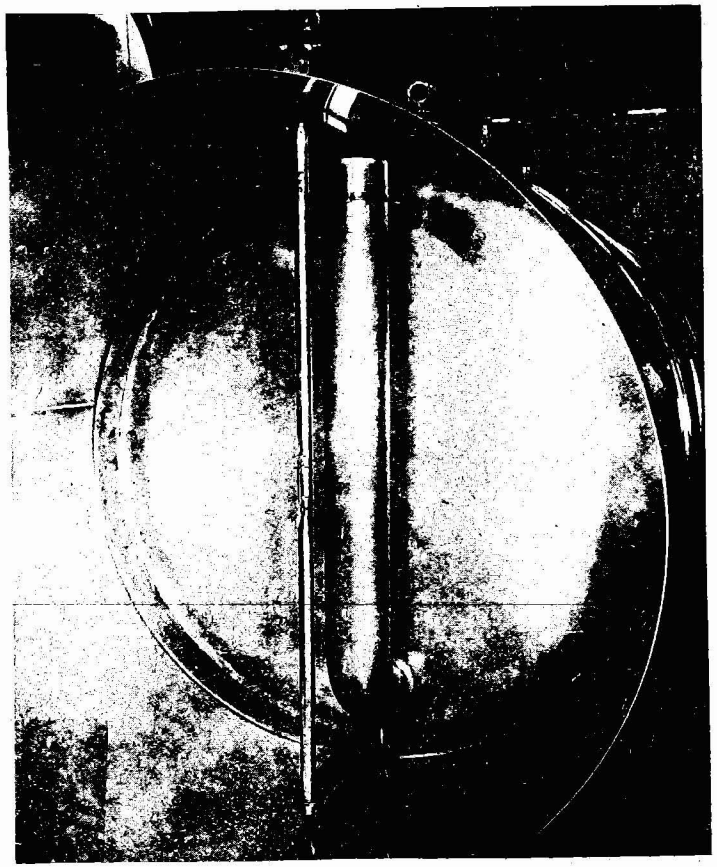

Figure 10. - Low-Pressure Tank, Baffled Configuration

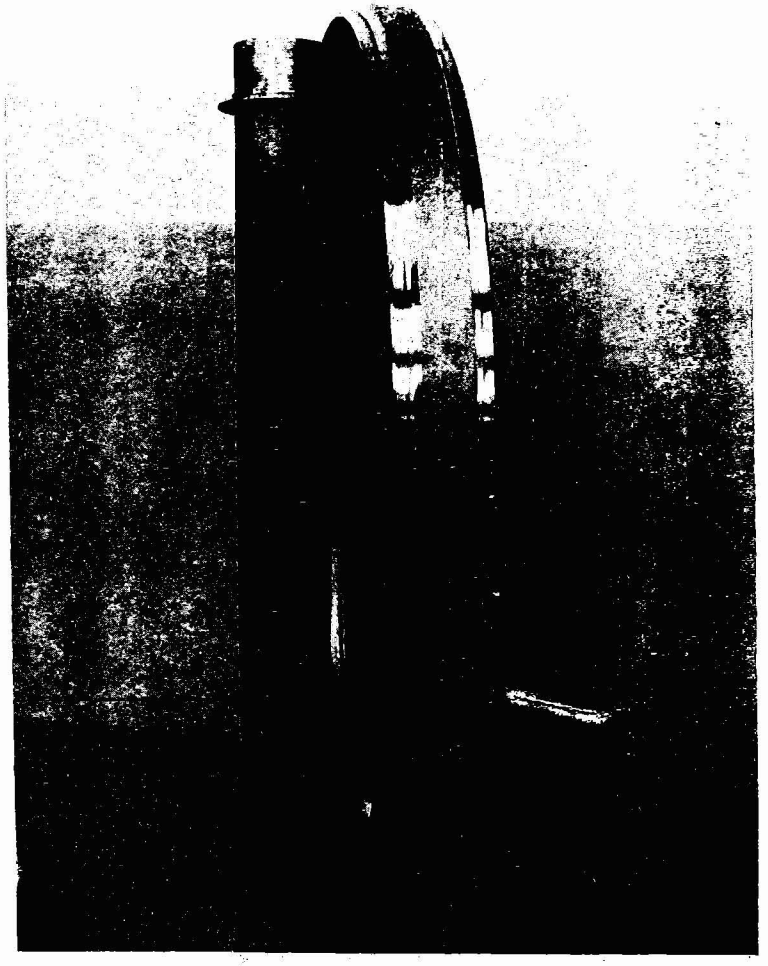

Figure 11. - Ring Section with Baffle and Line Installed

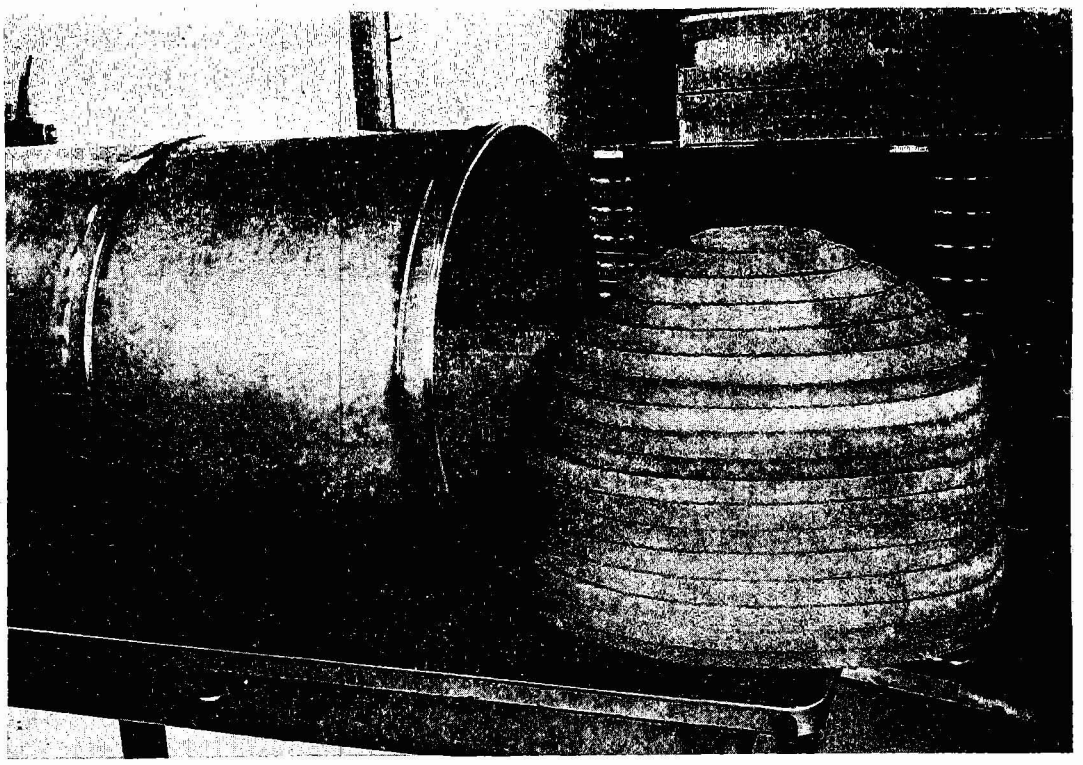

Figure 12. - Foam Sections Used to Fill Dome

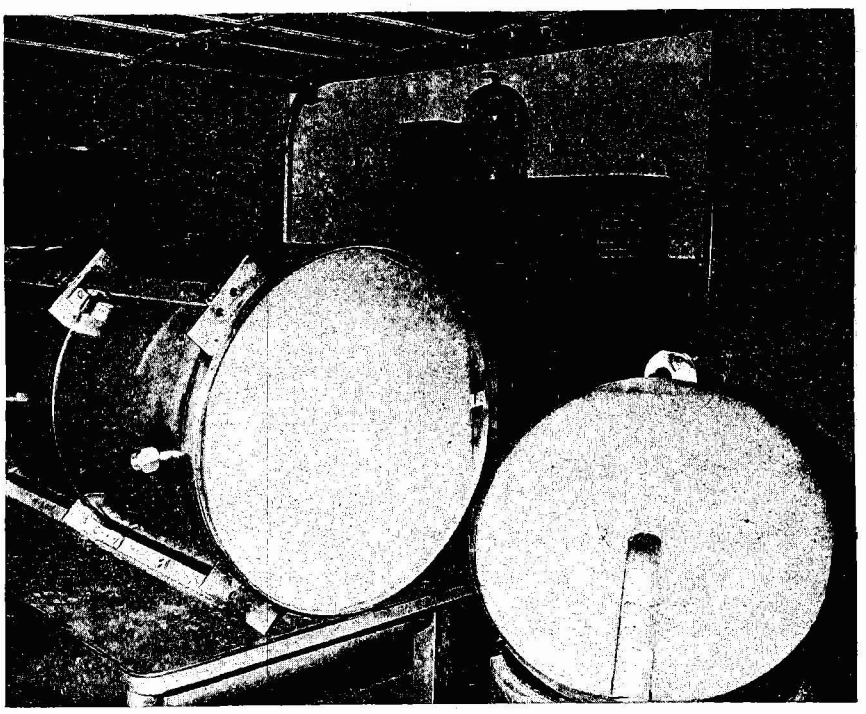

Figure 13. - Foam-Packed Tank Before Making Final Weld

taken off the top and bottom of each disk to provide gas and liquid channels during loading. Figure 13 shows the foam-packed tank before the final weld was made.

To prevent burning the foam while making the final weld, dry ice was packed between the two foam layers nearest the weld. This kept the foam separated from the weld area and held down the internal temperature in the area of the weld. The degree of success of this technique will only be determined when the tank is disassembled.

The tank penetrations for filling, venting, and instrumentation probes were similar to those used in the main tank of standpipe configuration, as was the method used to insulate the tank.

d. High-pressure tank.- This tank was similar in design and construction to the main tank portion of the standpipe configuration, except that it was designed and hydrostated for a higher operating pressure. Because it was intended to act as a receiver vessel during the fuel-transfer tests, it had to withstand pump heads above the level in the low-pressure tank. The design operating pressure for the high-pressure tank was 50 psig (34.5 N/cm^2), which required a wall thickness of 0.035 in. (0.089 cm).

Both the thickness of the insulation and the tank penetrations for filling, draining and instrumentation were similar to those used for the standpipe configuration.

2. Wing Section Design

The wing section was designed to provide structural support for the test tanks and to provide a representative heat path to the tanks. Since some of the structure was to be exposed to low temperatures, the basic framework has stainless steel. Figure 14 shows two of the four tank bays before the skin was installed. As shown, most of the basic structure consisted of steel angles welded into truss sections. The between-tank bulkheads were of stainless steel sheet welded to the truss sections.

The assembled truss structure was mounted on four pin-ended vertical legs to a base structure on the floor of the test cell. Figure 15 shows one of the vertical leg mounts, the hydraulic actuator used to produce slosh loads along the axis of the tank, and the tank-mounting clips within the wing structure. Structural steel sheet used to cover the wing section structure was painted black to increase absorptivity. Most skin sections were welded to the basic structure, but the top sections were bolted so the tanks could be installed and removed.

3. Liquid and Gas Supply Systems

Figure 16 shows the system used to supply the gaseous and liquid methane to the test fixture. The liquid methane was supplied from a 600-gallon (2.27 m^3) dewar which was resupplied between tests from a 4000-gallon (15.14 m^3) mobile

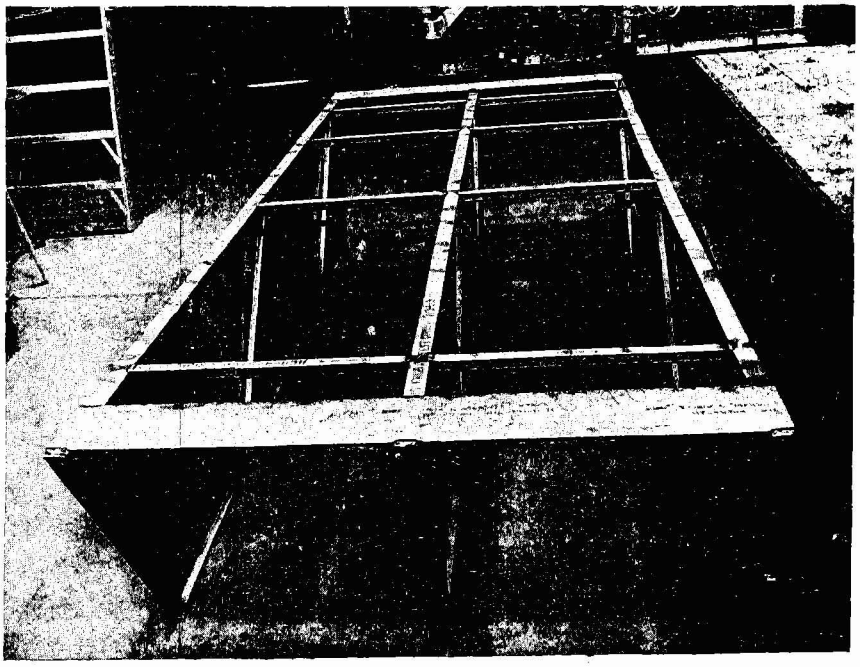

Figure 14.- Basic Structure of Tank Bays

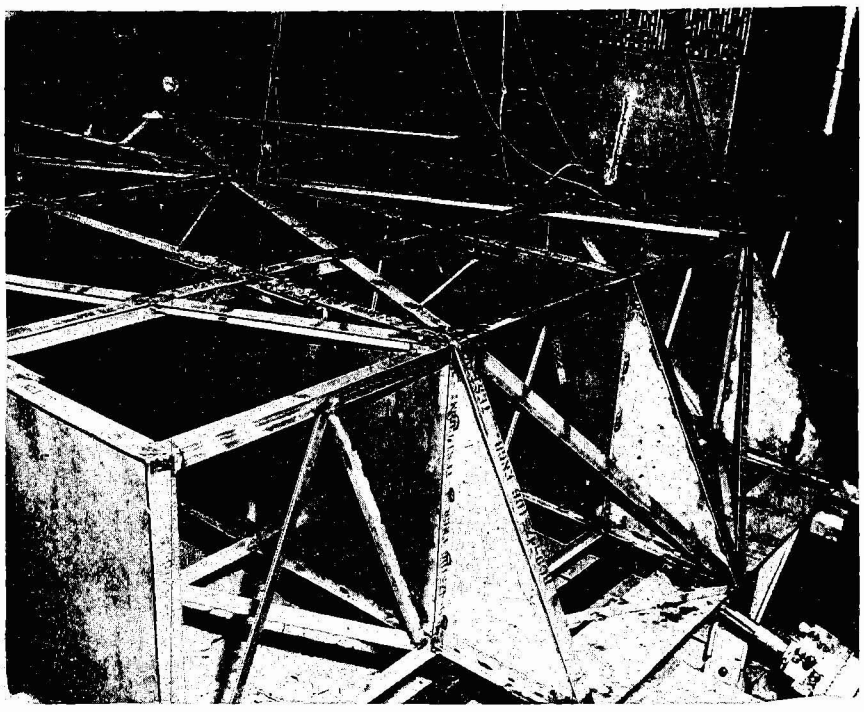

Figure 15.- Assembled Truss Structure in Test Cell

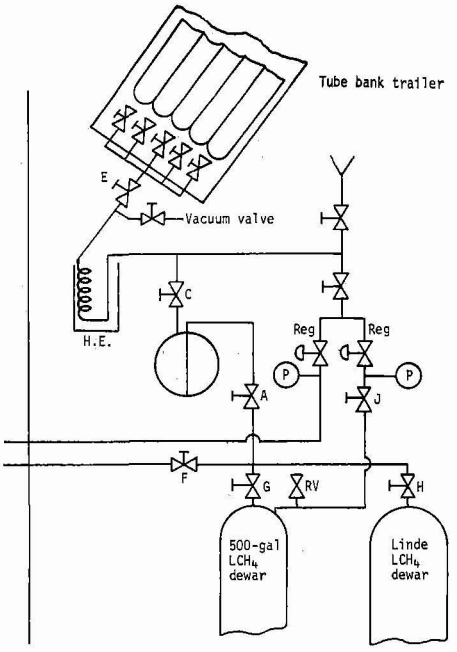

Figure 16.- Storage System for Liquid and Gaseous Methane

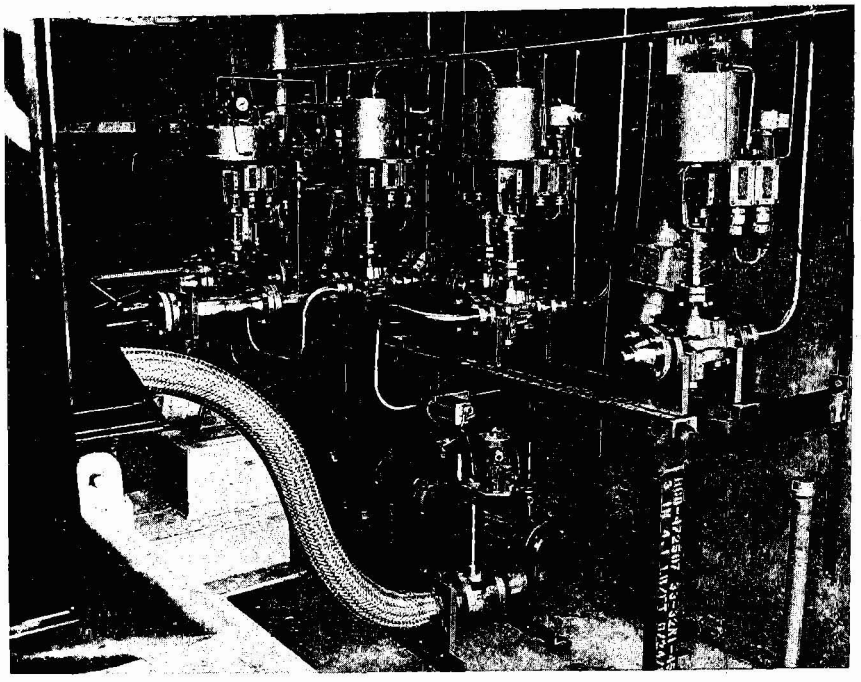

Figure 17.- Plumbing Used to Fill Tanks with Liquid Methane in Tests 1 through 37

methane dewar. Both dewars were separated from the test fixture by a concrete blast wall. Liquid nitrogen, when required, was supplied from a 600-gallon (2.27 m^3) dewar. All plumbing lines, fittings, valves, and meters were made of stainless steel. The liquid fill line from the supply dewar to the tank fill valves was not insulated. An analysis indicated that the heat lost to the flowing liquid due to insulation cooldown would be greater than the environmental heat loss because of the short flow times involved. Figure 17 shows the plumbing configuration used to fill the tanks with liquid methane in the first 37 tests.

The valve bodies were thermally isolated from the cell structure by Micarta support blocks. The lines from the fill valves to the tanks were flexible stainless steel hoses, which were insulated with polyurethane foam. These flexible sections were used to allow for up to 2 inches (5.08 cm) double amplitude movement of the wing during slosh loading.

The vent end systems were similar, although the flexible vent hoses from the tanks to the vent valves were not insulated. The pressurization gas was either methane or nitrogen. The methane was stored in a tube bank trailer on the other side of the blast wall, and the nitrogen was supplied directly from facility supply lines. With the exception of the dewar liquid supply valve and the pressurant supply valve and regulator, all valves were remote operating valves with limit switches for remote monitoring of proper operation.

4. Fuel Transfer System

The tank-to-tank fuel transfer system to pump liquid methane from the low-pressure tank to the high-pressure tank consisted of a pump, liquid flowmeter, and a parallel arrangement of an orifice and flow control valve. The system is shown schematically in figure 3.

The pump was mounted on the test cell floor outside the tanks and wing section as pictured in figure 17. It was a single stage centrifugal model designed specially for low NPSH operation with cryogens. The minimum NPSH was 4.5 feet (1.4 m) of liquid methane at the rated maximum flow of 100 gal/min (6309 cc/sec). More detailed pump specifications are contained in table 2.

The orifice was sized to give maximum rated flow with the flow control valve completely open. Thus, pumping rates could be varied from the minimum valve through the orifice alone to full capacity.

TABLE 2
PUMP SPECIFICATIONS

Type	Single Stage Centrifugal
Drive	Direct Coupled to 5 HP Electric Motor
Inlet Diameter (in.)	2.5
Outlet Diameter (in.)	1.5
Maximum Impeller Diameter (in.)	6.0
Maximum Flowrate (gal./min.)	100.0
Maximum Dynamic Head (ft.)	140.0
Maximum Speed (RPM)	3550.0
Minimum NPSH (ft. water)	4.5

5. Slosh System

This system consisted of a hydraulic piston actuator connected to the liquid fill end of the wing structure. The hydraulic actuator was capable of inducing slosh amplitides up to 2 in. (5.08 cm) double amplitude. A low-frequency function generator was used to drive the hydraulic pump and switching system. The 3000-psi (2068 N/cm^2) pressure provided accelerations up to 2.5 g (24.5 m/sec^2) on the 4000-lb (1814 kg) wing assembly.

6. Heating System

To simulate the wing heating rates experienced in supersonic flight, 440 quartz lamps were mounted in reflector pans above and below the wing skin. This system (fig. 18) provided 120 Btu/ft^2-hr (378 W/m^2) of heat to the outer skin of the wing. The system was driven by a solid-state ignition system to a peak power of 200 W per lamp. The total system power used was 88 kW.

Due to the size of the test fixure, difficulty of installing new lamps, and duration of the test program, it was necessary to minimize the common problem of lamp failures. This was achieved through a novel lamp holding device shown in figure 19. Most lamp failures occur due to overheating the lamp ends. This lamp holding device overcomes the problem by heat sinking the lamp ends to a small cooling fin located on the outside of reflector pans.

7. Wing Cavity Purge

A separate gaseous system, incorporating a shutoff valve and a regulator, was attached to the wing section. This system provided a manifold in each of the four wing bays to maintain a dry nitrogen atmosphere around the tanks during testing. Had the wing section not been completely airtight, the cooling down of the cavity gas would have caused air to be pumped into the wing. Thus, the moisture contained in the air would have been frozen out in the tank insulation. Over a number of cooldown cycles, the insulation would have become saturated with water, and the thermal conductivity would have increased substantially.

8. Instrumentation

In line with the objectives of the program, obtaining as much test data as possible was of paramount importance. A second consideration, however, was the acquisition, handling, and final presentation of these data at a reasonable cost. The complete system used for the program made this possible. This system is described in the following paragraphs.

a. Tank instrumentation.- As each of the four test tanks was fabricated a considerable number of instrumentation sensors was installed. In general, the temperature measurements were of primary importance. The various types of senso

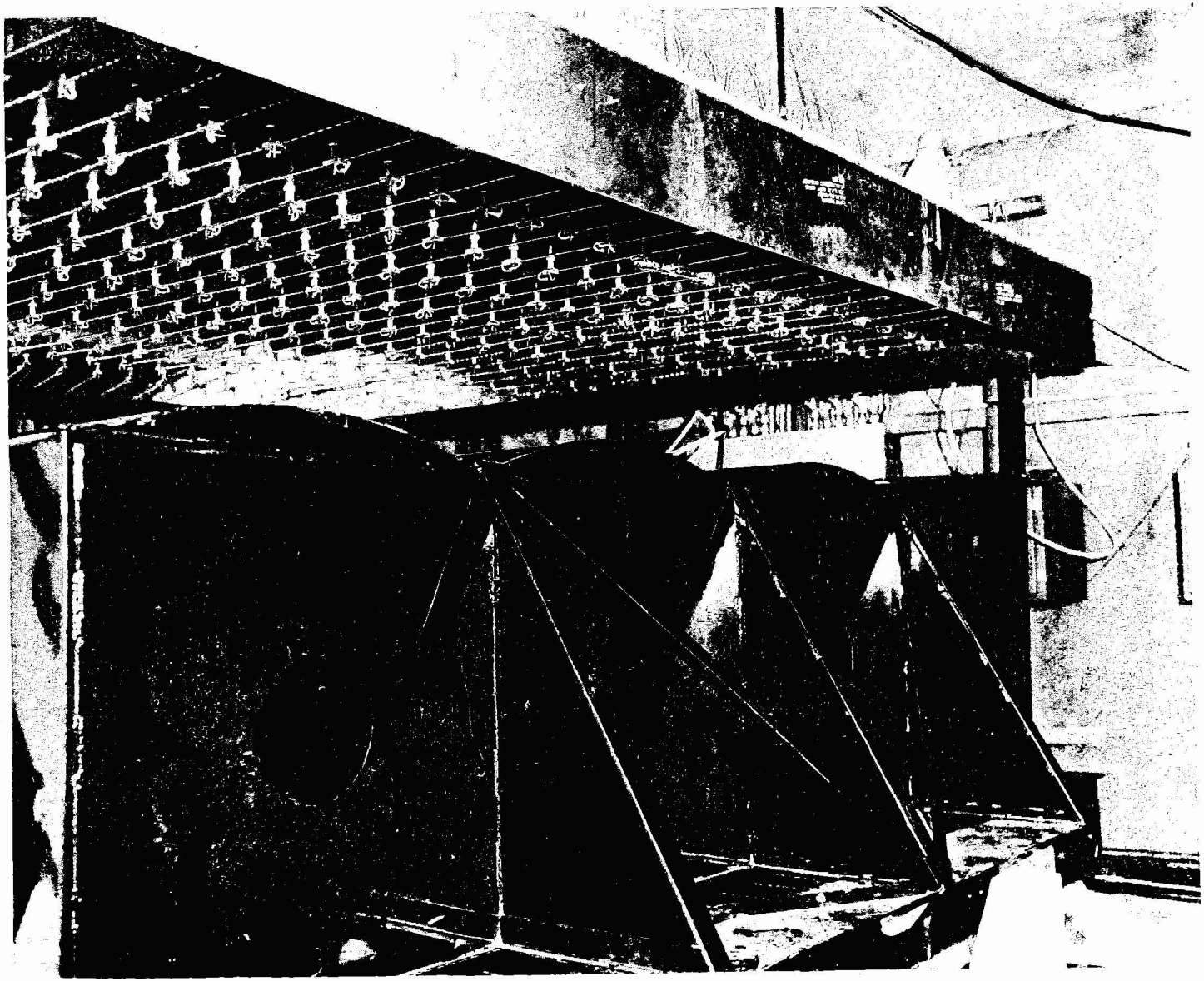

Figure 18. - Lighting System Used to Simulate Wing Heating

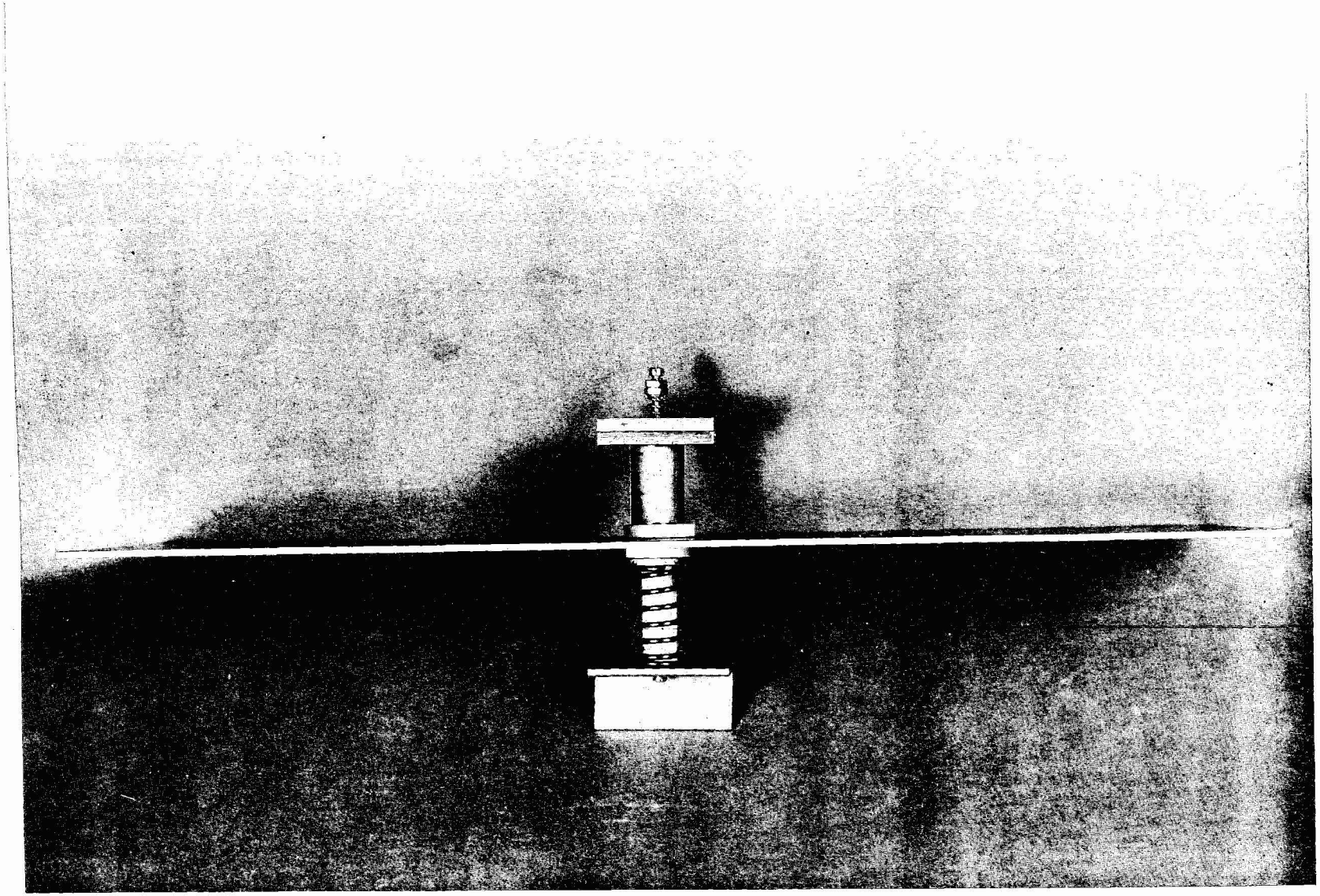

Figure 19.- Finned Lamp Holder

included thermocouples, platinum thermometers, carbon sensors to detect the level of the liquid, and nichrome wire slosh sensors. The temperature and level of the liquid and the slosh conditions were measured by instrumentation probes inserted through bosses on the centerline of the tank top. Figure 20 shows several probes during fabrication.

Table 3 lists the instrumentation used on the standpipe tank and gives its general location on the tank. Figure 21 shows the actual location of the standpipe tank instrumentation. The high-pressure tank and the foam tank were instrumented in a similar manner except they contained no slosh sensors. The baffled-tank instrumentation differed because of the various compartments, and is pictured in figure 22.

For the last 12 tests, the instrumentation in the standpipe tank was changed slightly. Nichrome wire sensors were used in place of carbon level sensors, and were placed at the 7, 47, 53, 75, and 90% levels.

b. Wing section instrumentation.- To complete the tank heat transfer picture, a number of thermocouples were attached to the wing structure. Four thermocouples were mounted on the center of the between-tank bulkheads; eight thermocouples were mounted on the upper and lower wing skins. A chromel/alumel thermocouple was also mounted on the upper wing skin to act as a control for the wing heater system.

c. Gas and liquid system instrumentation.- A number of instrumentation sensors were also provided in the liquid and gas systems outside the tank. Tank pressure transducers were mounted on the vent lines and were the only instrumentation sensors for tank measurements that were not mounted directly on the tanks. Four venturi-type flowmeters were mounted in the fluid transfer systems. One was used to measure liquid flow through the pump, two were used to measure vent gas flows from the center bay tanks, and one was used to measure pressurant gas flowing into the low-pressure test tank. Each flowmeter had an inlet pressure and ΔP pressure transducer, along with a thermocouple to measure fluid temperature. A pump case thermocouple was used to monitor pump cooldown before pumping began.

d. Data collection and recording.- Through a variety of standard amplifiers and power supplies, the signals from the sensors were conditioned to provide an analog voltage output in the range of ± 64 mV. These signals were then input to an IEC Subscriber Station (fig. 23 and table 4), which had a 100-channel, low-level analog input capability, a PCM output of 312 twenty-bit words, and a multiplexing and transmitting capability. This low-level, analog-to-digital acquisition system is transportable to permit the input of data in remote laboratories.

A permanent hard-wired link was used to transmit the data from the 501 unit to a central data recording station. At the station, the signal was input to a Lear-Seigler 670A telemetry processor (fig. 24 and 25, and table 5), which had a data-rate capability of 1 channel at 0.8 to 1 250 000 bits per sec of serial PCM data, or 14 channels at a maximum rate equal to 1.25/N (N = number of data

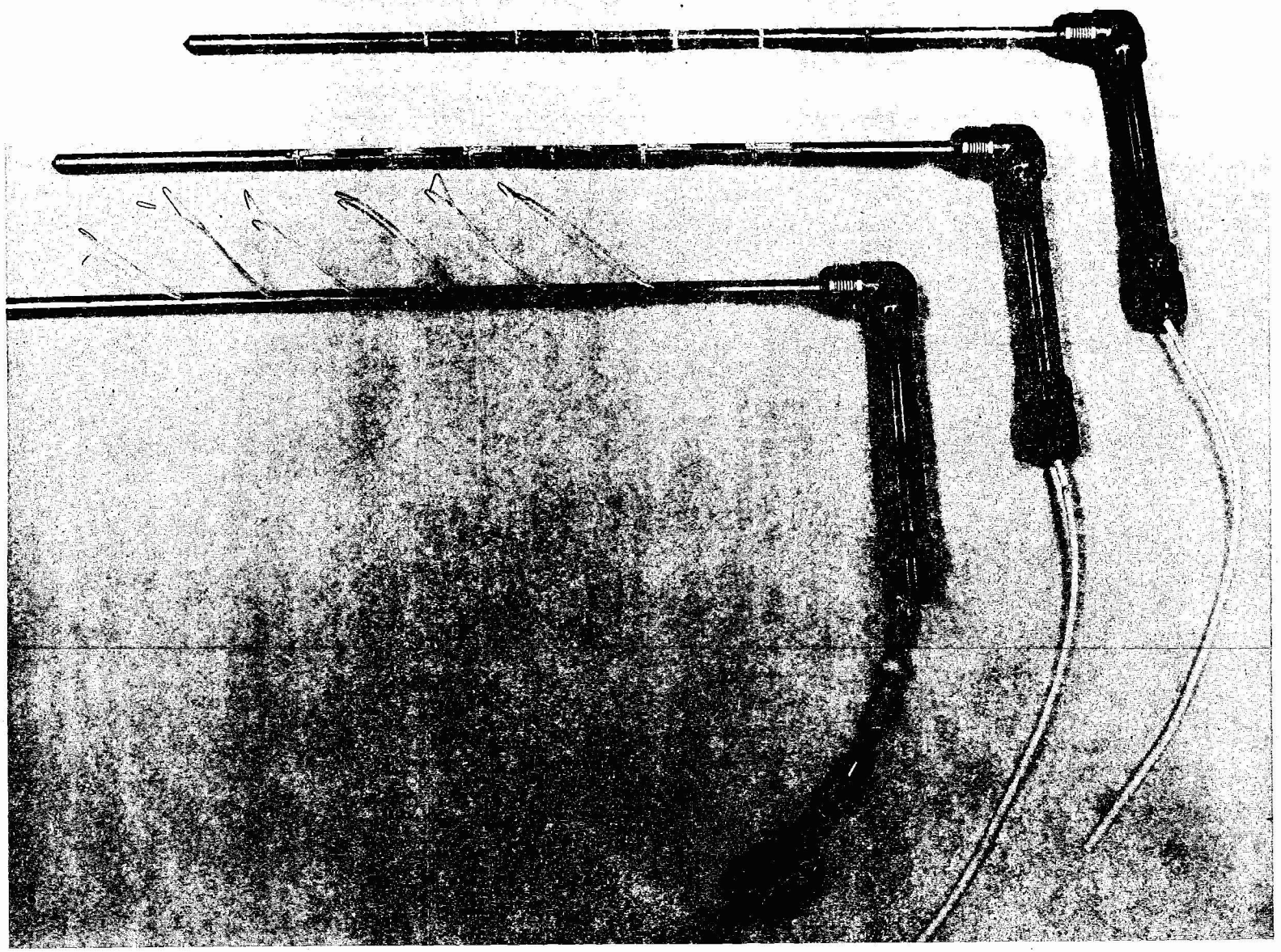

Figure 20.- Instrumentation Probes Being Fabricated

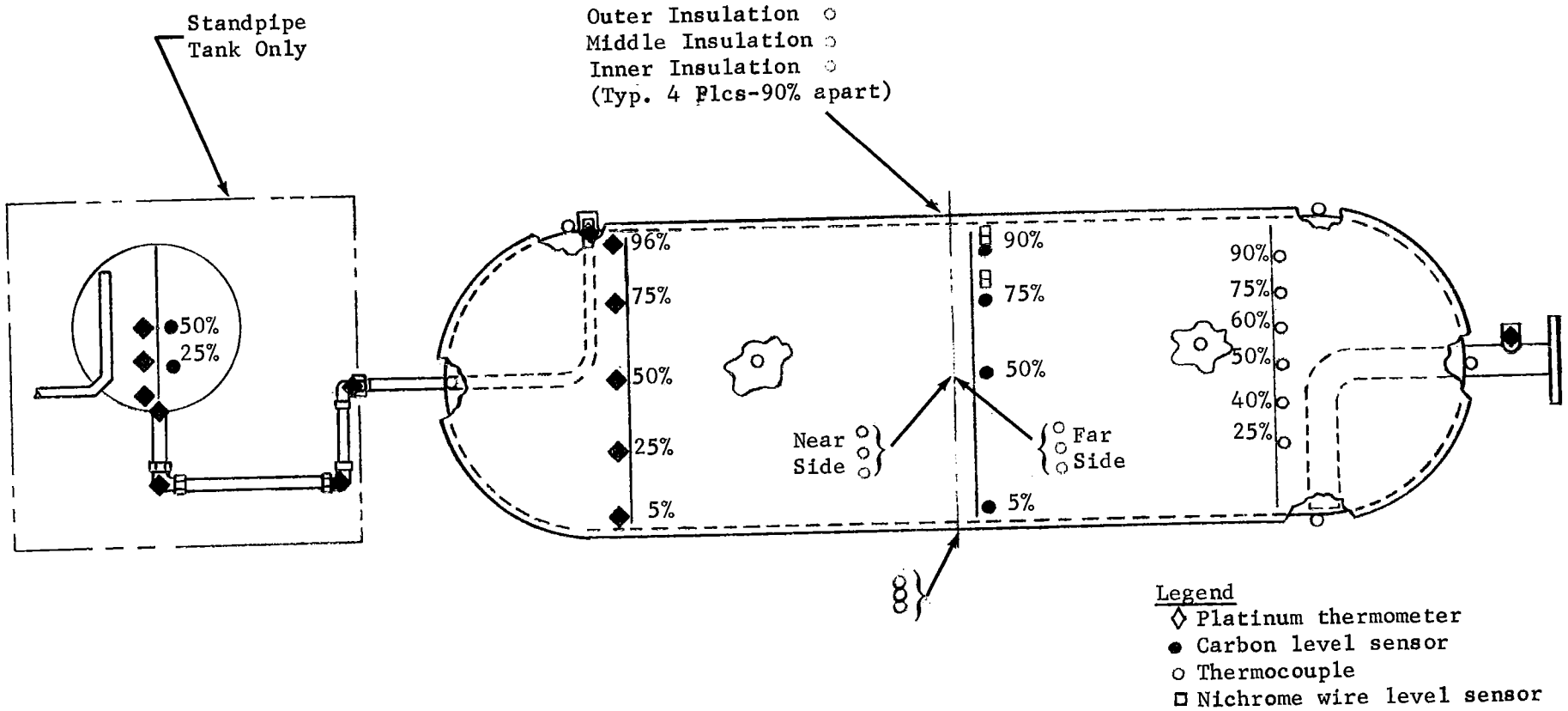

Figure 21.- Typical Instrumentation Drawing for the Standpipe Tank, Foam Tank and High-Pressure Tank

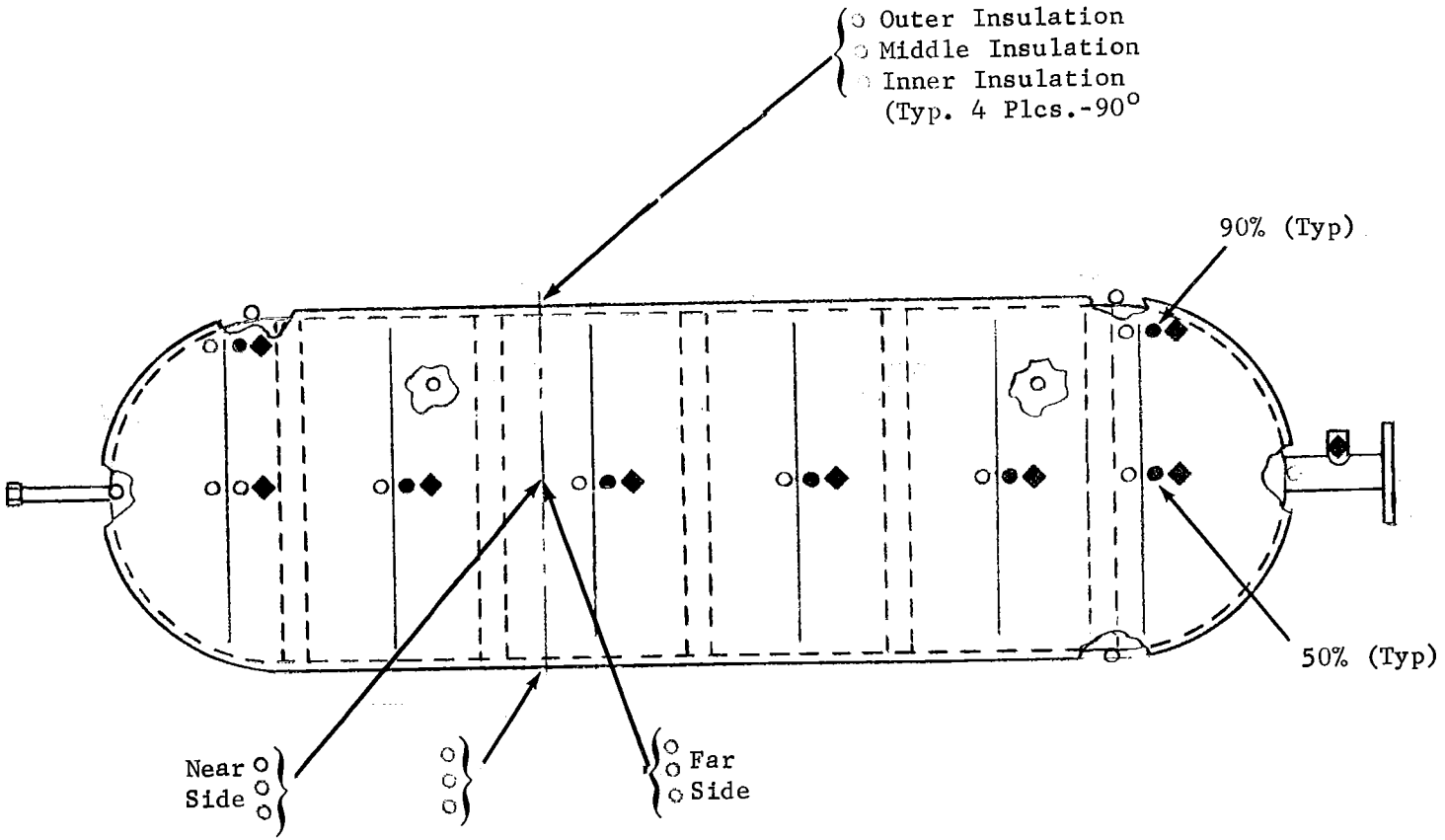

Figure 22.- Instrumentation Drawing for the Baffled Tank

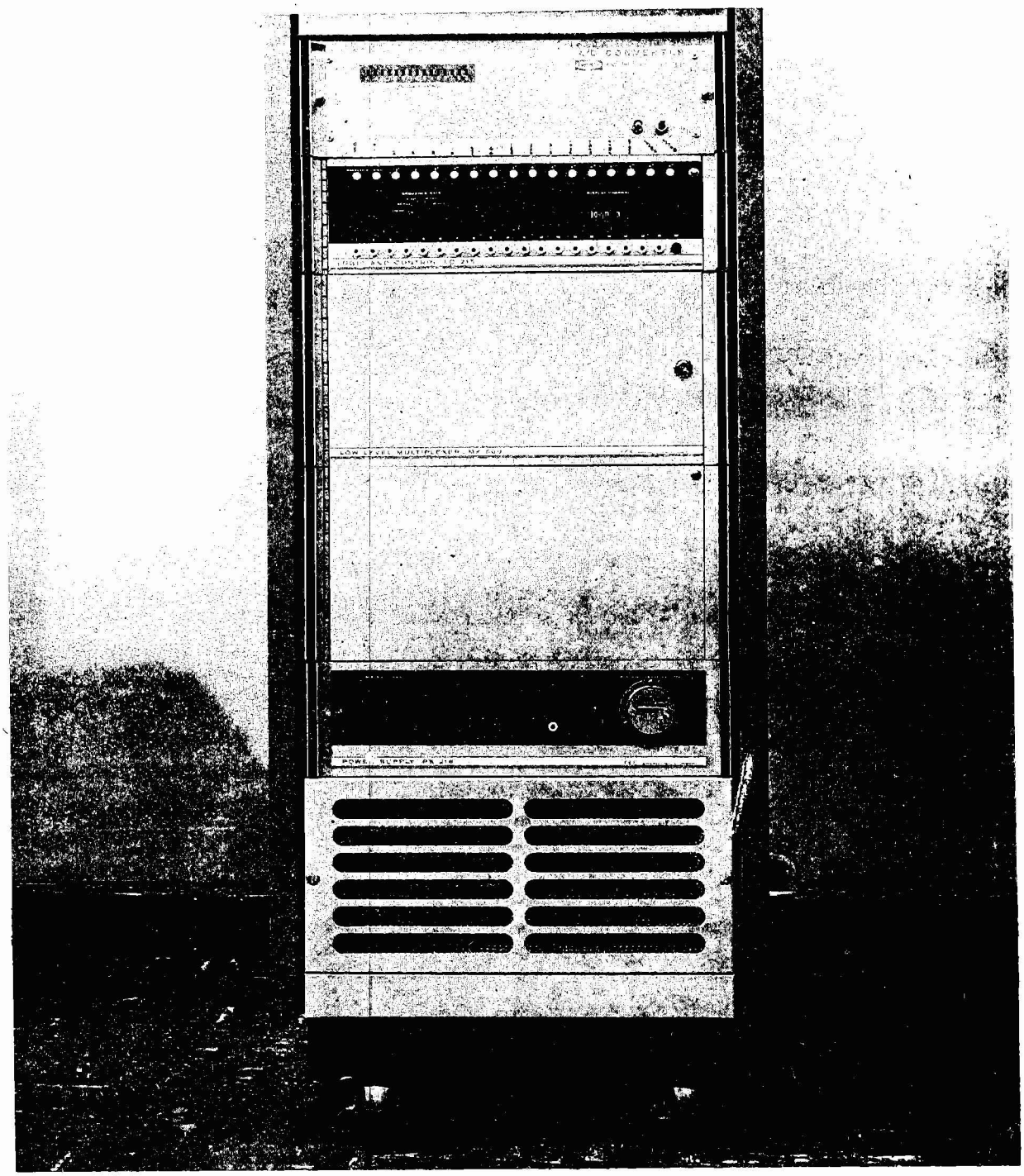

Figure 23. - 501 Data System

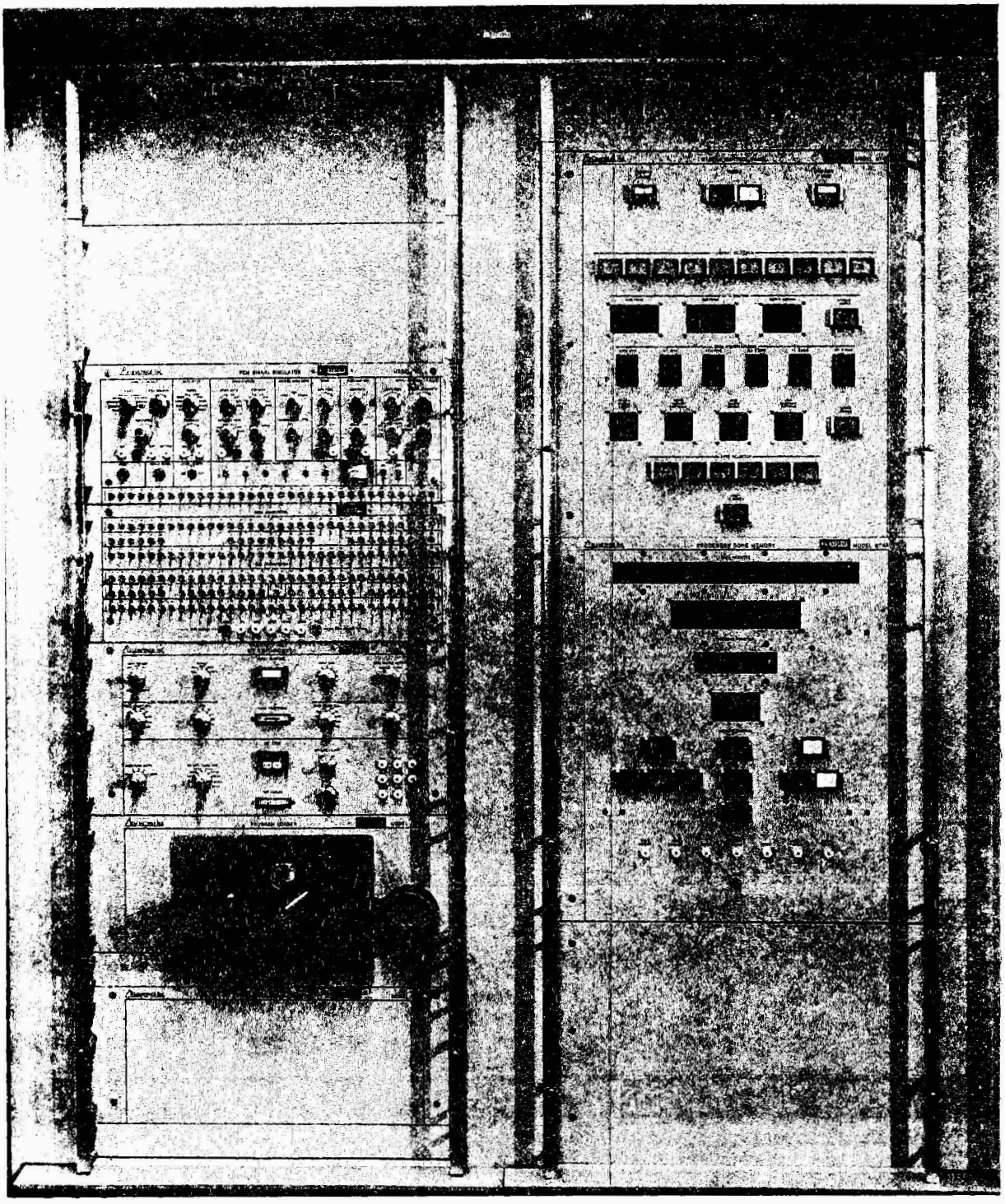

Figure 24.- 670A Telemetry Processor

Figure 25.- 6748 Magnetic Tape Formatter
and 729 Mod II Tape Drive

TABLE 3.- STANDPIPE TANK SENSORS

Type of sensor	Location	Purpose
Thermocouple chromel/ constantan	On a vertical probe at six levels in the tank	To measure the temperature of the gas and of the liquid in the tank
	Seven on the tank skin top, side, bottom, dome end, etc	To measure the temperature of the skin on the tank
	Twelve on the radiation shields in the three layers of tank insulation -- inner layer, middle layer, and outer layer	To obtain the temperature distribution across the insulation in order to calculate the heat loss
Platinum thermometer	On a vertical probe at five levels in the tank	To accurately measure the temperature of the liquid in the tank
	At the tank inlet and in the vent cup	To accurately measure the temperature of the liquid at the inlet and the temperature of the gas and of the liquid at the outlet
	Three in the line from the vent cup to the standpipe	To measure the temperature of the liquid as it passes between the two tanks
	At the inlet and at three levels in the standpipe	To measure the temperature variation of the liquid in the standpipe
Carbon level sensors	At the 5%, 50%, 75%, and 90% volume levels in the main tank	To determine the level of the liquid
	At the 25% and 50% levels in the standpipe	To determine the level of the liquid
Nicrome wire slosh sensors	Two just above the 75% level and two above the 90% level in the tank	To detect the presence of slosh waves in the tank

TABLE 4.- TECHNICAL SPECIFICATIONS FOR 501 DATA SYSTEM

Data input characteristics	
Type of inputs	Analog, differntial, shielded
Input amplitude	4, 8, 16, 32, 64 mV, full-scale
Number of inputs	100, expandable to 250
Common-mode input	10 V peak, dc to 60 Hz
Source impedance	Less than 1000 ohm
Common-mode rejection	100 dB, dc through 60 Hz
Sampling rate	1.25, 2.5, 5, 10, or 20 kHz steady-state
Output characteristics	
Type of output	PCM format, biphase-M (Manchester 1)
Amplitude out of data link line driver	Approximately 16 V, peak-to-peak
Amplitude out of data link receiver	1 V, rms
Frame length	312 words
Frame content	Frame synchronization word, information word, 10 calibration words, and 300 data words
Word length	20 bits
Environmental characteristics	
Temperature	0 to 50°C
Pressure altitude	Up to 10 000 ft
Humidity	0 to 90% without condensation
Power requirements	115 V ac ± 10%, 60 ± 2 Hz 5A
Size	
Main cabinet	22-1/16 in. wide x 25-1/2 in. deep x 54-7/6 in. high
Receiver enclosure	8 in. wide x 8 in. high x 4 in. deep
Multiplexer subsystem characteristics	
Accuracy	±0.05% of full seale
Crosstalk	±0.02%
Manual gain selection	2000, 1000, 500, 250, 125
Programmable gain selection	2000, 500, 125 by groups of 10 channels
Automatic gain selection	2000, 500, 125
Gain stability	0.05% in 200 hr
Analog-to-digital converter characteristics	
Input range	±8.192 V, full-scale
Bit weighting	4 mV per bit
Input impedance	100 megohm, minimum
Resolution	12 bits (11 bits and sign)
Output code	Negative number (two's complement)
Digital input and output	"1" = 4.5 ± 0.5, "0" = 0 ± 0.5 V
Digitizing accuracy	±0.05% of full scale ± 1/2 LSB

TABLE 5.- TECHNICAL SPECIFICATIONS FOR LEAR-SIEGLER 670A TELEMETRY PROCESSOR

Input power	115 V ± 10% at 45 to 400 cps single phase, 50 A
Power consumption	4 kW
Data input characteristics	
Types of input	Serial or parallel
Serial data	PCM NRZ-S data accompanied data input clock
Data rate	1 channel at 0.8 to 1 250 000 bits per sec.
Word length	From 1 to 64 bits, variable from word to word
Data alignment	MSB or LSB, or mixed MSB and LSB words
Parallel data	PCM NRZ-S data accompanied by data transfer pulse
Data rate	14 data channels at a maximum rate equal to 1.25/N, where N = number of data channels
Word length	From 1 to 64 bits, variable from word to word
Data alignment	MSB or LSB
Data output characteristics	
Type of output	Parallel
Data rate	500 000 words per sec, maximum
Word length	From 1 to 64 bits, variable from word to word
Data identification	A unique 11-bit I.D. code for each main frame and subframe word
Data use code	Provides for addressing up to 63 (511 optional) output peripheral devices. Any data channel may be addressed to any one of the 63 output devices
Core memory characteristics	Coincident-current storage element
Capacity	4096 36-bit words. Each word has three 12-bit addressable fields
Function modes	Operate (automatic), manual, or external
Access modes	Random or sequential address
Address modes	Direct-address, indirect-address, relative address, or no-address
Operating modes	Full cycle (clear/write and read/restore). Modify cycle (read/modify and restore)
Cycle times	Full cycle, 2 μsec Read only, 1.2 μsec Modify and restore, variable Data access, 0.85 μsec

TABLE 5.- TECHNICAL SPECIFICATIONS FOR LEAR-SEIGLER 670A TELEMETRY PROCESSOR - Concluded

Operation times (minimum including access)	
Add/subtract	2 μsec
Multiply	17 μsec
Logical (OR, AND, exclusive OR)	2 μsec
Data transfer	2 + 0.2 N μsec, where N = bits/word
Environmental characteristics	
Temperature	
Operating	50 to 100°F (operating time above 100°F limited to 4 hr)
Nonoperating	40 to 150°F
Relative humidity	95% maximum
Air conditioning	Refrigeration, 1 ton
Dimensions	76 in. high x 48 in. wide x 32 in. deep
Input/output unit characteristics	
High-speed paper tape reader, 8-level	300 characters per sec
Paper tape punch (optional)	50 characters per sec
Typewriter (optional	15.5 characters per sec
Bit synchronizer (optional)	1 250 000 bits per sec
Paper tape reader (optional)	50 characters per sec
PCM simulators (optional	
Digital-to-analog converter (optional	8- or 10-bit conversion
PAM/PDM-to-PCM converter (optional)	
Magnetic tape formatters	Systems presently operating with IBM, such as Mod II, IBM Mod IV Ampex TM3, and Ampex TM7
General-purpose computers	Systems presently operating with CDC 160A, IBM 1800, and SDS Sigma 11

channels) of parallel data. The main frame has 4096 36-bit words of core memory, and the formatter has 1024 18-bit words of core memory. After the PCM signal was decoded and conditioned to provide a binary digital output from the 670A unit, the output was recorded on a 7-track tape unit. These tapes were input to the CDC 6400/6500 computer along with the plot computer program.

The computer program:

1) Averages the data samples for each data channel over any specified time increment;

2) Skips any specified time increment between averages;

3) Compares each individual data point with the average and omits any point that differs from the average by more than a preselected amount. If a point is omitted, the remaining points are again averaged. This portion of the program is used to aliminate extraneous noise on the data signal whenever the noise affects less than half the data smaples;

4) Converts each of the averaged data points (in mV) to a temperature, pressure, liquid level, or flowrate of gas or liquid;

5) Plots as many as five channels per plot against a preselected time scale on a continuous roll of photosensitive paper. Plot titles, data point identification, annotations, and ordinate and abscissa nomenclature are printed on each plot. In addition, each plot is placed on microfilm;

6) Stores the averaged data points of Item 3 above on magnetic tape.

Data points may be replotted at any time with changes of scale, if required. This allows any section of the plot to be expanded for closer investigation.

9. Standpipe Tank Sampling System

For three of the last 12 tests, the liquid methane was pressurized with gaseous nitrogen and the nitrogen solubility was determined. To do this, a liquid sampling system was added to the standpipe tank. The system consisted of a 0.125-in. (0.318 cm) diameter stainless steel tube running from the 50% level in the standpipe tank to a manifold outside the cell wall. Ten evacuated sampling cylinders were attached to the manifold. When a sample was required, the manifold and tubing were bled down and a sample cylinder was filled. The samples were analyzed on a Perkin-Elmer gas chromatograph.

B. CHECKOUT

As a prelude to the systems tests using liquid methane, a number of component, subsystem, and system checkouts were made. Three of the tanks were

loaded and exposed to a water-filled hydrostatic test at 1.5 times the maximum operating pressure. This test was made after welding but before the insulation was installed. The foam-filled tank was omitted from this step to avoid the problem of drying the tank after the test. Afterward, each tank underwent a helium mass spectrometer leak check, with again, an exception made in the case of the foam tank.

Next, 7000 lb. (3175 kg) of lead weights were loaded into the wing, and the slosh system was activated to proof-load the wing structure. Then, after they were insulated and installed in the wing section, the three hydrostated tanks were filled with water and pressurized to operating pressure. The wing slosh system was activated on a one-g proof load test was made to prove the structural integrity of the tank mounts and tanks under axial loading.

After the foam-filled tank was installed in the wing, all the tanks were loaded with liquid nitrogen and pressurized to 1.5 times the maximum operating pressure. A final check was made by pressurizing all four tanks to the operating pressure with methane gas and checking for leaks with a portable methane detector.

The gaseous and liquid plumbing systems were pressurized to operating pressure using gaseous nitrogen and a bubble type leak check was made. Before making any tests, a final leak check was made with gaseous methane and the methane detector.

A complete system cold checkout was conducted using liquid nitrogen. During this series of checks, all operations which were to be done with liquid methane were done with liquid nitrogen, even to operating the cryogenic pump.

A high degree of confidence in system integrity and operation was now attained and the system was ready for liquid methane testing.

V. TEST PROGRAM

A comprehensive test program was designed and carried out to evaluate the problems involved in handling a cryogenic fuel under flight conditions. The original program consisted of 37 tests covering five basic areas of operation:

1. Fuel loading
2. Ground hold and taxi
3. Heat transfer
4. Fuel transfer
5. Flight simulation

Except for the fuel loading tests, all four tank configurations were evaluated in each phase of testing. Fuel loading tests were limited to the standpipe tank configuration since all other configurations should pose fewer problems.

Upon evaluation of the data from the first 37 tests it was decided that further loading tests and flight simulation tests were required. A second series of 12 tests were defined, with six tests directed toward series tank loading as apposed to the parallel loading used in the first tests, and six additional flight simulation tests using both methane and nitrogen as pressurant gases.

Table 6 gives a complete summary of the total test program. The table lists the test numbers related to each tank in every phase of testing as well as indicating the environmental conditions.

In the following sections a brief objective of each phase of testing is presented. A detailed test description is given along with typical pertinent data from the tests. Each section is concluded with a summary of the results for that phase of testing.

A. LOADING TESTS

All loading tests were conducted using the standpipe tank configuration. The major objectives of these tests were to obtain maximum bulk subcooling and to completely fill the standpipe tank. This test series involved twelve separate tests on the standpipe tank configuration. Tests 1 through 3 involved loading a tank which was initially at ambient temperature; tests 4 through 6 involved parallel loading a precooled tank. The test conditions simulated actual aircraft conditions; i.e., the wing tanks could be completely empty and be warmed up to ambient temperature or could contain a small amount of liquid from a previous flight. Tests 39 and 41 involved series loading of liquid methane while 38 and 40 served as a baseline case where liquid methane was loaded into a single ambient tank. Tests 40 and 41 had small quantities of helium gas added to the ullage at several times following loading. Tests 48 and 49 involved loading liquid nitrogen.

TABLE 6. - TEST PROGRAM MATRIX

		Ground Fill and Hold								Hold and Taxi			Heat Transfer		Fuel Transfer			Flight Simulation				
ST Tests		1, 2, 3	4, 5, 6	38	39	40	41	48	49	7	8		9	10	11	12	13	14	15	16	42, 43, 44	45, 46, 47
FT Tests										17	18	19	20	21	22	23	24	25	26	27		
BT Tests										28	29		30	31	32	33	34	35	36	37		
Liquid		Methane	Methane	Methane	Methane	Methane	Methane	Nitrogen	Nitrogen	Methane	Methane	Methane	Methane	Methane	Methane	Methane	Methane	Methane	Methane	Methane	Methane	Methane
Pressurant		Methane	Methane	Methane	Methane	Methane	Methane	Nitrogen	Nitrogen	Methane	Methane	Methane	Methane	Methane	Methane	Methane	Methane	Methane	Methane	Methane	Methane	Nitrogen
Initial Liquid Volume	LPT	~100%	~100%	~100%	~100%	~100%	~100%	~100%	~100%	~100%	5%	50%	~100%	~100%	~100%	~100%	~100%	~100%	~100%	~100%	~100%	~100%
	HPT	Empty	96%	Empty	96%	Empty	96%	Empty	96%	96%	50%	50%	96%	96%	25%	25%	25%	60%	60%	60%	96%	96%
	Guard	Empty	90%	Empty	90%	Empty	90%	Empty	90%	90%	90%	50%	90%	90%	90%	90%	90%	90%	90%	90%	90%	90%
Initial Liquid Temperature	LPT	-263°F	-263°F	-263°F	-263°F	-263°F	-263°F	-324°F	-324°F	-263°F	-263°F	-263°F	-263°F	-263°F	-263°F	-263°F	-263°F	-263°F	-263°F	-263°F	-263°F	-263°F
	HPT	Ambient	-237°F	Ambient	-263°F	Ambient	-263°F	Ambient	-324°F	-237°F	-237°F	-237°F	-237°F	-237°F	-237°F	-237°F	-237°F	-237°F	-237°F	-237°F	-263°F	-263°F
	Guard	Ambient	-237°F	Ambient	-263°F	Ambient	-263°F	Ambient	-324°F	-263°F	-263°F	-263°F	-263°F	-263°F	-263°F	-263°F	-263°F	-263°F	-263°F	-263°F	-263°F	-263°F
Tank Pressure Profile	LPT	Maintain at 36 psia	Maintain at 36 psia	Maintain at 36 psia	Maintain at 36 psia	Maintain at 36 psia	Maintain at 36 psia	Maintain at 49 psia	Maintain at 49 psia	Maintain at 36 psia	Maintain at 36 psia	Maintain at 36 psia	Vent	Vent	Vent	Vent	Vent	Flight Profile	Flight Profile	Flight Profile	Flight Profile	Flight Profile
	HPT	Vent	Vent	Vent	Maintain at 36 psia	Vent	Maintain at 36 psia	Vent	Maintain at 49 psia	Lock up at 36 psia, vent at 62 psia	Lock up at 36 psia, vent at 62 psia	Lock up at 36 psia, vent at 62 psia	Lock up at 36 psia vent at 62 psia	Lock up at 36 psia vent at 62 psia	36 psia maximum	36 psia maximum	36 psia maximum	Lock up at 36 psia, vent at 62 psia	Lock up at 36 psia, vent at 62 psia	Lock up at 36 psia, vent at 62 psia	Maintain at 36 psia	Maintain at 36 psia
	Guard	Vent	Vent	Vent	Maintain at 36 psia	Vent	Maintain at 36 psia	Vent	Maintain at 49 psia	Vent	Vent	Vent	Vent	Vent	Vent	Vent	Vent	Vent	Vent	Vent	Maintain at 36 psia	Maintain at 36 psia
Wing Temperature Profile		Ambient	Ambient	Ambient	Ambient	Ambient	Ambient	Ambient	Ambient	Ambient	Ambient	Ambient	400°F	400°F	400°F	400°F	400°F	Flight Profile	Flight Profile	Flight Profile	Flight Profile	Flight Profile
Slosh Schedule		None	None	None	None	None	None	None	None	5 minutes of moderate sloshing after initial thermal equilibrium is established 5 minutes of violent sloshing after thermal equilibrium is re-established from first slosh 5 minutes of violent sloshing after one hour			Moderate slosh every 5 minutes to wet walls	1 minute violent slosh at 40 and 80 minutes after test start	None	Continuous moderate sloshing	Violent sloshing for 30 seconds when the high pressure tank is 75% full	None	Continuous moderate sloshing	Violent slosh for 2 minutes during ascent and descent when LPT pressure reaches 19.4 psia	Continuous moderate sloshing	Continuous moderate sloshing
Miscellaneous Notes		Ambient tankage "Zero ullage" load Run 2 and 3 had helium added to tank prior to fill (3 and 10 psi resp.)	Precooled tankage "Zero ullage" load	Ambient single tank load	Series standpipe tank load	Ambient single tank load Helium injected into ullage 4 times after loading	Series tank load Helium injected into ullage 4 times after loading	Ambient single tank load	Series tank load	None	None	None	2 hour wet test followed by a 2 hour dry test on ST only	None	Pump fuel from LPT to HPT until HPT reaches 96%	Pump fuel from LPT to HPT until HPT reaches 96%	Pump fuel from LPT to HPT until HPT reaches 96%	Drain back LPT to 50% level after thermal equilibrium following ascent	Drain back LPT to 50% level after thermal equilibrium following ascent	Drain back LPT to 50% level after thermal equilibrium following ascent	Drain back LPT to 50% level after thermal equilibrium following ascent	Drain back LPT to 50% level after thermal equilibrium following ascent Take 10 liquid samples from 50% level on Run 46 to test for GN_2 solubility

1. Test Descriptions and Data

a. Test 1.- During Test 1, the standpipe tank was pressurized with methane gas to 36 psia (24.8 N/cm^2) from the tank vent valve to the liquid methane supply valve. All intermediate valves were open. The supply dewar system was pressurized to 40 psia (27.6 N/cm^2) up to the liquid methane supply valve to provide a transfer pressure of 4 psi (2.76 N/cm^2). Before being pressurized, the dewar system had been vented long enough to provide liquid saturated at ambient pressure, which was approximately 12 psia (8.27 N/cm^2). The test was started by opening the liquid methane supply valve to initiate the transfer. The dewar pressurization control valve was operated manually to maintain the transfer pressure.

Because the tank vent was closed, once the liquid methane supply valve was opened the pressure in the test tank rose to 40 psia (27.6 N/cm^2). When the vent valve was opened, the tank pressure dropped rapidly, and before the valve could be reclosed the pressure had dropped below 36 psia (24.8 N/cm^2). This method of attempting to maintain a constant tank pressure caused the tank pressure to cycle around the required pressure.

Figure 26 shows the tank pressure during the test. Figures 27 and 28 show the temperature of the liquid in the main tank and standpipe, respectively. The tank pressure was maintained near 36 psia (24.8 N/cm^2) throughout the test, except for a short period before any liquid was collected in the tank and again after the liquid methane was drained back to the dewar.

Figure 28 shows the temperature of the incoming liquid at the tank inlet. Note that, after fill system cooldown, this temperature stabilized at -252°F (-157.8°C). Immediately after filling, the temperature of the liquid in the main tank ranged from -249°F (-156.1°C) at the tank bottom to -240°F (151.1°C) at the tank top. This stratification of 9F° (5C°), however, did not vary linearly from bottom to top since the 75% level temperature was -246°F (-154.4°C). Thus, two-thirds of the stratification was between the 75% level and tank top.

The temperature of the liquid in the standpipe (fig. 28) was -237°F (-149.4°C) after loading. The 50% level, or surface temperature, was at saturation temperature for the liquid throughout the test. If the temperature recorded at the 50% liquid level is representative of the temperature of the bulk liquid in the main tank, then the subcooling from the standpipe to the main tank (fig. 26 and 27 is 10F° (5.6C°) after loading and 5F° (2.8C°) after the 27 minute hold period. Hence, a bulk subcooled loading of about 10F° (5.6C°) was attained.

Figures 29 and 30 show the temperature distribution across the tank insulation at two places during the test. Note that the inner temperature in each case is essentially the temperature of the tank skin. Comparing the inner temperature on the two figures shows that the tank did not fill completely: the top-inner temperature reached only -210°F (-134.4°C), but the side-inner temperature reached the temperature of the liquid, -245°F (-153.9°C). The liquid was within 1 in. (2.54 cm) of the top, however, as measured by the respective platinum probe in Figure 27.

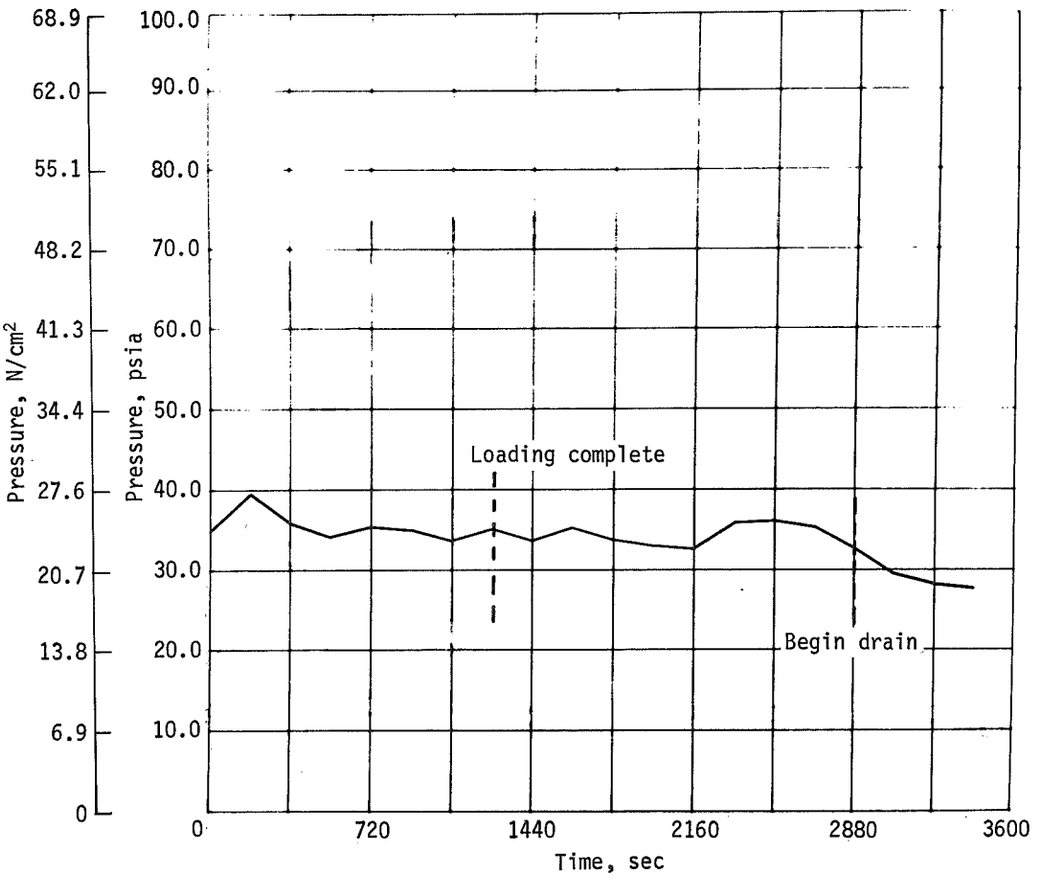

Figure 26.- Test Number I - Ambient Loading Tests, Methane Prepressurization: Pressure at Top of Standpipe Tank

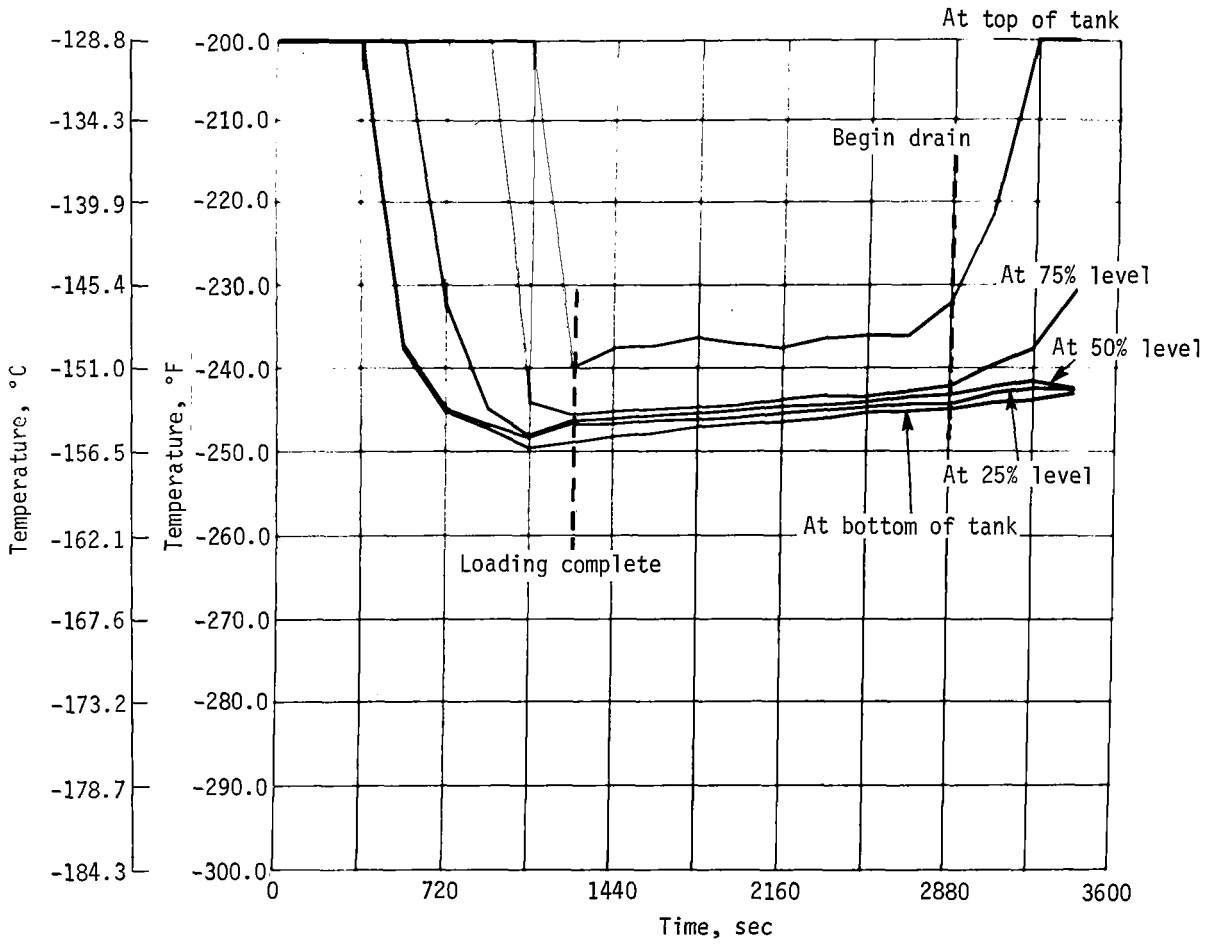

Figure 27.- Test Number I - Ambient Loading Tests, Methane Prepressurization: Temperature of Liquid in Standpipe Tank

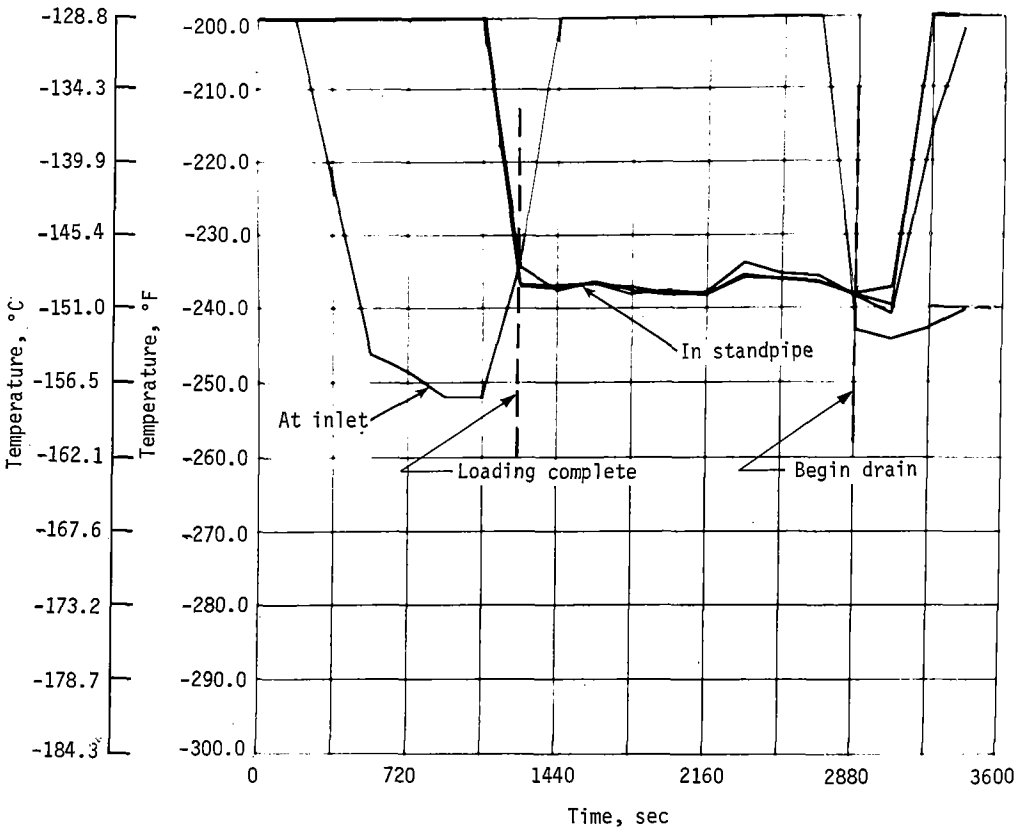

Figure 28.- Test Number I - Ambient Loading Tests, Methane Prepressurization: Temperature of Liquid in Standpipe and at Inlet of Standpipe Tank

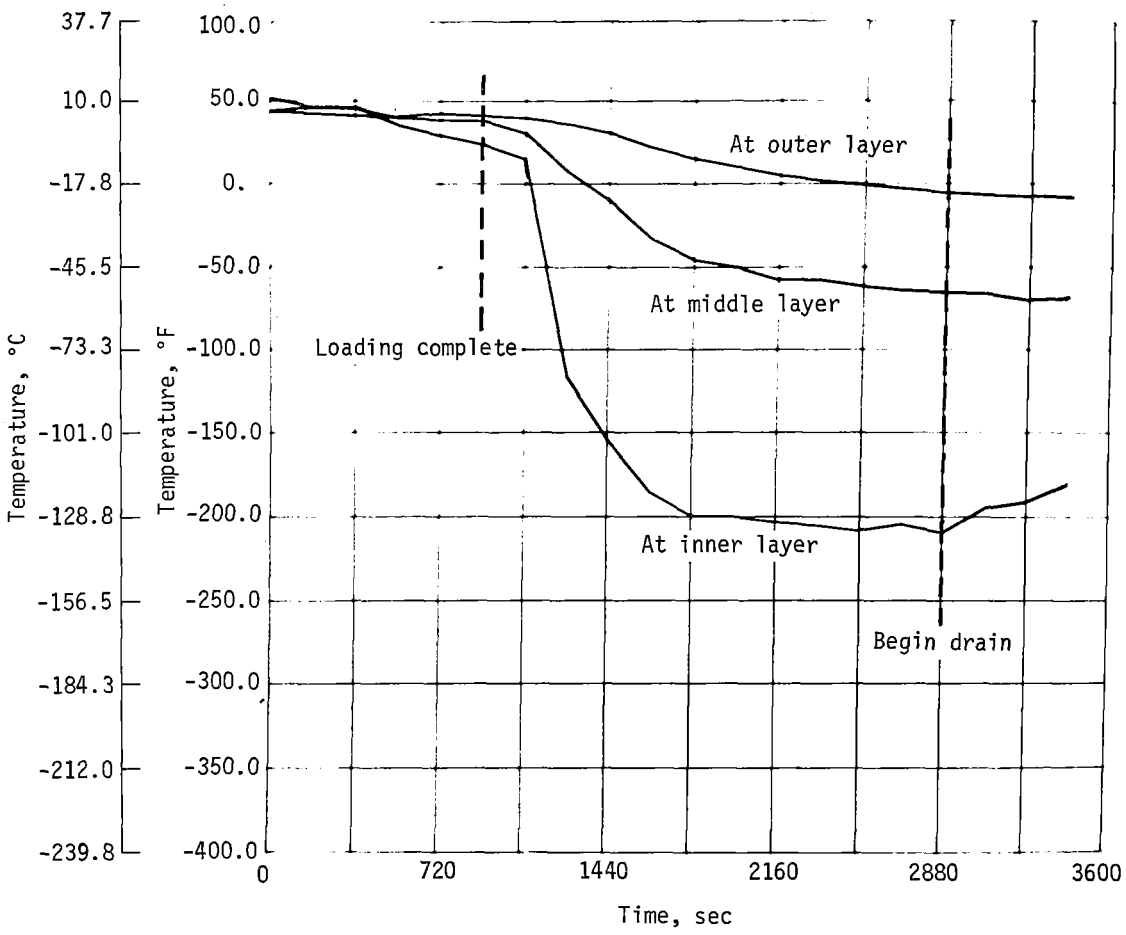

Figure 29.- Test Number I - Ambient Loading Tests, Methane Prepressurization: Temperature of Insulation at Top of Standpipe Tank

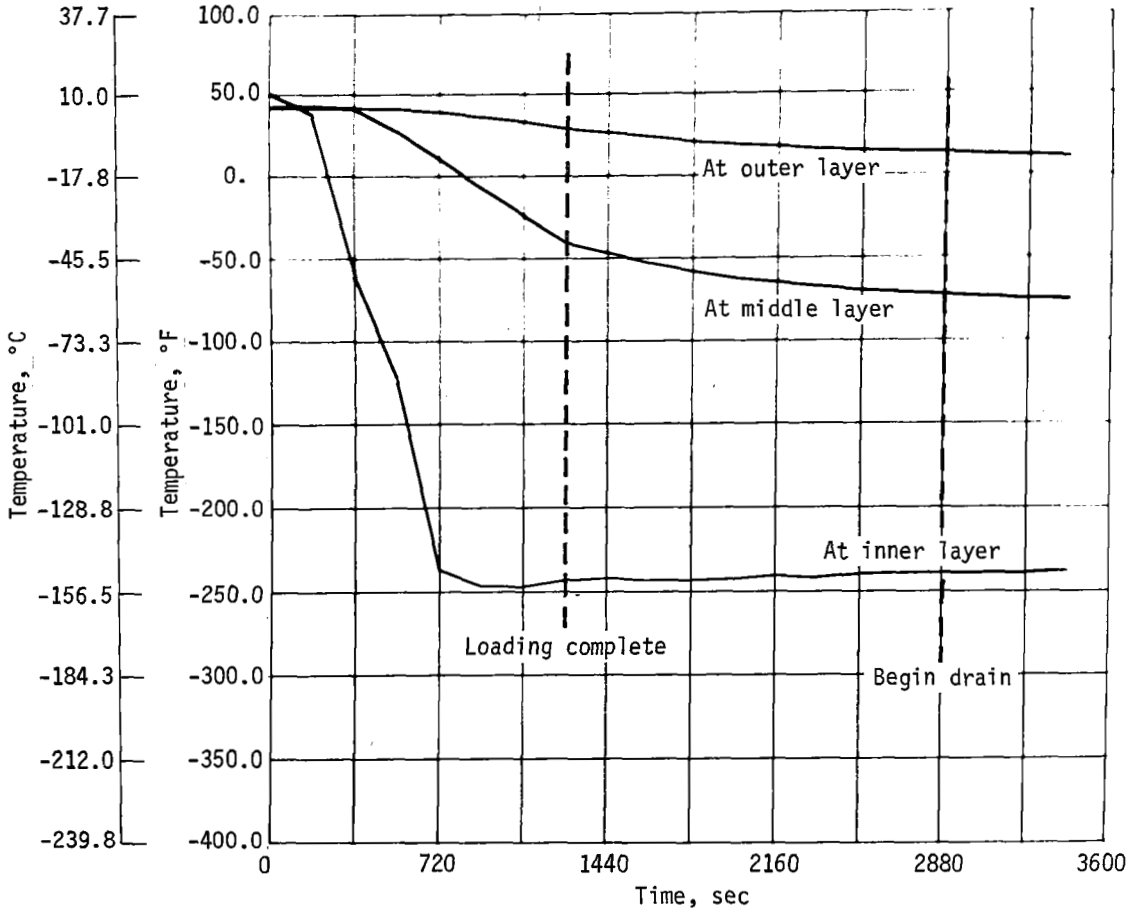

Figure 30.- Test Number I - Ambient Loading Tests, Methane Prepressurization: Temperature of Insulation on Side of Standpipe Tank

Figure 31 shows the pressurization rate to the standpipe tank. As can be seen, no pressurant gas was required at any time. Figure 32 shows the vent gas flowrate of the standpipe tank.

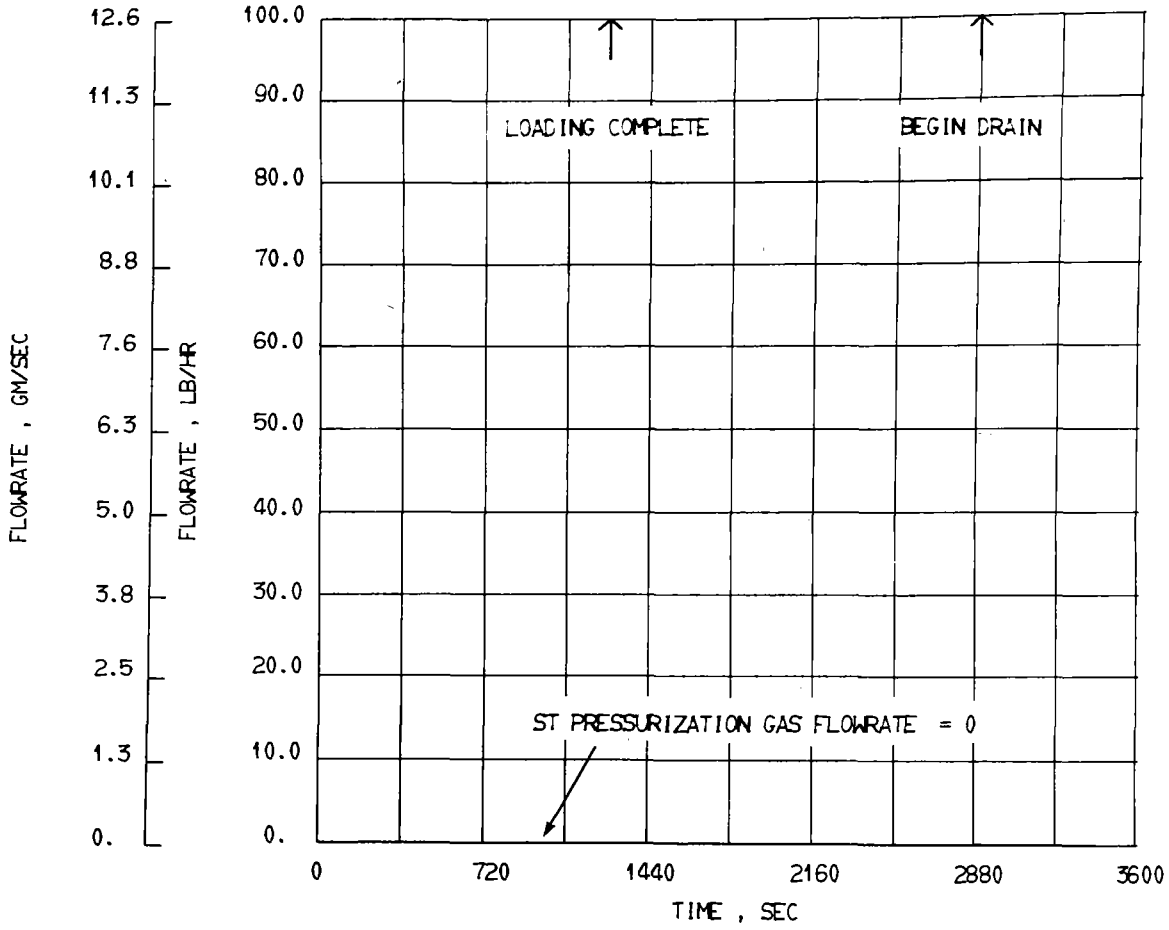

Figure 31.- Test Number I - Ambient Loading Tests, Methane Prepressurization: Flowrate of Standpipe Tank Pressurization Gas

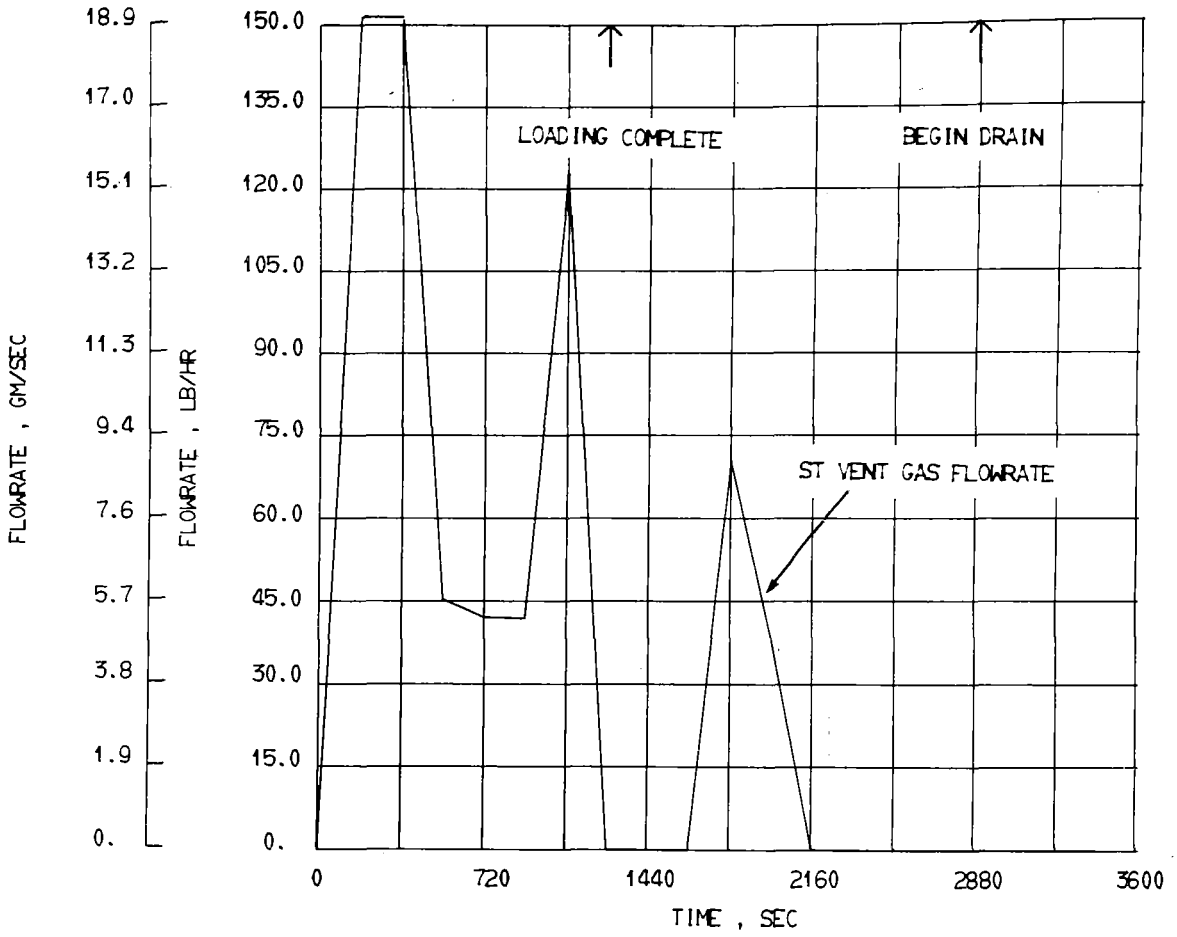

Figure 32.- Test Number I - Ambient Loading Tests, Methane Prepressurization: Flowrate of Standpipe Tank Vent Gas

b. Test 2.- Test 2 was conducted in much the same manner as Test 1. However, before loading, helium at 3 psi (2.07 N/cm^2) was added to the tank that initially contained methane at 12 psia (8.27 N/cm^2). Afterward, the test tank was pressurized to 36 psia (24.8 N/cm^2) with methane.

The loading technique used during Test 1 was repeated, and we attempted to hold the tank pressure as near 36 psia (24.8 N/cm^2) as possible. As in the first test, the pressure in the test tank tended to rise to that in the supply dewar until liquid began to collect in the test tank, so we had to vent the gas in the test tank to maintain the transfer pressure differential. The standpipe pressure is shown in figure 33.

As in Test 1, zero ullage loading was not attained because the temperature at the top of the inner layer of insulation only reached -115°F (-81.7°C).

During filling, the temperature at the tank inlet reached -250°F (-156.7°C). After filling, the temperature of the liquid at the bottom of the main tank reached -249°F (-156.1°C), but that at the 50% level was -247°F (-155.0°C), as shown by figure 34. After loading, the temperature stratification of the liquid in the tank was about 10F° (5.6C°).

As in test 1, the tank was vented during the entire fill process and there was no need for pressurization gas (figs. 35 and 36).

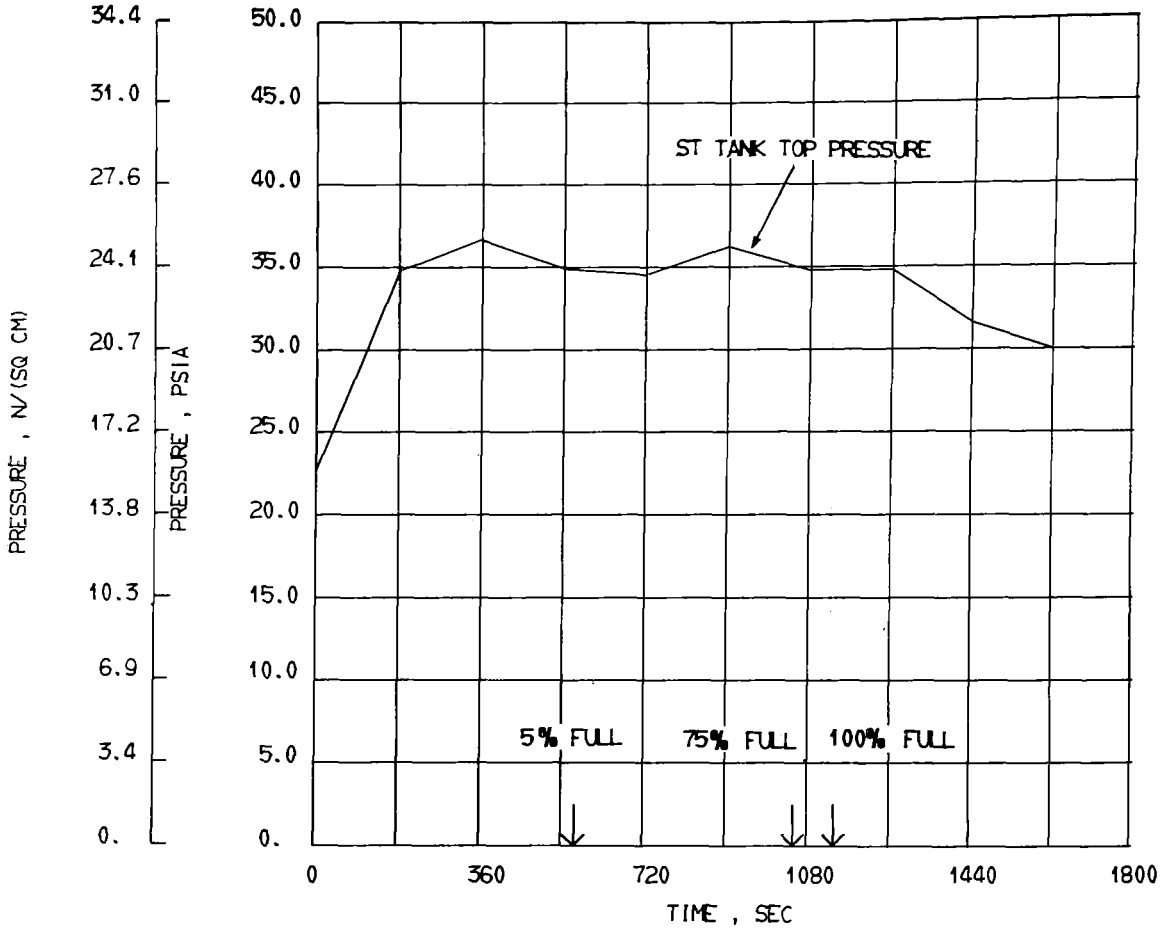

Figure 33.- Test Number 2 - Ambient Loading Tests, 3-psi (2.07 N/cm2) Helium Prepressurization: Pressure at Top of the Standpipe Tank

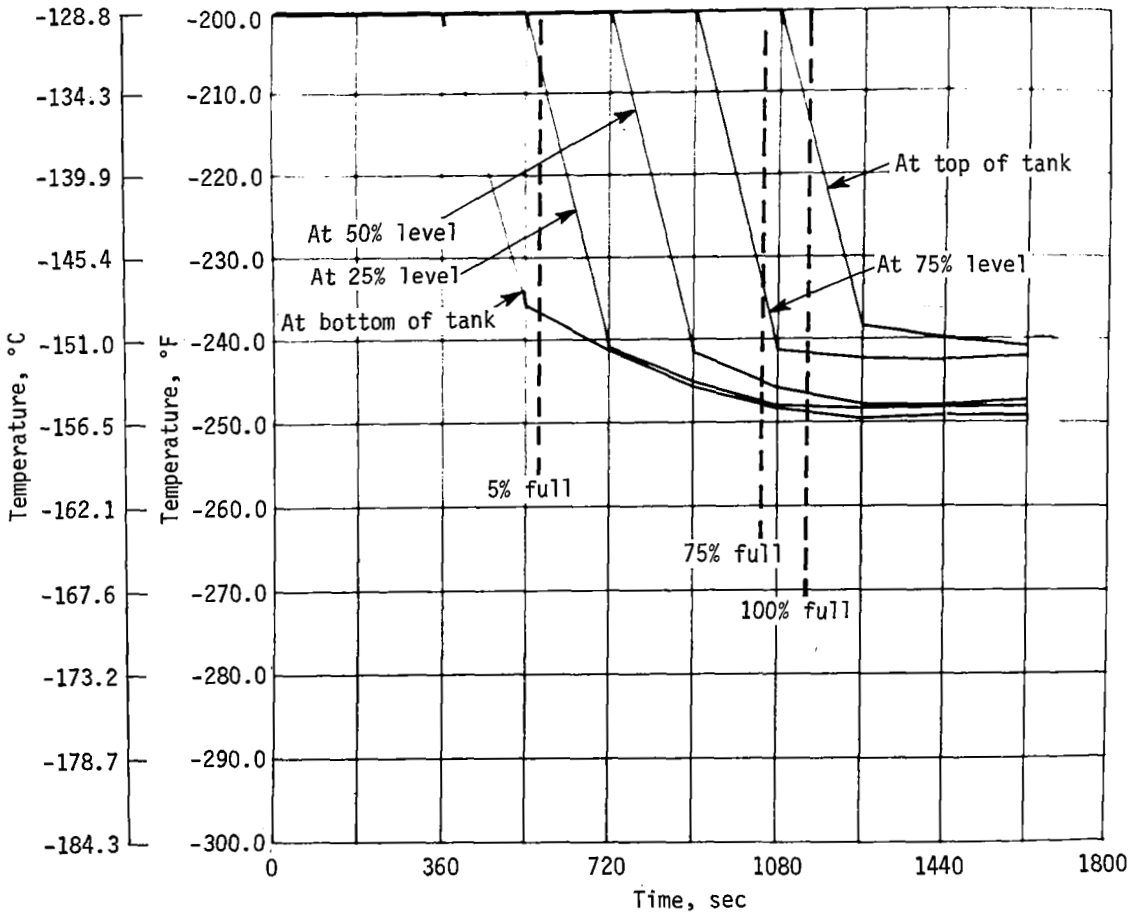

Figure 34.- Test Number 2 - Ambient Loading Tests, 3-psi (2.07 N/cm2) Helium Prepressurization: Temperature of Liquid in Standpipe Tank

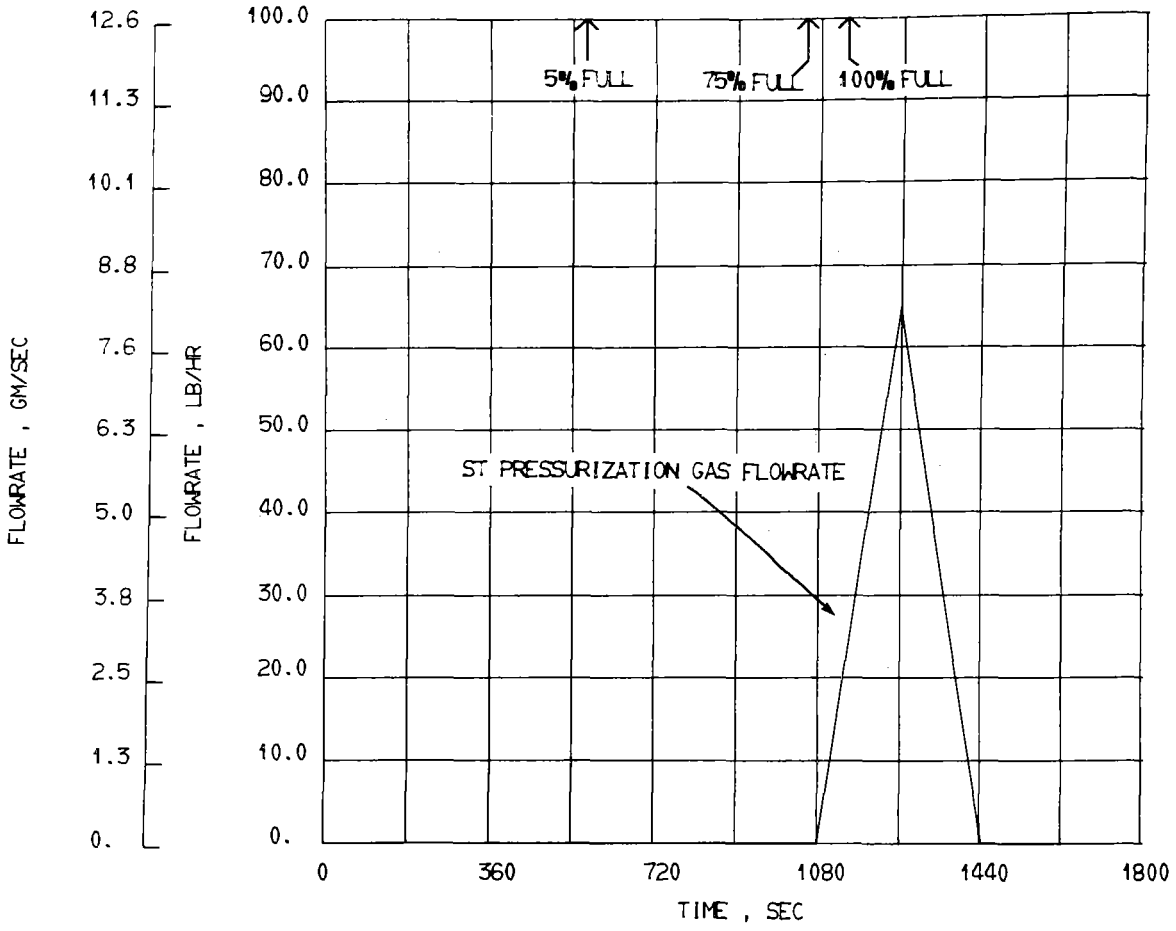

Figure 35.- Test Number 2 - Ambient Loading Tests, 3-psi (2.07 N/cm2) Helium Prepressurization: Flowrate of Standpipe Tank Pressurization Gas

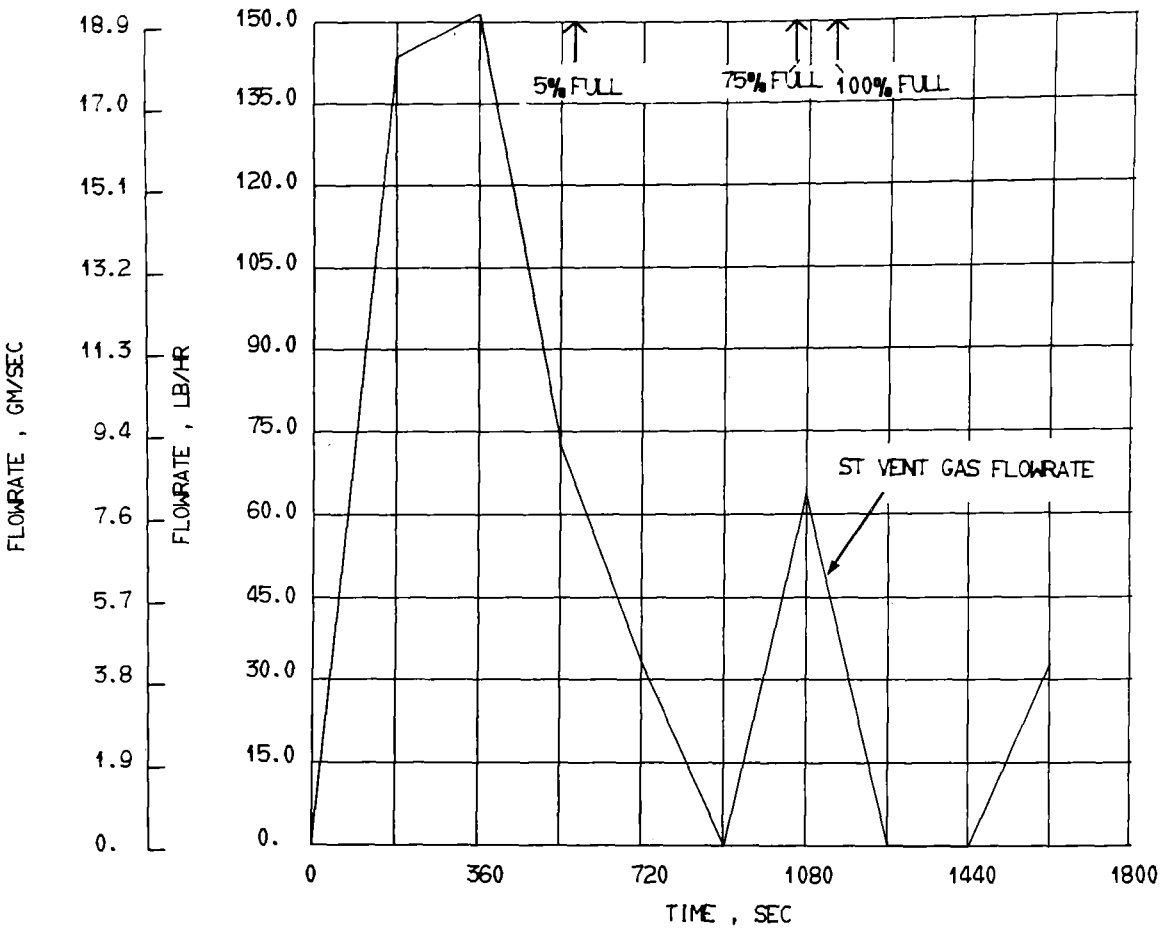

Figure 36.- Test Number 2 - Ambient Loading Tests, 3-psi (2.07 N/cm^2) Helium Prepressurization: Flowrate of Standpipe Tank Vent Gas

c. Test 3.- This test was similar to the first two ambient loading tests. except that a helium partial pressure of 10 psi (6.89 N/cm^2) was added to the methane preload to provide a total pressure of 36 psia (24.8 N/cm^2).

The data acquisition system was shut down early during the test, and we were unable to determine the temperature at which the liquid and gas stabilized after loading. However, the pressurization system behavior was the same as in tests 1 and 2.

d. Test 4.- This test was the first in a series of three tests involving the filling of a precooled tank. The standpipe tank had just been emptied before beginning these tests. After the guard tanks on each side of the test tank were filled, the test tank was pressurized to 36 psia (24.8 N/cm^2) before being loaded. Tank pressure is shown in figure 37.

Figures 38 and 39 show the temperatures in the main tank and in the standpipe during and after loading. As shown in figure 39, the liquid entering the tank dropped to -255°F (-159.4°C) during loading, but that in the standpipe reached -239°F (-150.6°C) after loading. The temperature stratification of the liquid in the main tank was 15F° (8.3C°) after loading, and varied from -254°F (-158.9°C) at the bottom to -239°F (150.6°C) at the top.

Using the temperature at the 50% level in the main tank as representative of the temperature of the bulk liquid (-253°F) (-158.3°C), the amount of subcooling between the main tank and the standpipe was 14F° (7.8°C) after loading.

The pressurization and vent flow rates are shown in figures 40 and 41. There was no pressurization requirement throughout the loading procedure, as indicated by figure 40.

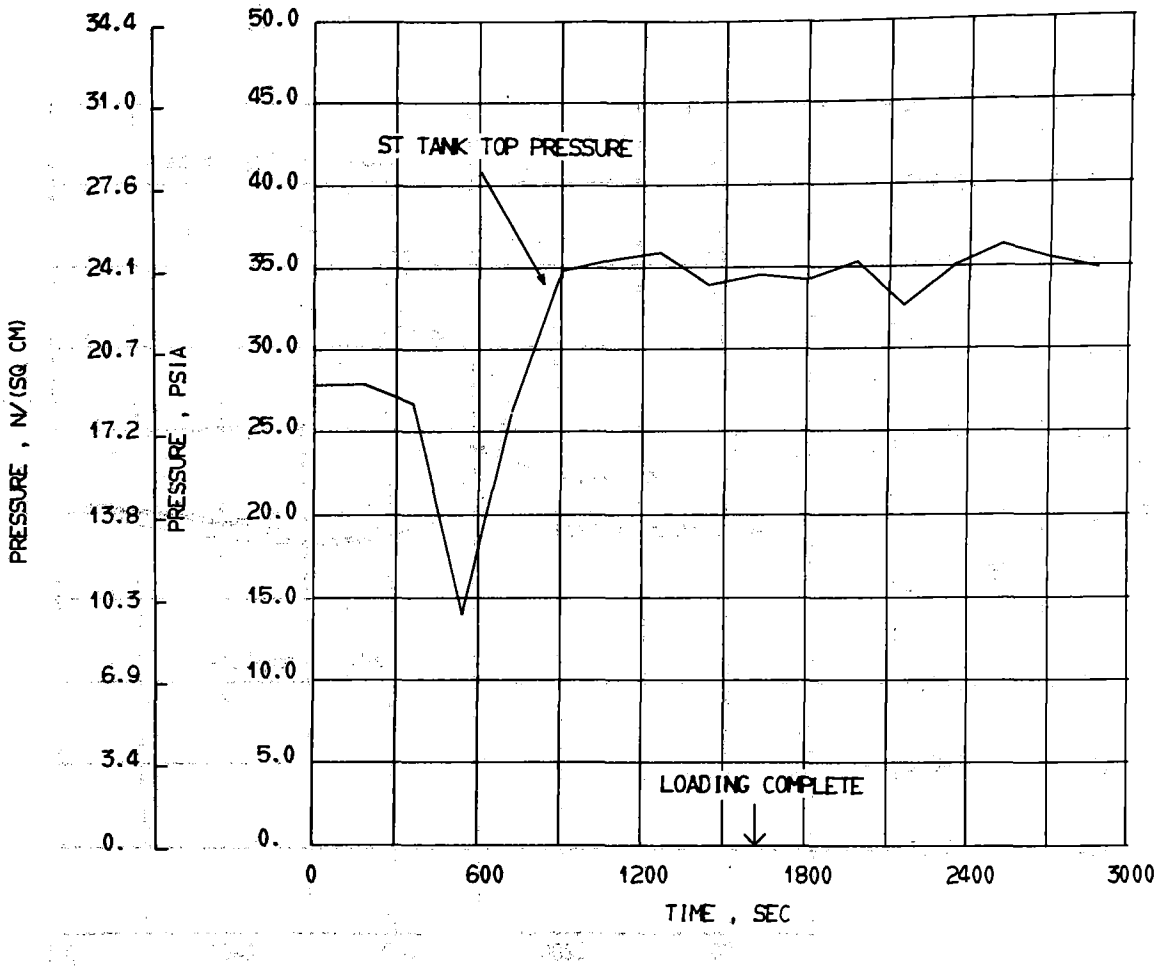

Figure 37.- Test Number 4 - Cold Loading Tests, Methane Prepressurization: Pressure at Top of the Standpipe Tank

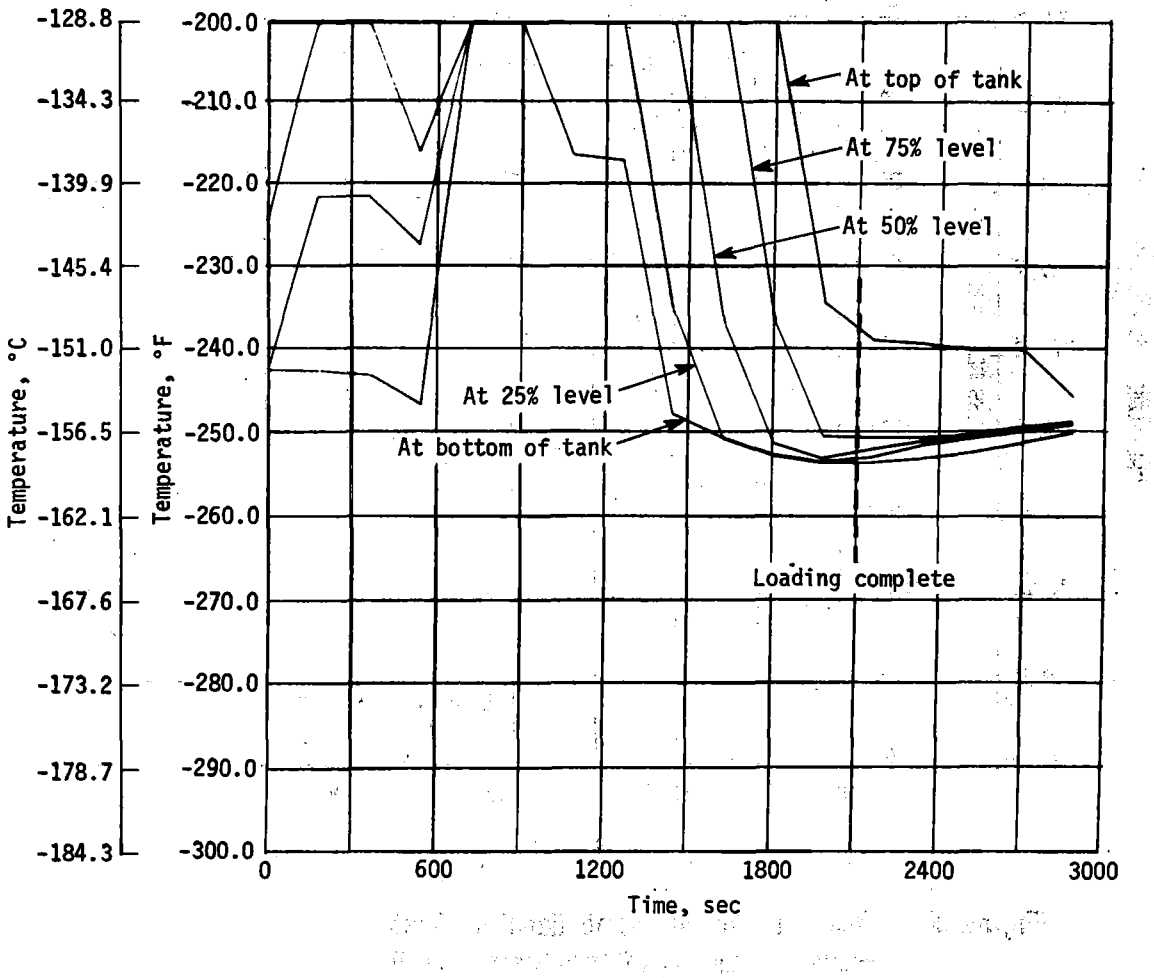

Figure 38.- Test Number 4 - Cold Loading Tests, Methane Prepressurization: Temperature of Liquid in Standpipe Tank

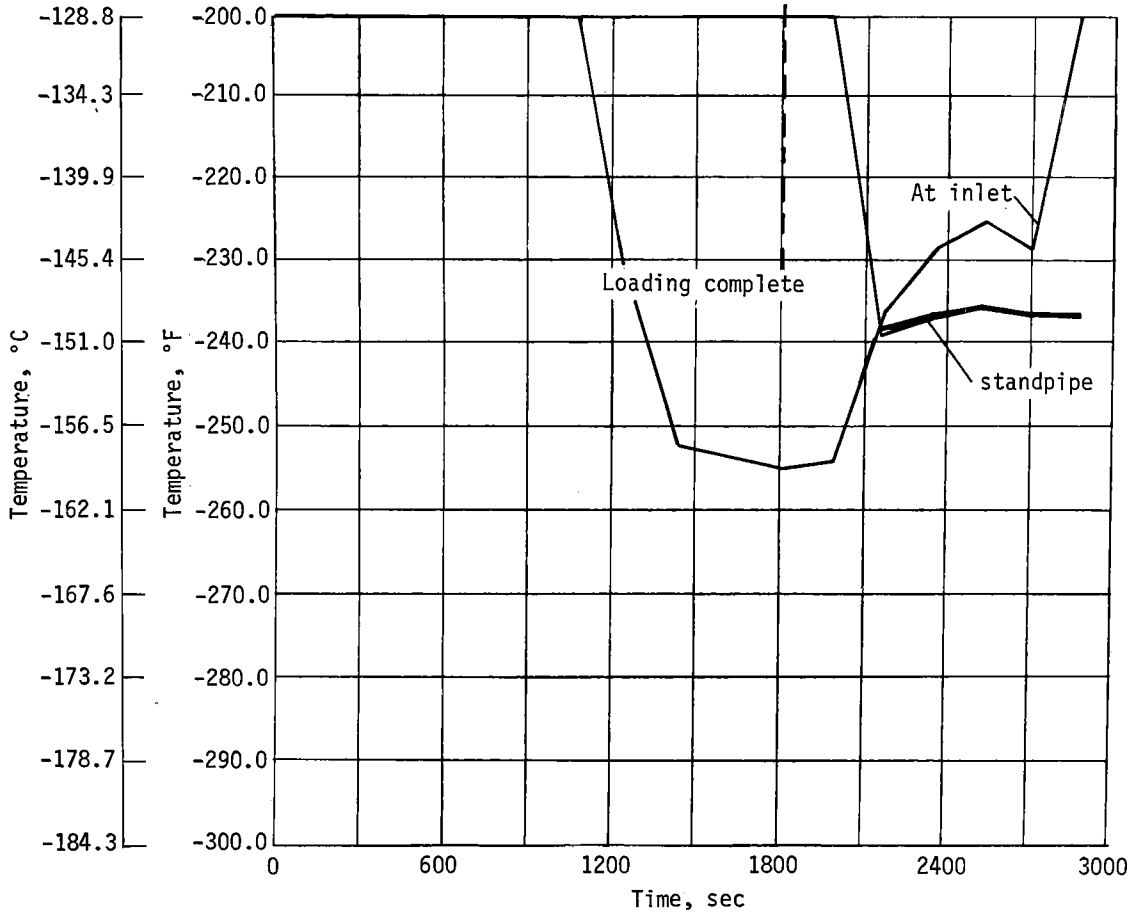

Figure 39.- Test Number 4 - Cold Loading Tests, Methane Prepressurization: Temperature of Liquid in Standpipe and at Inlet of Standpipe Tank

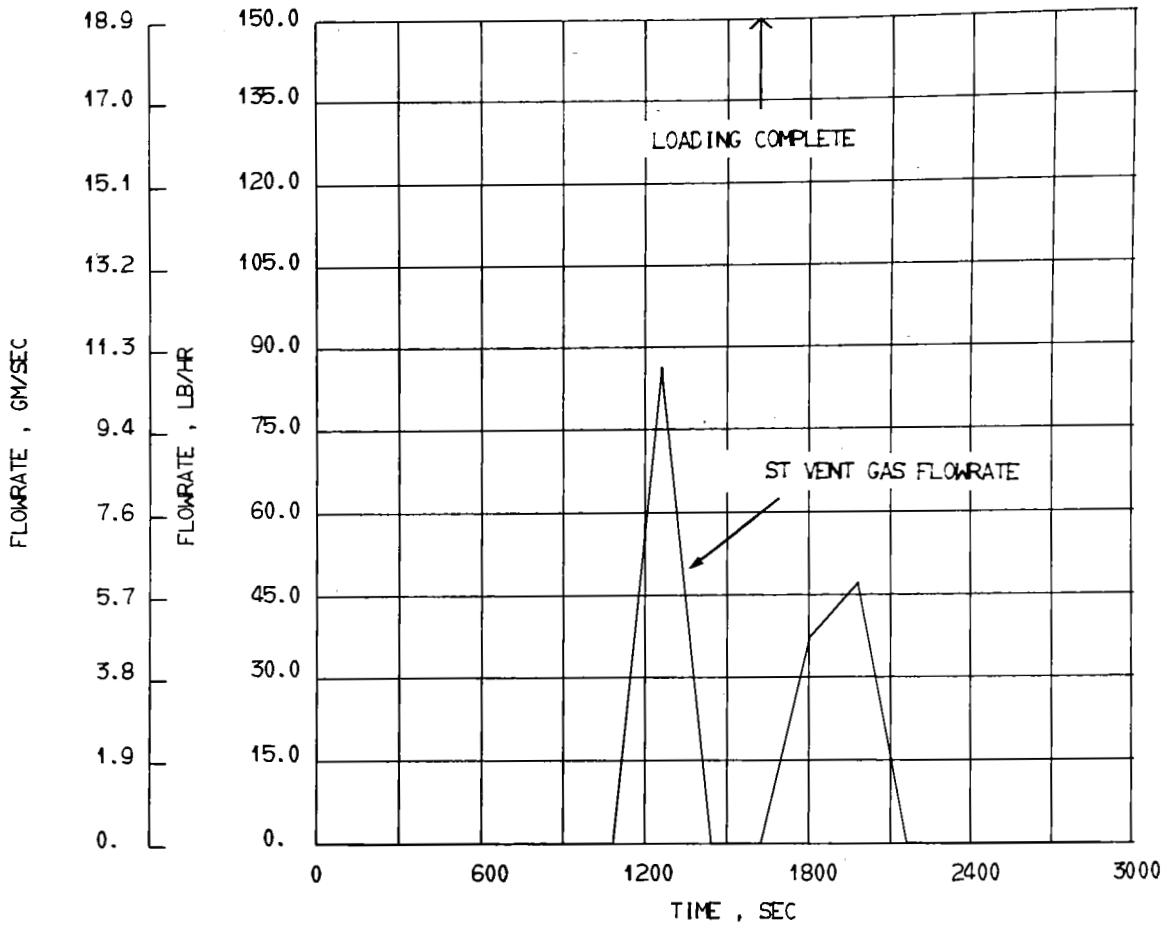

Figure 40.- Test Number 4 - Cold Loading Tests, Methane Prepressurization: Flowrate of Standpipe Tank Vent Gas

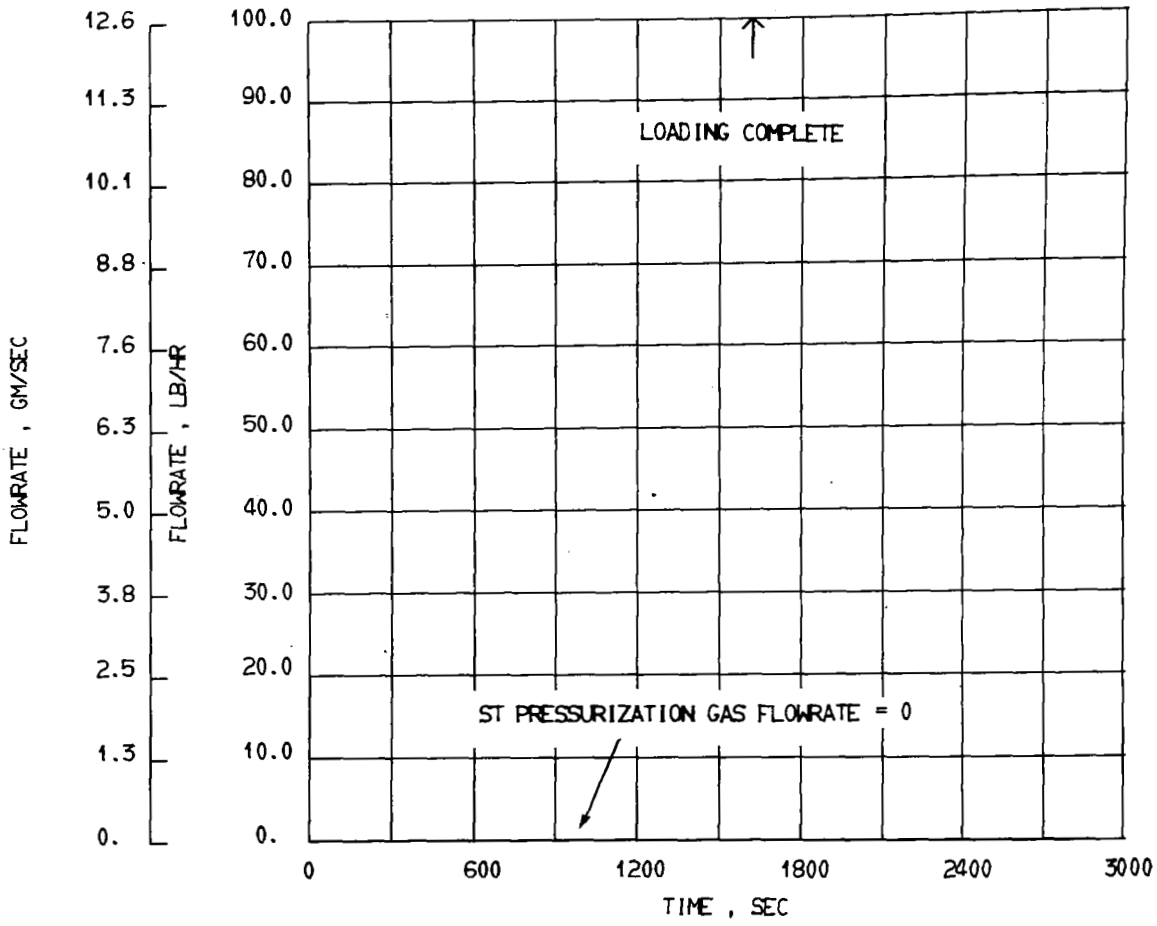

Figure 41.- Test Number 4 - Cold Loading Tests, Methane Prepressurization: Flowrate of Standpipe Tank Pressurization Gas

e. Test 5.- In this test, we had difficulty holding the pressure constant in the standpipe tank (fig. 42).

Figures 43 and 44 show the temperature of the liquid in the main tank and standpipe. During loading, the temperature at the tank inlet was -254°F (-158.9°C). After loading, the temperature at the bottom of the main tank was -253.5°F (-158.6°C). The temperature stratification in the main tank after loading was 10F° (5.6C°), but there was only a 4F° (2.2C°) spread from the bottom to the 75% level.

The temperature of the bulk liquid, based on the value recorded at the 50% level, was -253°F (-158.3°C). Immediately after loading, the liquid in the standpipe was at -246°F (-154.4°C), giving a main-tank subcooling of 7F° (3.9C°). This standpipe liquid temperature was saturated with respect to the tank pressure, and followed the tank pressure for the remainder of the test. The temperature stratification in the main tank decreased with time, and due to the low tank pressures, subcooling was lost 43 minutes into the test.

This was the first time a pressurant gas was required as shown in figure 45 and this was a very small amount. The pressure control problem appeared to be associated with the supply dewar rather than the test tank thermodynamics. Figure 46 shows the standpipe tank vent rate and figure 47 shows the high-pressure tank vent flowrate.

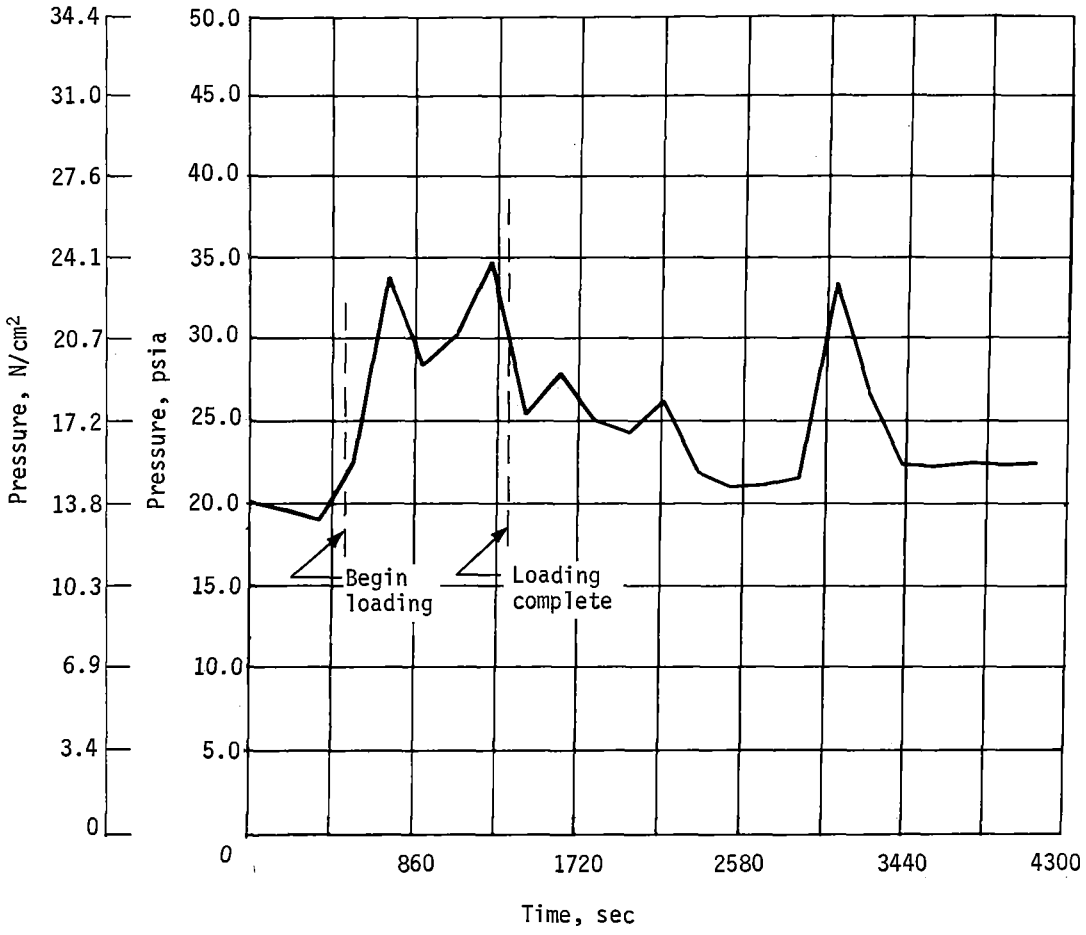

Figure 42. - Test Number 5 - Cold Loading Tests, Methane Prepressurization Pressure at Top of Standpipe Tank

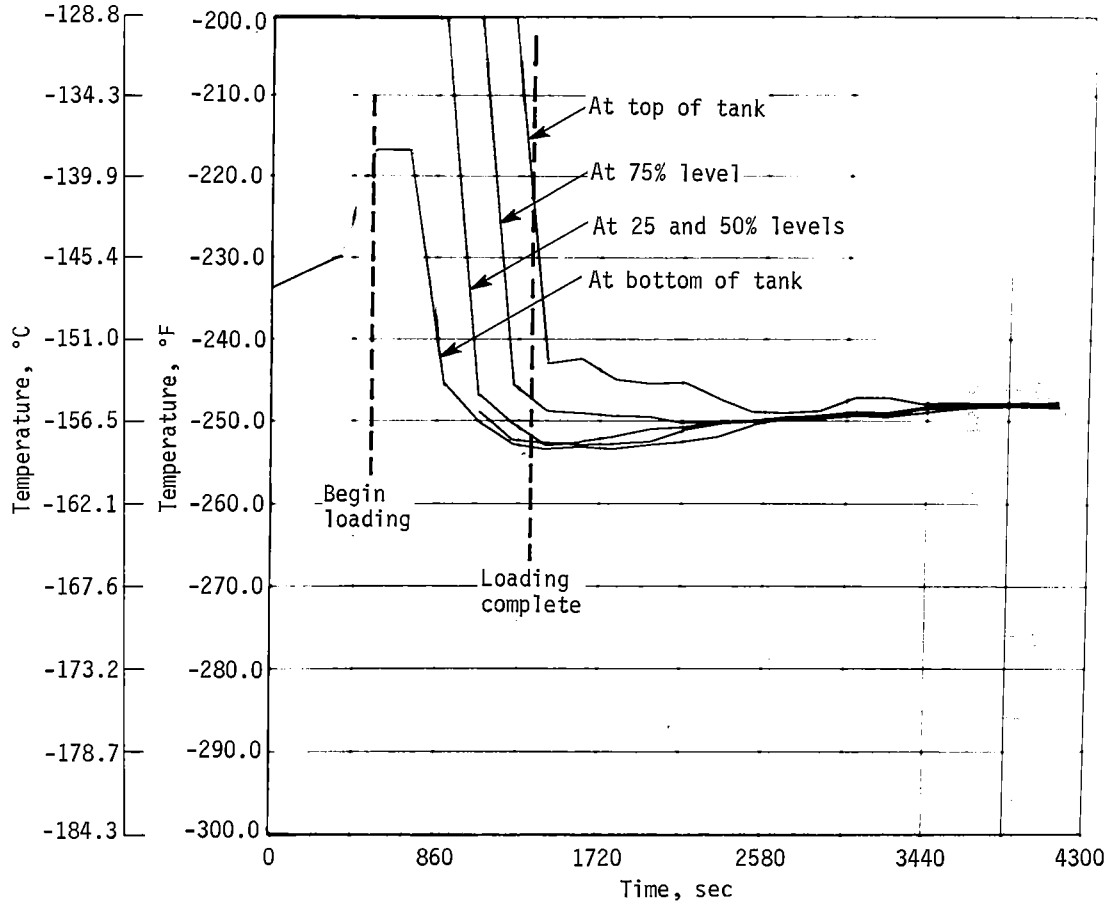

Figure 43.- Test Number 5 - Cold Loading Tests, Methane Prepressurization: Temperature of Liquid in Standpipe Tank

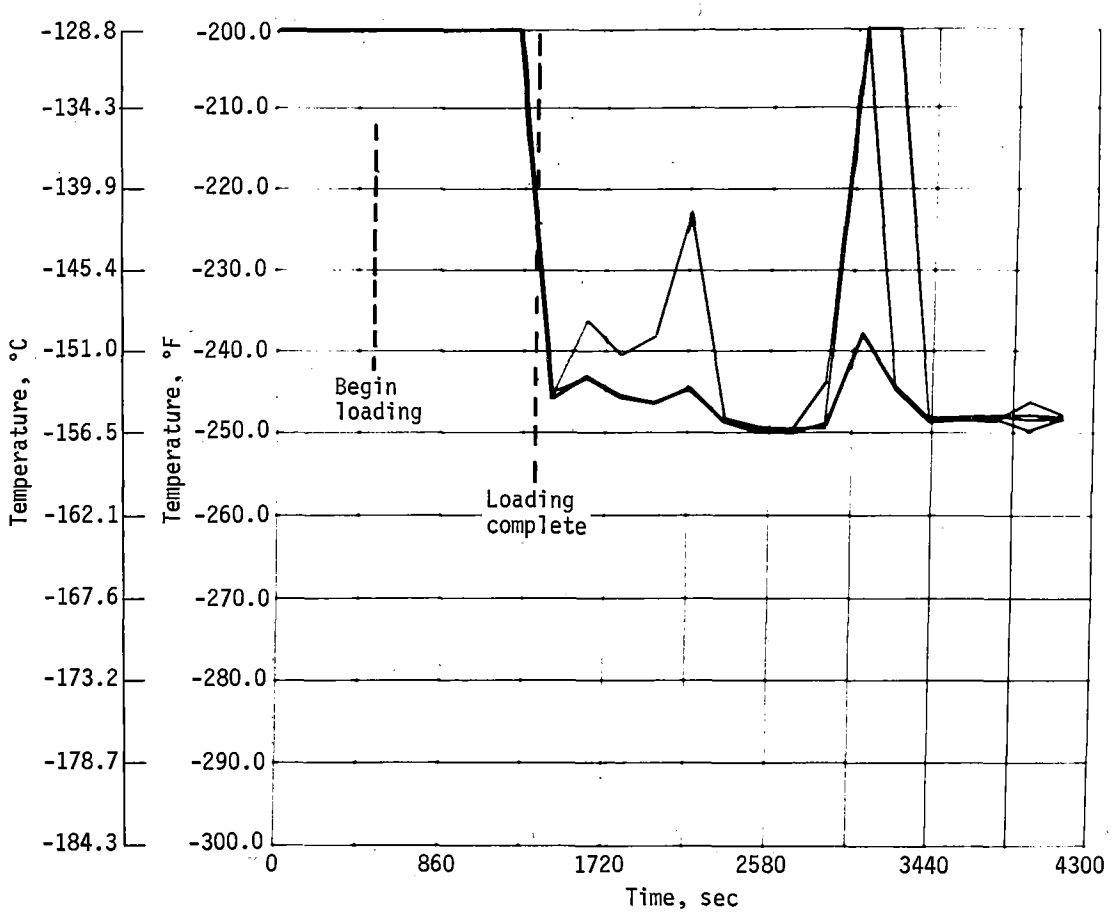

Figure 44.- Test Number 5 - Cold Loading Tests, Methane Prepressurization: Temperature of Liquid in Standpipe

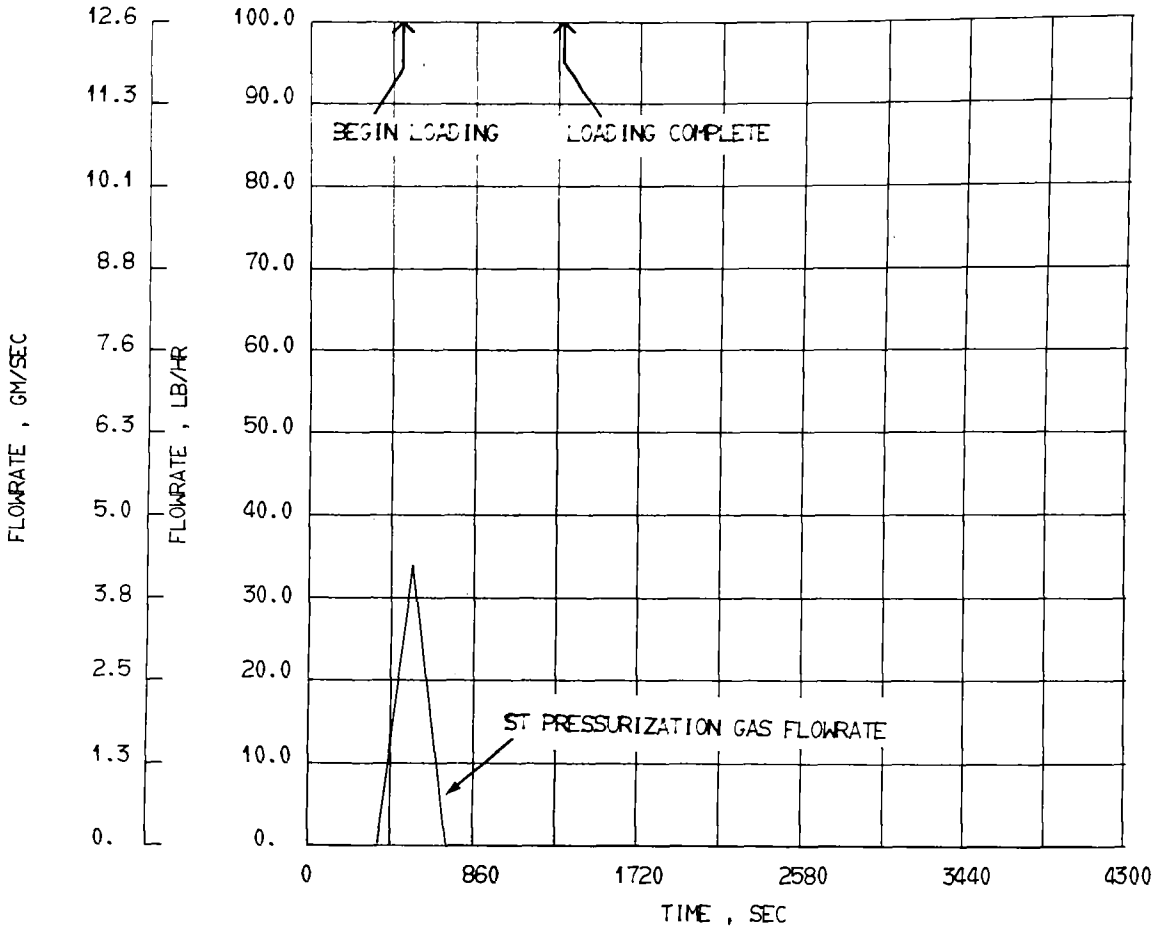

Figure 45.- Test Number 5 - Cold Loading Tests, Methane Prepressurization: Flowrate of Standpipe Tank Pressurization Gas

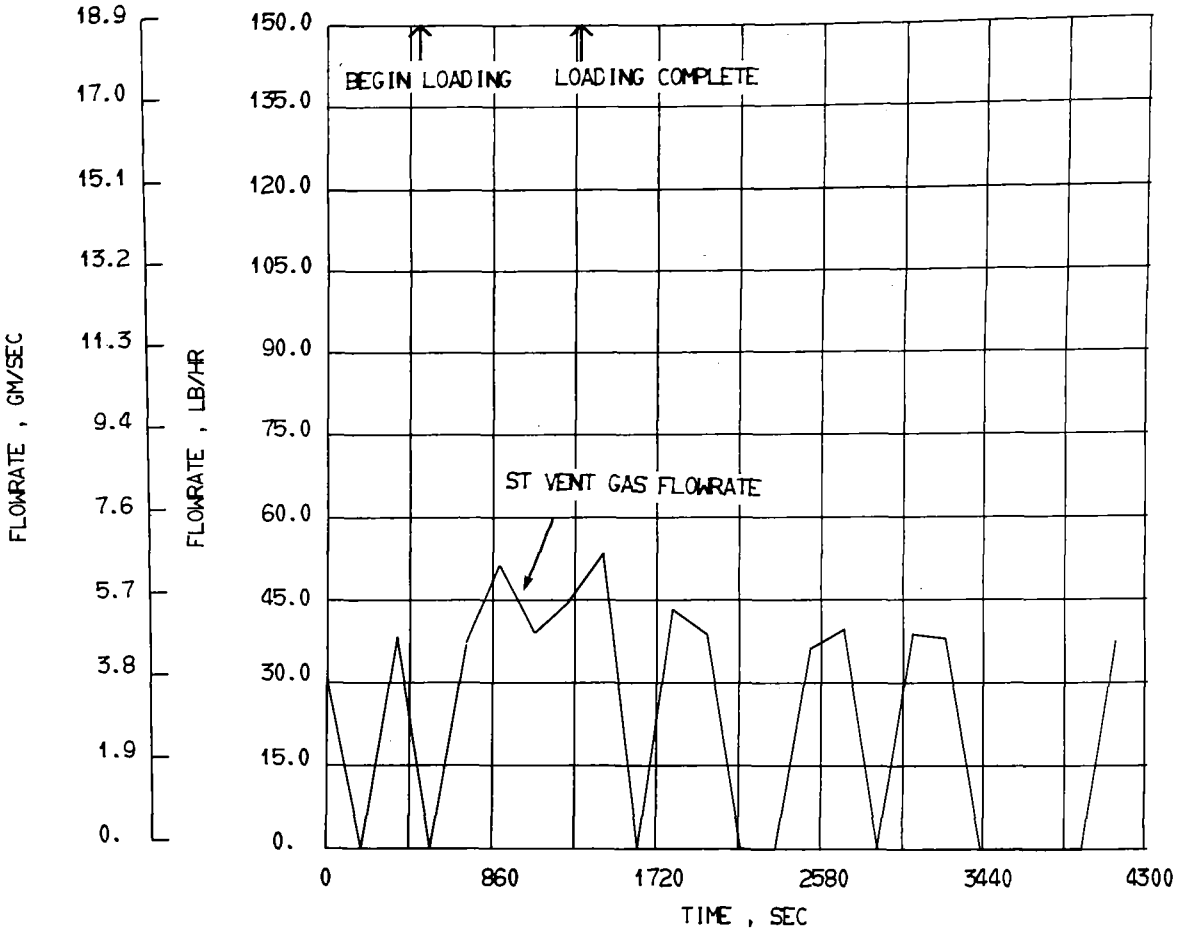

Figure 46.- Test Number 5 - Cold Loading Tests, Methane Prepressurization: Flowrate of Standpipe Tank Vent Gas

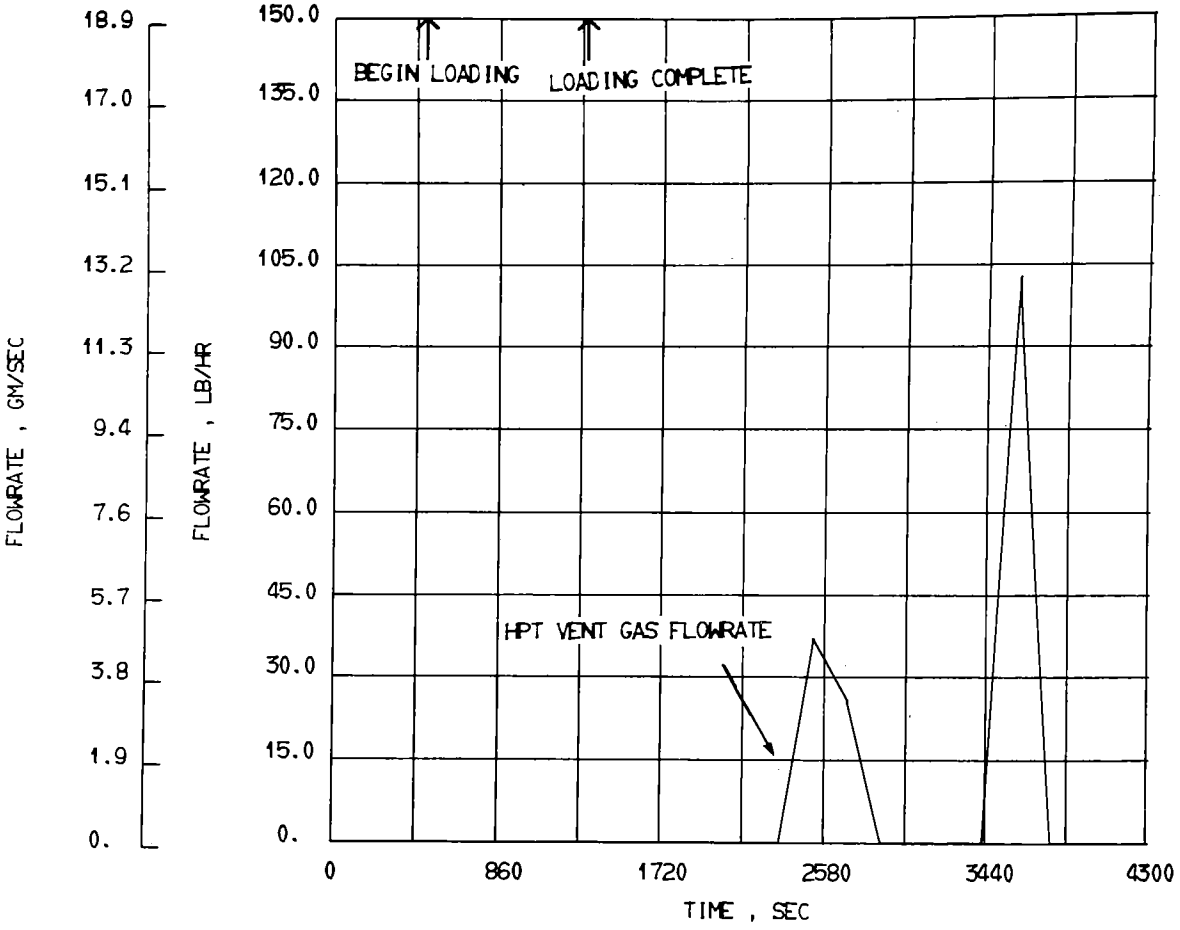

Figure 47.- Test Number 5 - Cold Loading Tests, Methane Prepressurization: Flowrate of High-Pressure Tank Vent Gas

f. Test 6.- The procedure for this test was the same as used in Tests 4 and 5. As shown in figure 48, the tank pressure remained near 36 psia (24.8 N/cm^2) throughout the loading.

Figures 49 and 50 show the temperatures of the liquid in the main tank and in the standpipe. The liquid entering the tank was at -249.5°F (-156.4°C), but that at the bottom of the main tank was at -249°F (-156.1°C). After loading, the temperature of the liquid varied 11F° (6.1C°), mainly in the region between the 75% and 100% levels; the spread from the bottom to the 75% level was only 2F° (1.1C°).

After loading, the average bulk temperature in the main tank was -248.5°F (-155.9°C) and the temperature of the liquid in the standpipe was -238°F (-150.0°C), which provided 10.5F° (5.8C°) of subcooling.

Figures 51 and 52 show the temperatures at two points on the insulation of the tank. The temperature differences shown in these two figures again indicate that the tank was not loaded to zero ullage even though the standpipe was filled. The temperature at the start of the test (fig. 52) shows the precooled condition of the standpipe tank.

The gas pressurant flowrates and standpipe tank vent flowrate are shown in figures 53 and 54, while the high-pressure tank vent flowrate is shown in figure 55. Once again, there was no pressurization requirement during loading.

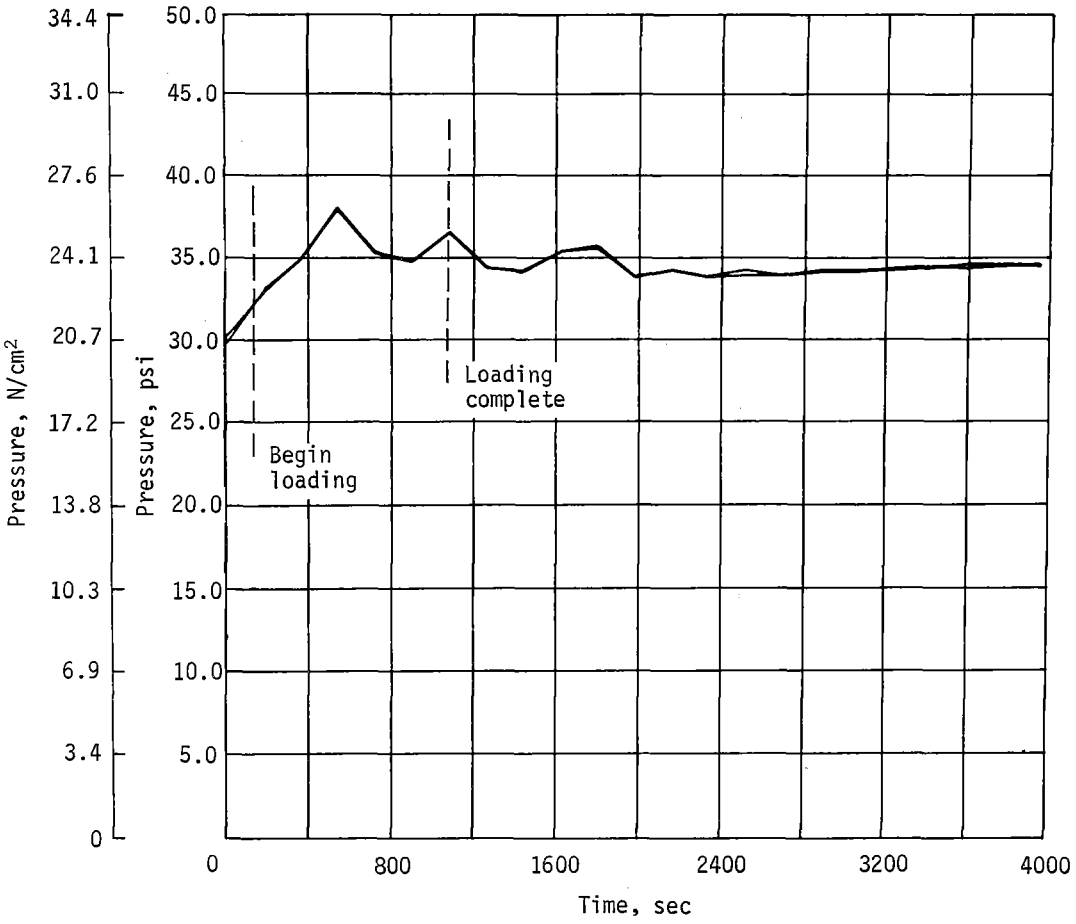

Figure 48. - Test Number 6 - Cold Loading Tests, Methane Prepressurization: Pressure at Top of Standpipe Tank

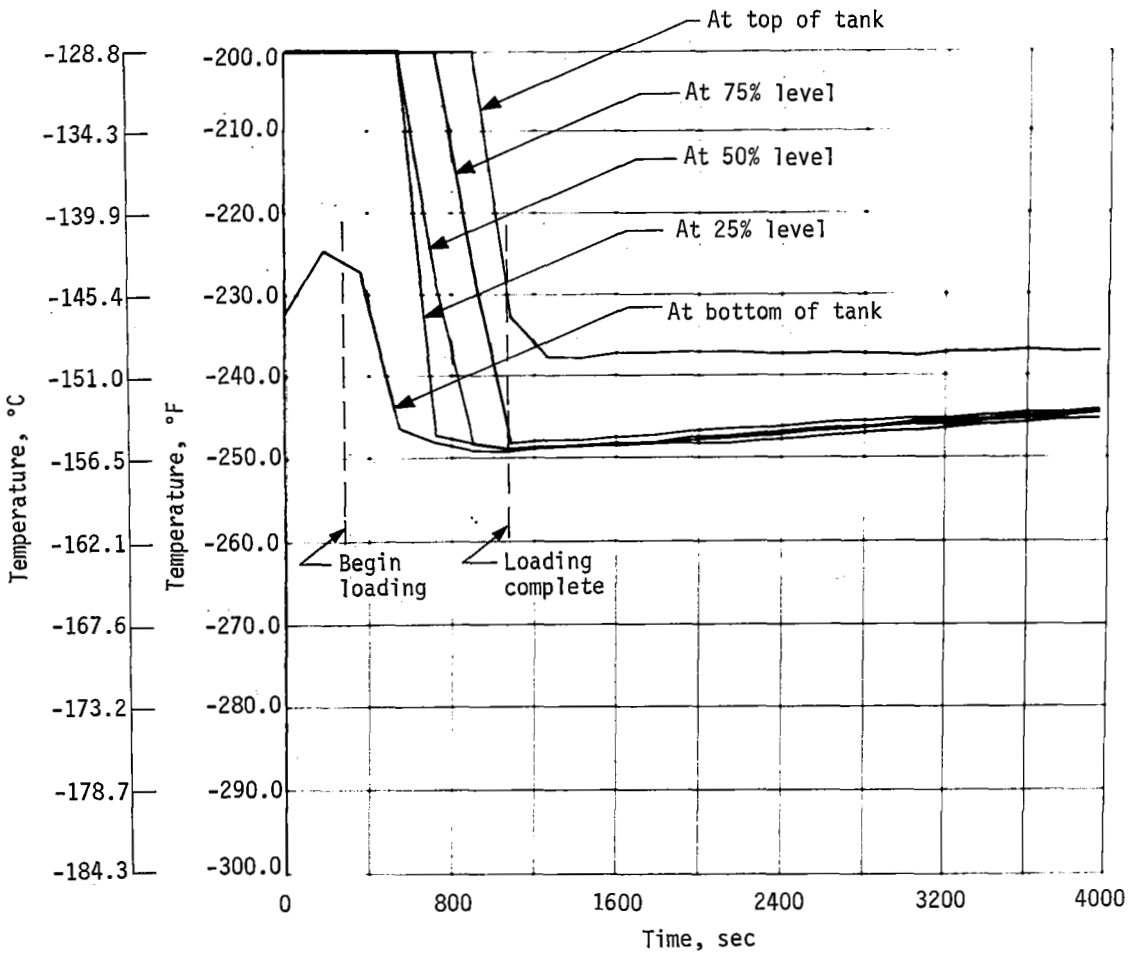

Figure 49.- Test Number 6 - Cold Loading Tests, Methane Prepressurization: Temperature of Liquid in Standpipe Tank

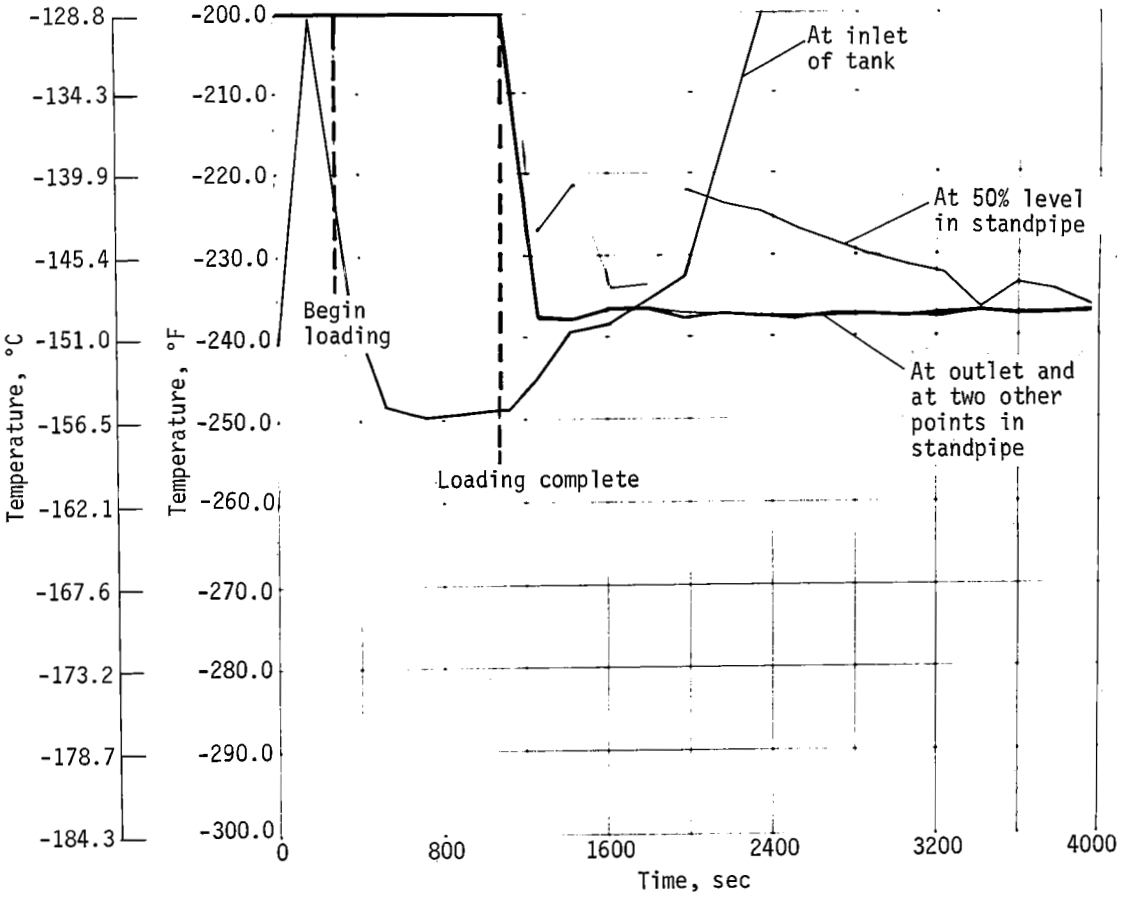

Figure 50.- Test Number 6 - Cold Loading Tests, Methane Prepressurization: Temperature of Liquid in Standpipe and at Inlet of Standpipe Tank

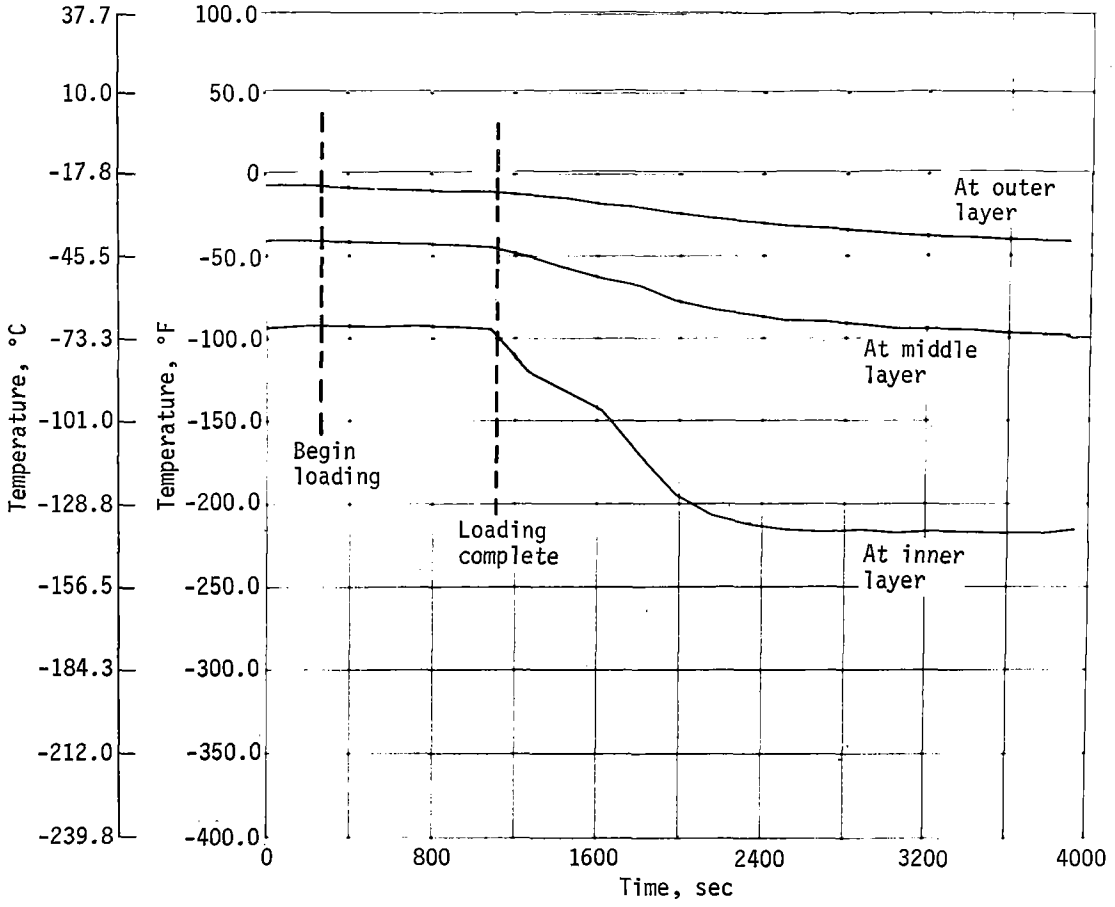

Figure 51.- Test Number 6 - Cold Loading Tests, Methane Prepressurization: Temperature of Insulation at Top of Standpipe Tank

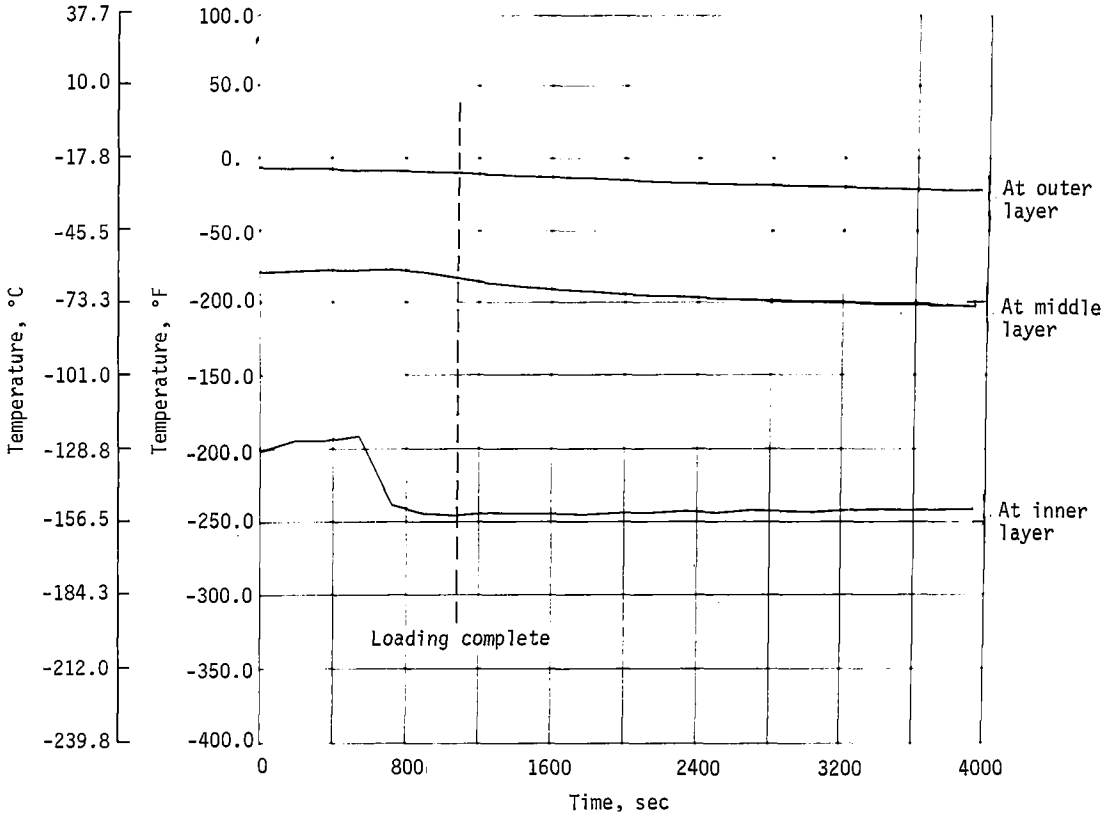

Figure 52.- Test Number 6 - Cold Loading Tests, Methane Prepressurization: Temperature of Insulation on Side of Standpipe Tank

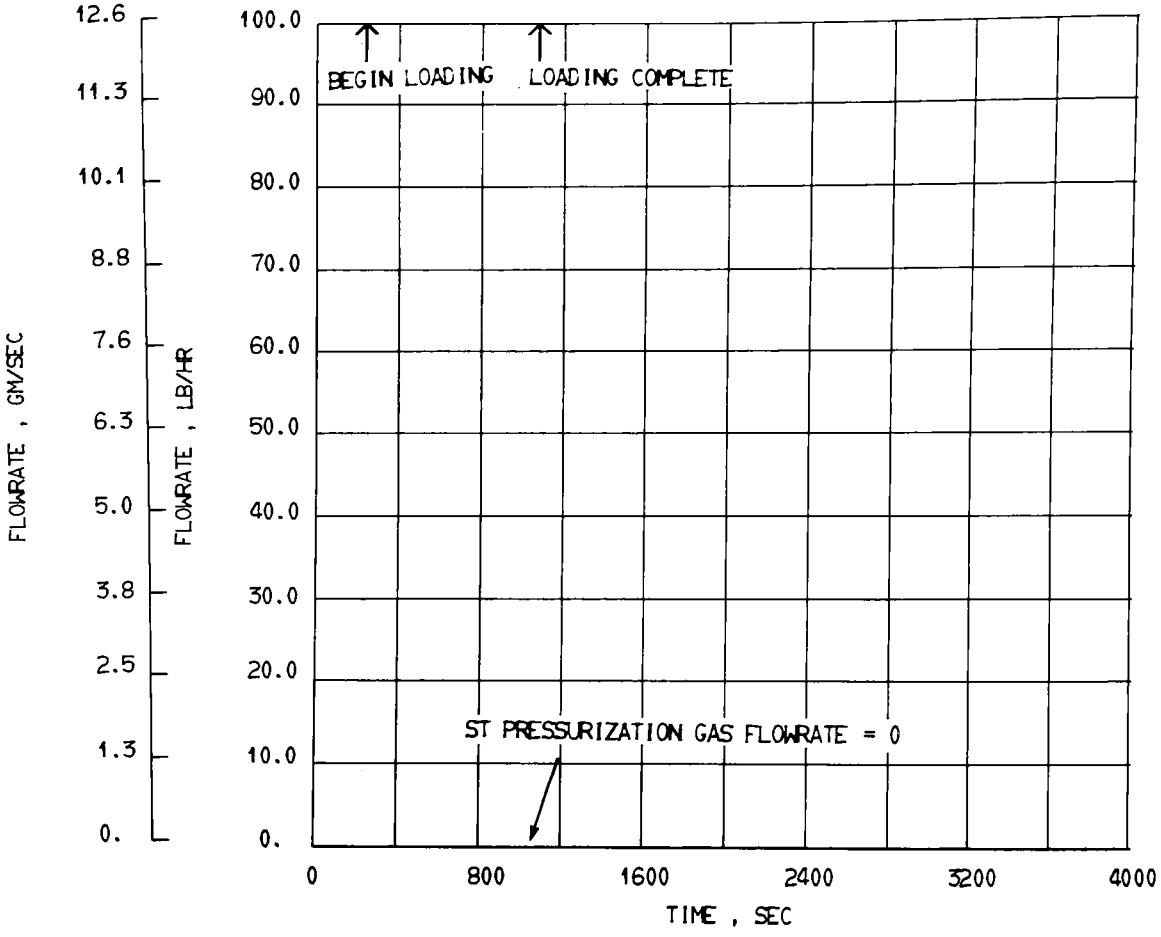

Figure 53.- Test Number 6 - Cold Loading Tests, Methane Prepressurization: Flowrate of Standpipe Tank Pressurization Gas

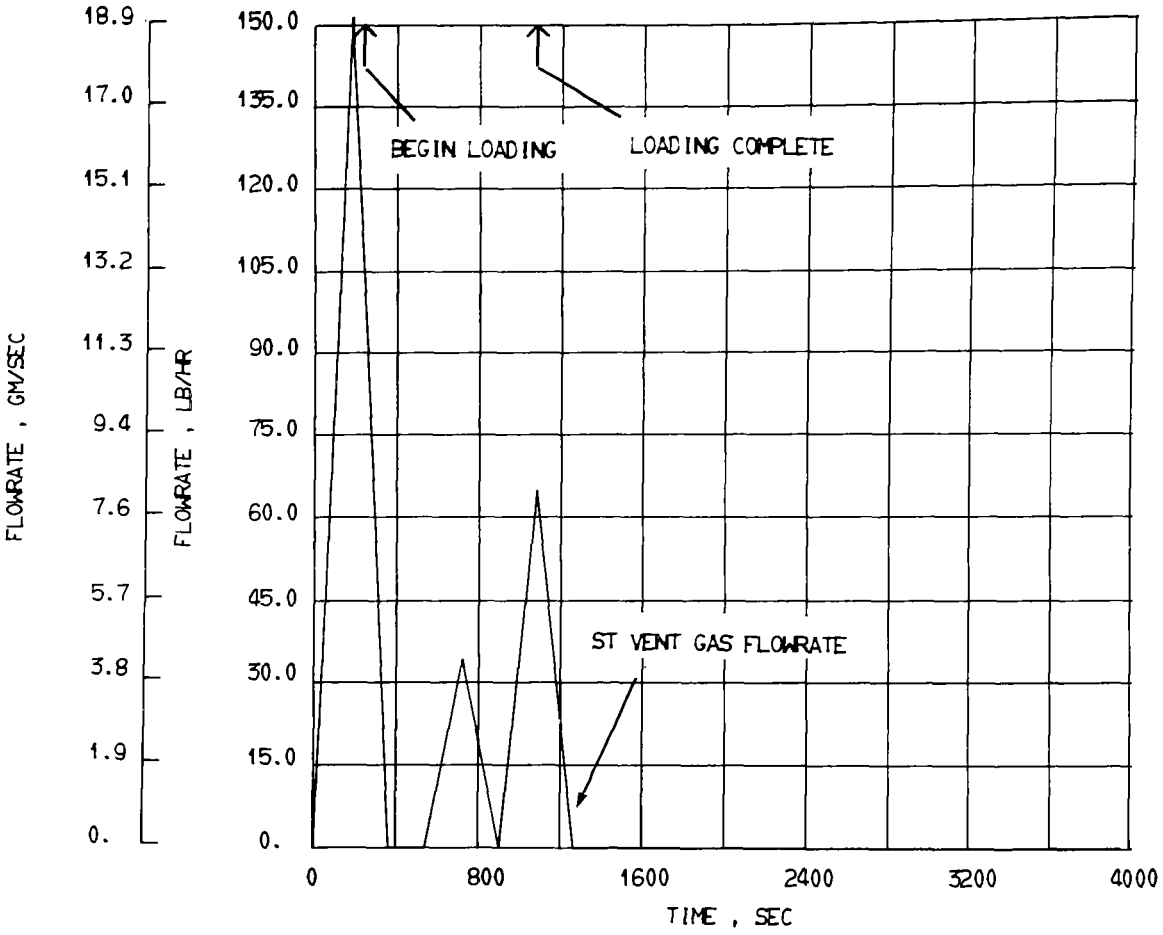

Figure 54. - Test Number 6 - Cold Loading Tests, Methane Prepressurization: Flowrate of Standpipe Tank Vent Gas

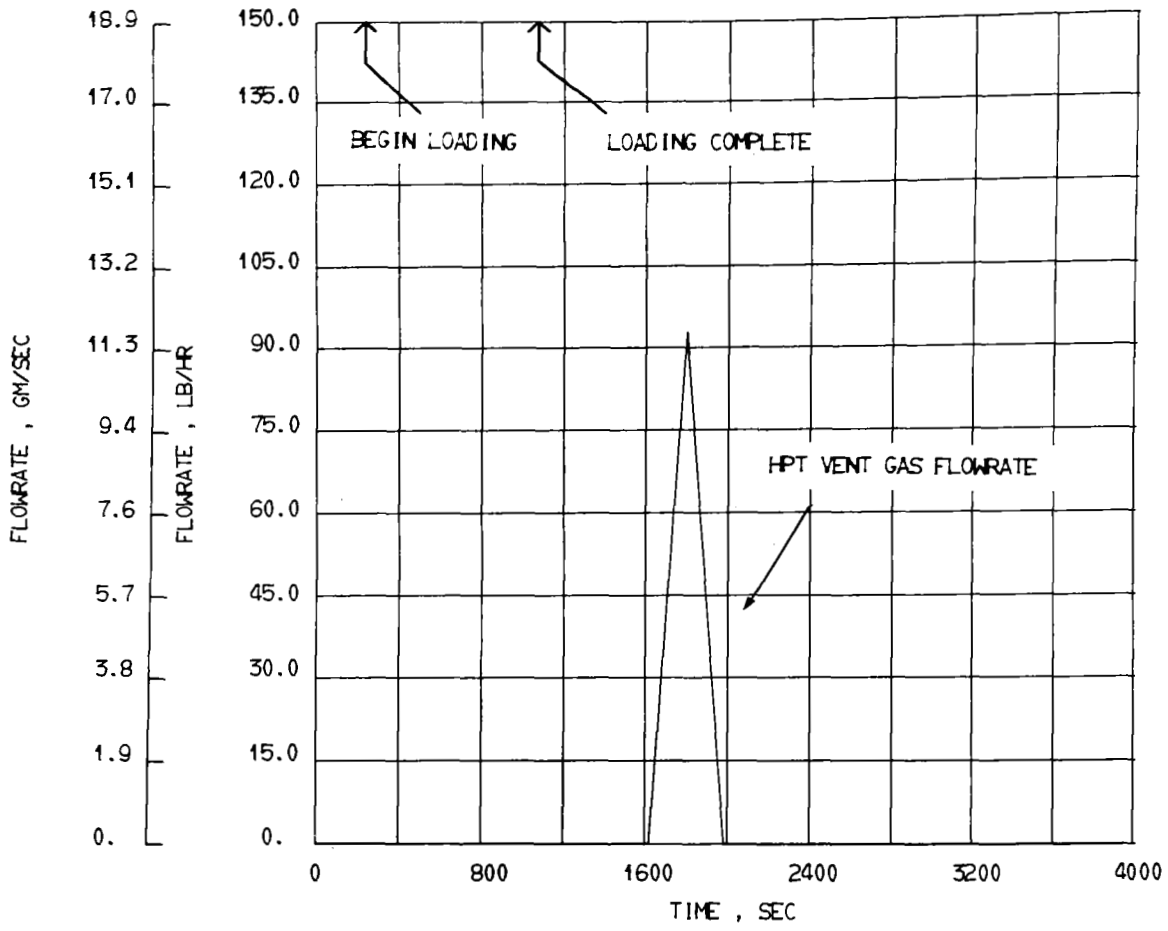

Figure 55.- Test Number 6 - Cold Loading Tests, Methane Prepressurization: Flowrate of High-Pressure Tank Vent Gas

g. Test 38.- During this test, the standpipe tank was pressurized to 36 psia (24.8 N/cm^2) with methane gas throughout the loading and hold period. Before starting the test, the source dewar was vented long enough for the liquid to reach equilibrium at ambient pressure. Then, just before starting the test, the source dewar was pressurized to 40 psia (27.6 N/cm^2).

The standpipe tank was filled and the pressure in the tank was held close to the desired level (figure 56) until equilibrium was established. The temperatures in the standpipe main tank are shown in figures 57 and 58, respectively. The liquid in the standpipe appears to be in equilibrium with the tank pressure at all times. The liquid entering the main tank was at -257°F (-160.6°C). After loading, the liquid at the tank bottom was at -256°F (-160.0°C). There was less than 2F° (1.1C°) of stratification from the bottom to the 50% level, and about 6F° (3.3C°) of stratification from the bottom to the 75% level. The liquid at the top of the tank was at -237°F (-149.4°C), which corresponds to equilibrium in terms of the pressure in the tank.

If the temperature of the liquid at the 50% level is representative of the temperature of the bulk liquid, there was 16F° (8.9C°) of subcooling immediately after loading. This subcooling was lost in approximately 1 1/2 hr (fig. 58).

Once again, the standpipe tank was not filled to zero ullage, as indicated by observing the inner insulation temperatures in figure 59. As in previous loading tests tank venting was nearly continuous and no pressurant gas was required (figures 60 and 61).

As shown in figure 57, most of the platinum probes appear to become covered at the same time (just before 1800 sec), rather than in sequence as they should. This anomaly was traced to the data acquisition system into which the temperatures were read.*

This problem was not discovered until the testing was finished, so there are data dropouts in each of the last 12 tests. There were backup thermocouples in the tank, so no critical data were lost. In some cases, the thermocouples could not give the desired accuracy, so the thermocouple data were superimposed on the platinum-probe plots in order to determine thermocouple corrections or biases.

---

* The platinum probes were scanned sequentially. The impedance of the first probe in the series did not exactly match that of the acquisition system. When the probes were scanned in order over a certain temperature range where an impedance mismatch occurred, the data for the first few probes were lost because of the recovery time of the acquisition system.

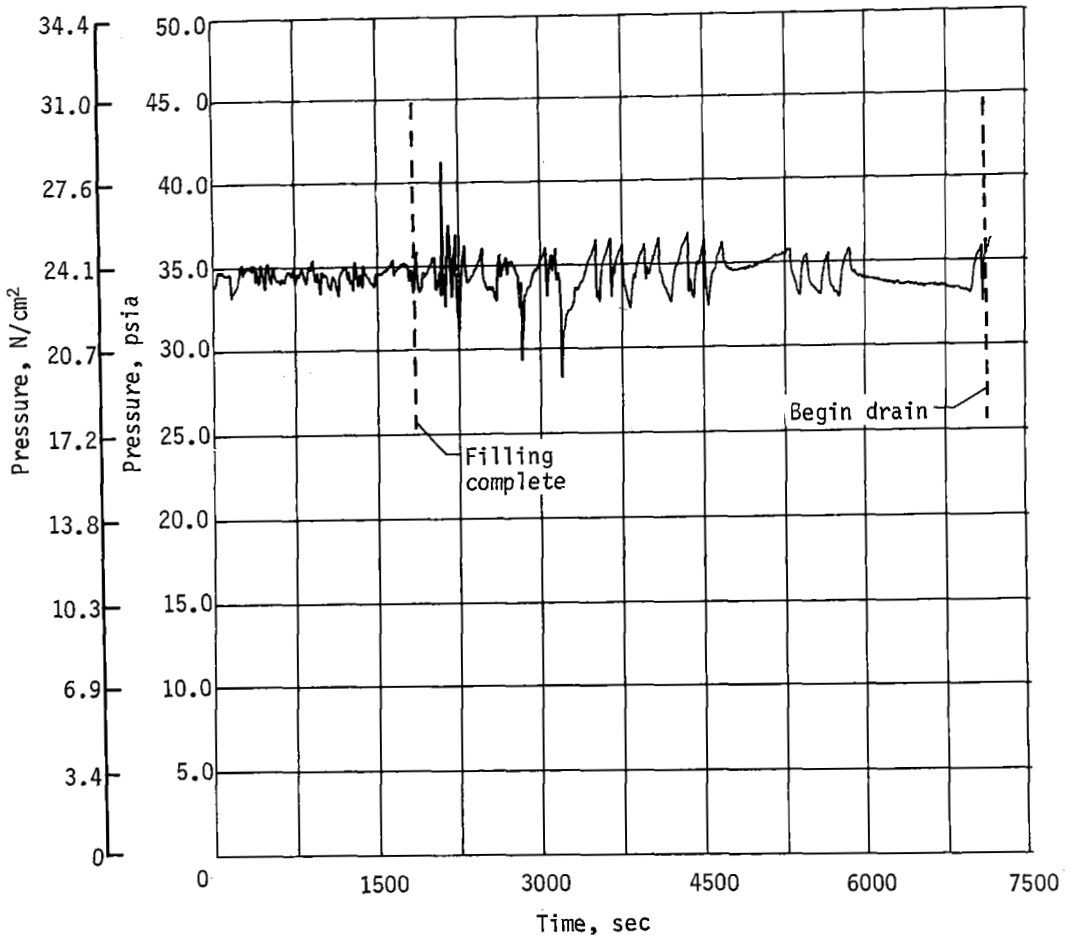

Figure 56.- Test Number 38 - Single Tank Loading with Methane: Pressure at Top of Standpipe Tank

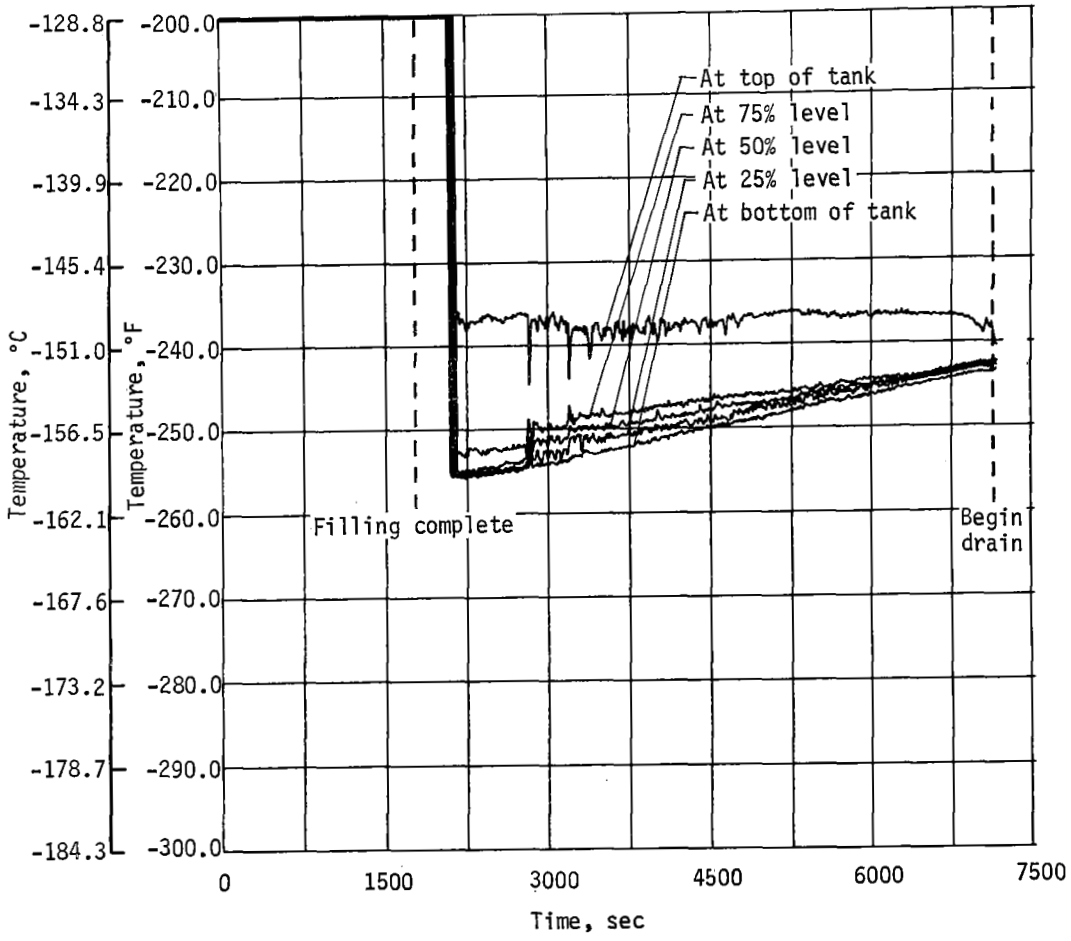

Figure 57.- Test Number 38 - Single Tank Loading with Methane: Temperature of Liquid in Standpipe Tank

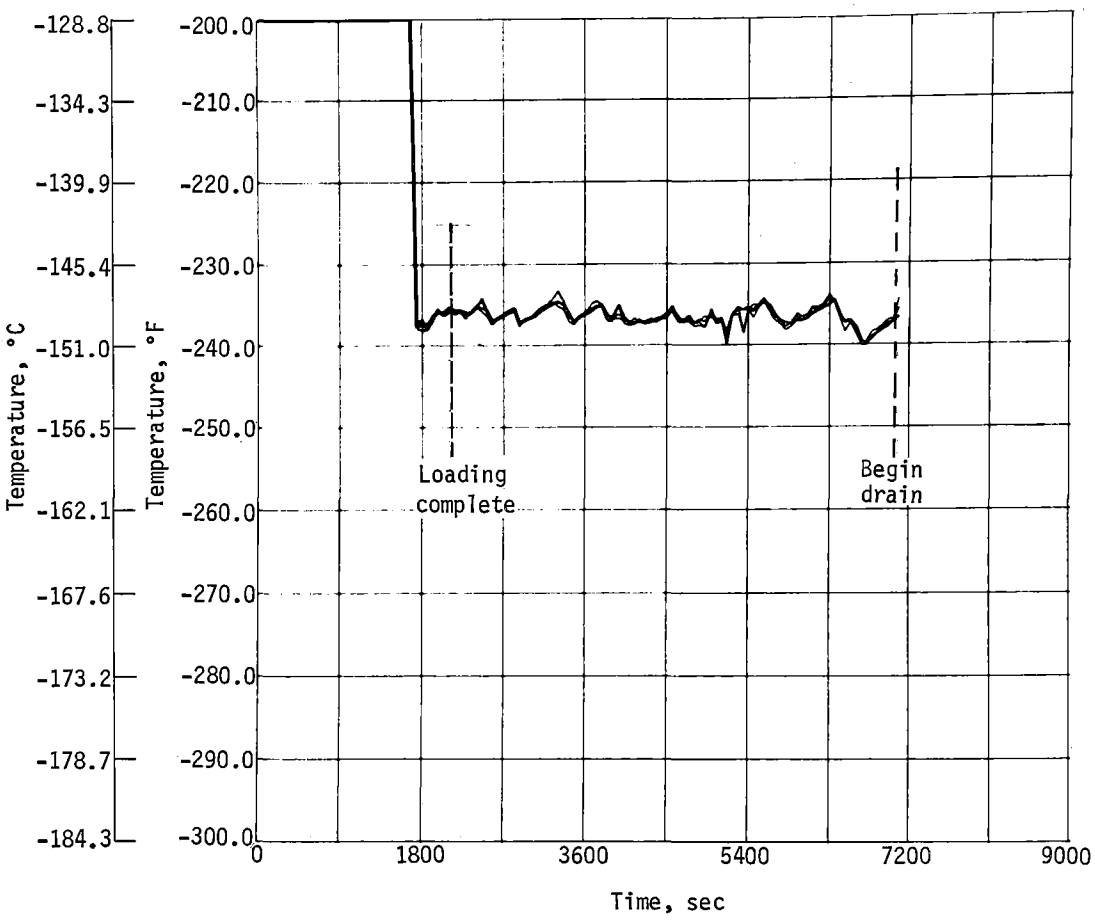

Figure 58. - Test Number 38 - Single Tank Loading with Methane: Temperature of Liquid in Standpipe

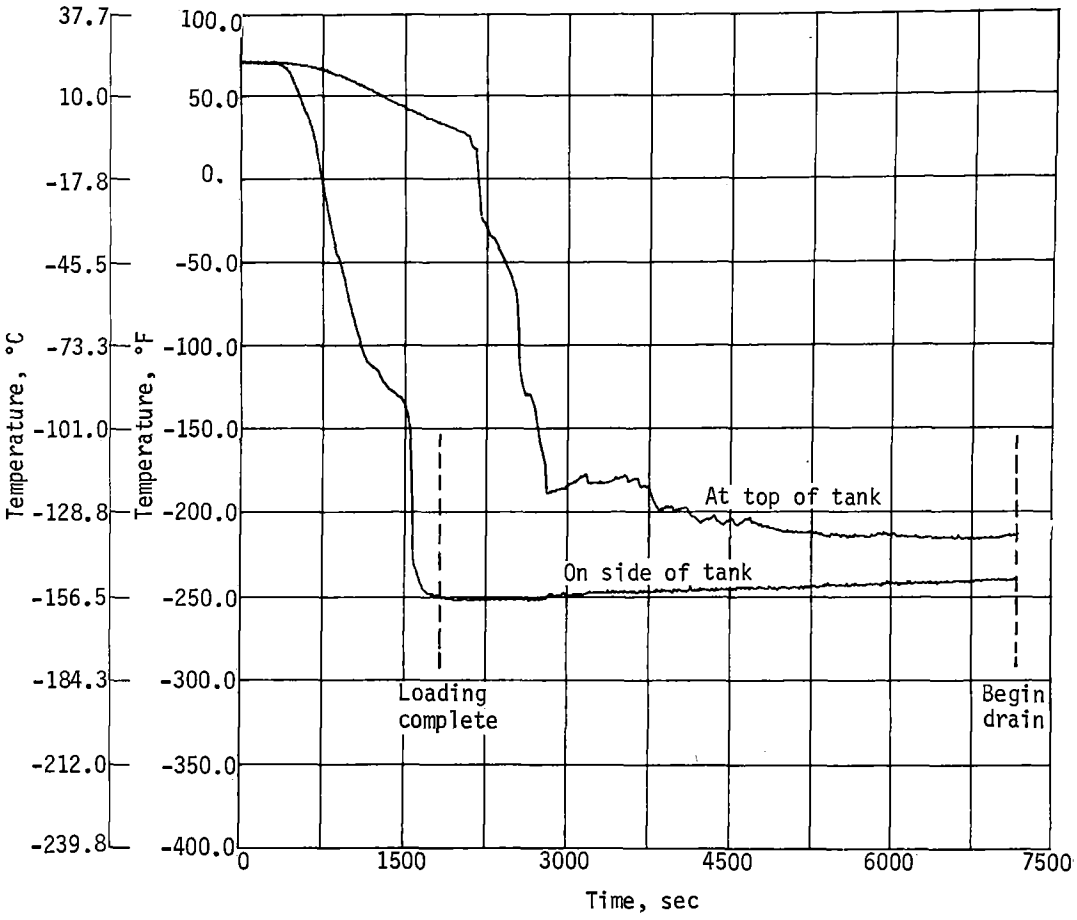

Figure 59.- Test Number 38 - Single Tank Loading with Methane: Temperature of Inner Layer of Insulation at Top and Side of Standpipe Tank

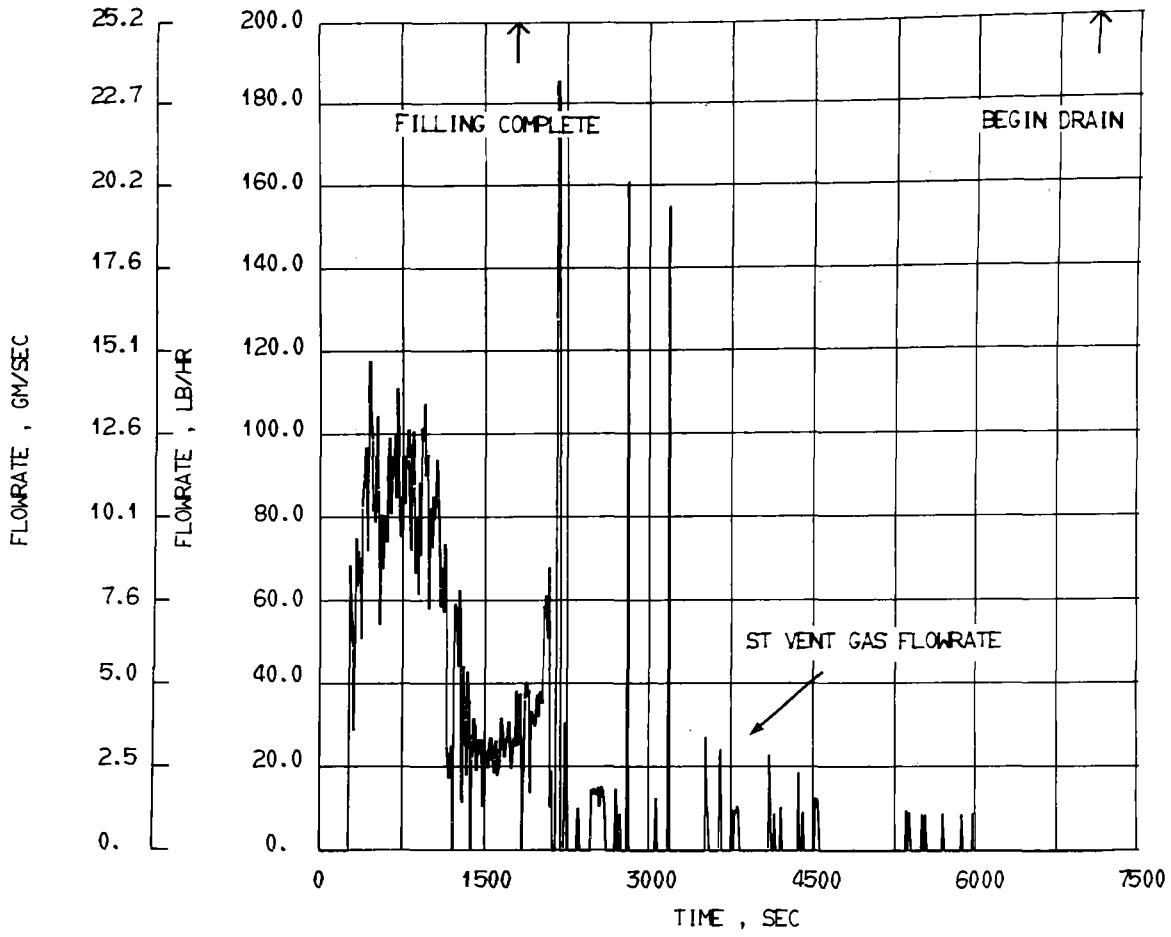

Figure 60.- Test Number 38 - Single Tank Loading with Methane: Flowrate of Standpipe Tank Vent Gas

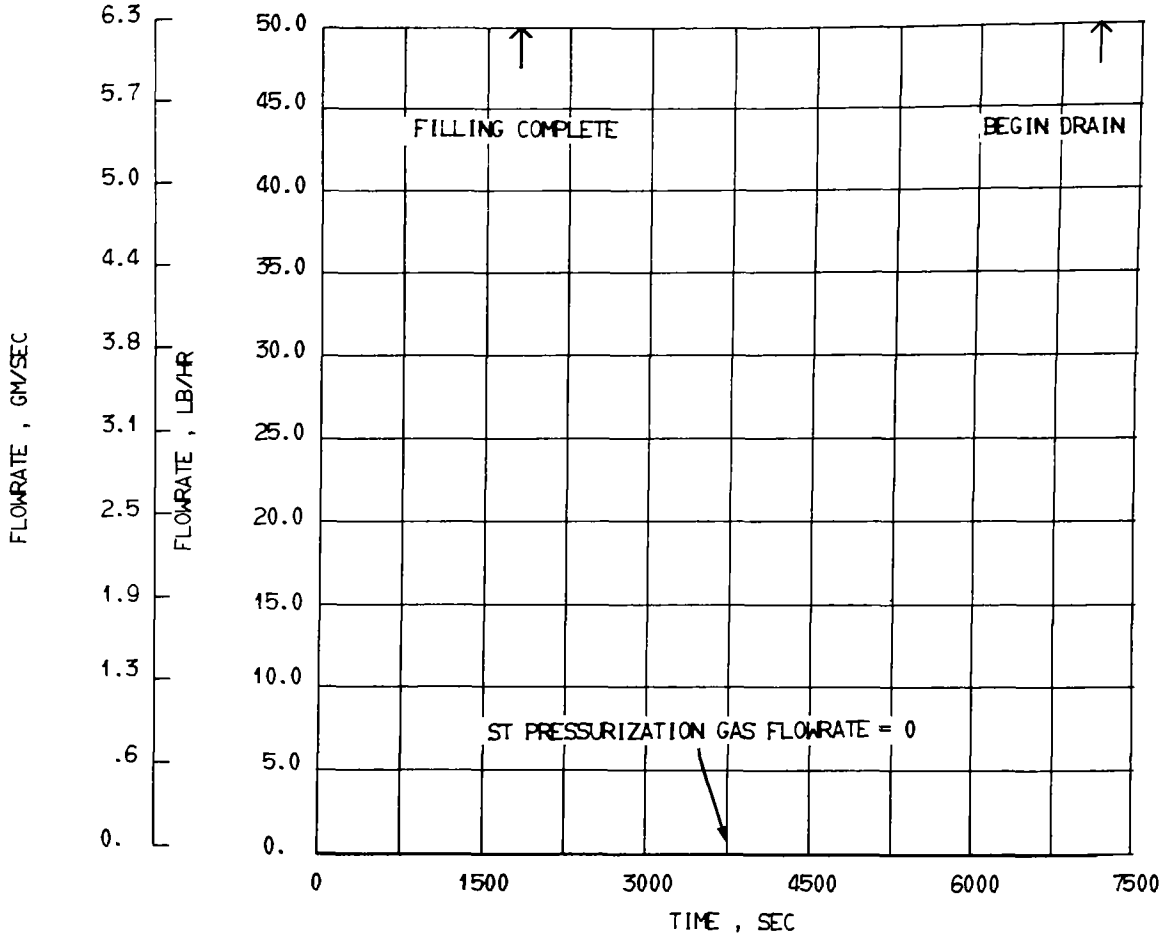

Figure 61.- Test Number 38 - Single Tank Loading with Methane: Flowrate of Standpipe Tank Pressurization Gas

h. Test 39.- Test 39 consisted of series filling the standpipe tank and holding the pressure constant until the system was at equilibrium. The tank pressure, (fig. 62) was held near 36 psia (24.8 N/cm^2) until the end of loading when the supply dewar pressure dropped too low to maintain this level.

The temperature of the liquid in the standpipe main tank is shown in figures 63 and 64, respectively. Note that the liquid in the standpipe was subcooled during the series loading, but reached equilibrium with the tank pressure shortly after the loading was complete.

During filling, the temperature at the inlet to the standpipe tank was -256°F (-160°C), while that at the bottom of the tank reached -254°F (-158.9°C). However, by the time loading was complete, the fill rate had slowed considerably due to the low dewar pressure and the temperature at the inlet had risen to about -235°F (-148.3°C), as shown in figure 64. Consequently, the liquid in the tank varied from -246 to -248°F (-154.4 to -155.6°C) after loading, for a subcooling of only about 8F° (4.4C°). Before the inlet temperature began to rise, the subcooling was around 13F° (7.2C°).

As seen in figure 65, the goal of zero ullage was nearly attained. Just after loading, the sensor at the top layer of insulation appeared to be reading the temperature of the liquid for a short period before slowly warming up.

Figure 66 shows that it was necessary to pressurize the standpipe tank at various times during the series loading. Consistant with this is the decreased vent flowrate shown in figure 67.

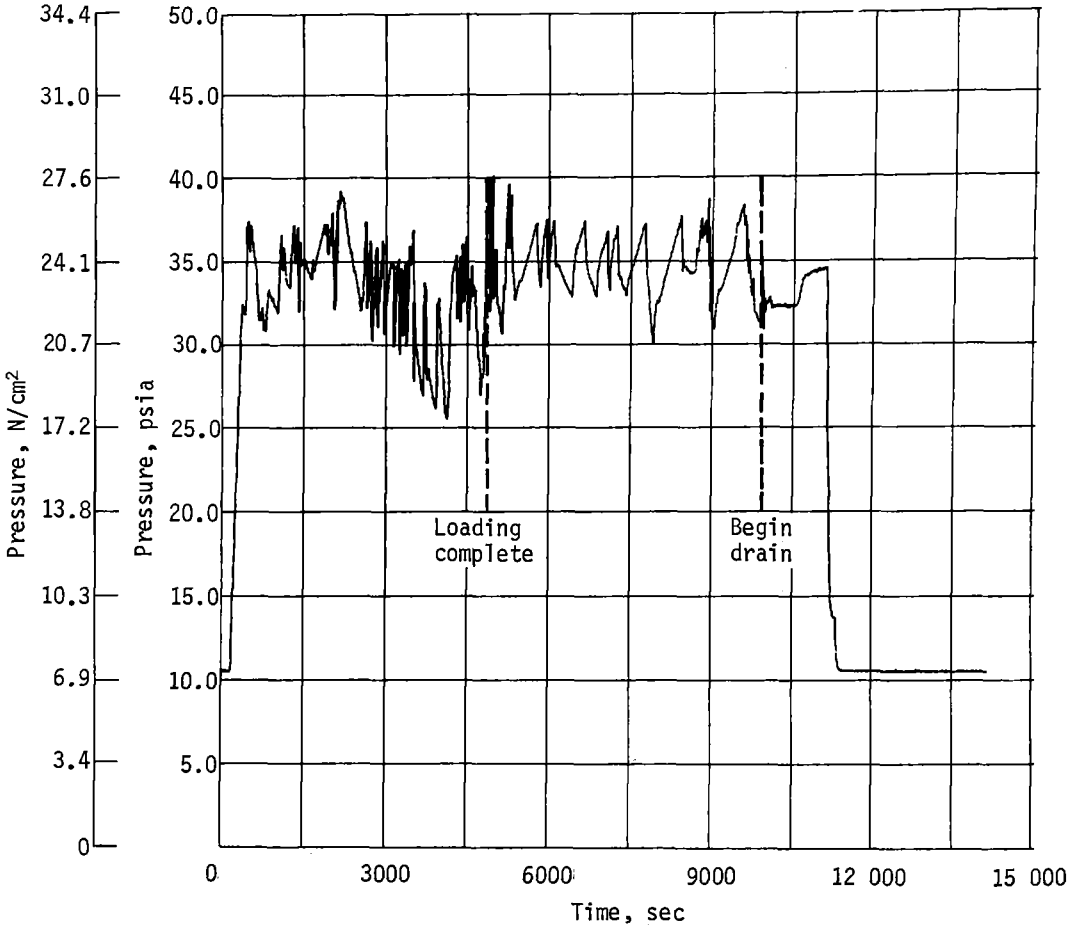

Figure 62.- Test Number 39 - Series Tank Loading with Methane: Pressure at Top of Standpipe Tank

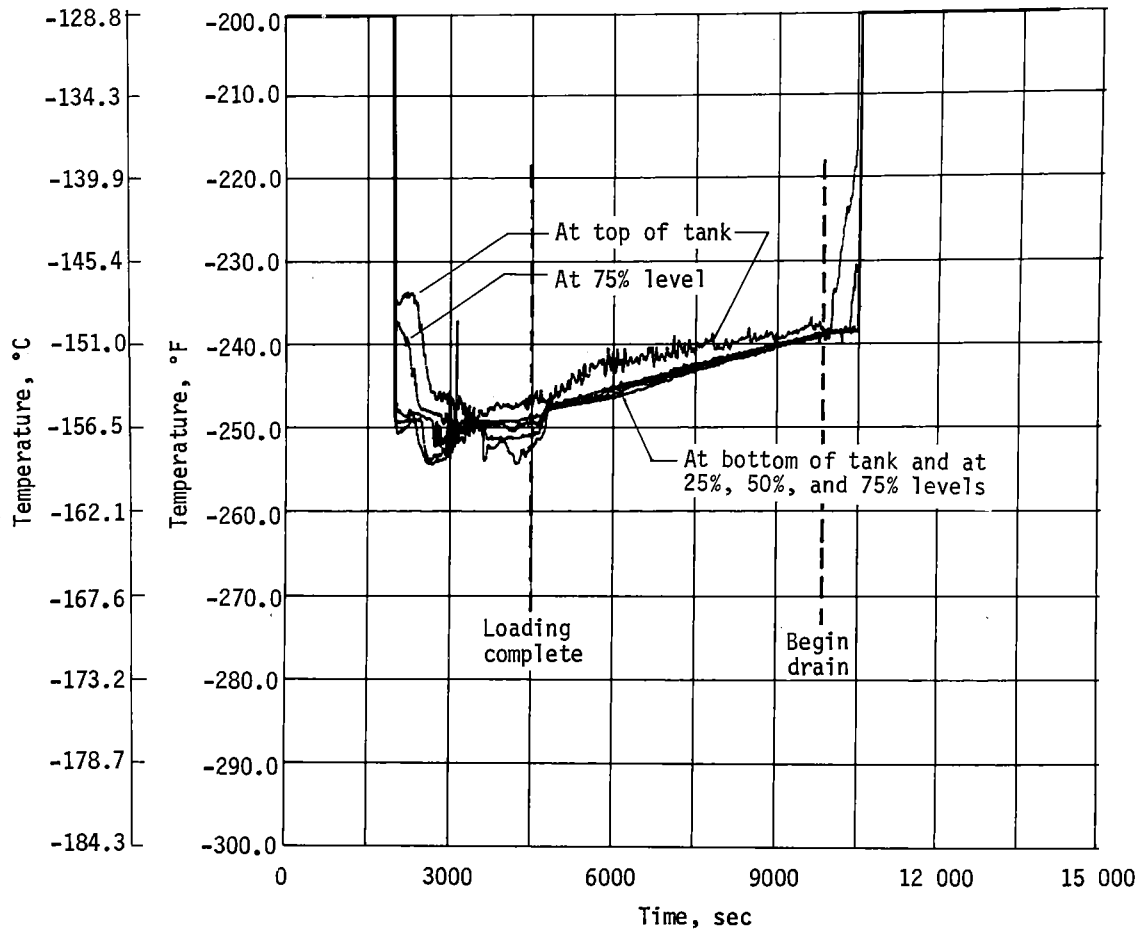

Figure 63.- Test Number 39 - Series Tank Loading with Methane: Temperature of Liquid in Standpipe Tank

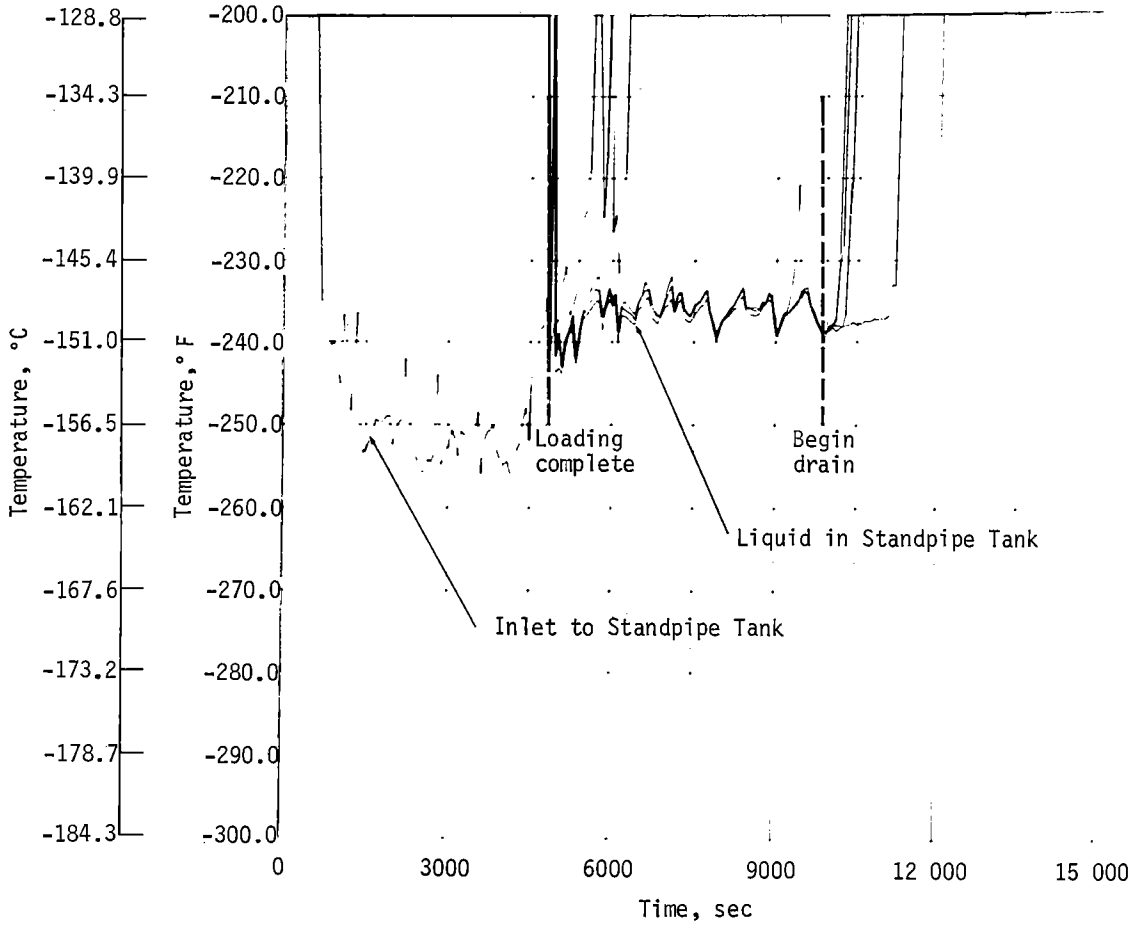

Figure 64.- Test Number 39 - Series Tank Loading with Methane: Temperature of Liquid in Standpipe and Inlet to Standpipe Tank

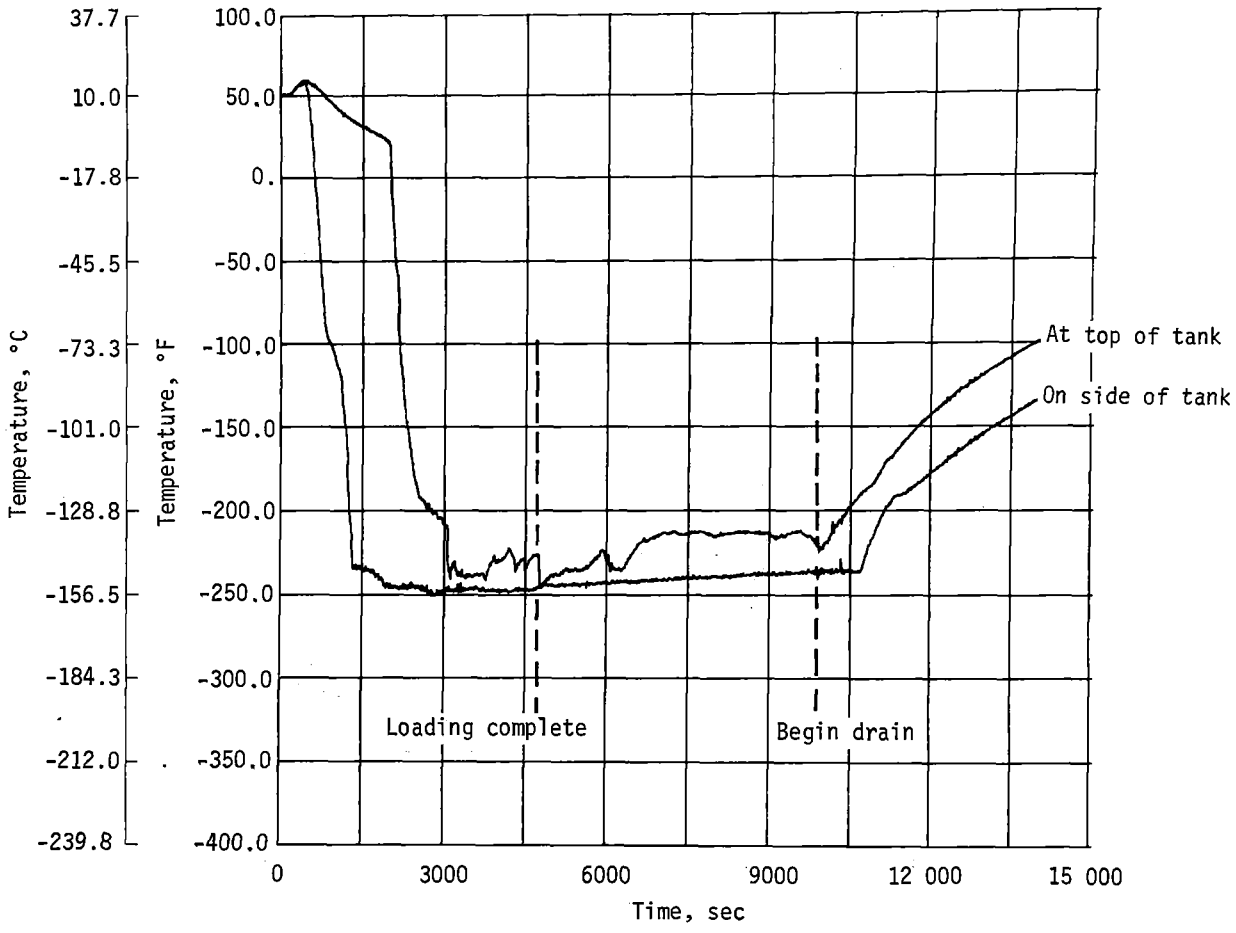

Figure 65.- Test Number 39 - Series Tank Loading with Methane: Temperature of Inner Layer of Insulation at Top and Side of Standpipe Tank

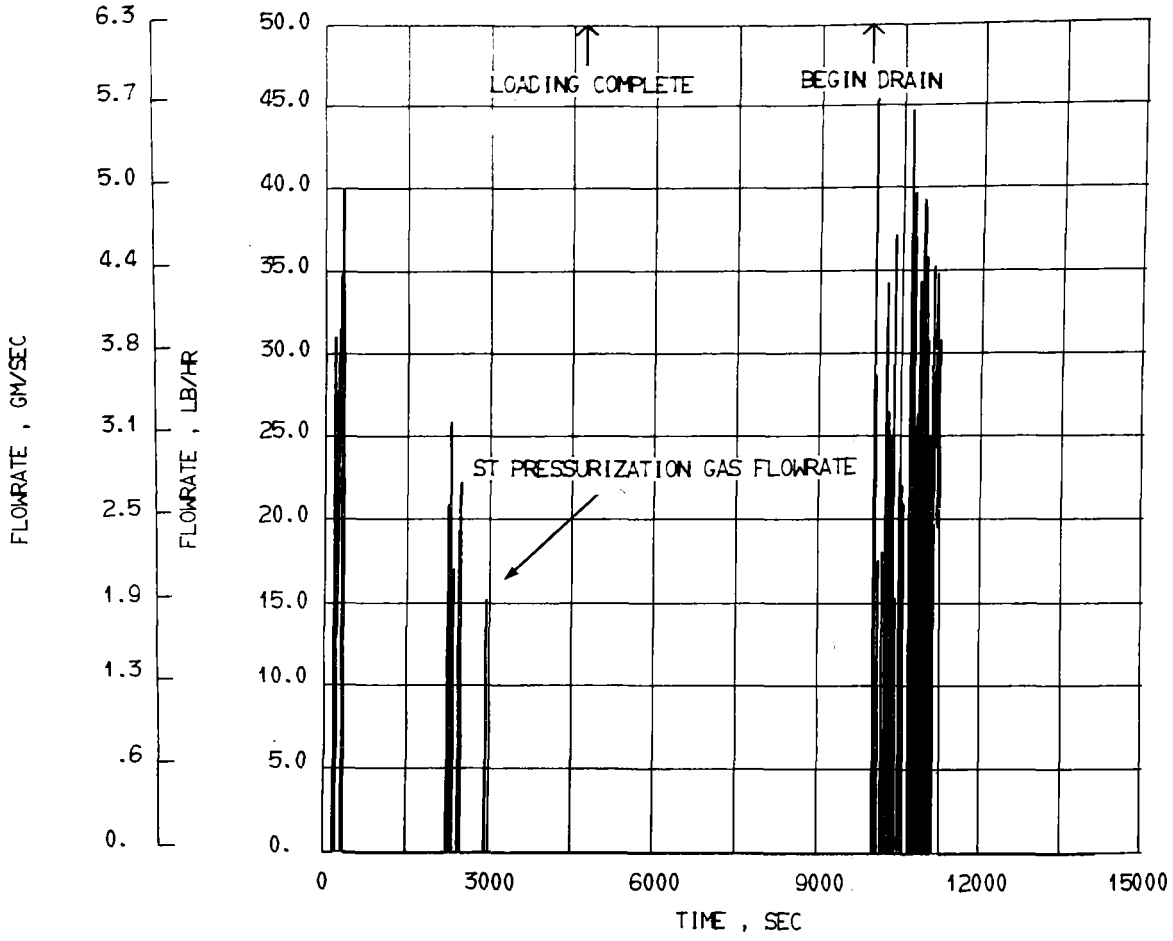

Figure 66.- Test Number 39 - Series Tank Loading with Methane: Flowrate of Standpipe Tank Pressurization Gas

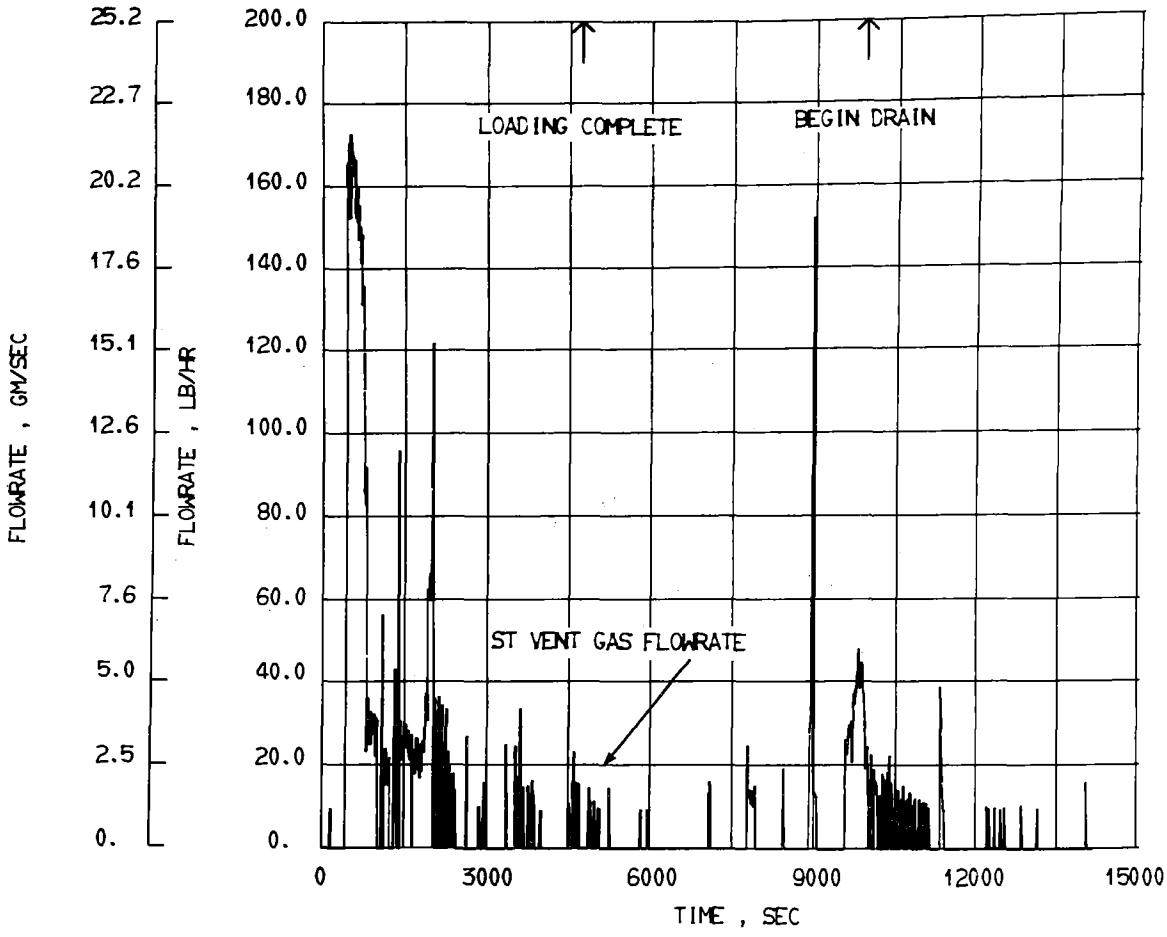

Figure 67.- Test Number 39 - Series Tank Loading with Methane: Flowrate of Standpipe Tank Vent Gas

i. Test 40.- The procedure for this test was to fill only the standpipe tank with subcooled methane and inject gaseous helium into the methane pressurant gas at specific times throughout the hold period. There was a 15-minute delay between the helium additions to allow any system changes to occur.

The tank pressure during Test 40 is shown in figure 68.

By the end of loading, the liquid in the inlet to the standpipe tank had reached -257°F (-160.6°C), while that at the bottom of the tank (fig. 69) was down to -255°F (-159.4°C). The stratification from the bottom of the tank was 1 1/2F° (0.84C°) to the 50% level, 7F° (3.9C°) to the 75% level, and about 20F° (11.1C°) to the tank-top probe. If the temperature of the liquid at the 50% level is again assumed to represent the temperature of the bulk liquid, the subcooling was 17F° (9.4C°). The temperature of the liquid in the standpipe (fig. 70) was about -237°F (-141.9°C), which was near equilibrium with the tank pressure at all times.

Based on the temperatures at the top of the tank (fig. 69) and those at the inner layer of insulation, the surface of the liquid was about 1 in. (2.54 cm) from the top of the tank. After the test pressure had been achieved no additional pressurant was needed. The pressurization flowrate and vent gas flowrate are shown in figures 71 and 72, respectively.

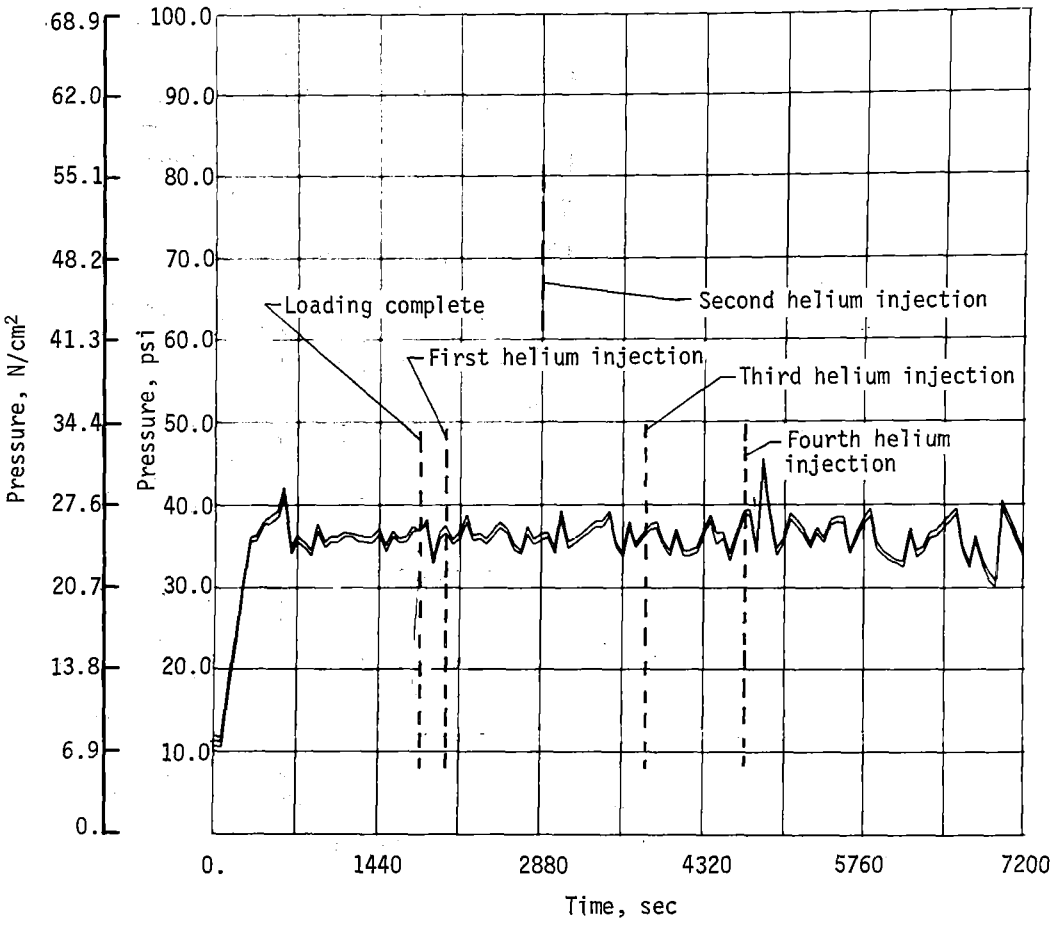

Figure 68.- Test Number 40 - Single Tank Loading with Helium Injected after Loading: Pressure at Top of Standpipe Tank

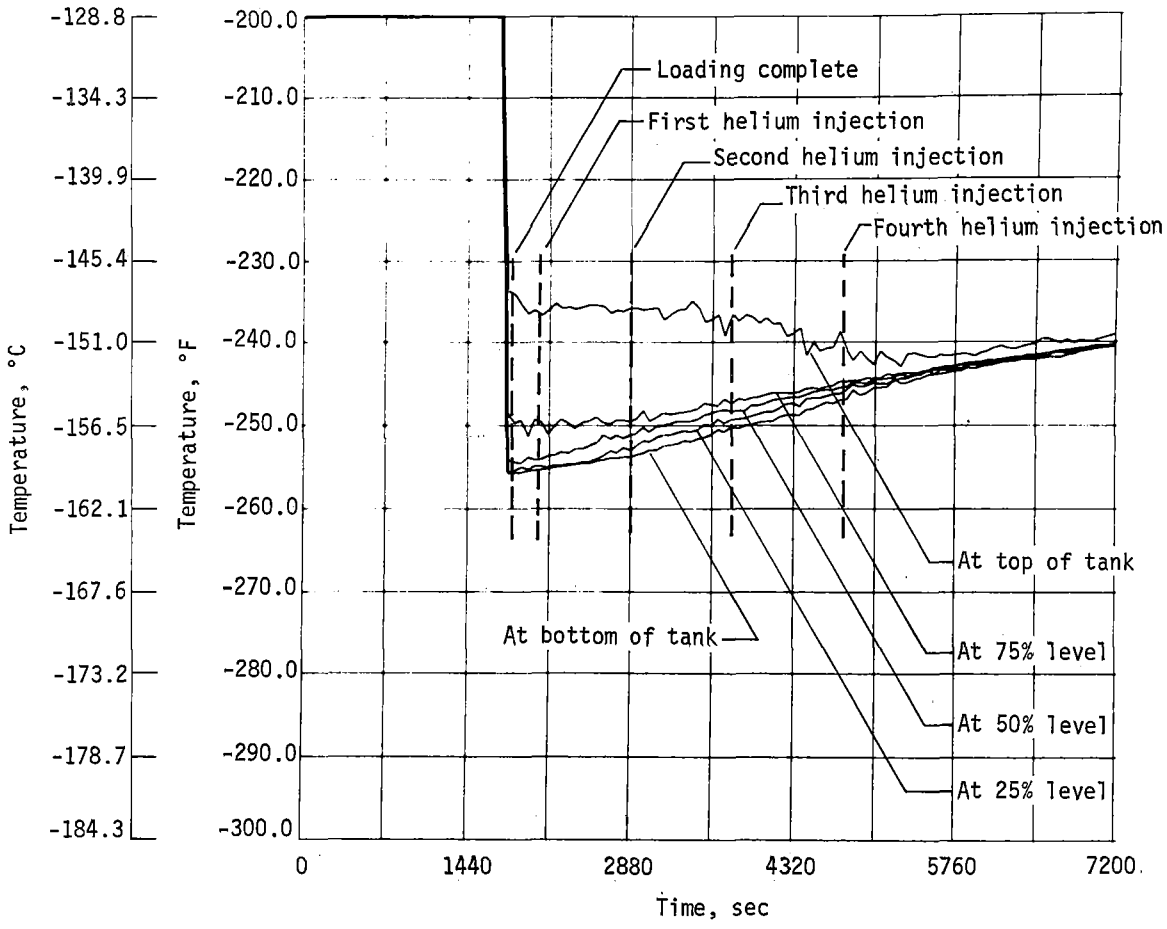

Figure 69.- Test Number 40 - Single Tank Loading with Helium Injected after Loading: Temperature of Liquid in Standpipe Tank

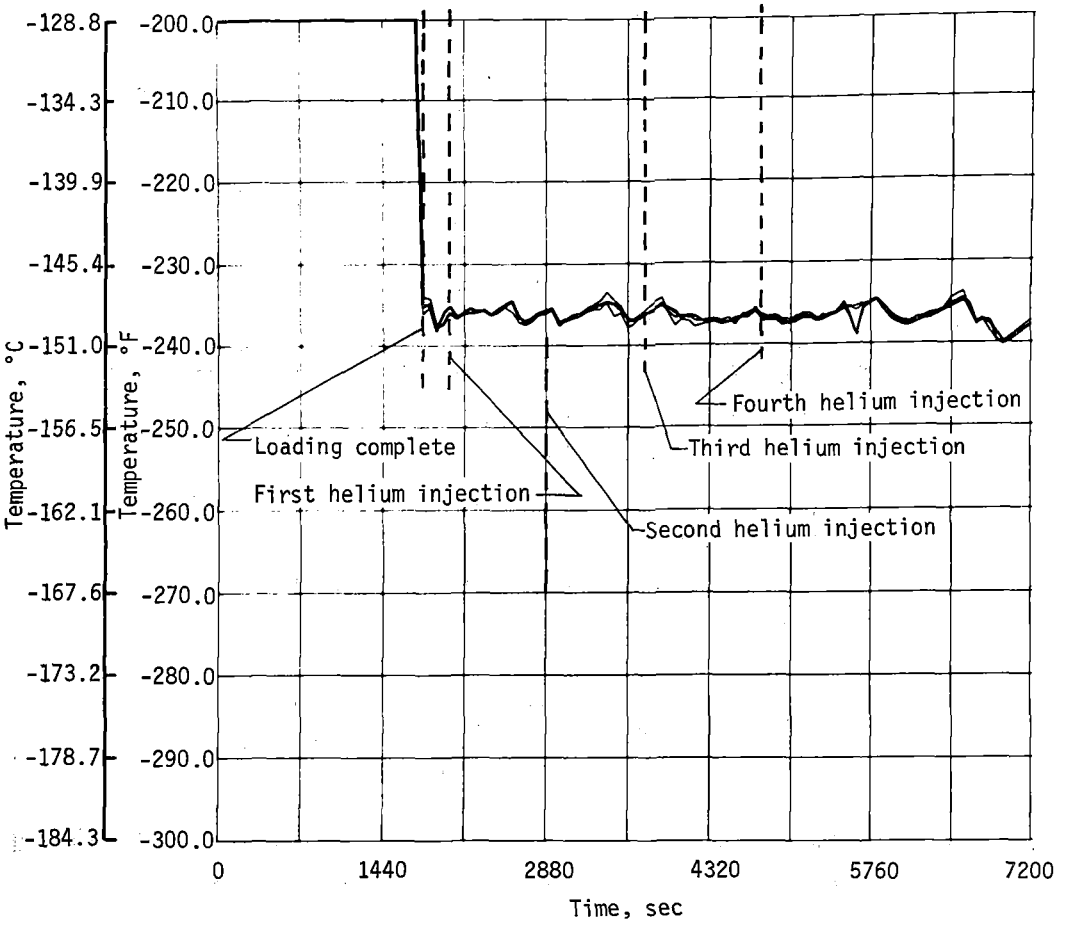

Figure 70.- Test Number 40 - Single Tank Loading with Helium Injected after Loading: Temperature of Liquid in Standpipe

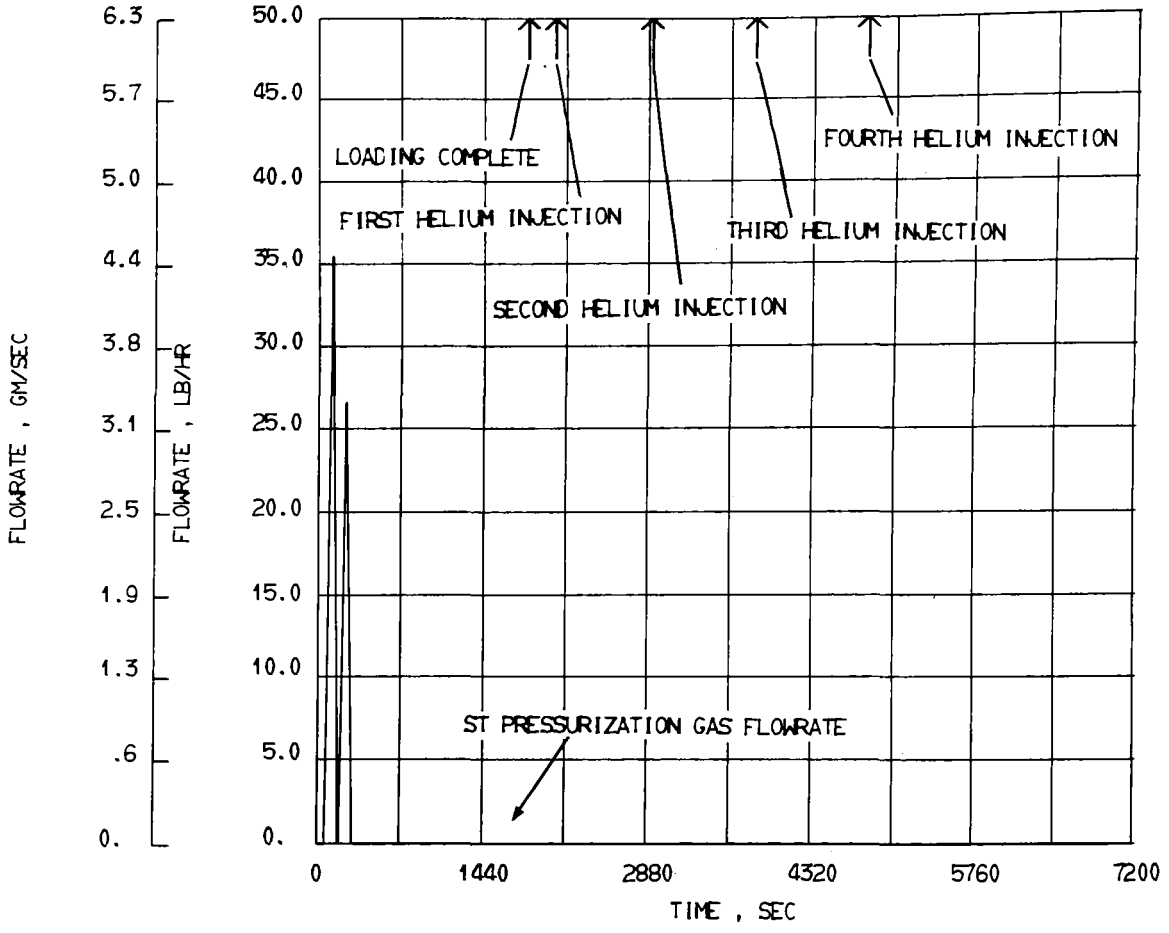

Figure 71.- Test Number 40 - Single Tank Loading with Helium Injected after Loading: Flowrate of Standpipe Tank Pressurization Gas

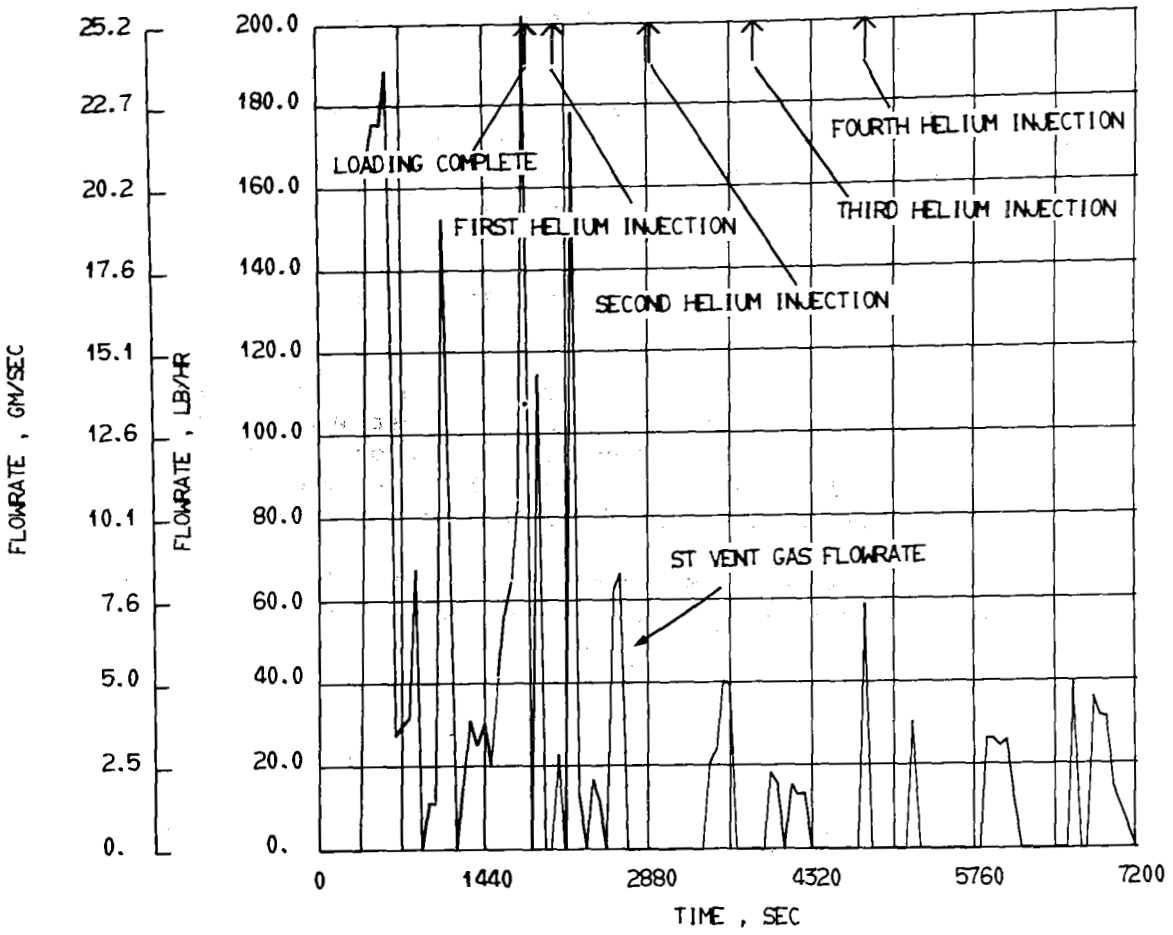

Figure 72.- Test Number 40 - Singel Tank Loading with Helium Injected after Loading: Flowrate of Standpipe Tank Vent Gas

j. Test 41.- Test 41 followed the same procedure as Test 40, except that the standpipe tank was series-loaded. As shown in figure 73, the tank pressure trace dropped off with the dropping supply pressure at the end of loading. Immediately after loading, the pressure was raised to the desired level.

The incoming liquid reached -257°F (-160.6°C) before warming up from the slower flowrate at the end of loading. Figure 74 shows the temperature of the liquid in the main tank. Note that, at the end of loading, this converged to -256°F (-160°C) with no stratification; this represented a subcooling of about 9F° (5C°) since the tank pressure had dropped off to 24 psia (16.6 N/cm^2).

The series filling resulted in the liquid in the standpipe being subcooled (fig. 75). Once the filling stopped, the standpipe subcooling was lost in about 1500 sec.

The liquid was much nearer the top of the tank for the series loading in this test than for the single tank loading in Test 40. The temperature at the top of the inner layer of insulation (fig. 76) dropped slightly below -250°F (-156.7°C) when loading was complete, and then slowly warmed to around -240°F (-151.1°C), where it remained until the tank was drained.

Again no pressurant gas was required during fill, figure 77. The vent flowrate was relatively low, figure 78, because of trouble in maintaining dewar pressure.

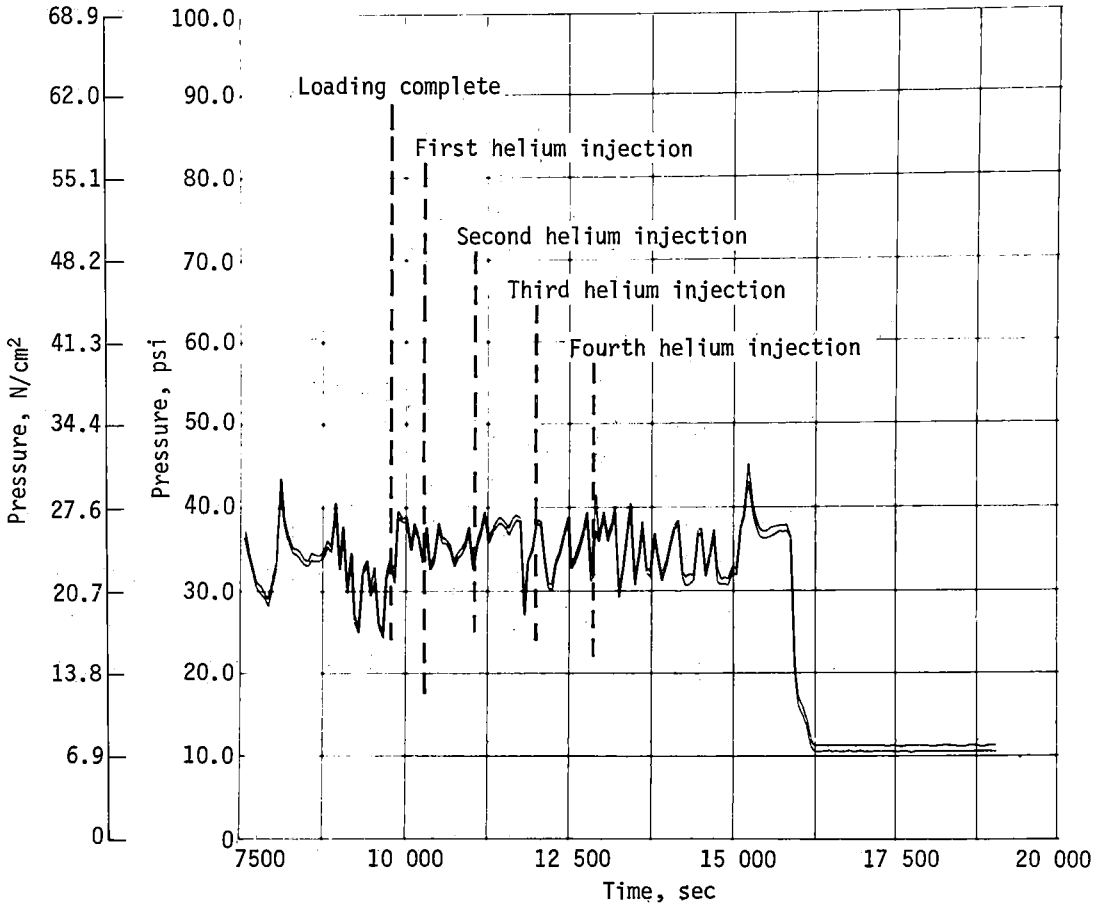

Figure 73.- Test Number 41 - Series Tank Loading with Helium Injected after Loading: Pressure at Top of Standpipe Tank

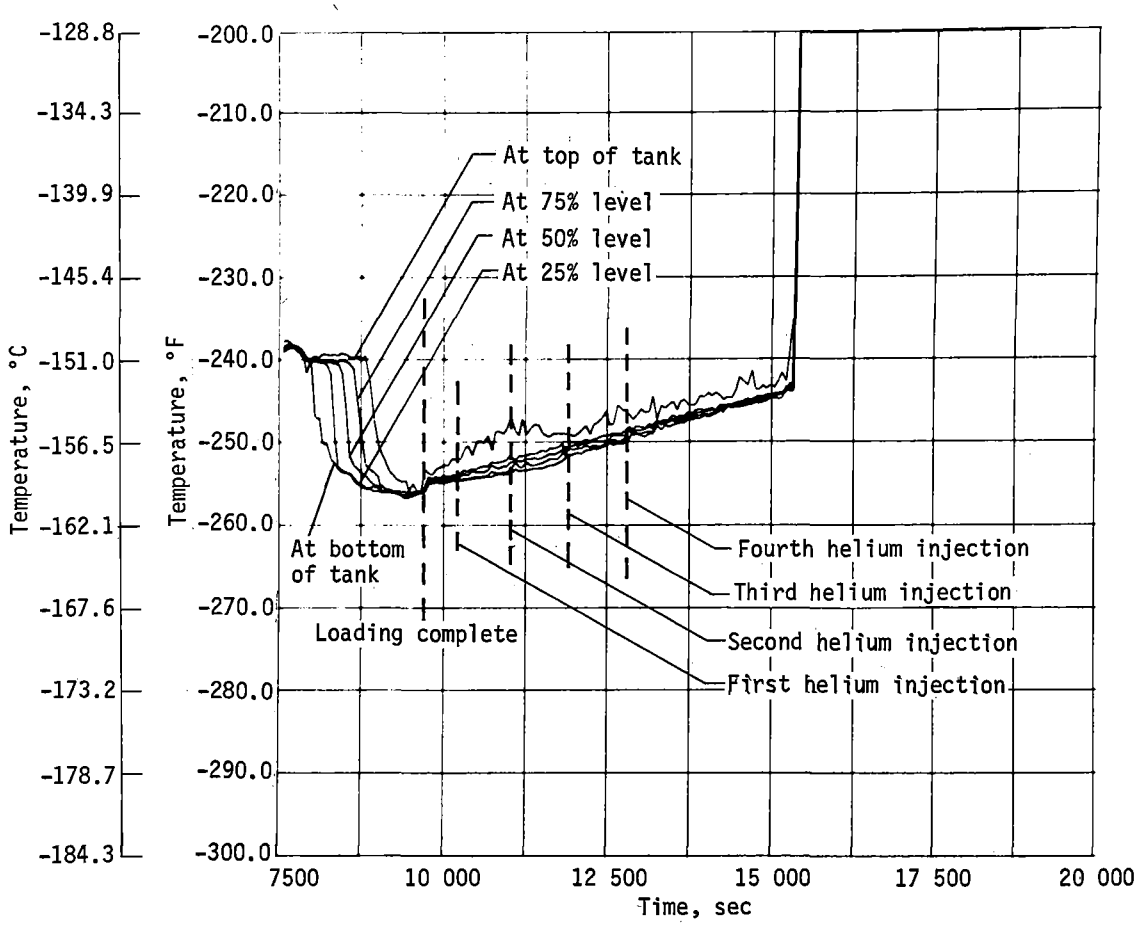

Figure 74.- Test Number 41 - Series Tank Loading with Helium Injected after Loading: Temperature of Liquid in Standpipe Tank

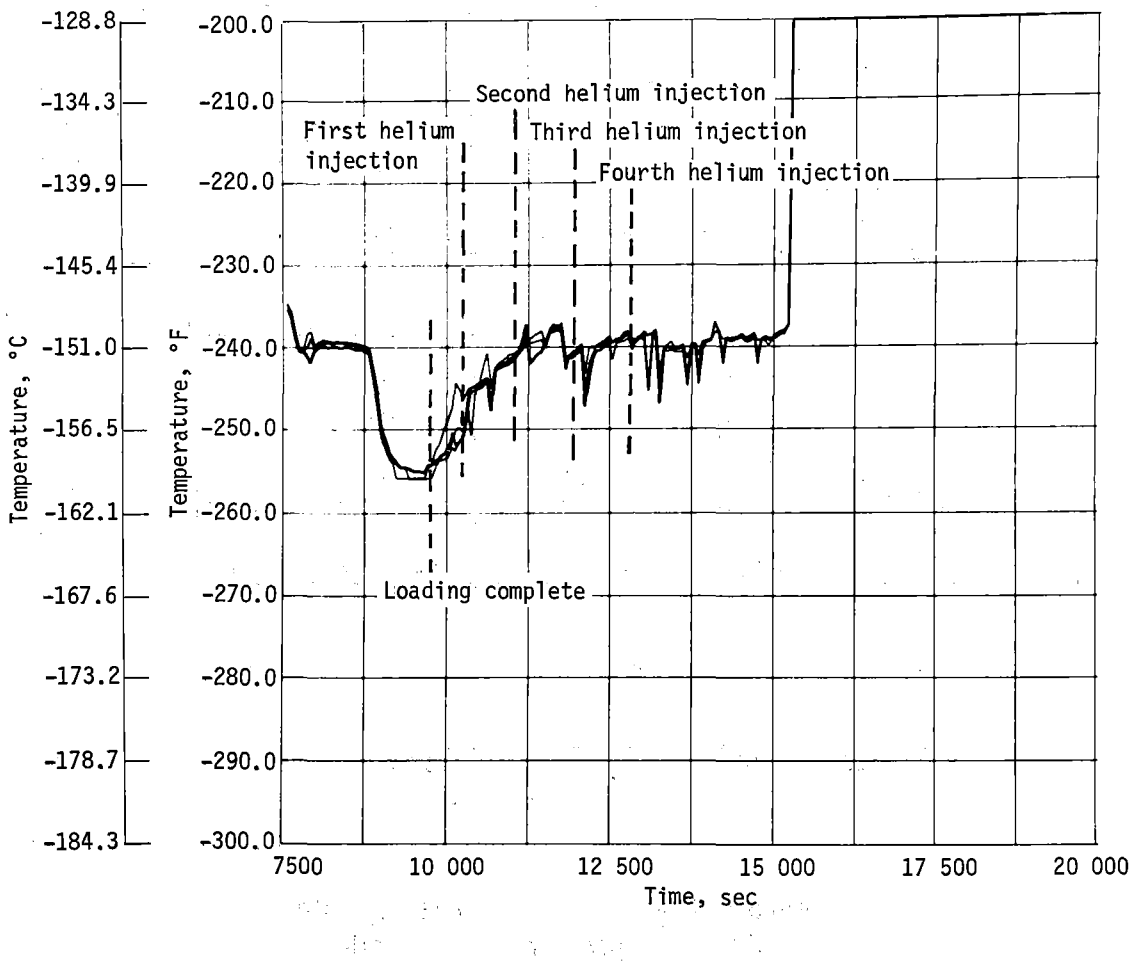

Figure 75.- Test Number 41 - Series Tank Loading with Helium Injected after Loading: Temperature of Liquid in Standpipe

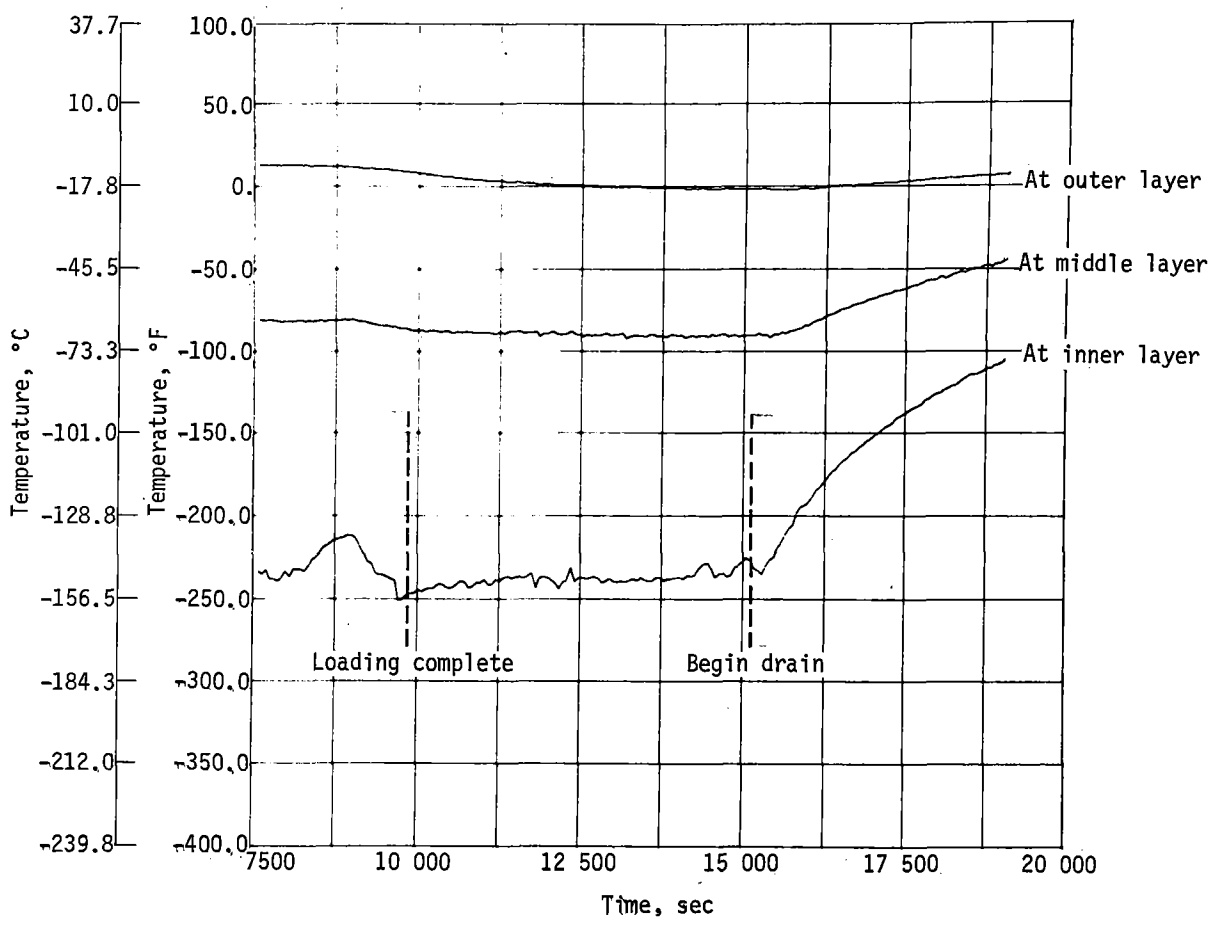

Figure 76.- Test Number 41 - Series Tank Loading with Helium Injected after Loading: Temperature of Insulation at Top of Standpipe Tank

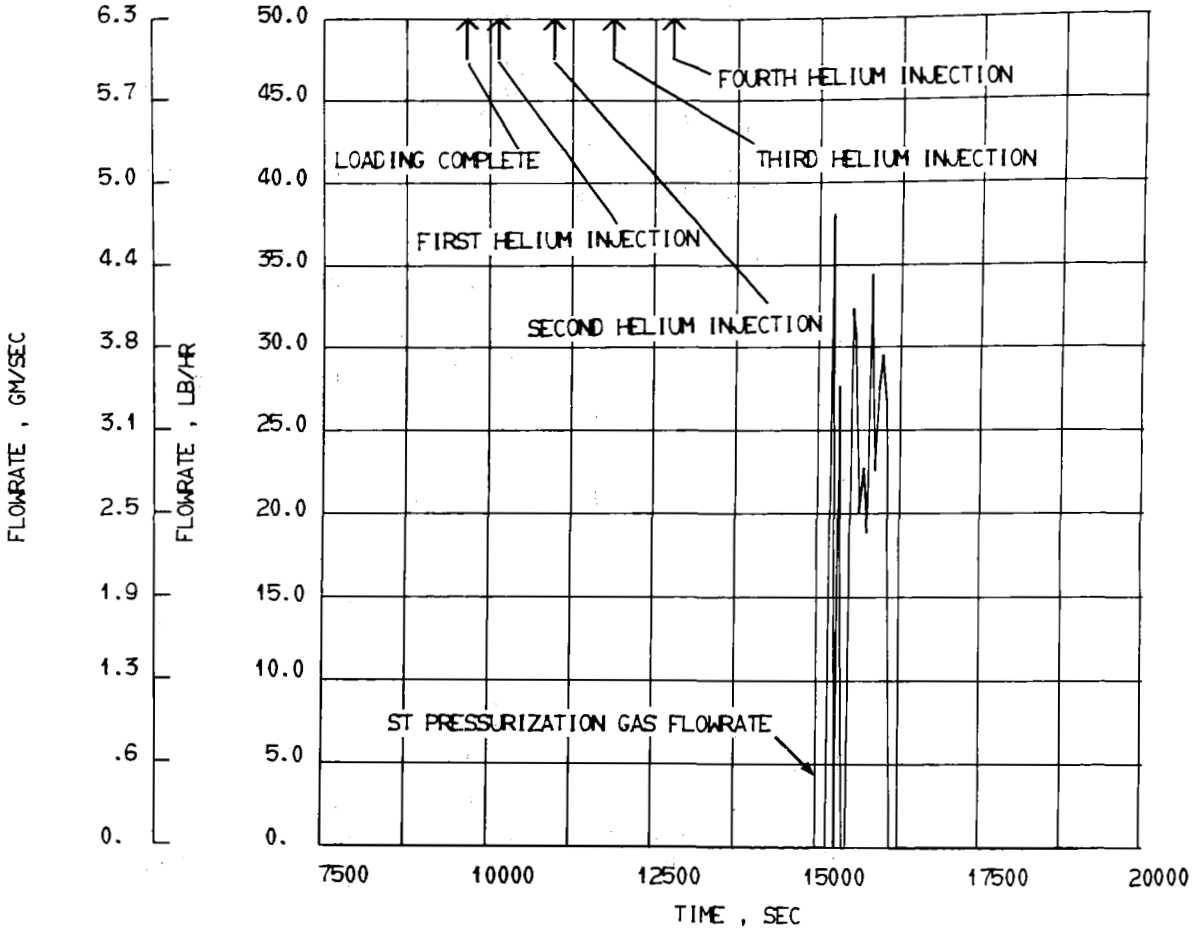

Figure 77.- Test Number 41 - Series Tank Loading with Helium Injected after Loading: Flowrate of Standpipe Tank Pressurization Gas

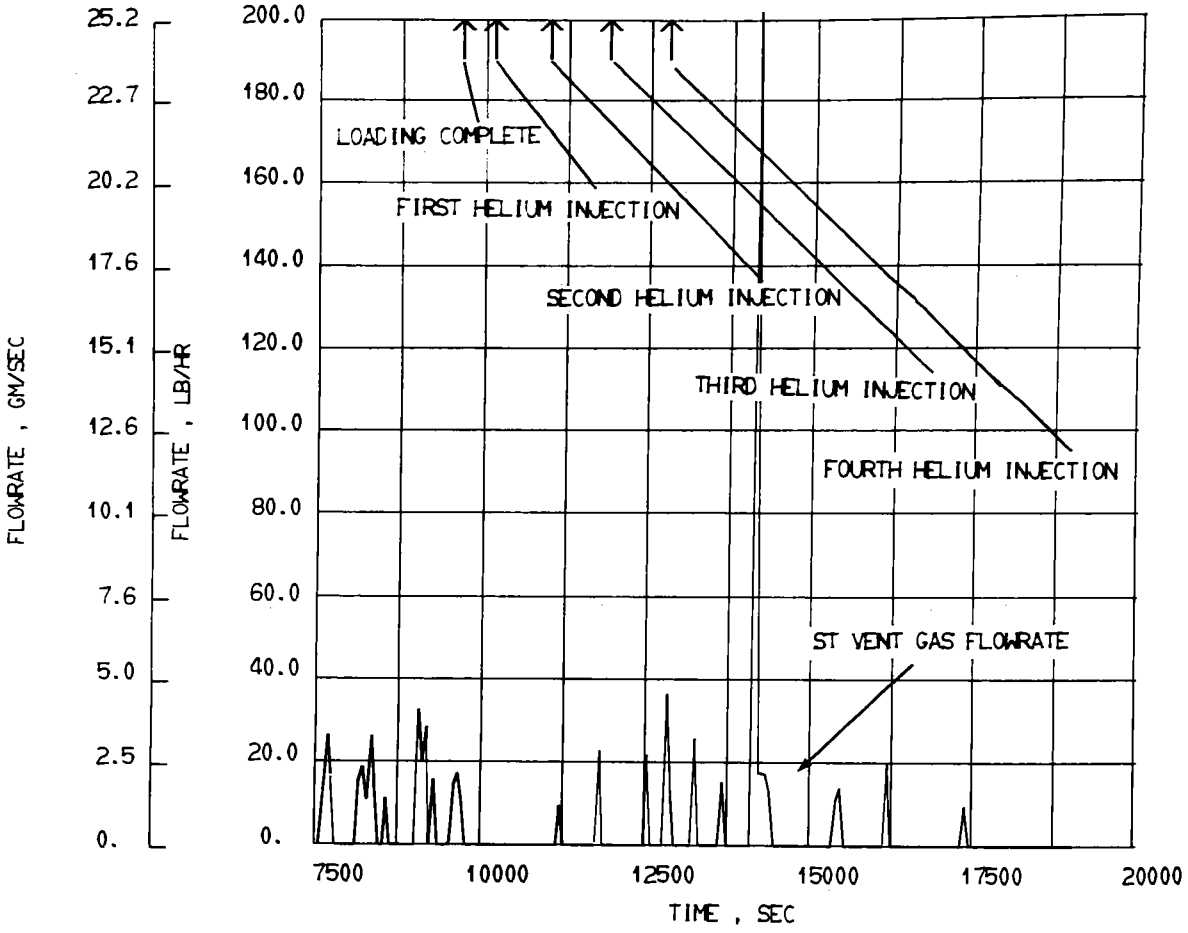

Figure 78.- Test Number 41 - Series Tank Loading with Helium Injected after Loading: Flowrate of Standpipe Tank Vent Gas

k. Test 48.- During this test, the standpipe tank was filled with liquid nitrogen pressurized to 48 psia (33.1 N/cm^2) with gaseous nitrogen and held at that level throughout the loading and hold period. The equilibrium temperature corresponding to this pressure is -299°F (-183.9°C), or 25F° (13.9C°) warmer than the equilibrium conditions of 12 psia and -324°F (-197.8°C). Before the test, the source dewar was vented long enough for the liquid to reach equilibrium. The dewar was then pressurized to 52 psia (35.9 N/cm^2) just before starting to transfer liquid.

Only the standpipe tank was filled during this test. The tank pressure (fig. 79) was close to the desired level except during the fill, because not enough gaseous nitrogen was flowing to the supply dewar to over come the condensation of the warm gas and maintain the pressure at 52 psia (35.9 N/cm^2).

During loading, the temperature of the fill line was -320°F (-195.6°C). The temperature of the liquid in the standpipe tank is shown in figure 80. When the loading was complete, the temperatures at the bottom, 50% level, and top of the tank were -310°F (-190°C), -307.5°F (-188.6°C), and -301°F (-185°C), respectively. After 3300 seconds into the holding period, the tank top had reached -299°F (-183.9°C), while all other probes read -300°F (-184.4°C).

As shown in figure 81, the liquid in the standpipe momentarily reached -306°F (-187.8°C) during the loading before quickly rising to an equilibrium value of -299°F (-183.9°C) with the tank pressure. Just after loading the subcooling in the main tank was 8.5F° (4.7C°).

Again, the standpipe tank was not loaded to zero ullage (fig. 82): the temperature of the inner layer of insulation at the top of the standpipe tank reached only -265°F (-165°C), instead of being close to the temperature of the liquid as it would have been for zero ullage.

The pressurization gas flowrate and the vent gas flowrate for this test are shown in figures 83 and 84, respectively.

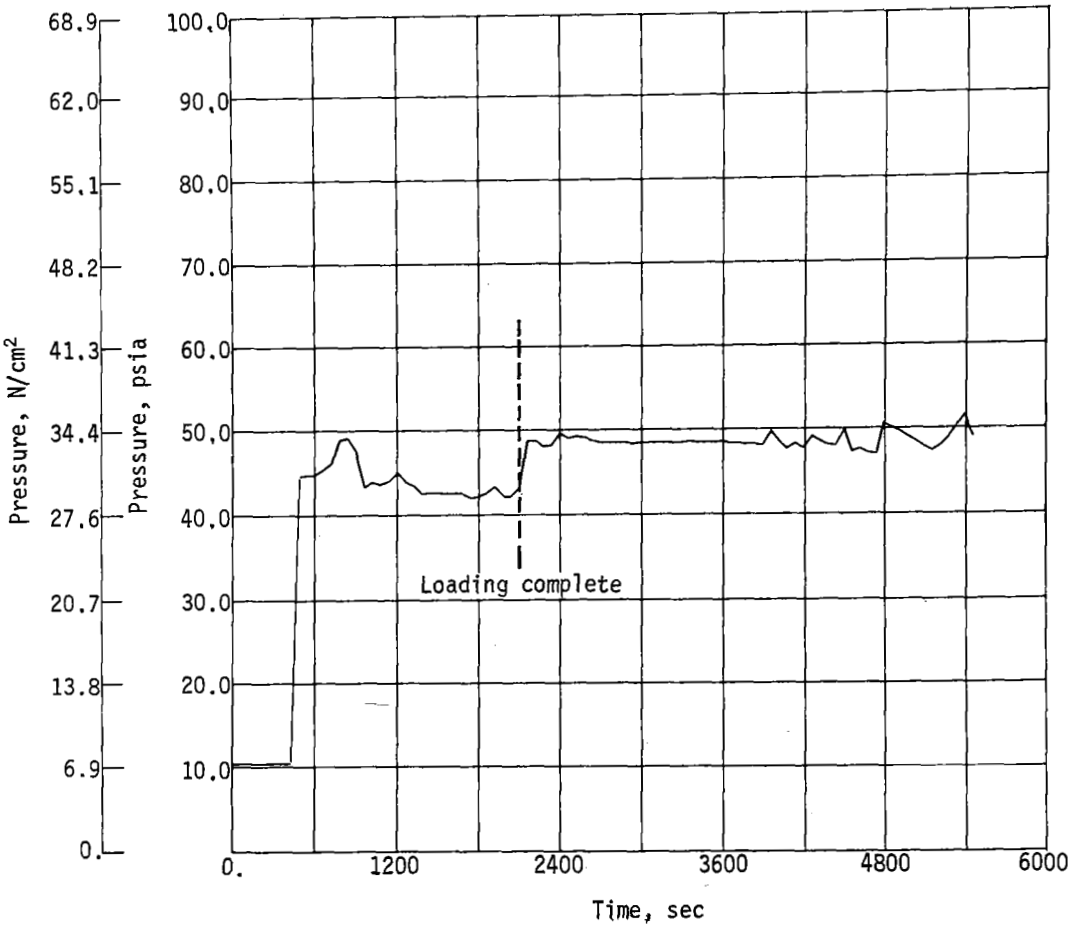

Figure 79.- Test Number 48 - Single Tank Loading with Liquid Nitrogen: Pressure at Top of Standpipe Tank

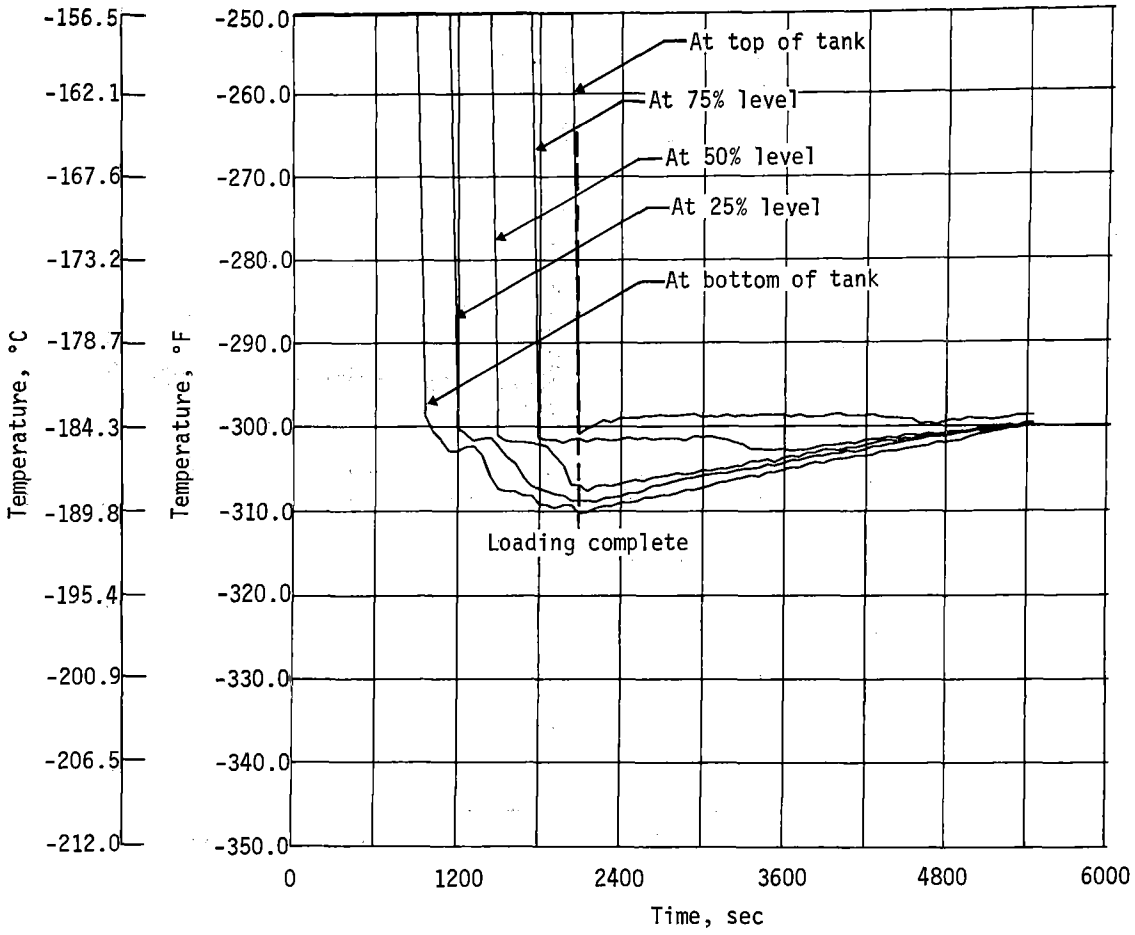

Figure 80.- Test Number 48 - Single Tank Loading with Liquid Nitrogen: Temperature of Liquid in Standpipe Tank

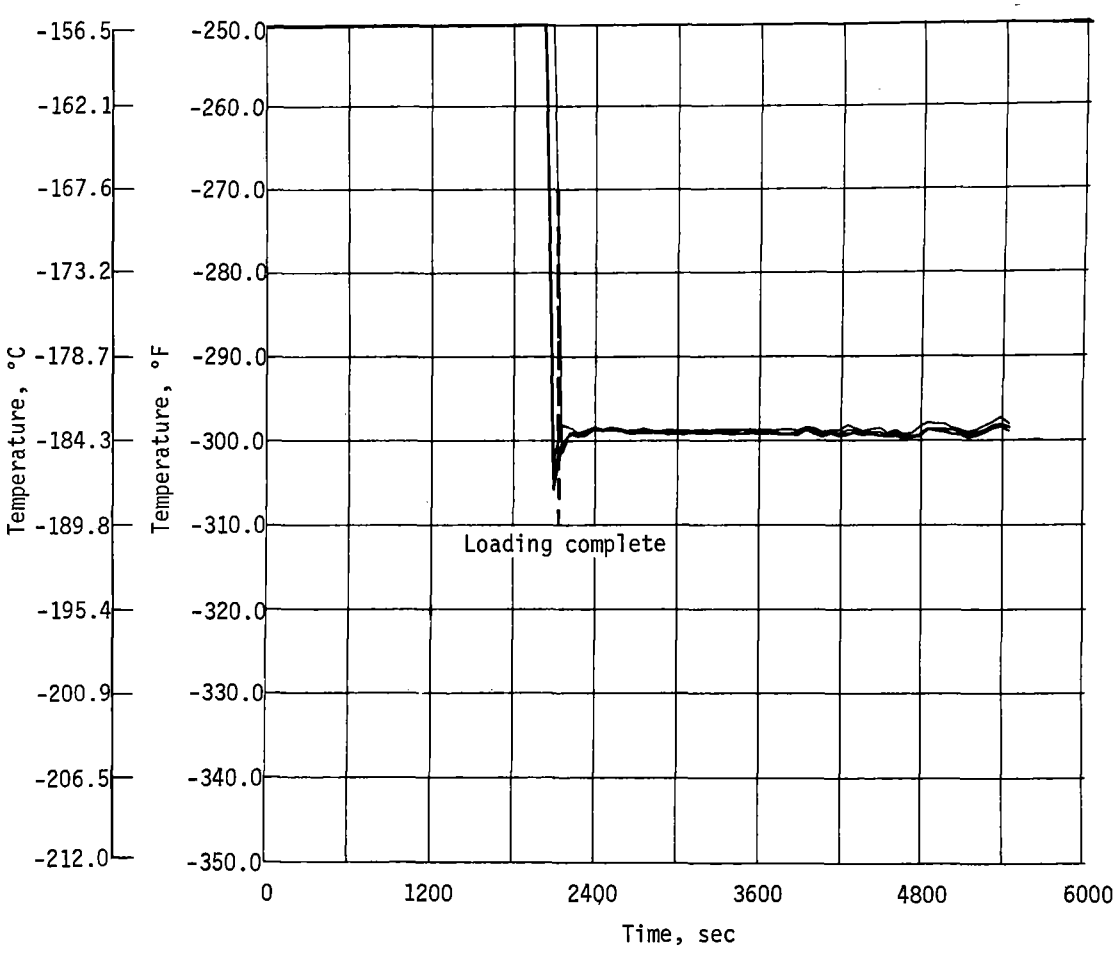

Figure 81.- Test Number 48 - Single Tank Loading with Liquid Nitrogen: Temperature of Liquid in Standpipe

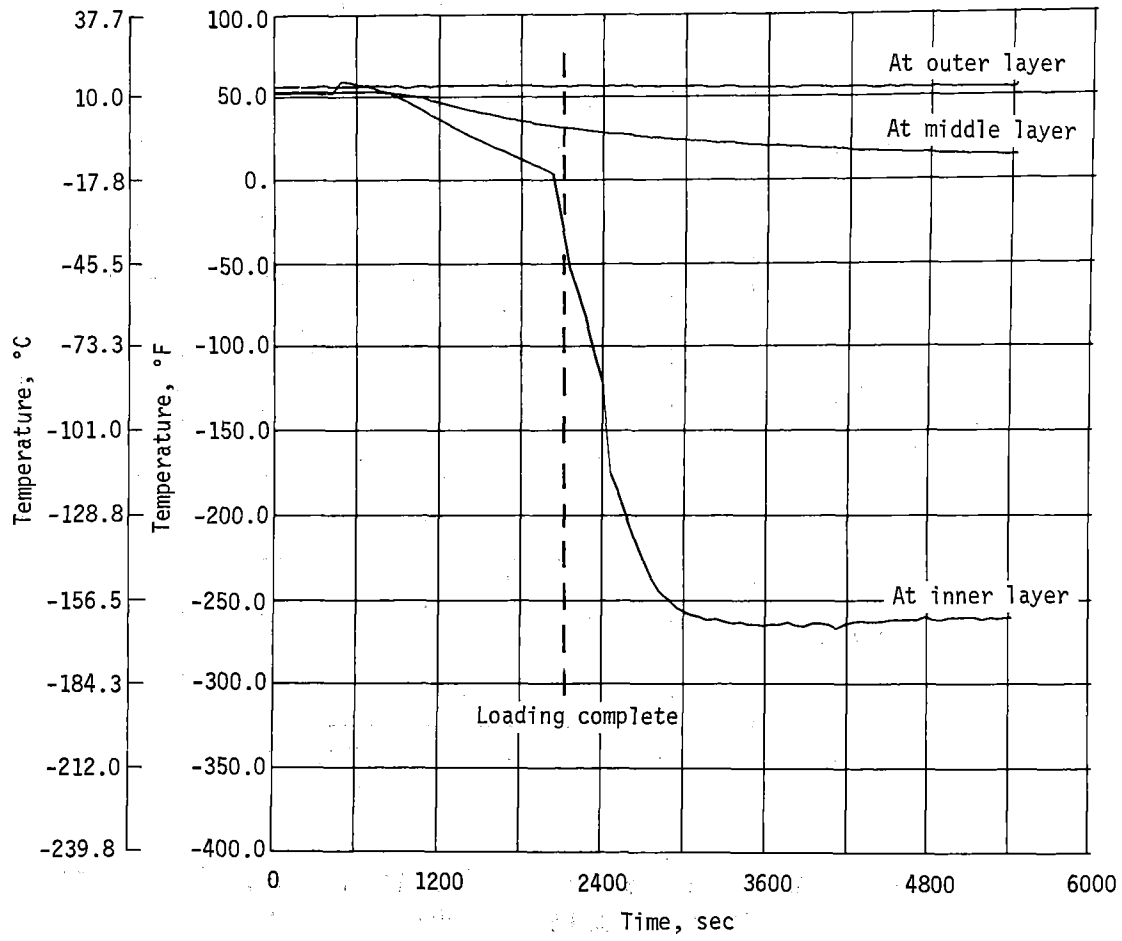

Figure 82.- Test Number 48 - Single Tank Loading with Liquid Nitrogen: Temperature of Insulation at Top of Standpipe Tank

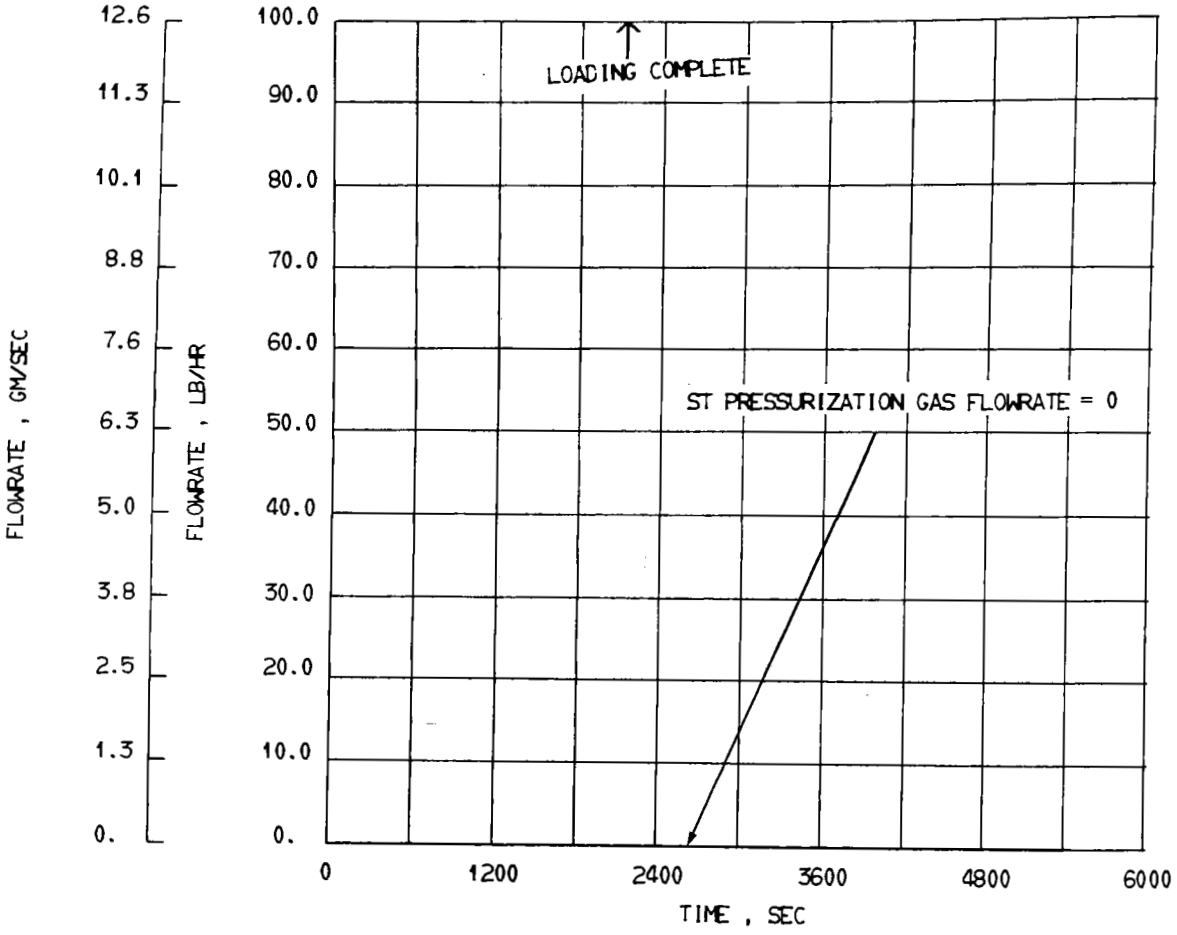

Figure 83.- Test Number 48 - Single Tank Loading with Liquid Nitrogen: Flowrate of Standpipe Tank Pressurization Gas

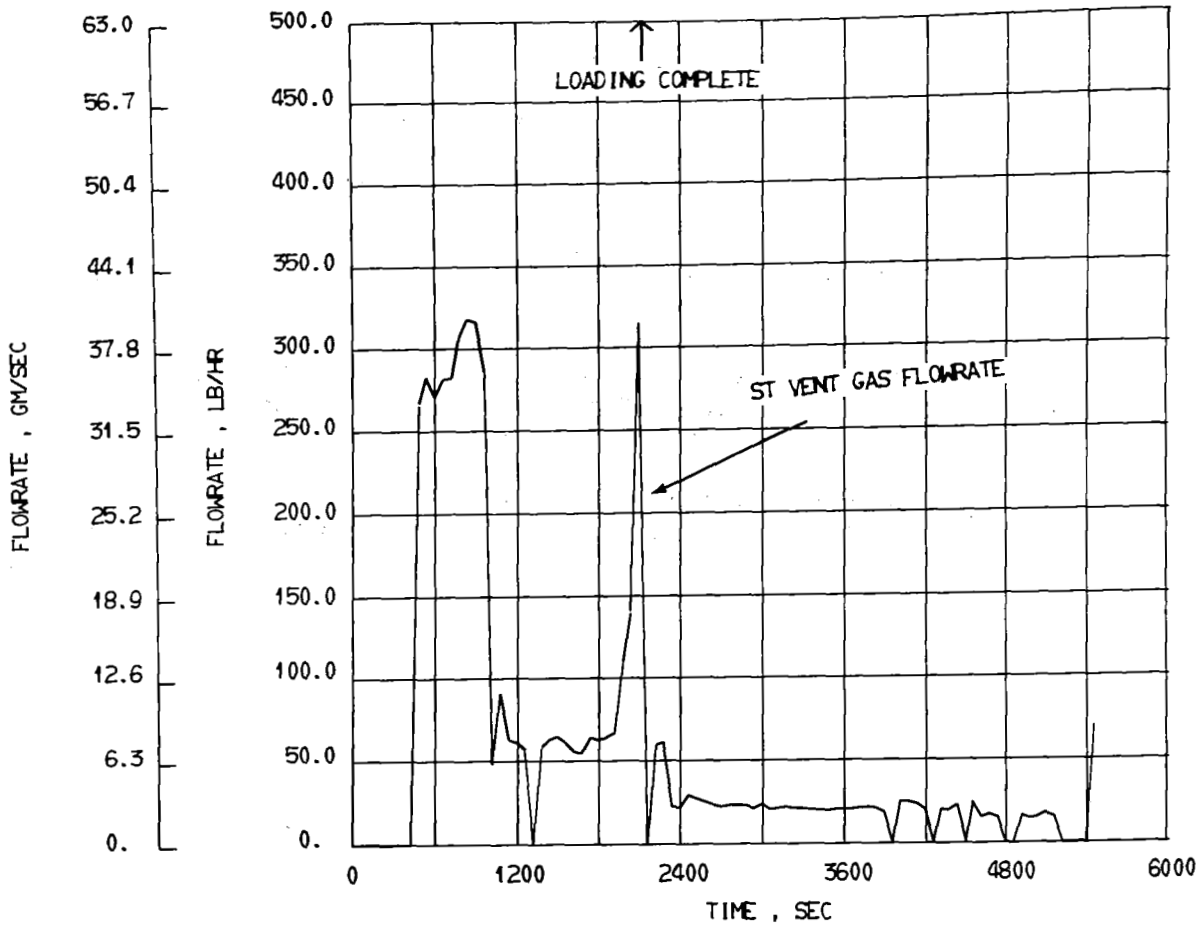

Figure 84.- Test Number 48 - Single Tank Loading with Liquid Nitrogen: Flowrate of Standpipe Tank Vent Gas

1. Test 49.- Test 49 was similar to Test 48, except thatthe standpipe tank was series-loaded. At the end of Test 48, the tank was vented to allow the liquid to cool down to loading temperature before starting the series loading for Test 49. Figure 85 shows the pressure in the standpipe tank. Again, not enough nitrogen pressurant was flowing into the supply dewar to maintain the desired pressure during loading, although it was established immediately after loading.

The standpipe tank temperatures (figure 86) show that the tank was loaded with vented liquid before the start of the series load. When loading was complete, there was no stratification from the top of the tank to the bottom because the supply dewar pressure had dropped to the point where the liquid was at saturation temperature. Shortly thereafter, the tank pressure was increased to 48 psia (33.1 N/cm^2), which left the liquid subcooled $6F^o$ ($3.3C^o$) with respect to the higher pressure.

As shown in figures 87 and 88, zero ullage was not achieved. Near the end of loading, however, the temperature of the inner layer of insulation at the top of the tank dipped momentarily to the temperature of the liquid.

Figure 89 shows that no pressurant gas was required during loading while figure 90 shows the relatively low rate of vent gas flow obtained in series loading.

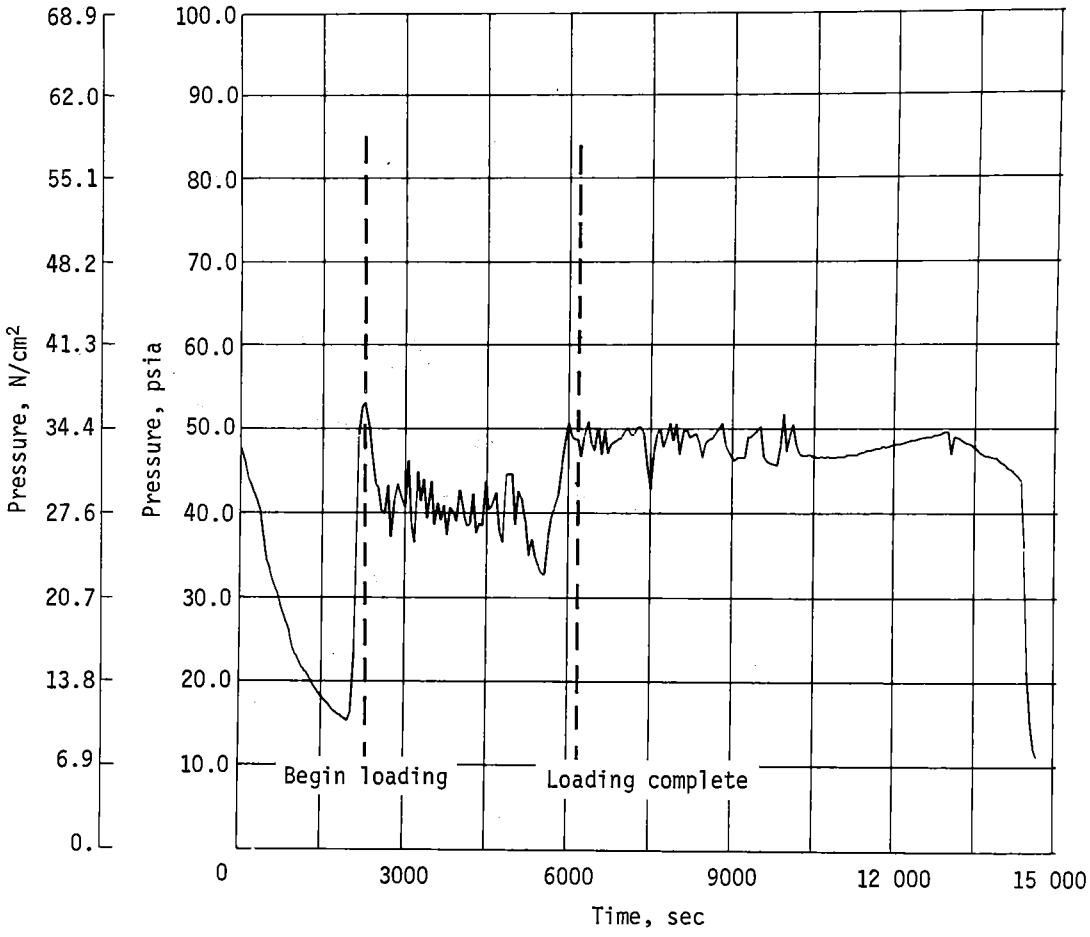

Figure 85.- Test Number 49 - Series Tank Loading with Liquid Nitrogen: Pressure at Top of Standpipe Tank

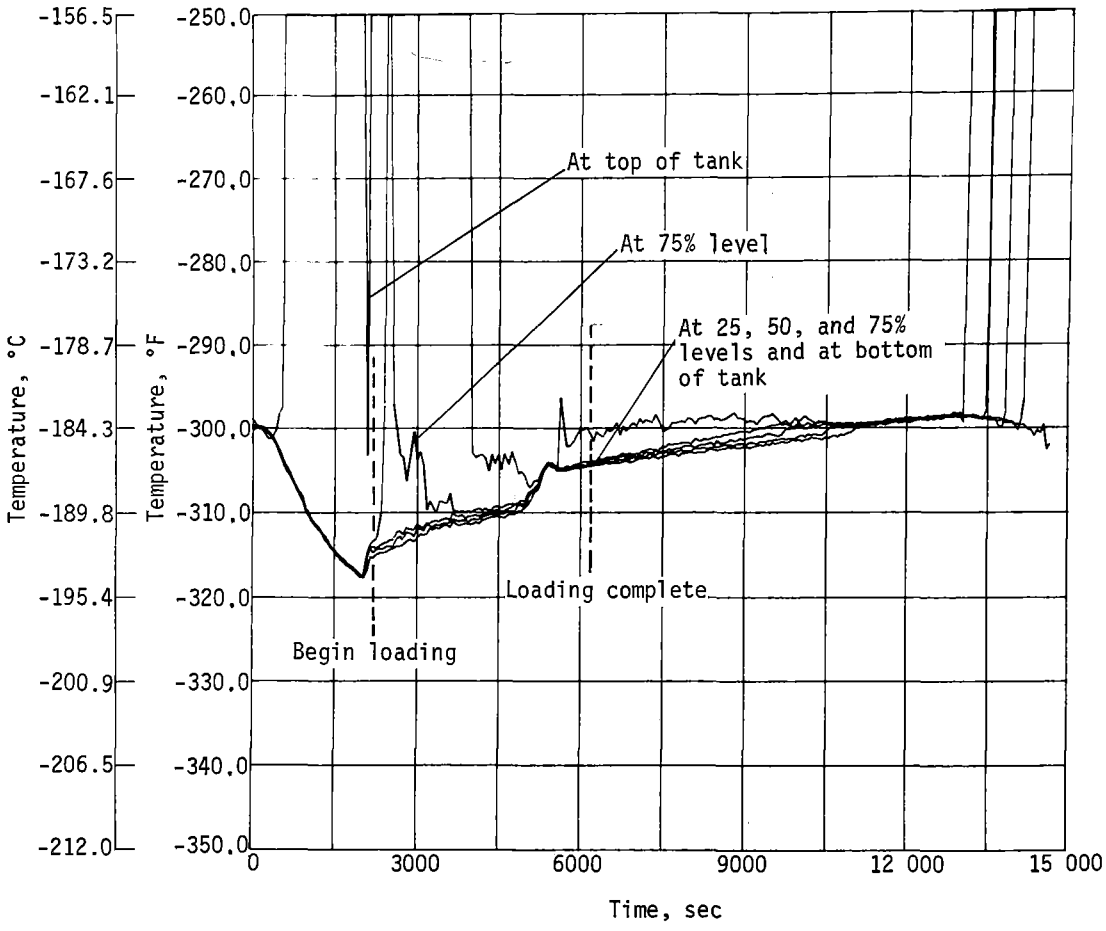

Figure 86.- Test Number 49 - Series Tank Loading with Liquid Nitrogen: Temperature of Liquid in Standpipe Tank

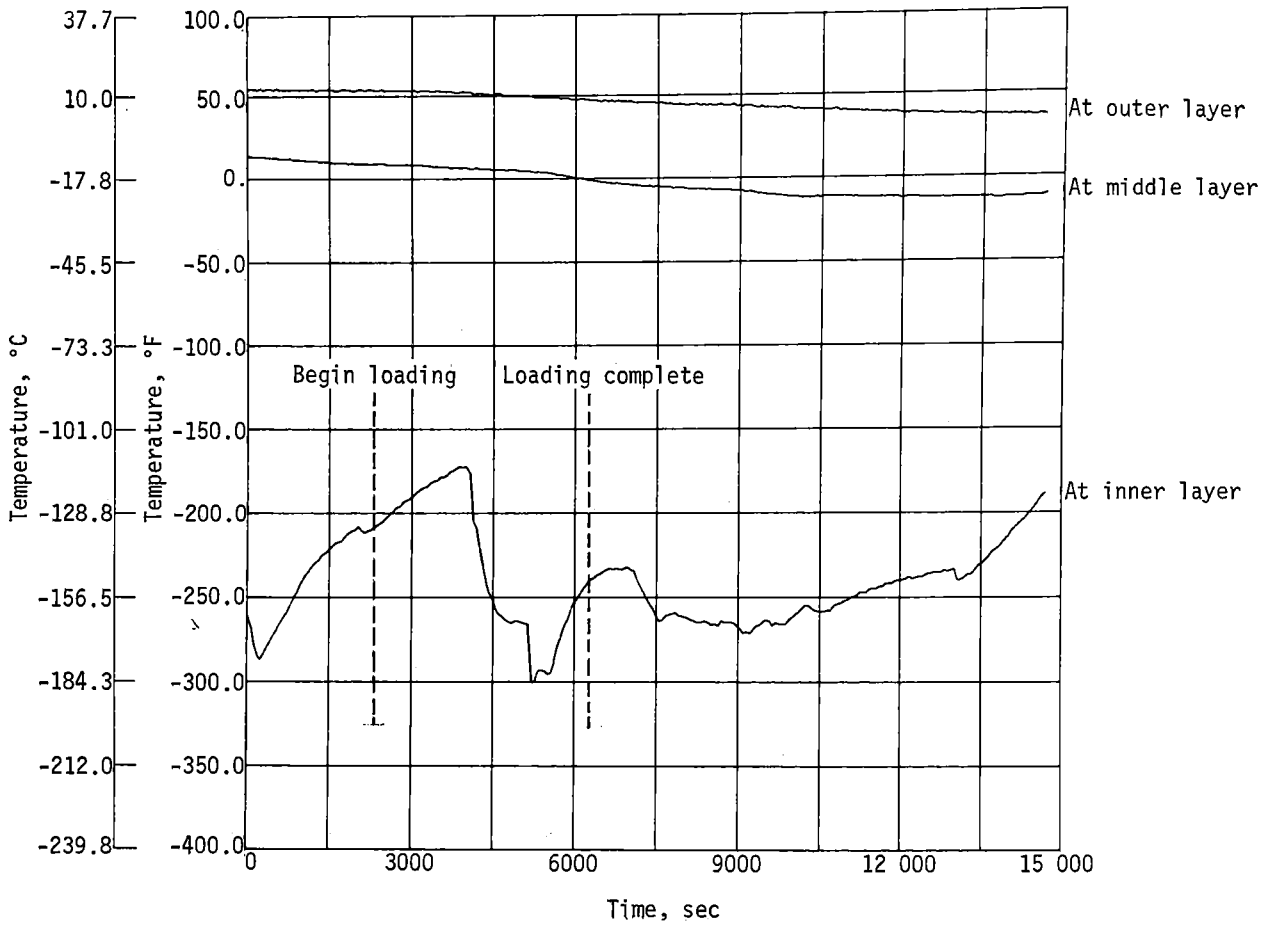

Figure 87.- Test Number 49 - Series Tank Loading with Liquid Nitrogen: Temperature of Insulation at Top of Standpipe Tank

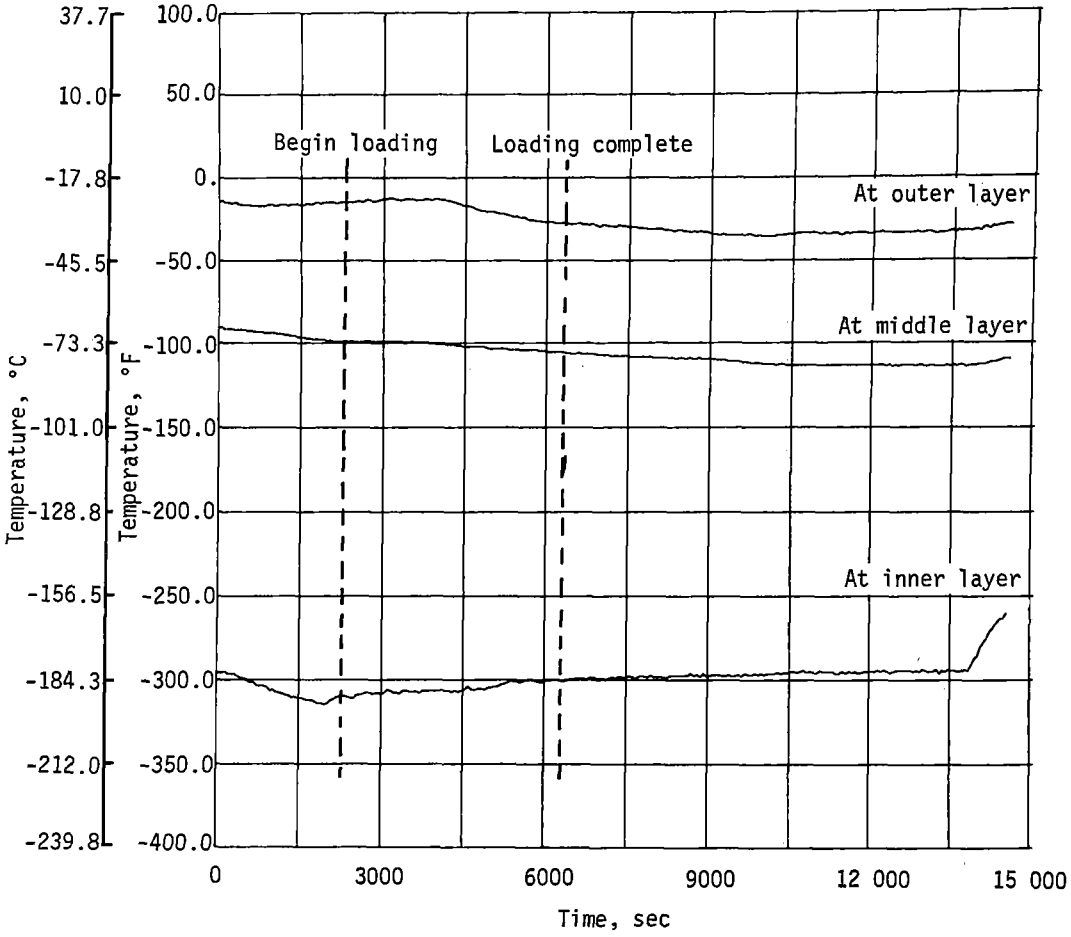

Figure 88.- Test Number 49 - Series Tank Loading with Liquid Nitrogen: Temperature of Insulation on Side of Standpipe Tank

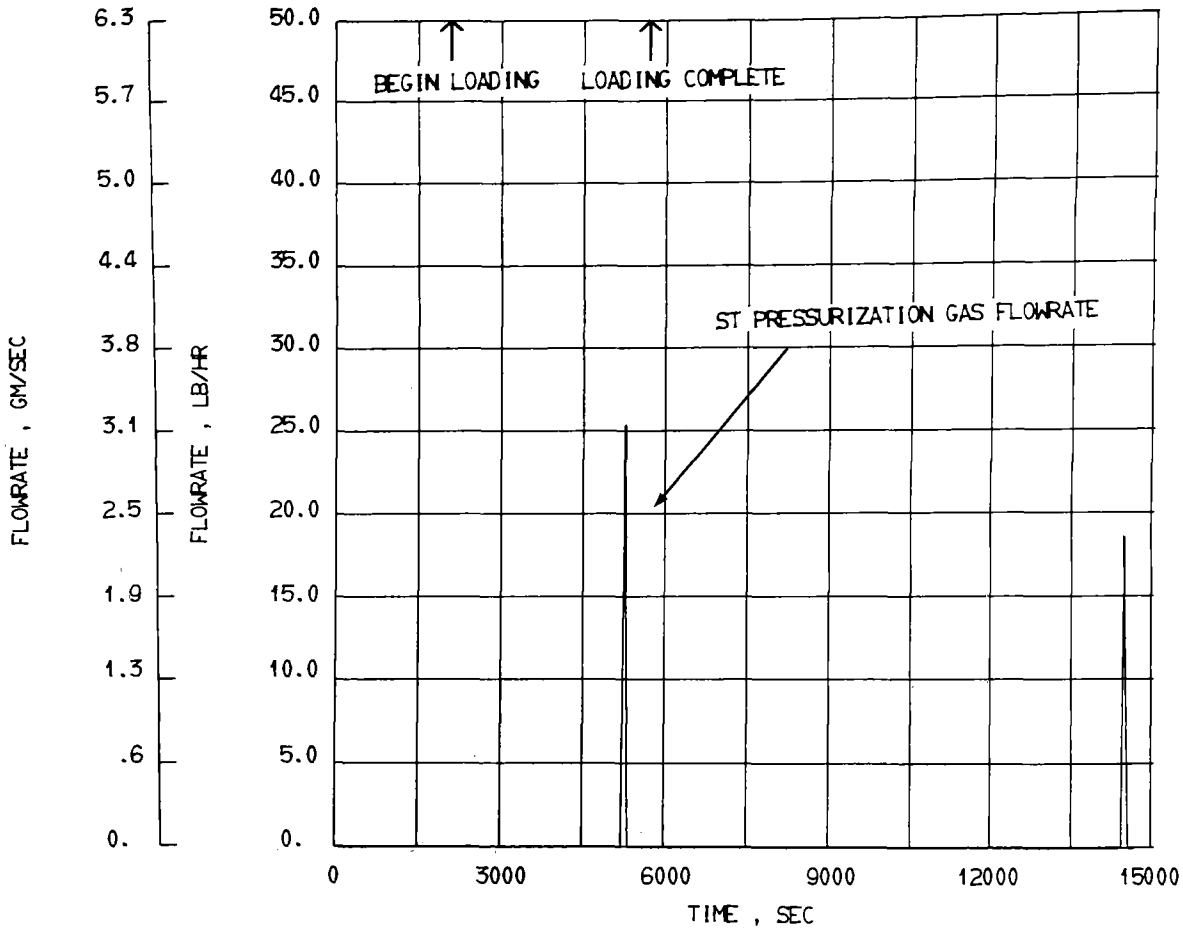

Figure 89.- Test Number 49 - Series Tank Loading with Liquid Nitrogen: Flowrate of Standpipe Tank Pressurization Gas

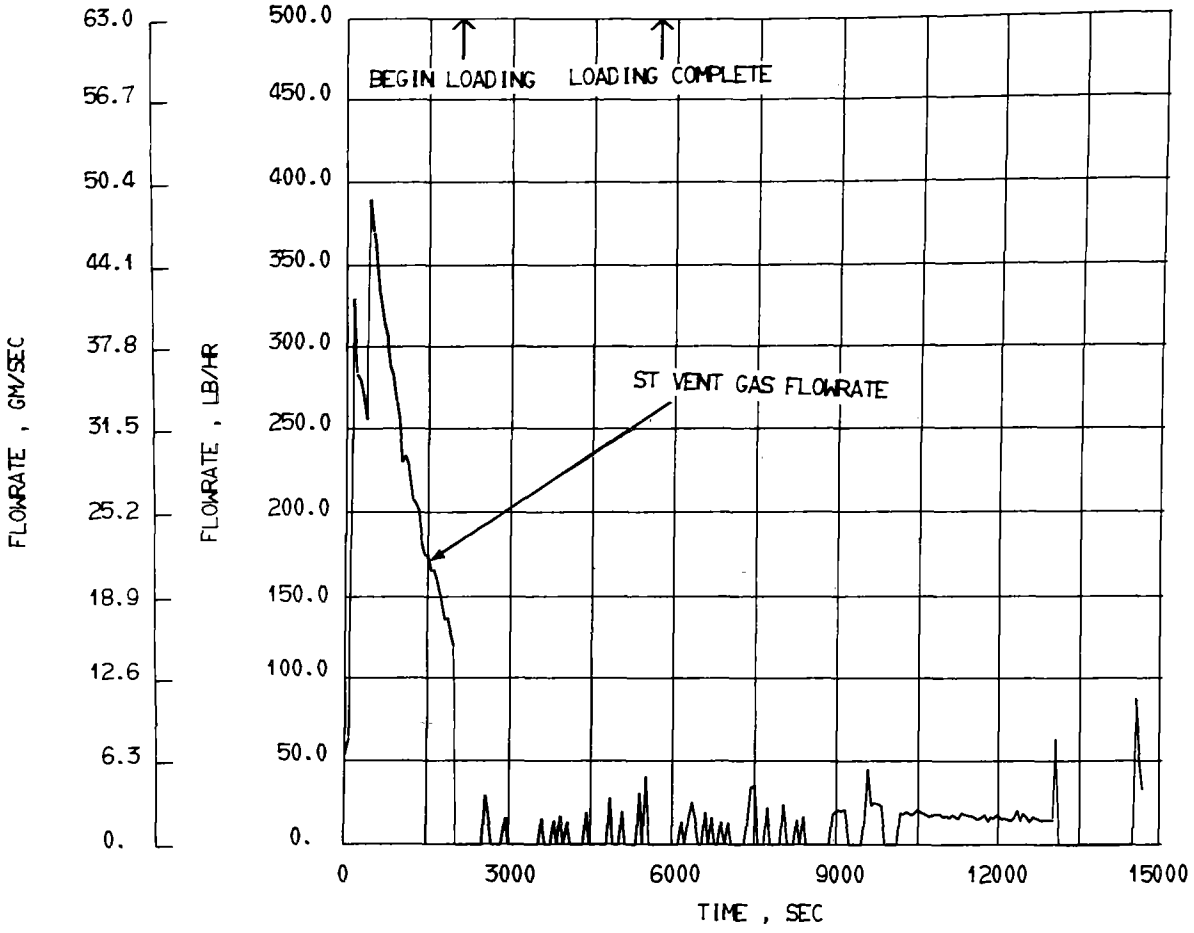

Figure 90.- Test Number 49 - Series Tank Loading with Liquid Nitrogen: Flowrate of Standpipe Tank Vent Gas

2. Test Summary

The standpipe tank loading tests addressed three major areas of concern, pressure control during loading, loading to zero ullage and obtaining maximum bulk subcooling in the loaded tank. Test results pertaining to these three areas are discussed below.

There were no significant problems uncovered during this test sequence associated with loading subcooled cryogens. The tests included loading a single ambient tank with and without a non-condensible pre-pressurization, loading a single precooled tank and loading four tanks in series through the test tank.

In all tests the tank continued to vent intermittantly throughout the loading and no pressurant gas was required. Stratification in the liquid was quickly established so that the liquid surface was at saturated conditions. This prevented gas condensation and the associated pressure collapse. Because of the equilibrating stratification there was no distinquishing differences between loading an ambient tank with no helium pre-pressurization (Test 1) and loading a tank after various degrees of helium pressurization (Tests 2 and 3).

There was no more difficulty in loading ambient tanks (tests 1, 2 and 3) than there was loading pre-cooled tanks (tests 4, 5 and 6). There was considerably more difficulty in maintaining pressure in a series load than was prevalent in a single tank loading under the same conditions. This is evident by comparing tests 38 and 39, 40 and 41, or 48 and 49. However, the pressure control problem during series loading was due to the size of the source dewar used for supplying the test tanks. The source dewar volume was essentially the same size as the total volume of the four test tanks. Thus during a series load the ullage volume in the supply dewar became very large and it was difficult to maintain pressure.

Zero ullage in the standpipe tank was never completely accomplished. To determine whether or not zero ullage was accomplished the tank skin temperature at the top and on the side were compared. The only time zero ullage seemed to be approached was during the series load in test 39 (figure 65). In this test the upper skin temperature briefly approached liquid temperature just as loading was completed. The temperature almost immediately increased again. This brief cooling was attributed to liquid entrained in the gas.

In analyzing the data with respect to bulk subcooling the two most important parameters are the total magnitude of stratification and the temperature profile in the liquid. The total stratification is an indication of the amount of energy required to bring the liquid to saturated condtions. The liquid temperature profile is an indication of heat transfer mechanism within the liquid, i.e. the degree of liquid mixing. The most desirable profile in this instance is one in which most of the stratification takes place near the liquid surface.

In the first three tests where ambient tanks were loaded with and without pre-pressurization with a noncondensible gas (helium), there appeared to be no difference in the stratification (figs. 27 and 34). The maximum subcooling was about $10^{\circ}F$ ($5.55^{\circ}C$)

In tests 4, 5 and 6 pre-cooled tanks were loaded with the expected result of somewhat more maximum subcooling, 10°F (5.55°C) to 15°F (8.33°C). The notable difference between these three runs is the liquid temperature profile of test 5 (fig. 43) compared to tests 4 and 6 (figs. 38 and 49). As can be seen the temperature profile is much more pronounced at the surface in tests 4 and 6. It is noted that in test 5 the tank pressure was not controlled as well as in the other two tests and that in the middle of the loading sequence a pressure decrease of more than 6 psi (4.14 N/cm^2) occurred. This was the first evidence that pressure control was extremely important to the amount and character of the liquid stratification obtained. This point is dramatically emphasized in comparing the stratification and pressure curves in tests 38 and 39 or tests 40 and 41. As pointed out earlier, the pressure control in tests 39 and 41 was poor due to the large source dewar ullage during series loading. This resulted in essentially no stratification.

Table 7 shows the amount and shape of stratification in each loading test immediately after loading was completed. Without exception the tests where the ratio of the stratification above the 75% level to the total stratification is lowest the tank pressure control was poor.

Although pre-pressurization of the tanks with a non-condensible gas did not appear to be needed for pressure control during loading injection of a non-condensible after loading the tanks did significantly affect the liquid subcooling. This was noted in test 40. At completion of loading there was significant stratification with the liquid surface being at the saturation temperature consistant with the tank pressure. The liquid surface temperature began to decrease as helium was injected.

TABLE 7 - LIQUID STRATIFICATION AT COMPLETION OF LOADING

TEST #	ΔT 90-75%	ΔT 90-50%	ΔT 90-7%	$\frac{\Delta T\ 90\text{-}75\%}{\Delta T\ 90\text{-}7\%}$
1	6.1	6.7	9.3	.66
2	4.2	9.6	10.2	.41
3	-	-	-	-
4	11.8	13.	14.8	.79
5	5.8	10.	10.6	.55
6	10.6	11.1	11.1	.95
38	15.2	17.2	18.1	.84
39	0.5	1.7	3.6	.13
40	15.8	20.4	21.6	.73
41	0.0	0.0	.2	.00
48	1.3	8.9	10.1	.13
49	.9	2.7	3.0	.3

B. HOLD AND TAXI TESTS

The need to investigate hold and taxi operations for aircraft using liquid methane fuel arises from the potential tank gas pressure collapse problem; thus, the primary objective of the hold and taxi tests were to determine the effect on tank gas pressure of a taxi manuever following a long quiescent period, and whether these pressure effects could be reduced or eliminated using specially designed tanks. In order to accomplish these objectives, each of the four tank configurations was tested with various ullage volumes and slosh levels. All tests attempted to simulate the actual conditions experienced in an aircraft during ground hold and taxi operations.

1. Test Description and Data

Each of the low pressure tanks was tested full and between 5 and 25% full. One additional test was performed on the foam tank with a 50% ullage to complete the picture of the effect of ullage volume. The test procedure was the same for each tank and consisted of filling the tanks to the desired levels and holding until thermal equilibrium was established, moderately sloshing along the longitudinal axis, holding until thermal equilibrium was re-established, violently sloshing along the longitudinal axis, holding for 1 hour, and again violently sloshing along the longitudinal axis. Each slosh period lasted 5 minutes.

The standpipe and high-pressure tanks were locked-up after loading and the pressure was allowed to increase to 36 and 62 psia (24.8 and 42.7 N/cm^2) respectively, before being maintained at these levels by venting. The high-pressure tank was tested at both the 96 and 50% liquid levels, while the guard tanks were filled to 90% and vented throughout each test.

Moderate and violent slosh levels are, of course, a function of liquid level and internal tank configuration. That is, the frequency and amplitude necessary to produce a violent slosh in an open tank would be different for a baffeled tank, and similarly for the same tank filled to different levels. To facilitate the comparison of the different tank configurations the standpipe tank filled to the 90% level was selected for defining moderate and violent slosh frequencies and amplitudes to be used with all tanks and liquid levels. The standpipe tank was equipped with nichrome wire sensors near the 90% level that essentially served as high-response, liquid-level sensors. After the tank was filled to the 90% level, the frequency at the first slosh mode was determined and the amplitude of the slosh actuator was varied to provide moderate and violent levels of liquid action. Moderate sloshing was defined as slight surface agitation in the tank with 10% ullage (i.e., sloshing in which the liquid just covers and uncovers the sensor). Violent sloshing was defined as sloshing at the same first mode frequency, but with enough force to wet the ends and top of the tank. Wetting was verified by observing the drop in temperature at the top skin of the tank.

a. Standpipe tank tests.

1) Test 7: After being fully loaded, the standpipe tank was sloshed at the moderate level for 5 minutes. Since the sloshing caused no noticeable change in the tank pressure, the thermal equilibrium was not upset and the planned wait for re-establishment of equilibrium was meaningless. Instead, the tank was held stable for 30 minutes before the first violent slosh.

As shown in figure 91, there was no effect on tank pressure from either the moderate or violent slosh level. During the first and third sloshes, tank pressure was rising before and during the sloshes at the same rate. We had some difficulty holding the tank pressure constant, which might have masked a subtle effect from sloshing, but not any appreciable pressure rise or collapse.

Figure 92 shows the temperature plots for the liquid at various levels in the tank. These data show no significant mixing of the various levels as a result of the sloshing. A possible exception might be during the moderate slosh when the tank top and 75% level liquid temperatures move together as if the liquid levels were mixing; however, this tendendancy did not reoccur during either violent slosh.

The high-pressure tank, which was 96% full during the test, was also examined for slosh effects. The tank pressure curve (figure 93) shows no appreciable change during the moderate slosh, but shows pressure decreases during each of the violent sloshes. The first violent slosh occurred before tank pressure had reached 62 psia, (42.7 N/cm^2) and thus the tank vent had not been opened yet. This observation affirms that the 3 psi (2.1 N/cm^2) pressure drop was due to sloshing rather than tank venting. The second violent slosh occurred concurrently with a pressure drop of 5 1/2 psi (3.8 N/cm^2), although it appears likely that some of the decrease was due to venting, as the pressure curve was nearing the 62 psia (42.7 N/cm^2) level just prior to the slosh.

The tank liquid temperature curves are shown in figure 94. The tank top liquid temperature dips about 1 or 2F° (0.56 or 1.11C°) during each of the violent sloshes.

Evidence of the physical sloshing inside the tanks was offered by one set of insulation temperatures on top of the high-pressure tank, figure 95. The inner layer thermocouple was located against the skin on top of the tank at the tangency point of the dome and barrel section. A lesser effect was noted at the moderate slosh level, but there were significant skin temperature drops during violent sloshing.

The pressurization and vent flowrate curves for the standpipe tank are shown in figures 96 and 97, respectively; and the vent flowrate for the high-pressure tank is shown in figure 98.

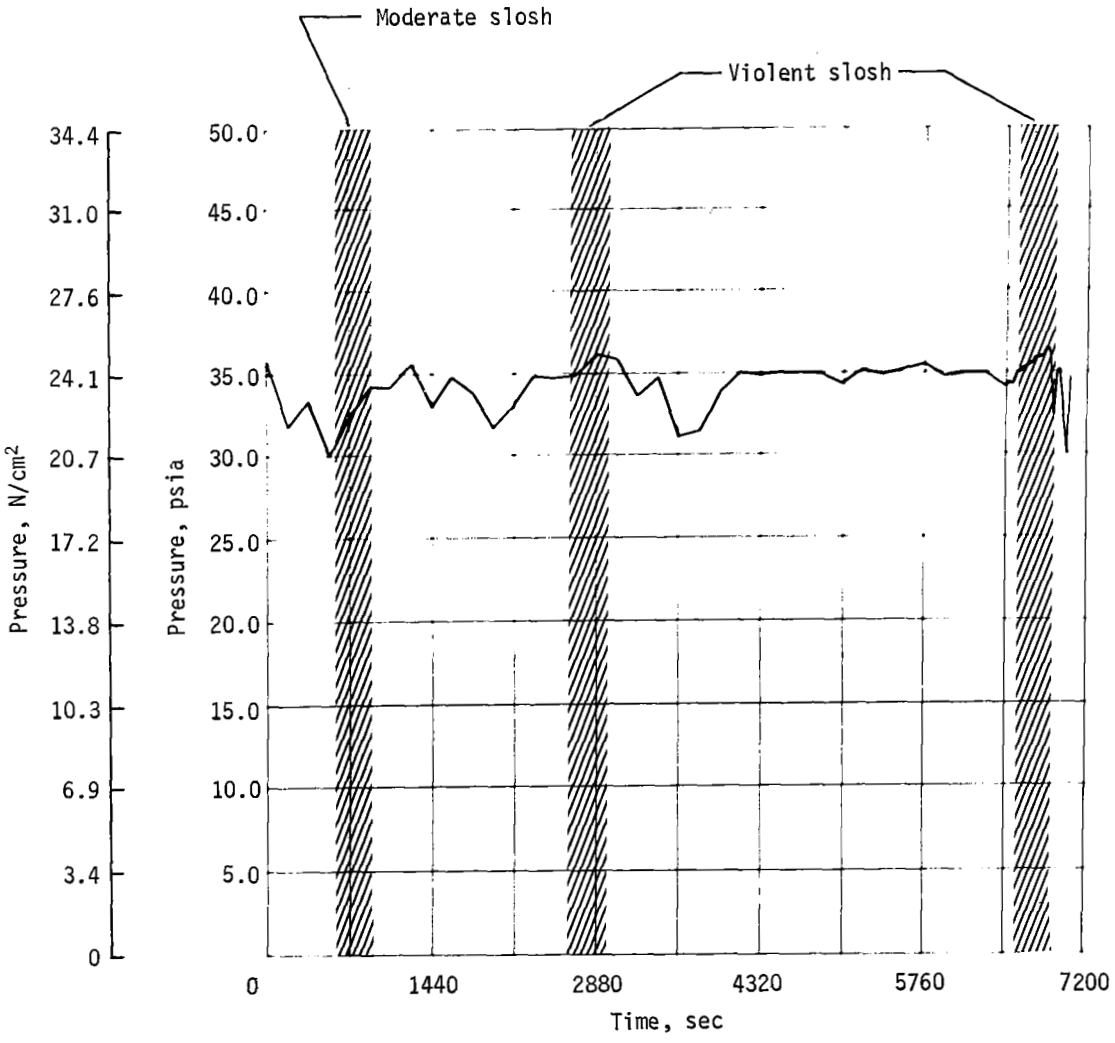

Figure 91.- Test Number 7 - Ground Hold and Taxi: Pressure at Top of Standpipe Tank

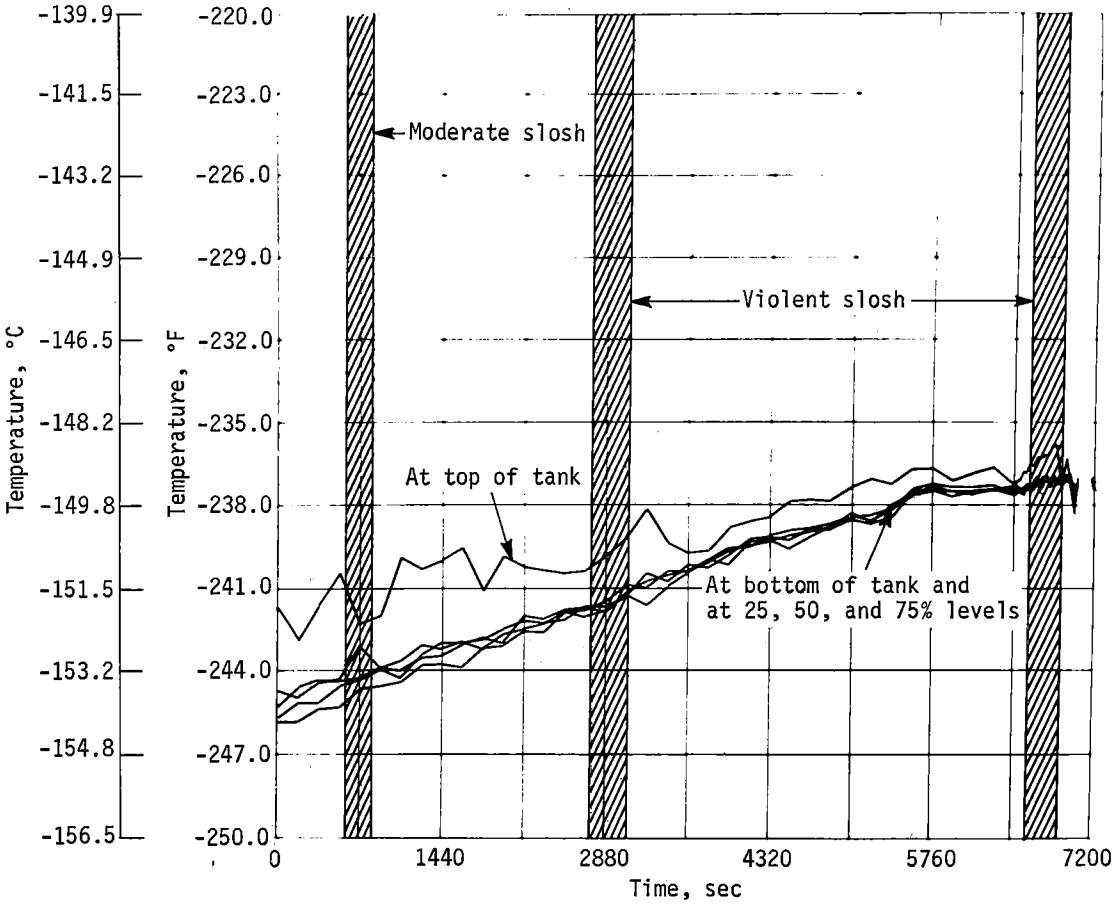

Figure 92.- Test Number 7 - Ground Hold and Taxi:
Temperature of Liquid in Standpipe Tank

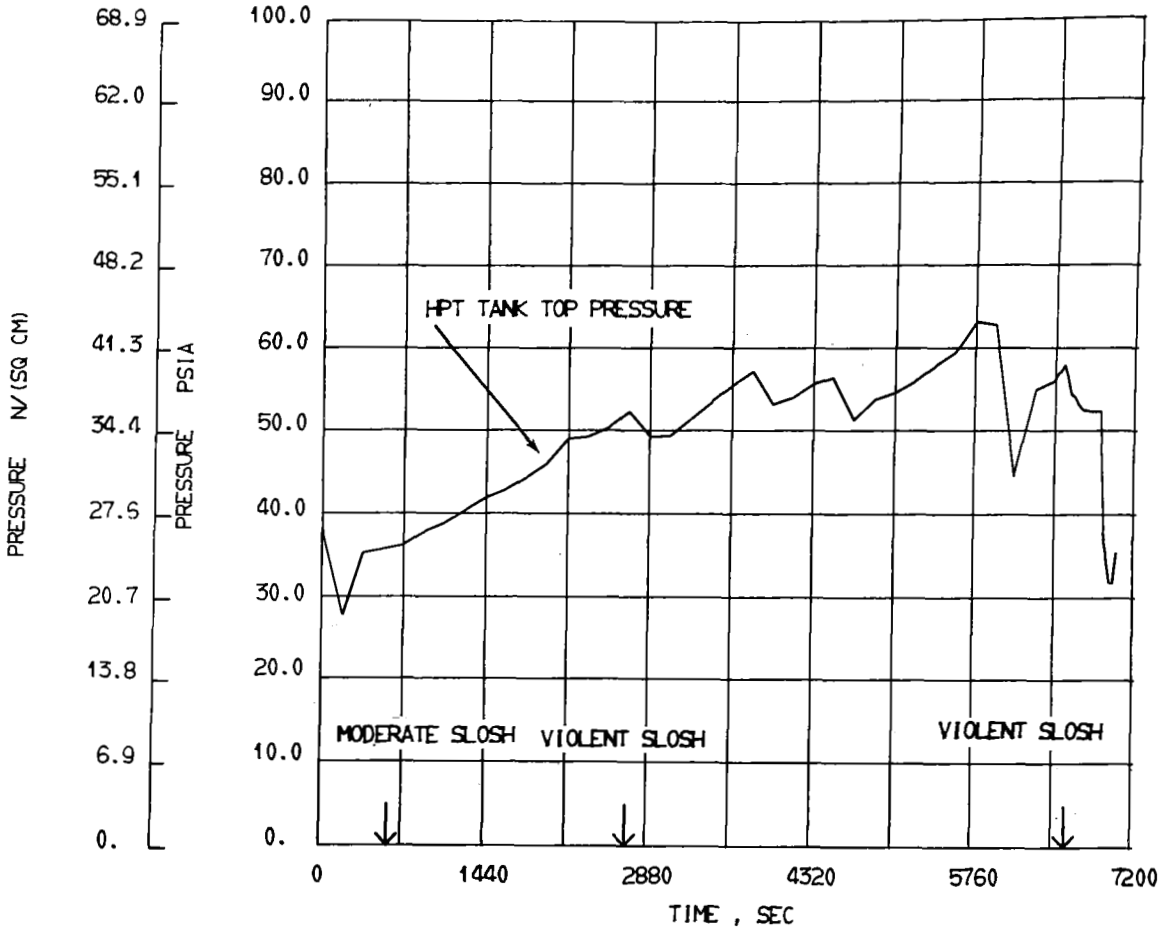

Figure 93.- Test Number 7 - Ground Hold and Taxi: Pressure at Top of High-Pressure Tank

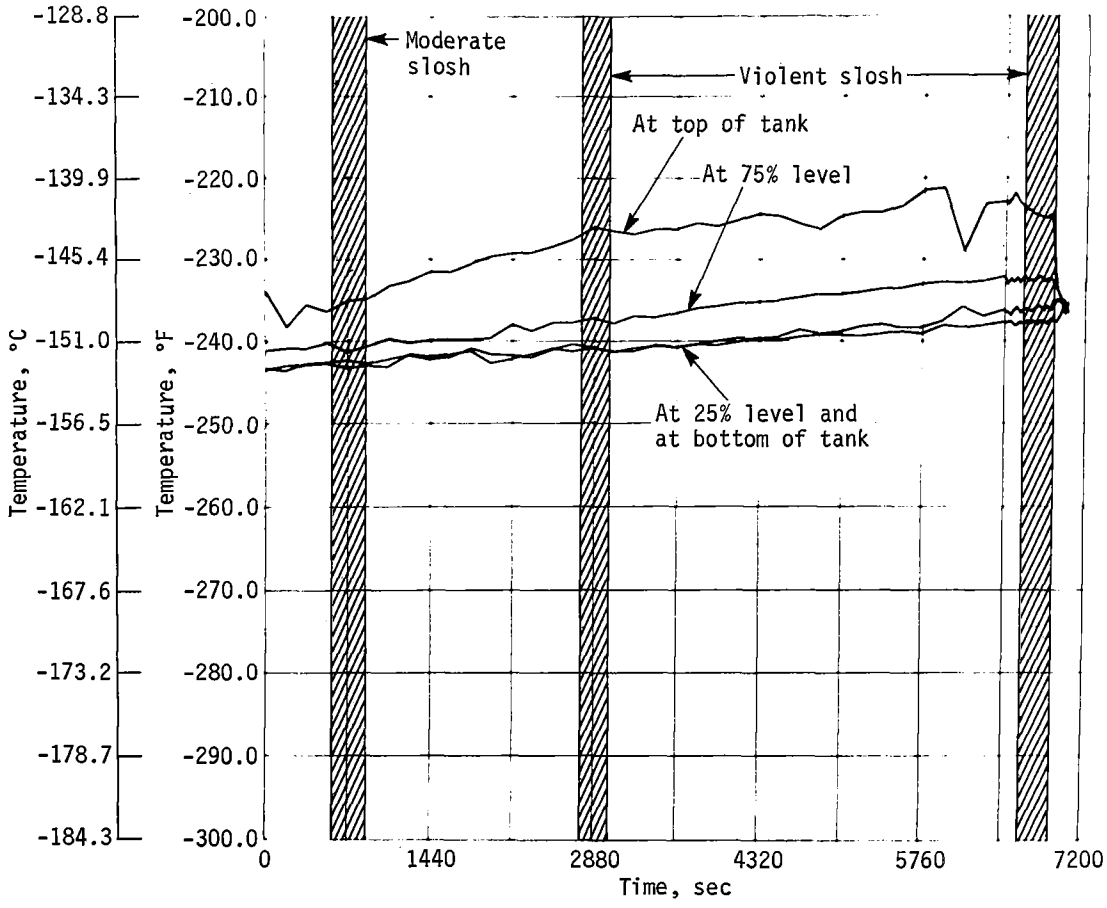

Figure 94.- Test Number 7 - Ground Hold and Taxi: Temperature of Liquid in High-Pressure Tank

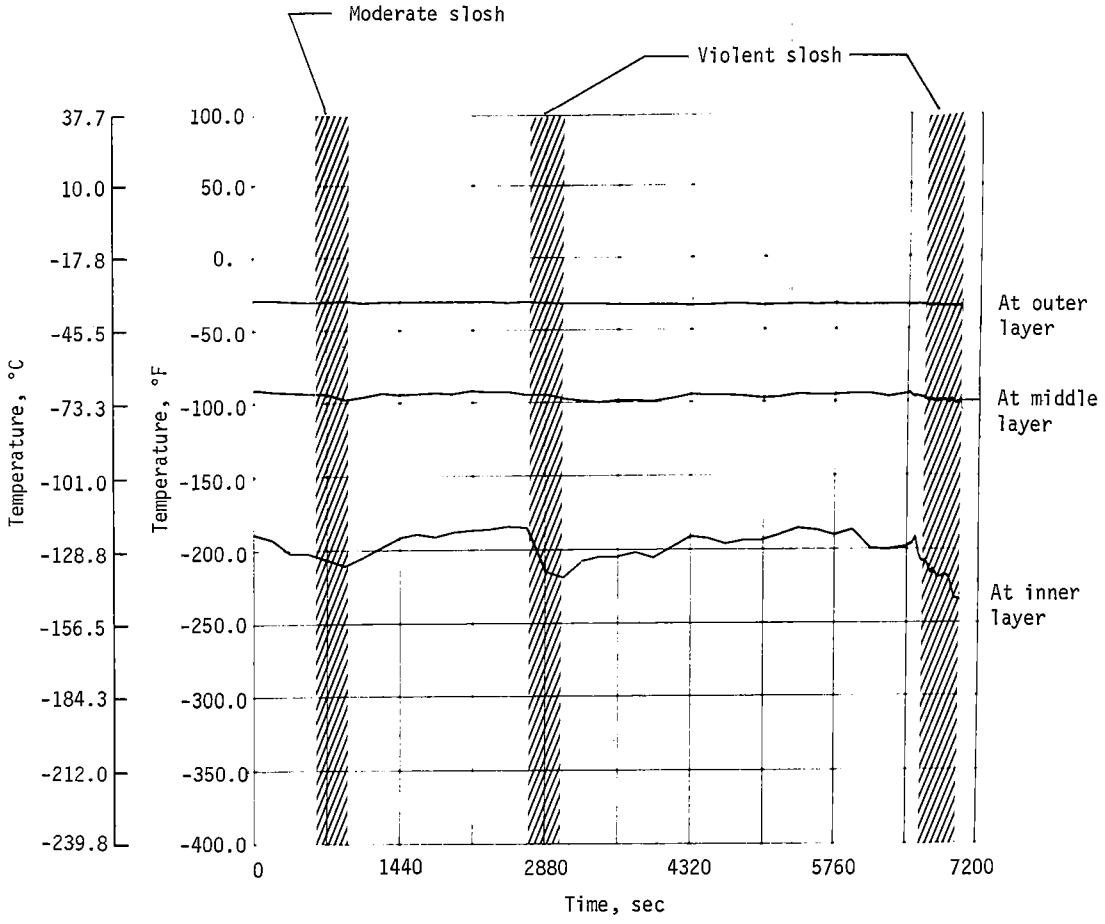

Figure 95.- Test Number 7 - Ground Hold and Taxi: Temperature of Insulation at Top of High-Pressure Tank

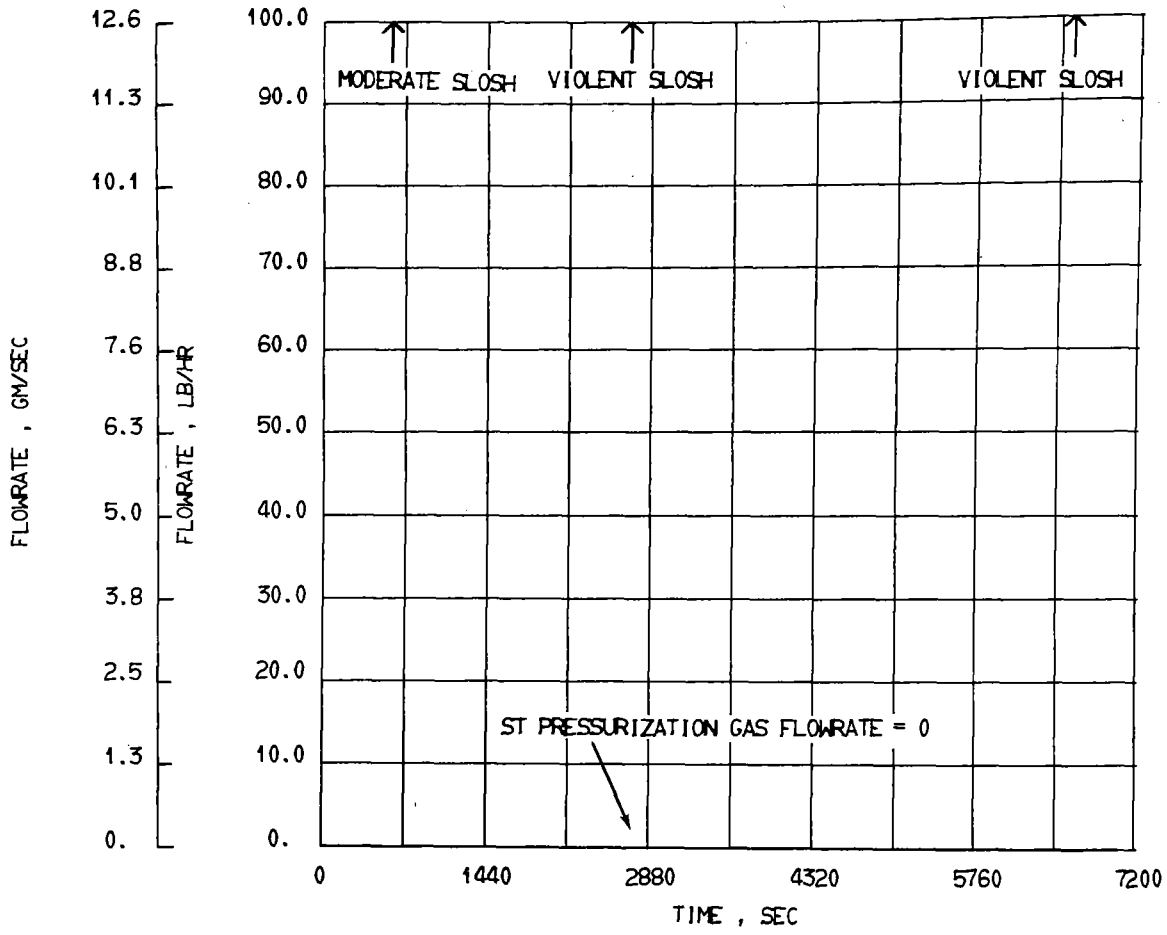

Figure 96.- Test Number 7 - Ground Hold and Taxi:
Flowrate of Standpipe Pressurization Gas

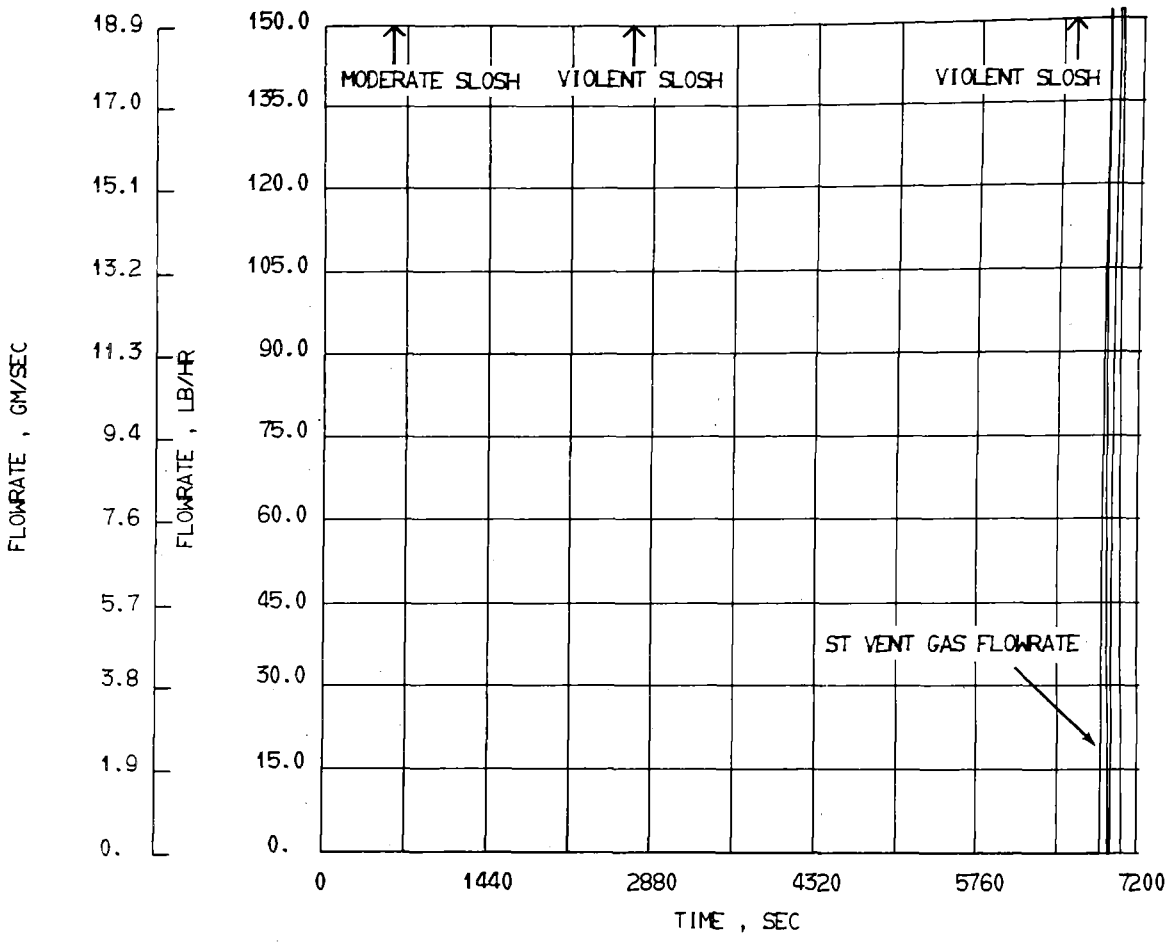

Figure 97.- Test Number 7 - Ground Hold and Taxi:
Flowrate of standpipe Vent Gas

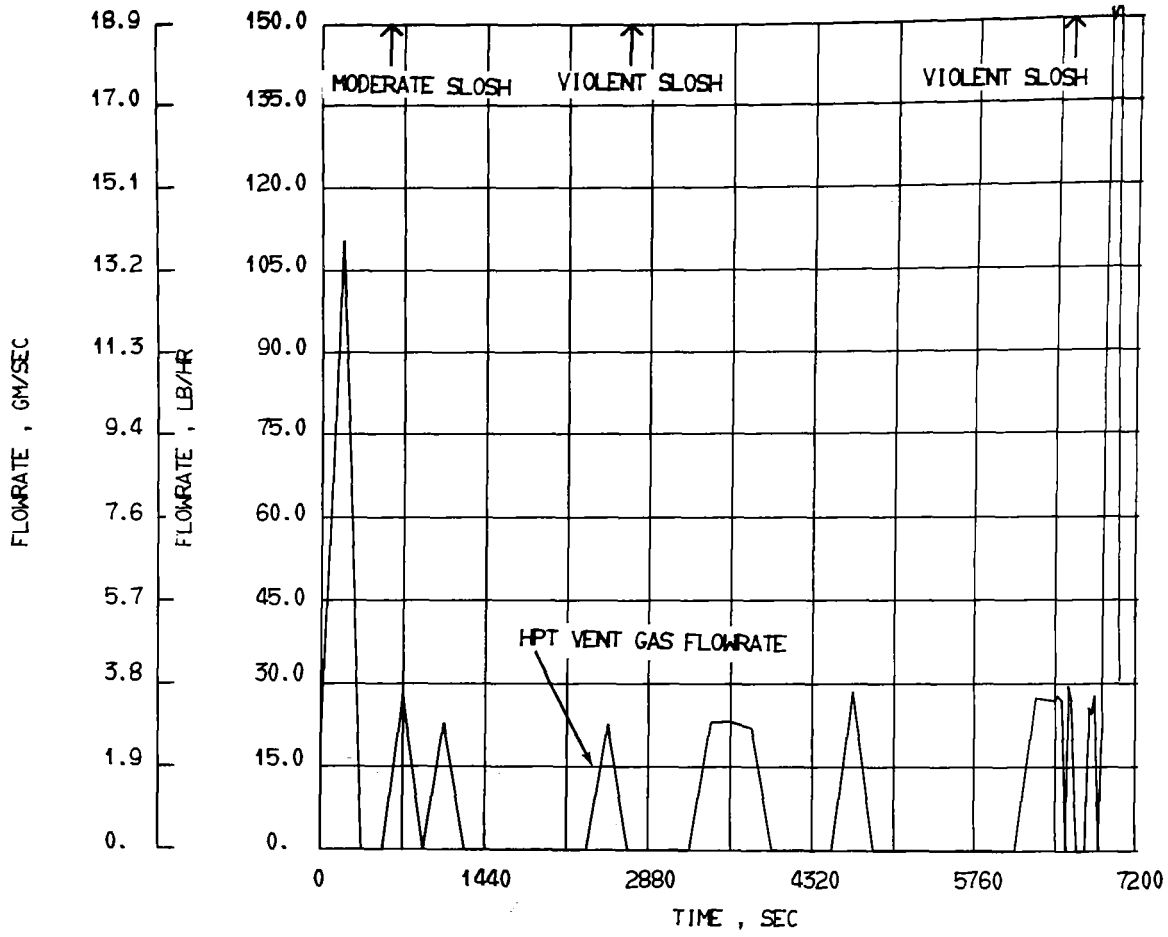

Figure 98.- Test Number 7 - Ground Hold and Taxi: Flowrate of High-Pressure Vent Gas

2) Test 8: For this test, the standpipe tank was filled to between 5 and 25% and the high-pressure tank was filled to 50%. No effect on tank pressures or liquid temperatures was noted for either tank during any of the three slosh periods (fig. 99 through 102). Figure 103 shows the gas temperature throughout the ullage and the negligible mixing during sloshing.

During the hold between the first two slosh periods, a problem arose in the test cell and the tanks had to be vented so personnel could safely enter the area. This reduced the temperature of the liquid at the bottom of the standpipe tank by 13F^{o} (7.2C^{o}) and that at the 25% level in the high-pressure tank by 5F^{o} (2.8C^{o}).

The pressurization and vent flowrate curves for the standpipe tank are shown in figures 104 and 105, respectively; and the vent flowrate for the high-pressure tank is shown in figure 106.

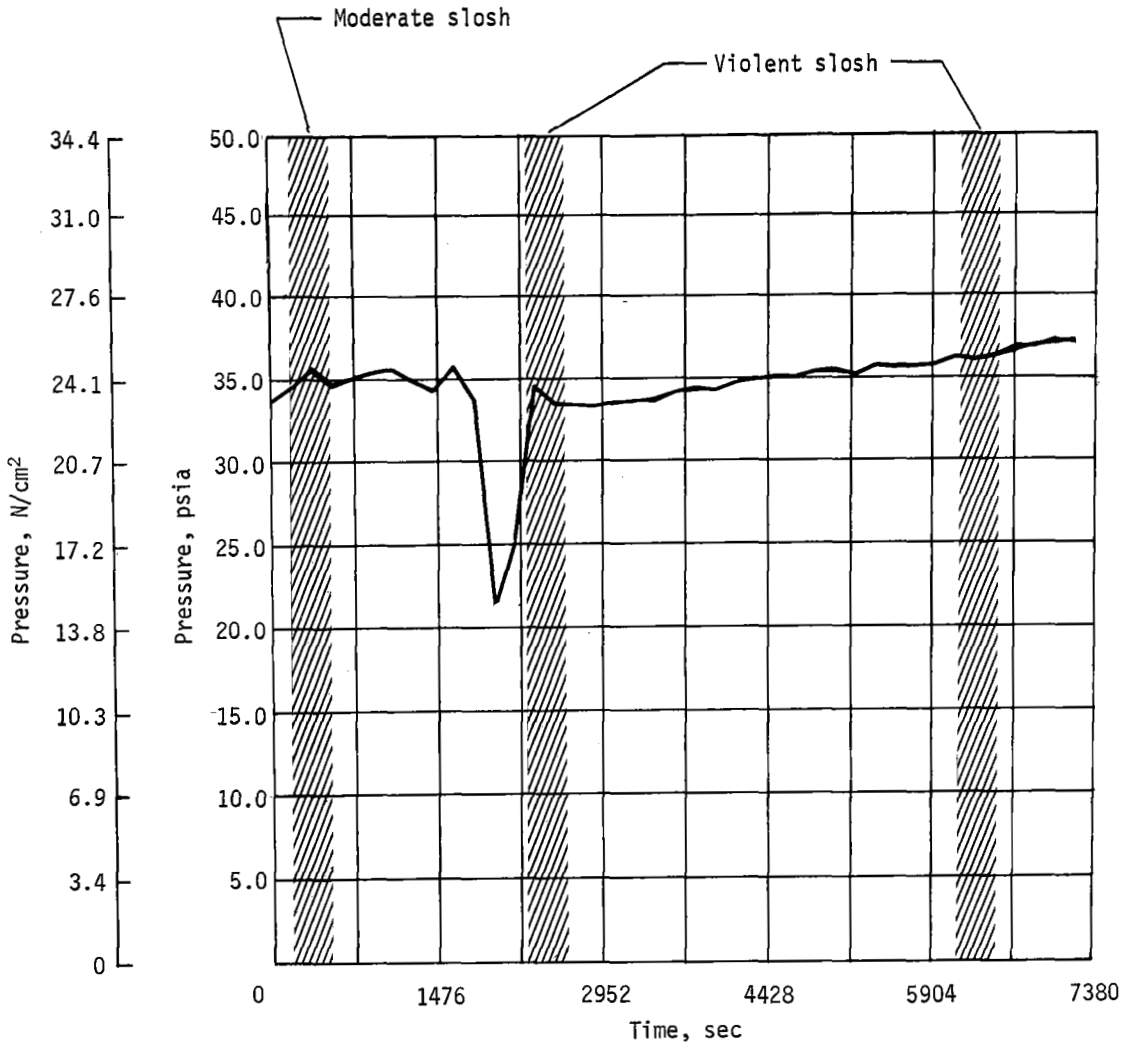

Figure 99.- Test Number 8 - Ground Hold and Taxi: Pressure at Top of Standpipe Tank

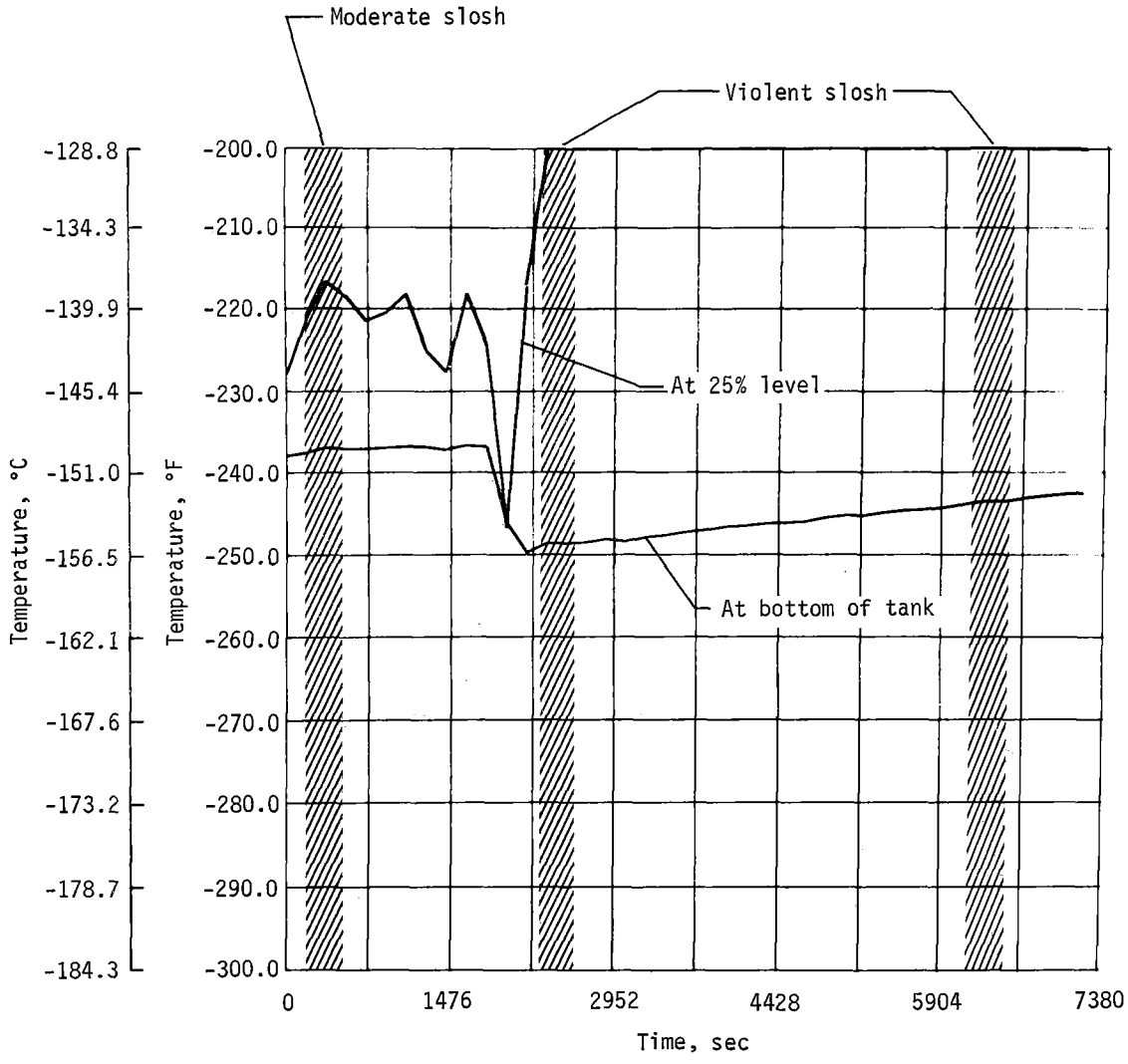

Figure 100.- Test Number 8 - Ground Hold and Taxi:
Temperature of Liquid in High-Pressure Tank

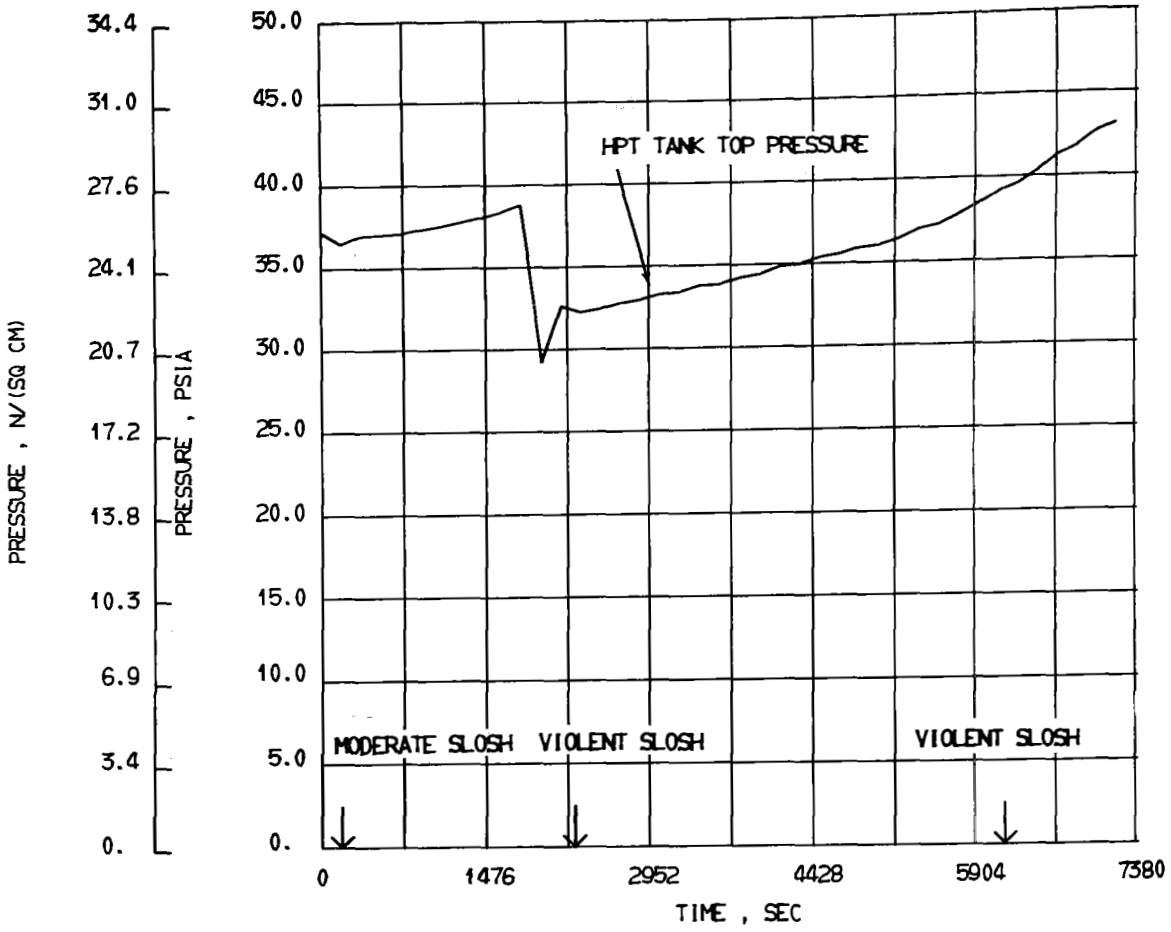

Figure 101.- Test Number 8 - Ground Hold and Taxi: Pressure at Top of High-Pressure Tank

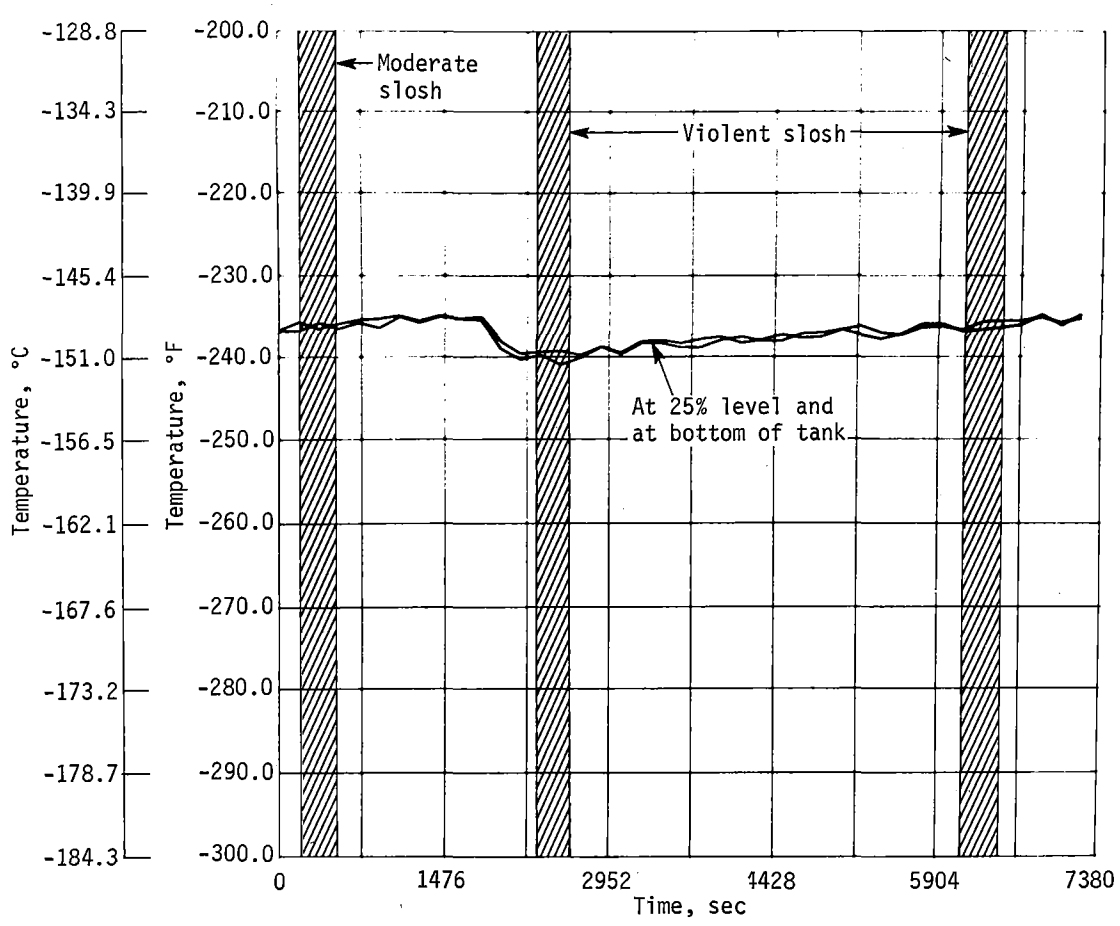

Figure 102.- Test Number 8 - Ground Hold and Taxi: Temperature of Liquid in High-Pressure Tank

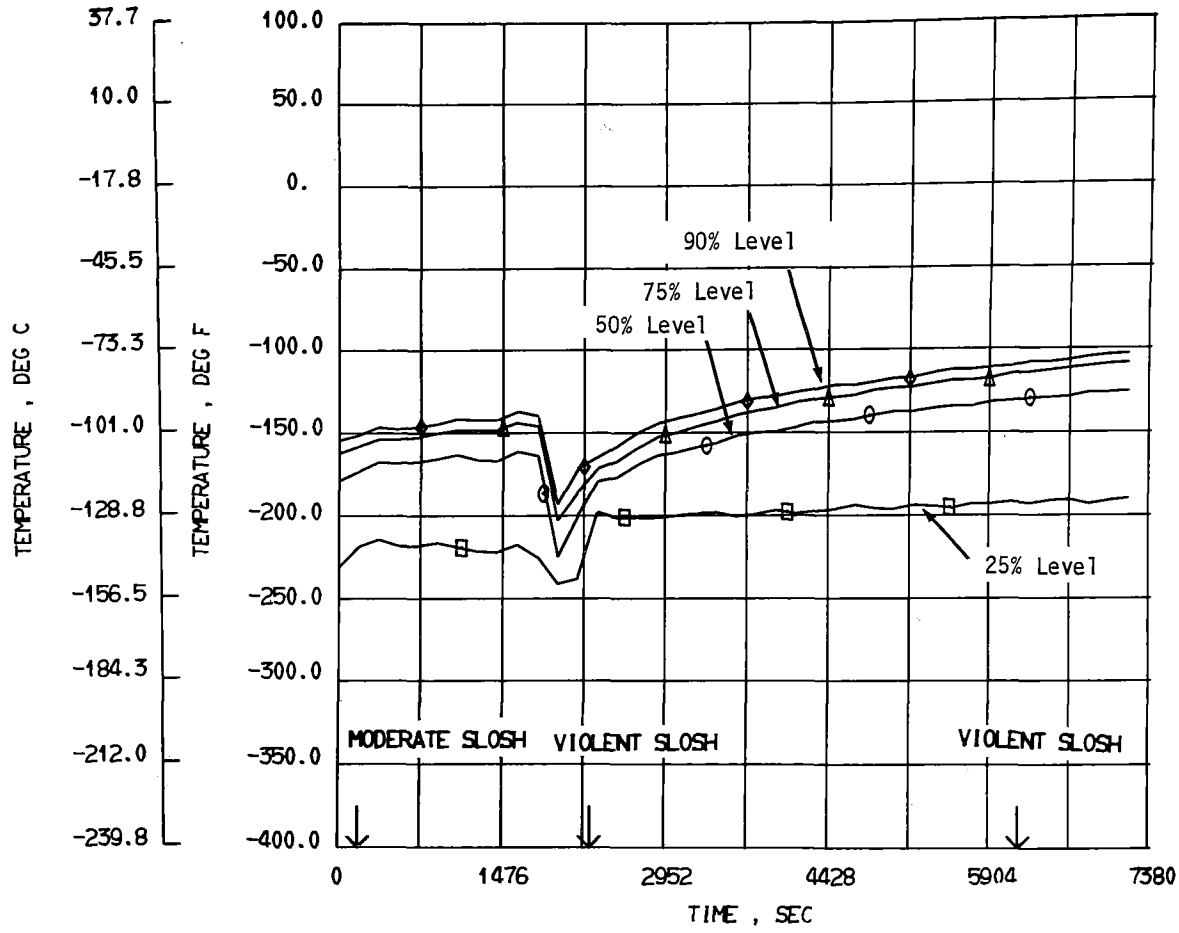

Figure 103.- Test Number 8 - Ground Hold and Taxi: Temperature of Gas in High-Pressure Tank

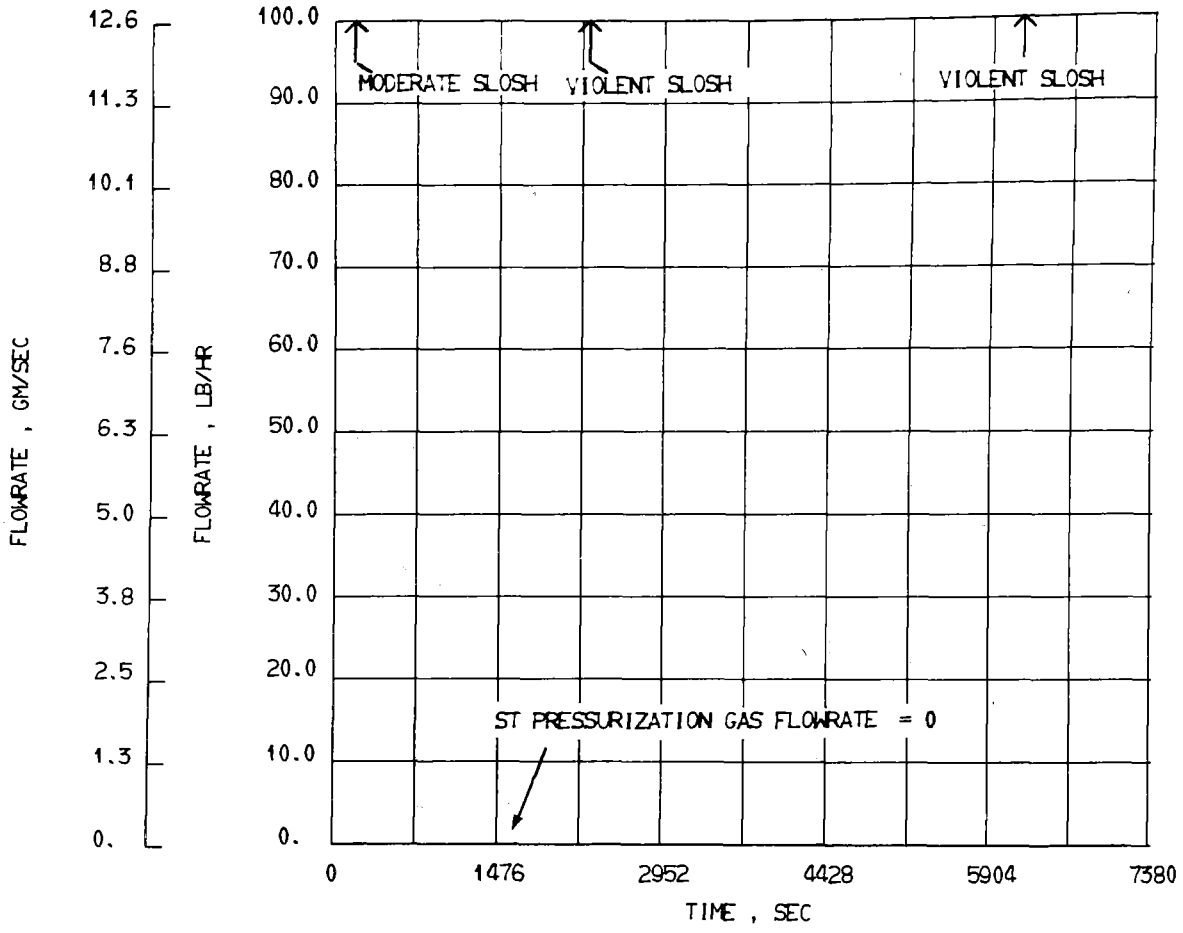

Figure 104.- Test Number 8 - Ground Hold and Taxi:
Flowrate of Standpipe Tank Pressurization Gas

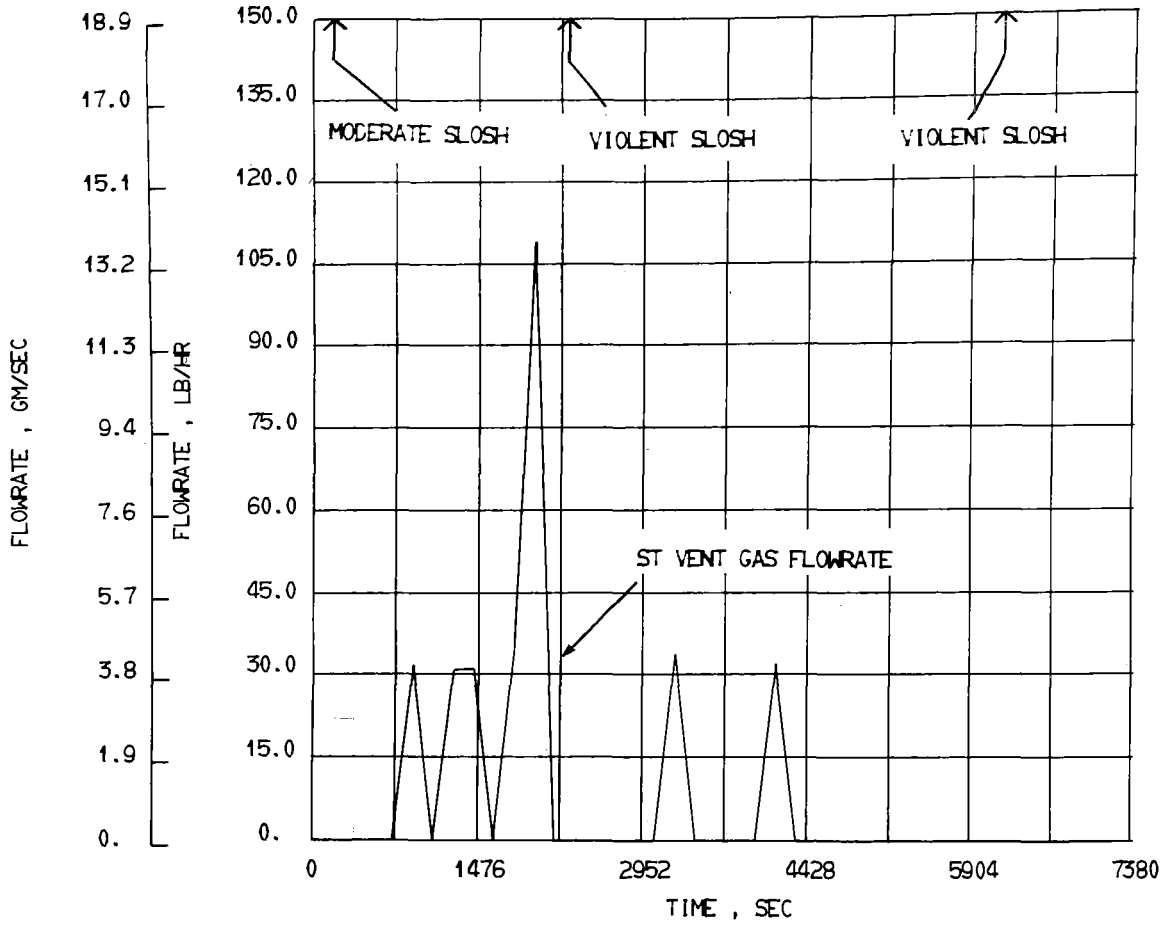

Figure 105.- Test Number 8 - Ground Hold and Taxi: Flowrate of Standpipe Tank Vent Gas

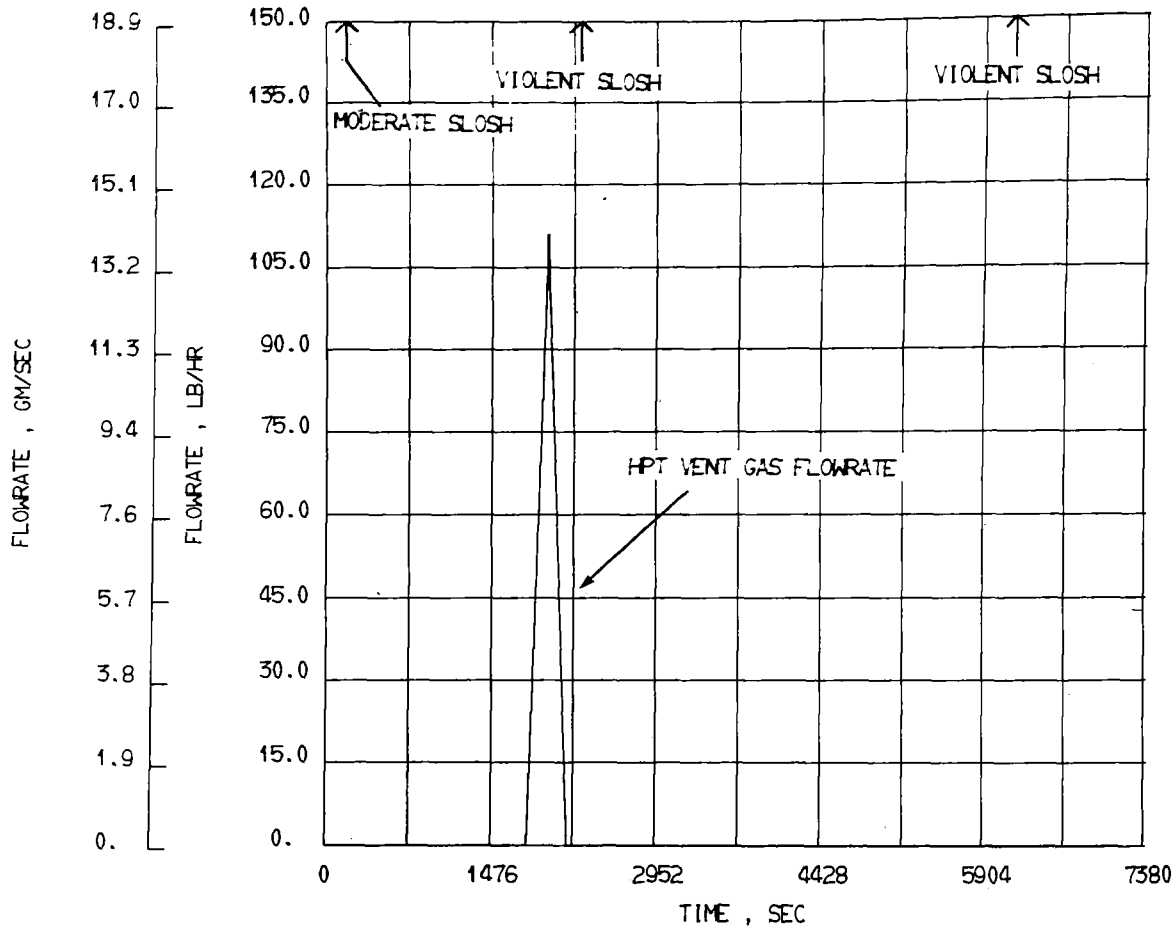

Figure 106.- Test Number 8 - Ground Hold and Taxi:
Flowrate of Standpipe Tank Vent Gas

b. Foam-filled tank tests.

1) Test 17: During test 17, the foam tank was filled to 90% and the high-pressure tank was filled to 96%. As can be seen by the foam tank gas pressure curve in figure 107, the first and third sloshes occurred during tank venting periods, which make it difficult to determine any correllation between sloshing and pressure control. Fortunately, the second slosh does provide good data and indicates that tank pressure was totally unaffected by the violent slosh period. The liquid temperature curves (fig. 108) indicate no liquid mixing during this period, as expected from the pressure curve.

The high-pressure tank pressure curve (fig. 109) was also examined for slosh effects. The pressure curve showed no change during the moderate sloshing but pressure decreases of about 7 psia (4.8 N/cm^2) during each of the violent sloshes. The pressure decrease curve during the first violent slosh had a characteristic concave shape significantly different than the typical vent curve, which was an almost vertical straight line. This same shape was not as noticeable during the second violent slosh; however, the pressure had reached 62 psia simultaneously with the start of the slosh and venting was started.

The curves of liquid temperature in the high pressure tank (fig. 110) show no change in temperature or degree of stratification identifiable with sloshing.

Figures 111 and 112 show the pressurization and vent flowrates in the foam tank, while figure 113 shows the vent flowrate in the high-pressure tank.

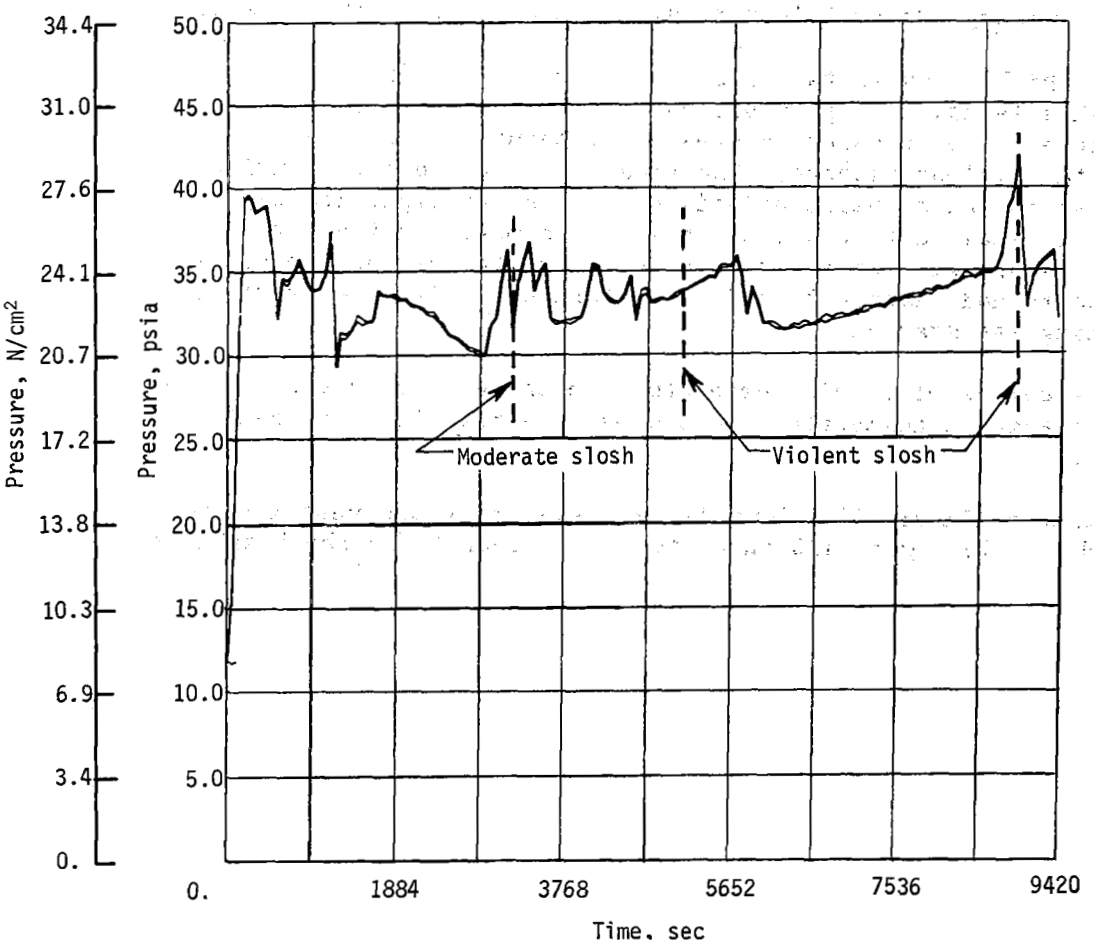

Figure 107.- Test Number 17 - Ground Hold and Taxi: Pressure at Top of Foam-Filled Tank

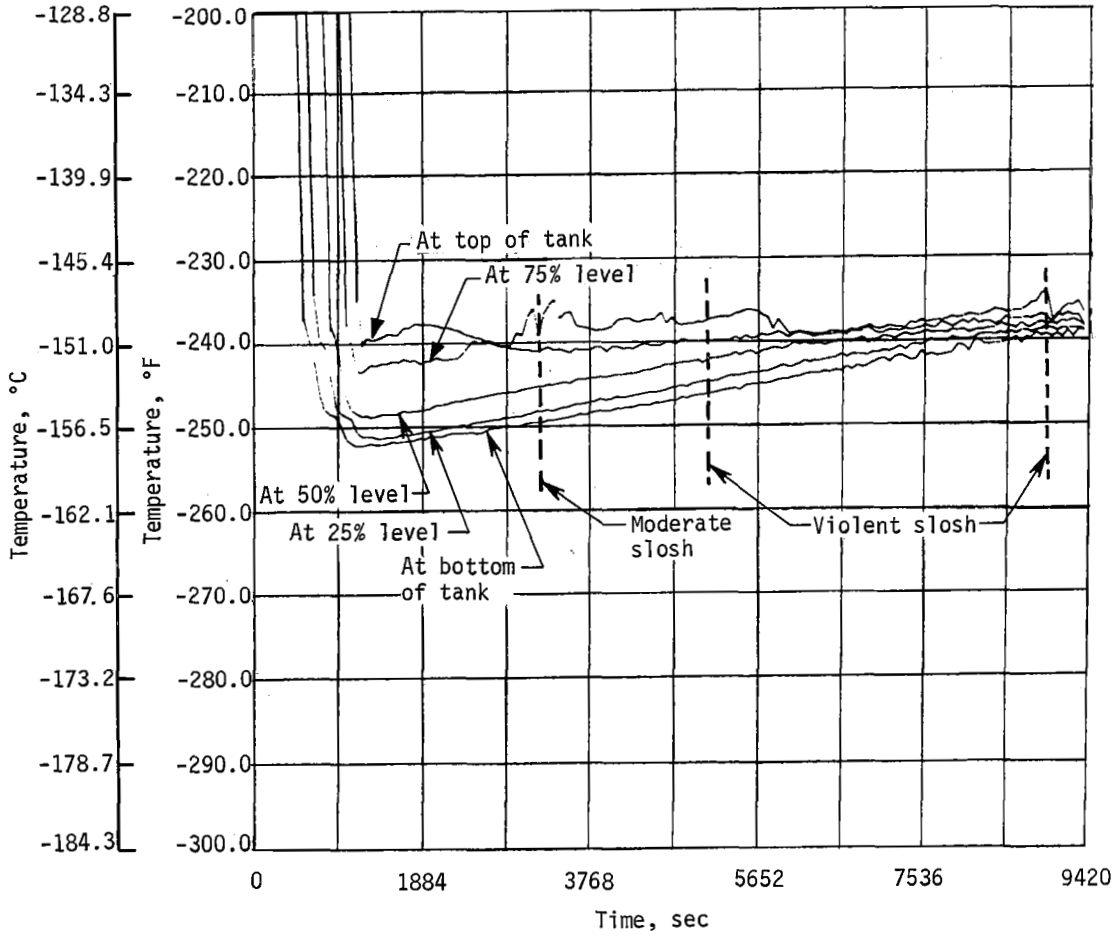

Figure 108.- Test Number 17 - Ground Hold and Taxi: Temperature of Liquid in Foam-Filled Tank

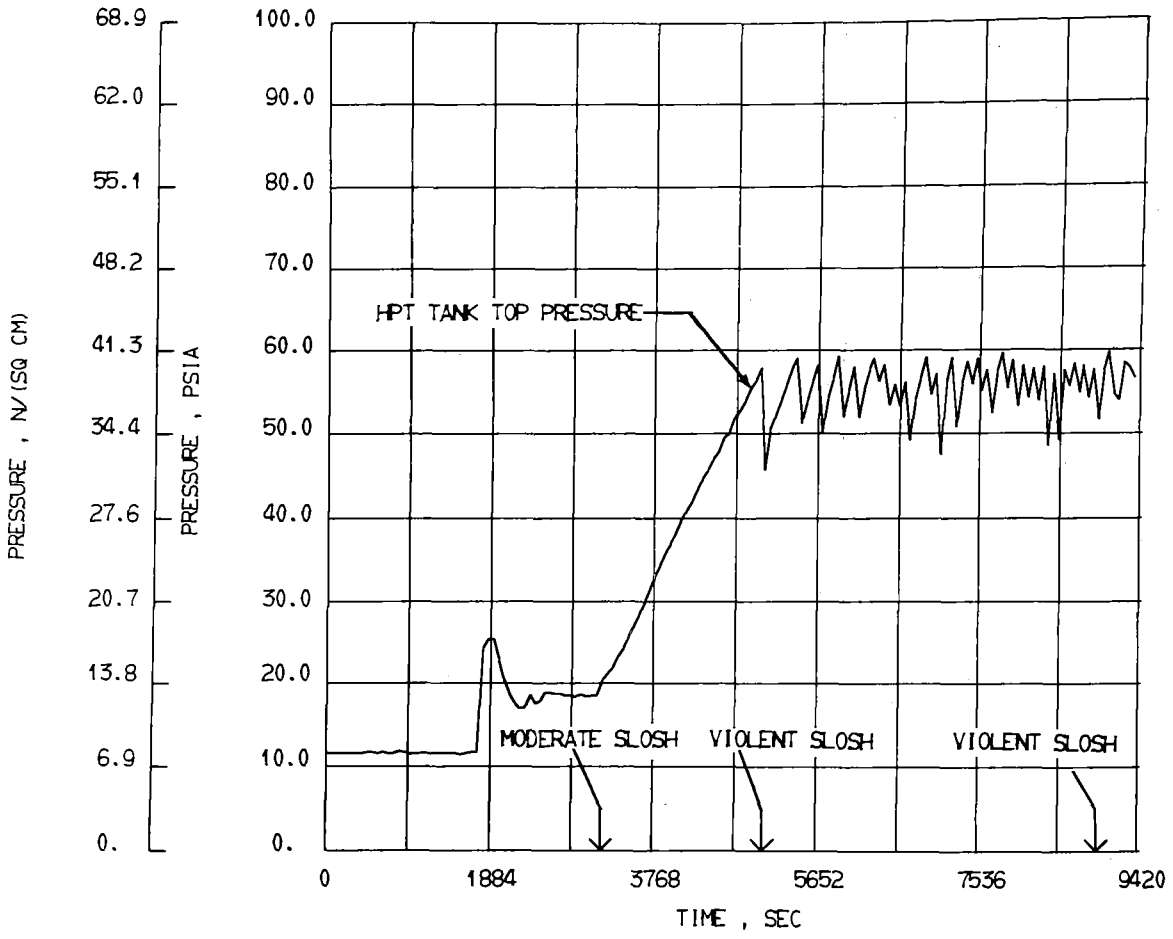

Figure 109.- Test Number 17 - Ground Hold and Taxi:
Pressure at Top of High-Pressure Tank

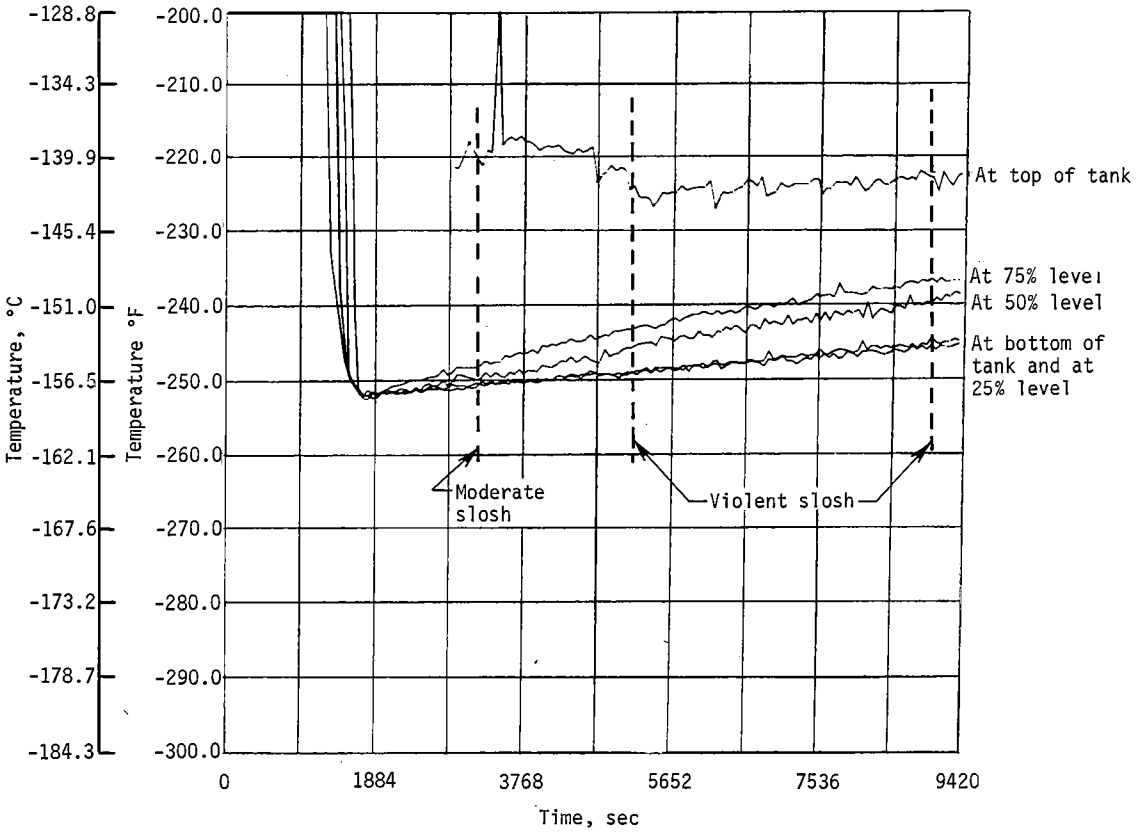

Figure 110.- Test Number 17 - Ground Hold and Taxi: Temperature of Liquid in High-Pressure Tank

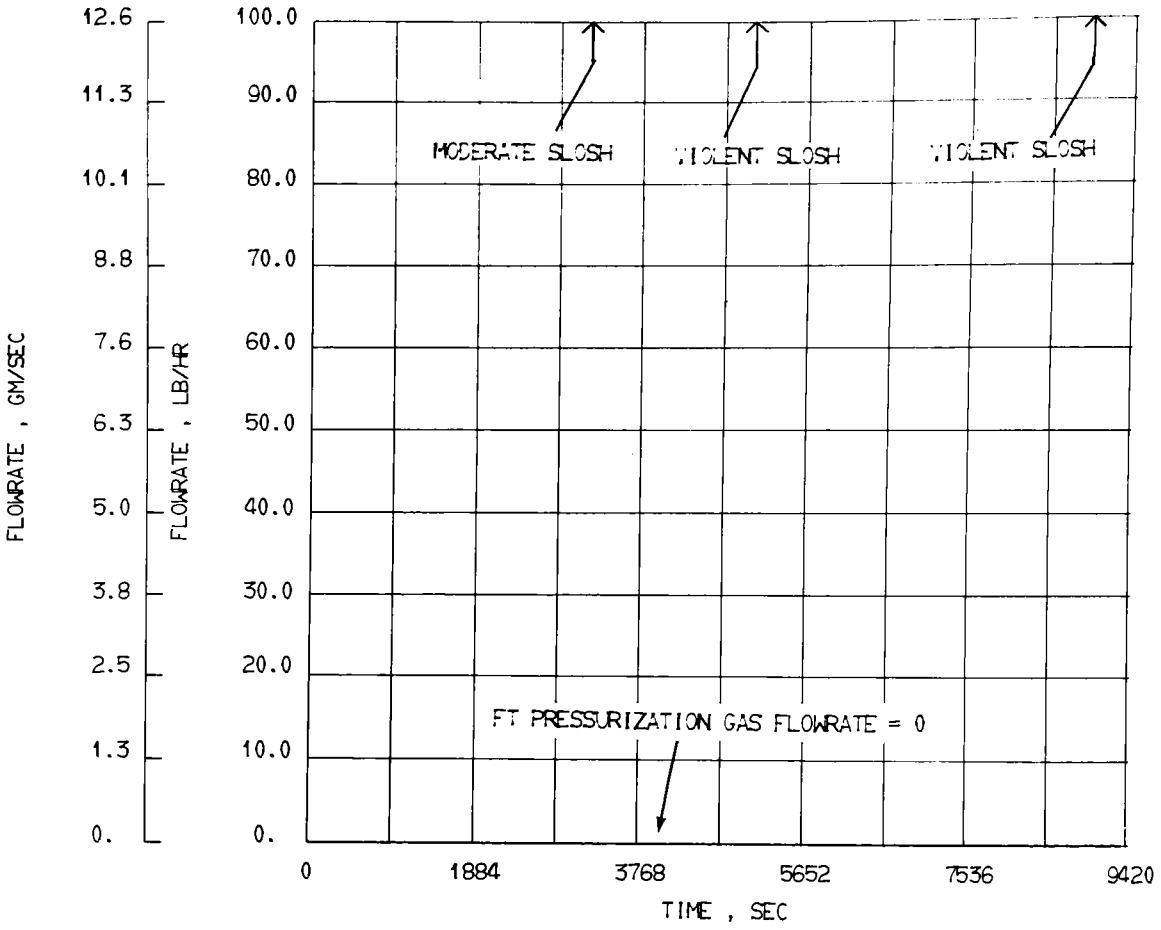

Figure III.- Test Number 17 - Ground Hold and Taxi:
Flowrate of Foam-Filled Tank Pressurization Gas

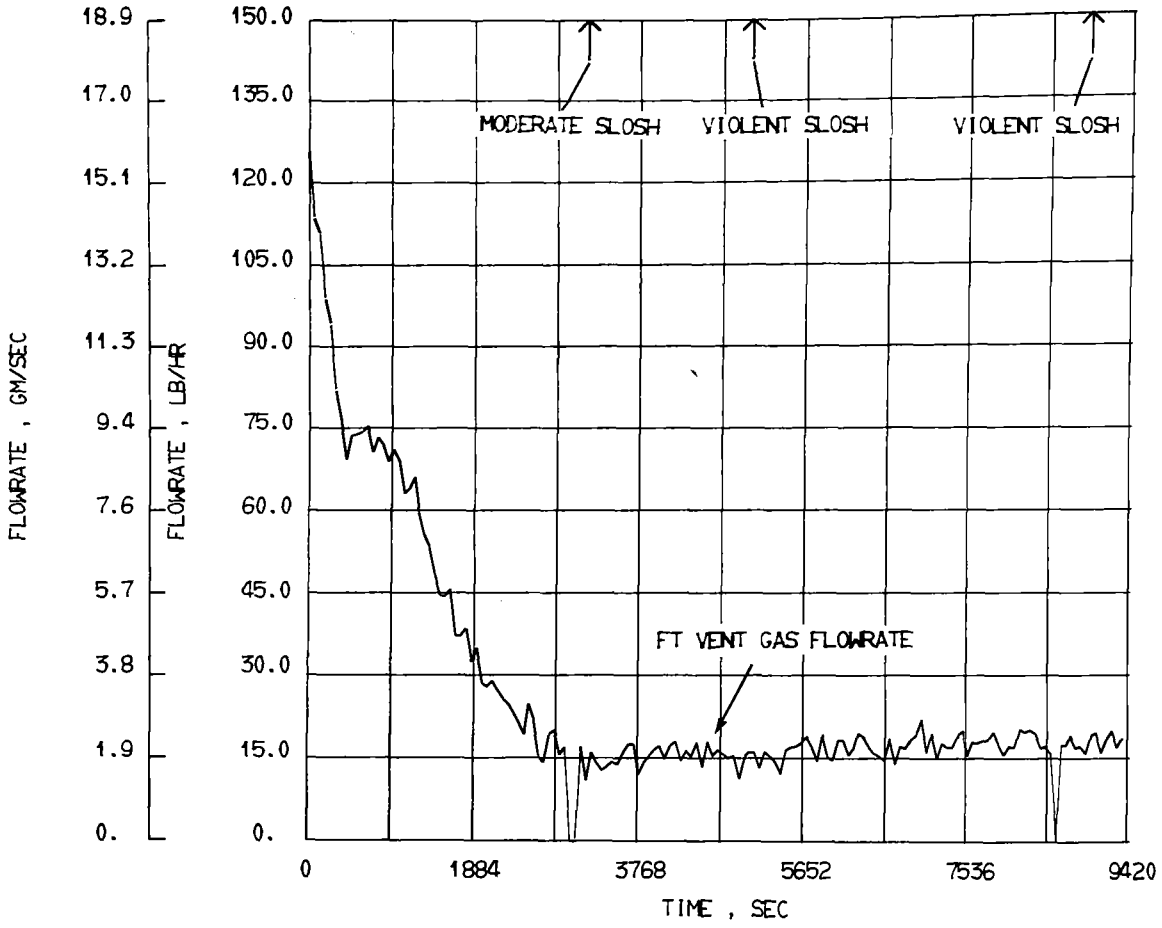

Figure 112.- Test Number 17 - Ground Hold and Taxi: Flowrate of Foam-Filled Tank Vent Gas

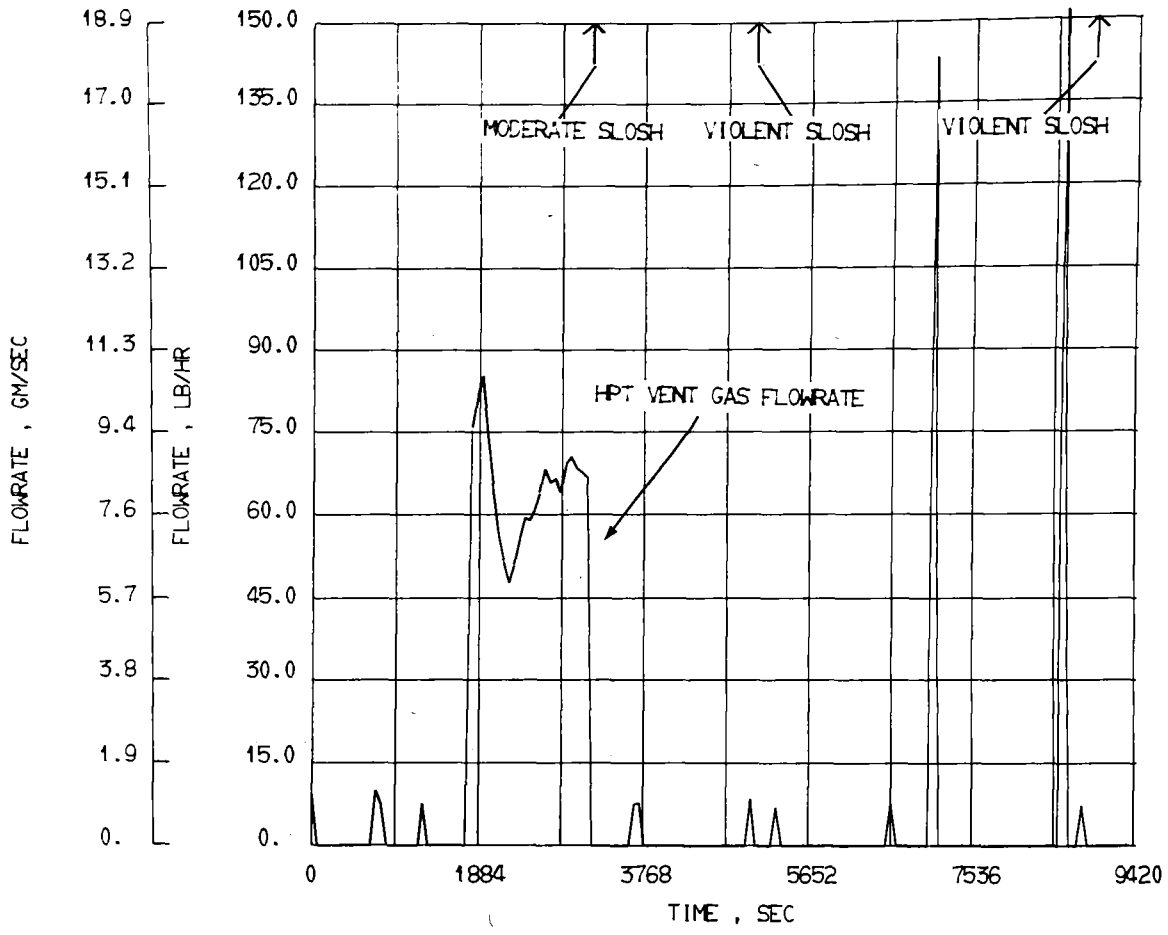

Figure 113.- Test Number 17 - Ground Hold and Taxi:

2) Test 18: This test was run with the foam tank filled to between 5 and 25% full and the high-pressure tank 50% full. As was the case in Test 8 with the standpipe and high-pressure tanks filled to these same levels, no effect on tank pressures or liquid temperatures was noted for either tank during any of the three slosh periods. Figures 114 and 115 show the tank pressure curves for the two tanks.

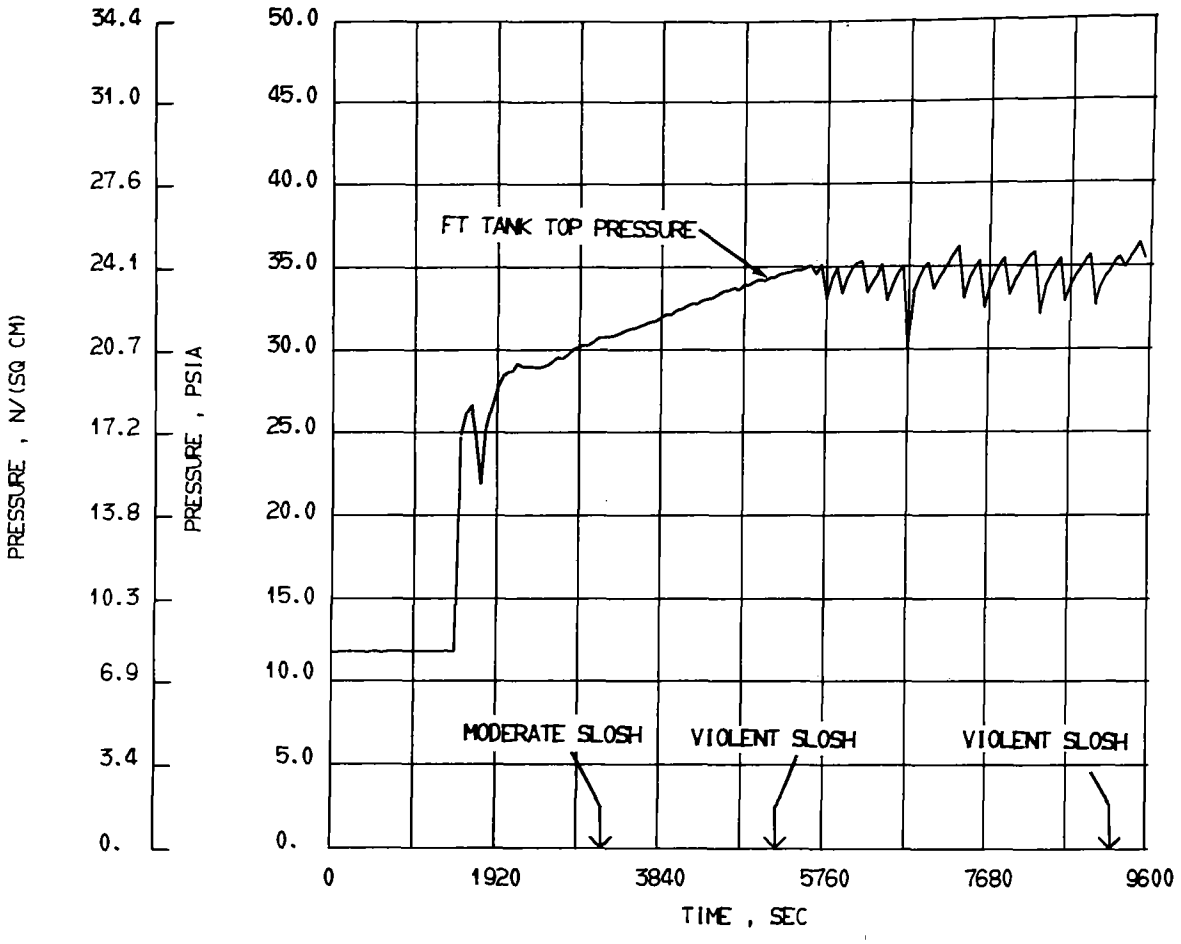

Figure 114.- Test Number 18 - Ground Hold and Taxi: Pressure at Top of Foam-Filled Tank

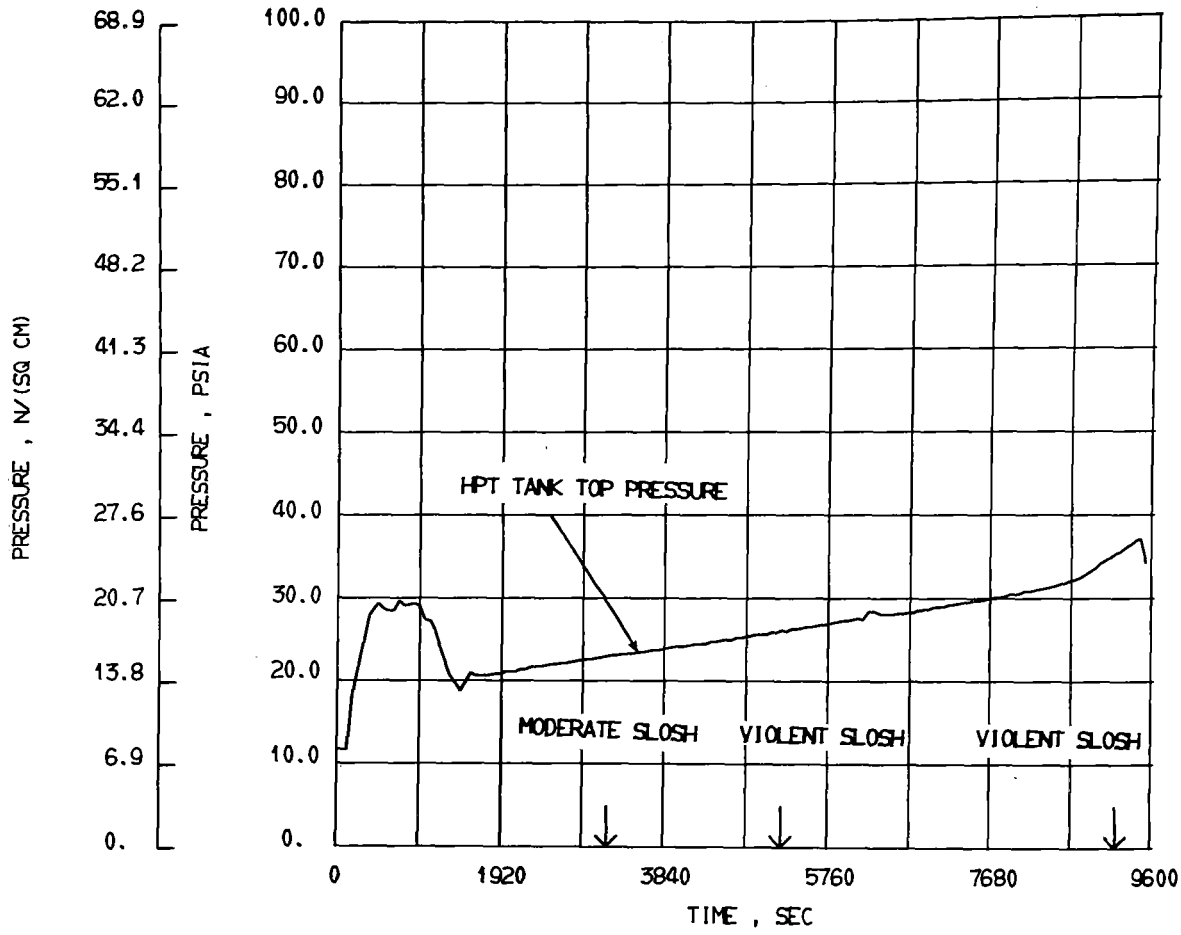

Figure 115.- Test Number 18 - Ground Hold and Taxi: Pressure at Top of High-Pressure Tank

3) Test 19: This test was run with both the foam tank and the high-pressure tanks filled to 50%, and provided a data point for a low-pressure tank between the 5% and 100% filled cases. No effect on either pressure or liquid temperature was noted on either tank during any of the sloshes. Figure 116, the foam tank gas pressure, is representative of this observation.

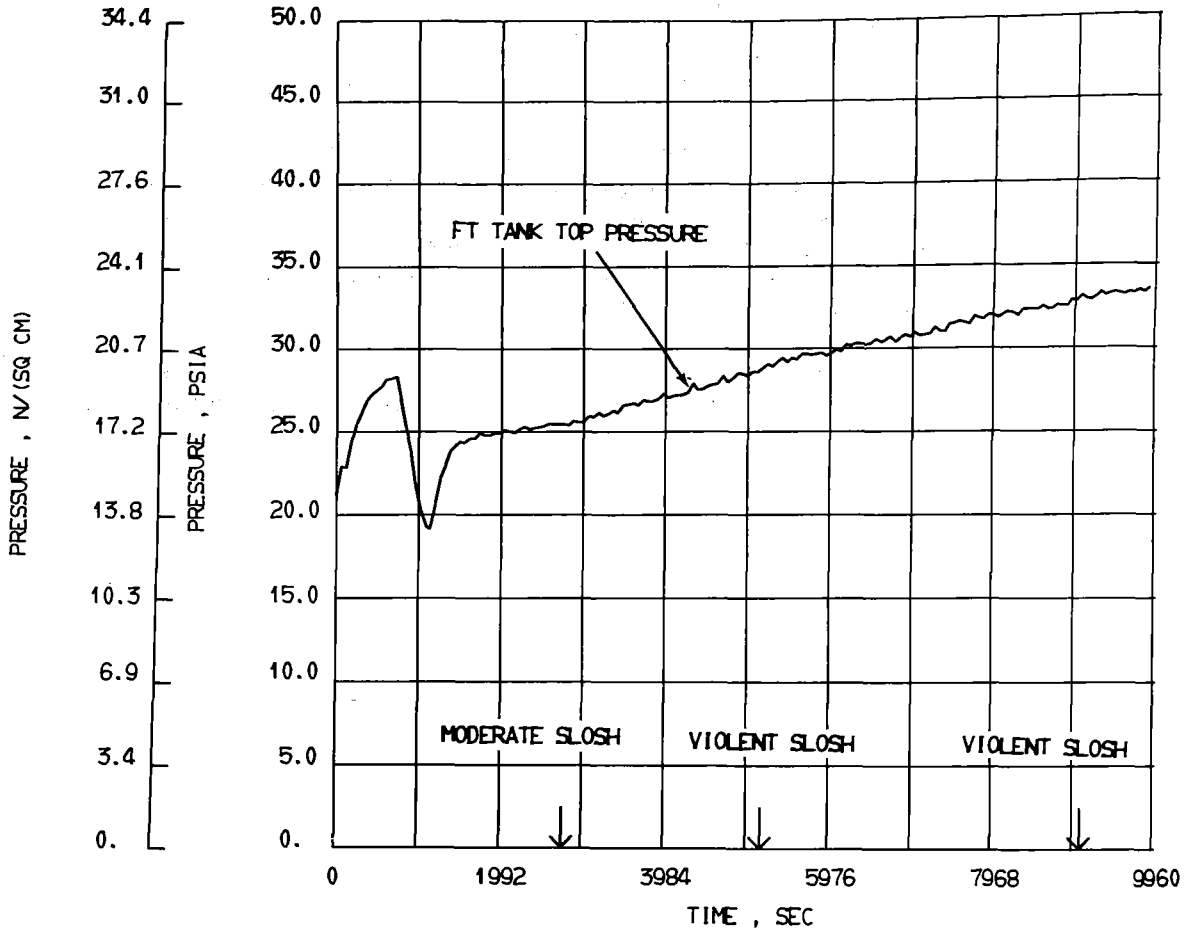

Figure 116.- Test Number 19 - Ground Hold and Taxi: Pressure at Top of Foam-Filled Tank

c. Baffled tank tests.

1) Test 28: During this test, the baffled tank was filled to 90% (i.e., the first four compartments were filled to their overflow height and the vent-end compartment was filled to the 90% level sensor) and the high-pressure tank was filled to 96% full. The baffled tank pressure and liquid temperature curves (figs. 117 and 118) were not affected by the sloshing.

As in previous runs with the high-pressure tank filled to the 96% level, The tank gas pressure curve (fig. 119) did show the same characteristic, concave-shaped pressure collapses. The moderate slosh caused about a 1 psi (0.7 N/cm^2) drop while the two violent sloshes caused approximately 3 psi (2.1 N/cm^2) drops. No particular pattern was noticeable on the curves of liquid temperature during the slosh periods.

The baffled tank pressurization and vent flowrate curves are shown in figures 120 and 121, while the high pressure vent flowrate is shown in figure 122.

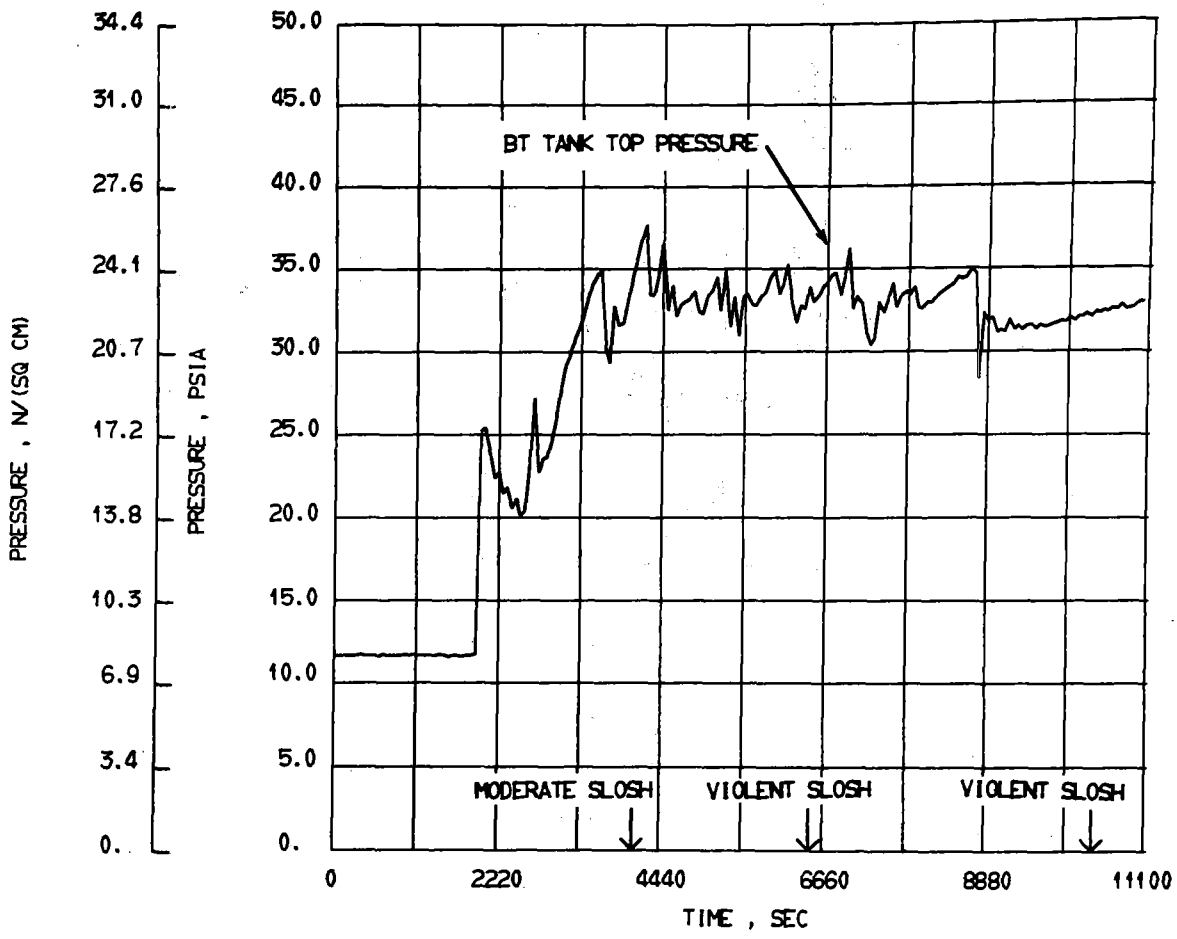

Figure 117.- Test Number 28 - Ground Hold and Taxi: Pressure at Top of Baffled Tank

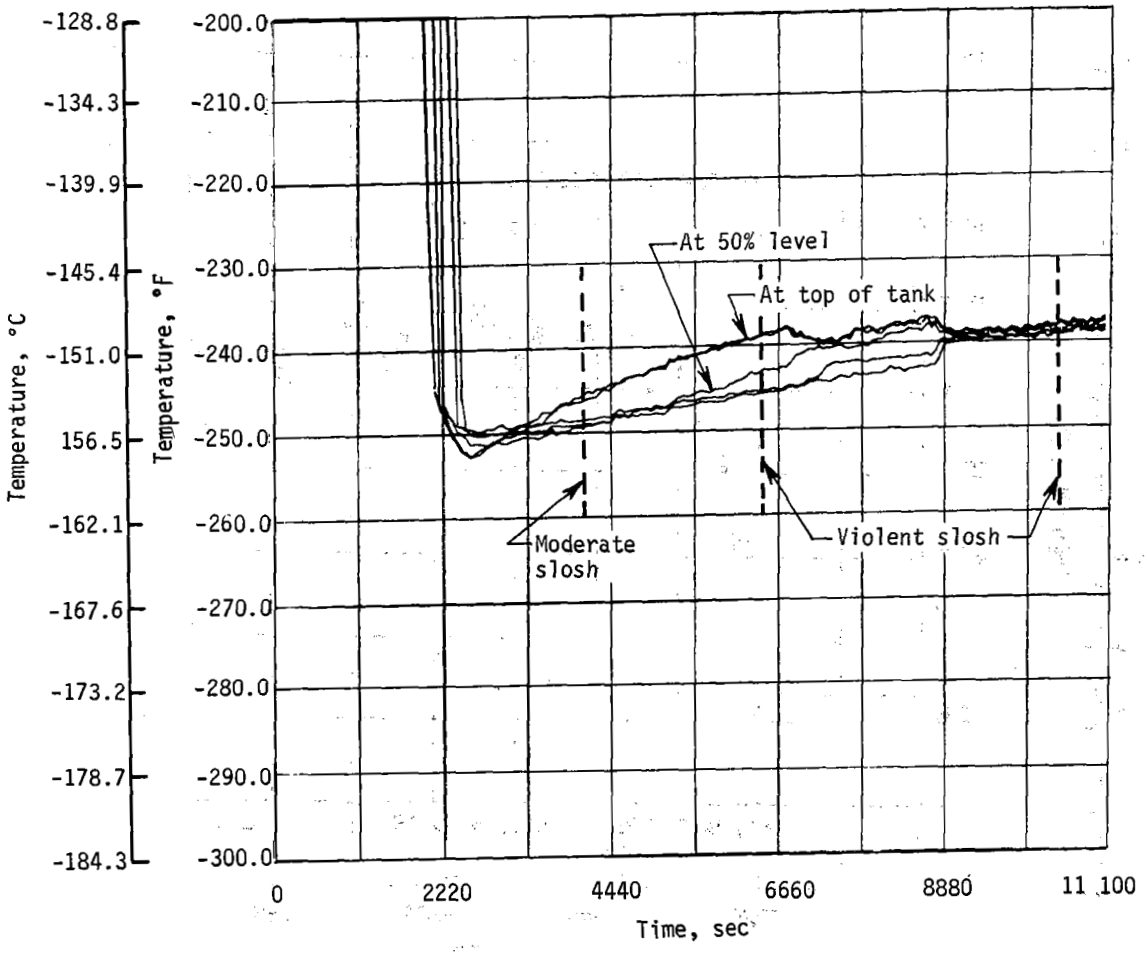

Figure 118.- Test Number 28 - Ground Hold and Taxi: Temperature of Liquid in Baffled Tank

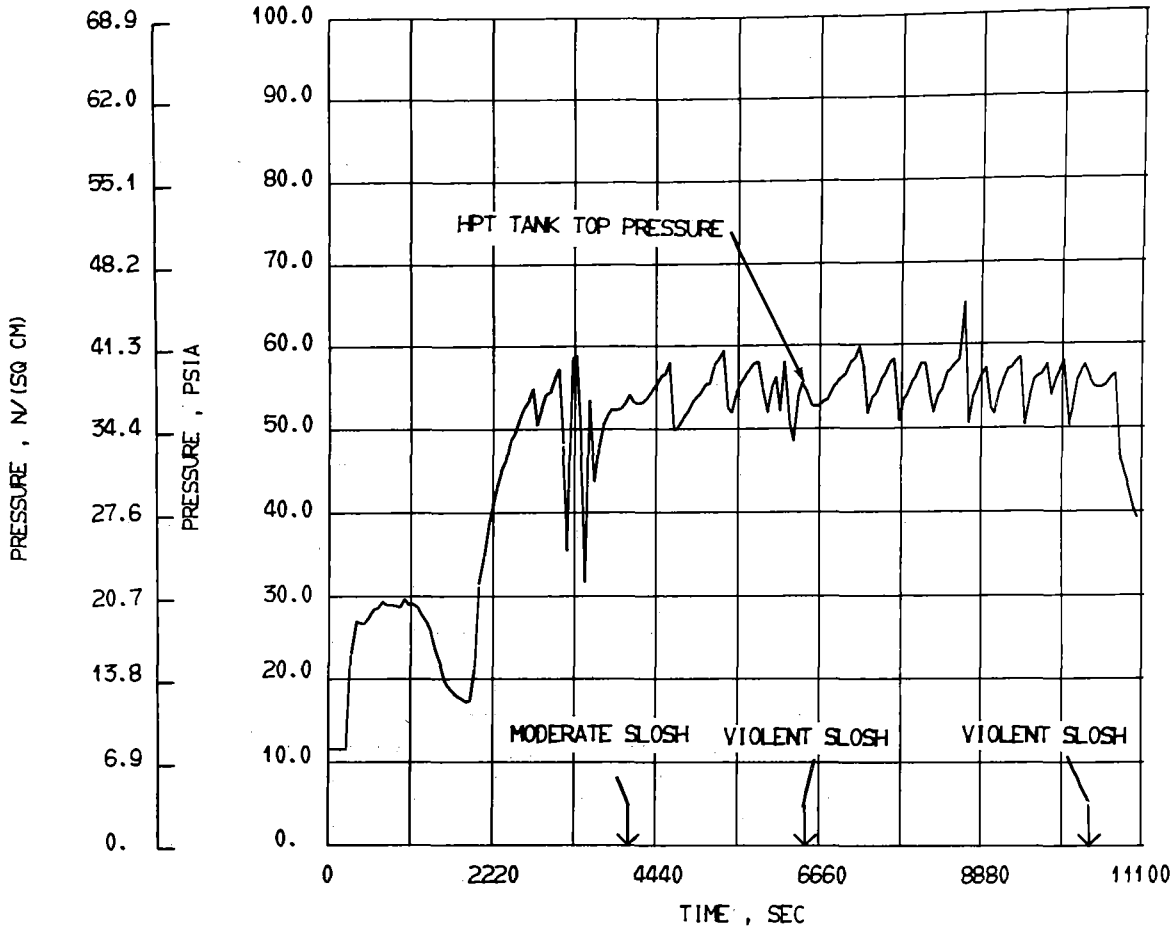

Figure 119.- Test Number 28 - Ground Hold and Taxi: Pressure at Top of High-Pressure Tank

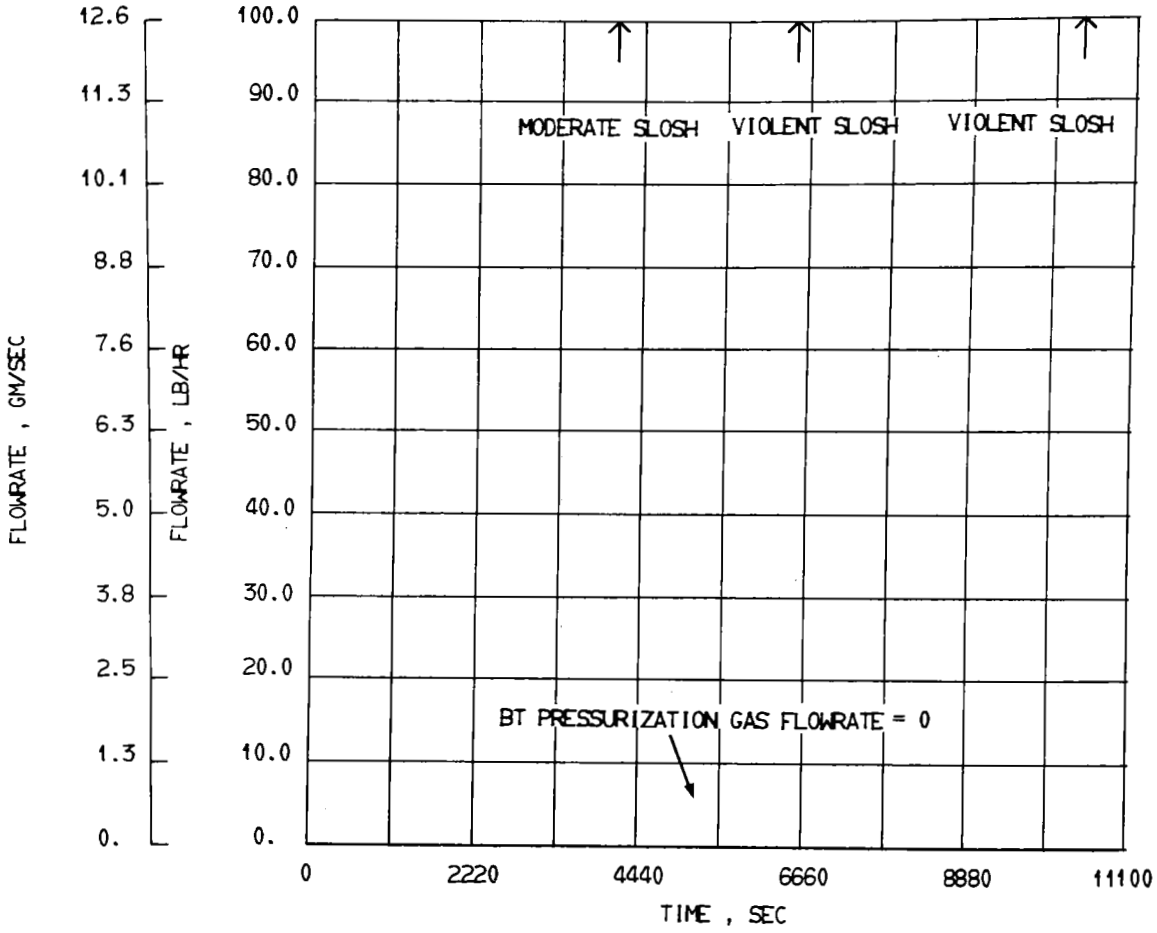

Figure 120.- Test Number 28 - Ground Hold and Taxi:
Flowrate of Baffled Tank Pressurization Gas

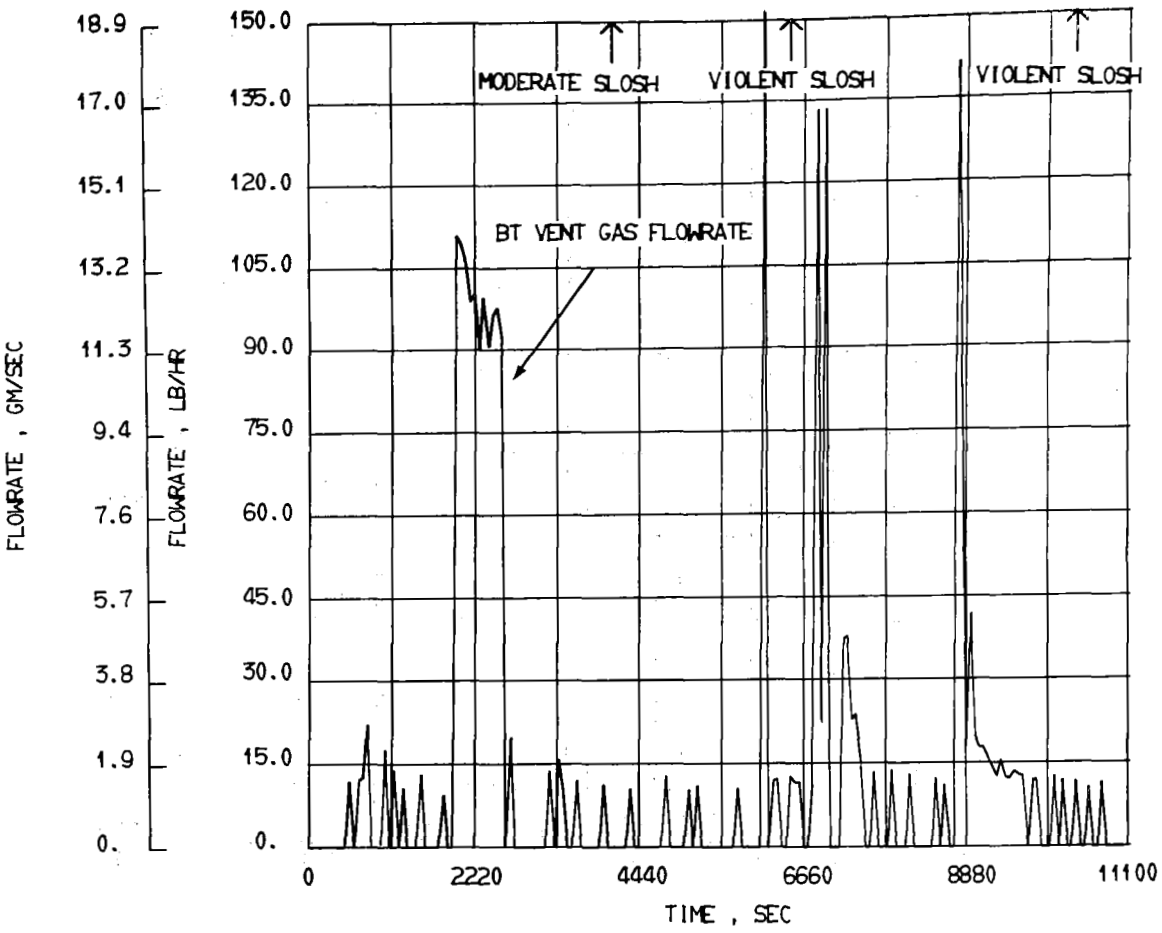

Figure 121.- Test Number 28 - Ground Hold and Taxi:
Flowrate of Baffled Tank Vent Gas

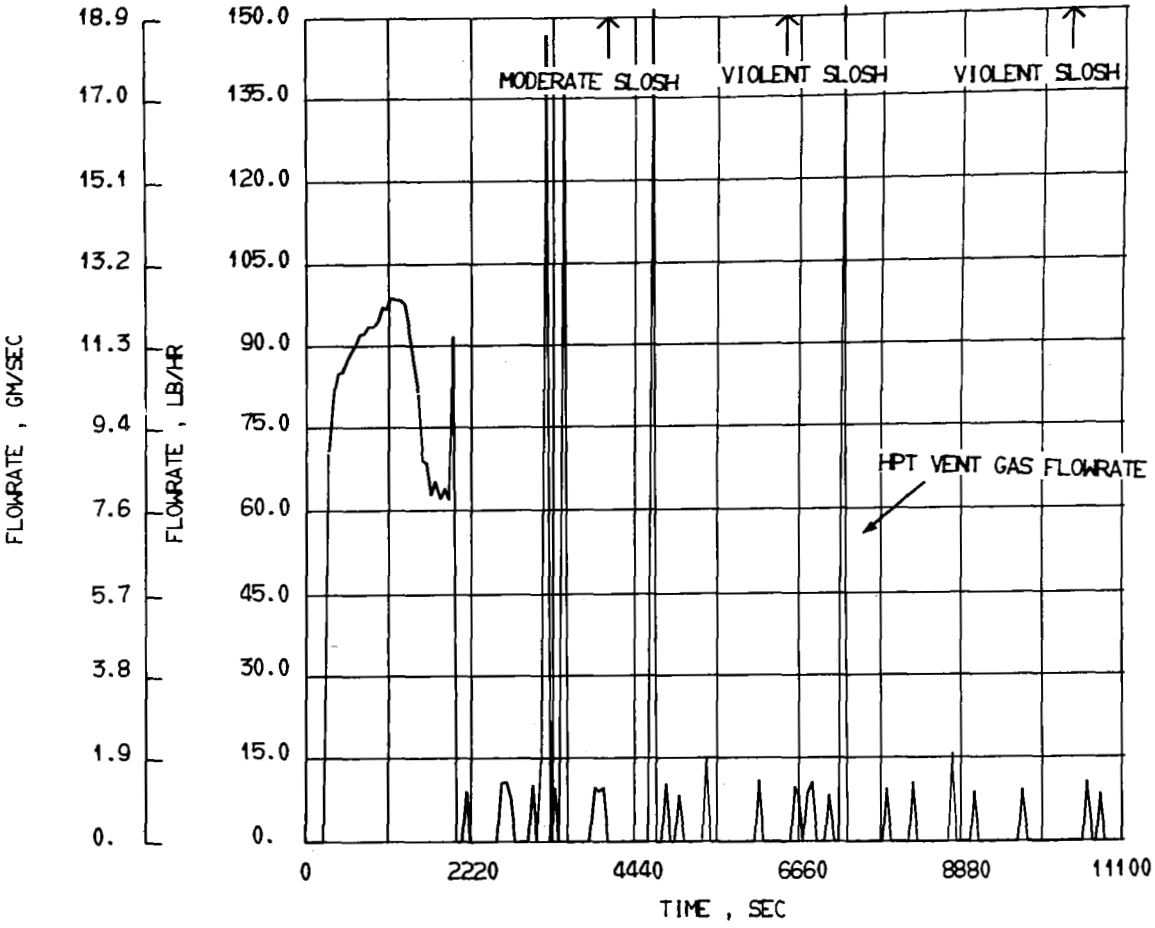

Figure 122.- Test Number 28 - Ground Hold and Taxi:
Flowrate of High-Pressure Tank

2) Test 29: This test completed the hold and taxi series, with the baffled tank between 5 and 25% full and the high-pressure tank 50% full. The actual level chosen for the baffled tank was the upper liquid level sensor in the first compartment. As with previous tests at these ullage levels, sloshing presented no problems with pressure control.

2. Test Summary

As stated previously, the two main objectives of the hold and taxi tests were to determine if tank gas pressure control problems would result from the taxi maneuver and whether the problems, if any, were a function of tank configuration (in particular, internal geometry designed to reduce pressure collapse). The data from the 7 hold and taxi have been evaluated and at least partially answer both these questions.

Four different tank configurations were tested, three specially designed low-pressure tanks and the high-pressure tank. Of the four, only the high-pressure tank experienced a pressure control problem. The problem was minimal with the moderate sloshing, ranging from no effect to about 1 psi (0.7 N/cm^2), but more severe with violent sloshing, ranging from 3 to 7 psi (2.1 to 4.8 N/cm).

The interior of the standpipe tank is the same as the high-pressure tank but did not exhibit the same pressure collapse characteristics. Had zero ullage been achieved this result would have been expected. The reasons for the absence of pressure collapse may be related to the presence of a large source of saturated liquid in the standpipe. This added source of saturated liquid would increase the total vaporization due to small pressure reduction and would, therefore, further counteract any condensation occurring in the main tank. Since the high-pressure tank was the only tank affected and is the only tank with no special apparatus for pressure control, it appears that pressure collapse is a function of tank geometry. Each of the three schemes employed on the low-pressure tanks appeared to perform satisfactorily.

The various ullage volumes tested included "zero ullage," 10%, 50% and 75 to 95% for the low-pressure tank and 4% and 50% for the high-pressure tank. As stated above, there was no effect on any of the low-pressure tanks from sloshing. This included the full range of ullage volumes. Ullage volume was, however, a factor in the high-pressure tank. Of the two different values tested, only the 96% full tank experienced a pressure control problem.

If the ullage volume is sufficiently small, a large percentage of both the small liquid surface and mass of ullage gas is thoroughly mixed by the sloshing. Conversely, if the tank is only half-filled, the liquid surface area and ullage mass are now much greater and not significantly affected by the same level of sloshing.

In each case where the high-pressure tank pressure curve was affected by sloshing, the corresponding liquid temperature curves were either undisturbed or appeared to be disturbed at some time after the pressure curve dip. This could be indicative that the pressure collapse was caused primarily by mixing of the ullage gas rather than mixing of the liquid. However, a second explanation is that since the tank top liquid temperature probe was measuring a point under the surface, and not at the surface, the actual surface liquid may have mixed and caused the pressure collapse. Depending on the depth of the temperature probe and the severity of the pressure collapse the liquid there may or may not have been affected by the pressure drop at some finite time later.

C. HEAT TRANSFER TESTS

This series of tests was designed to determine the overall effectiveness of the tank insulation system. This overall effectiveness may be different than the thermal conductivity of the insulation material due to tank supports, fill lines, vent lines, etc. Tests 9 and 10 were performed on the standpipe configuration; tests 20 and 21 on the foam-filled tank; and tests 30 and 31, on the baffled tank.

1. Test Description and Data

The test procedure for all the tests in this series consisted of loading the low-pressure tank to 100%, the high-pressure tank to 96%, and the guard tanks to 90%, and then increasing the wing skin temperature to 400°F (204.4°C). The low-pressure tank was operated at approximately 12 psia (8.27 N/cm^2), ambient pressure at the test site. The high-pressure tank was locked up, allowed to self-pressurize to 62 psia (42.7 N/cm^2), and held there by venting. The data is presented here only for test 9 since the data on all heat transfer tests was very similar. In test 9 the standpipe tank was filled and held with the vent open for 2 hr. During this hold period, the tank was sloshed every 5 minutes to wet the tank walls. At the end of 2 hr, the tank was drained and held for an additional 2 hr to observe the warmup.

Figure 123 shows the temperatures within the wing cavity. Figure 124 shows the temperature profile through 1 1/4 inch of insulation on the side of the tank. The resulting vent flow rate is shown in figure 125. The integrated average flowrate during the test is 21.0 lb/hr (2.66 g/sec). This is equivalent to a tank heat leak of 104 BTU/hr-ft^2 (327 w/m^2). As is seen in figure 126 there was no pressurant gas required during the test.

2. Test Summary

There was no significant difference in the results of any of the six heat transfer tests. The pertinent results of the six tests are tabulated in table 8. This table shows the integrated average vent flowrate for the low pressure tank, the integrated average outer insulation temperature, the average temperature difference across the insulation and the "effective" thermal conductivity of the system. The values of thermal conductivity are based on a heat of vaporization of 219 BTU/lb (509.8 J/gm) and a surface area of 44 ft^2 (4.09 m^2).

There was no identifiable difference between continuous moderate slosh (tests 9, 20 and 30) and occasional violent slosh (tests 10, 21 and 31). There is considerable scatter in the data which might be expected on a thermal test of this type. However, except for test 10 all values of "effective" thermal conductivity are in close agreement with the value of 0.0186 BTU/hr-ft-°F (0.769 cal/sec-m-°C) which was determined for this insulation material using a calorimeter under similar test conditions. No explanation could be found for the apparent high value of conductivity in test 10. The relatively close agreement of all other values as compared to the calorimetry

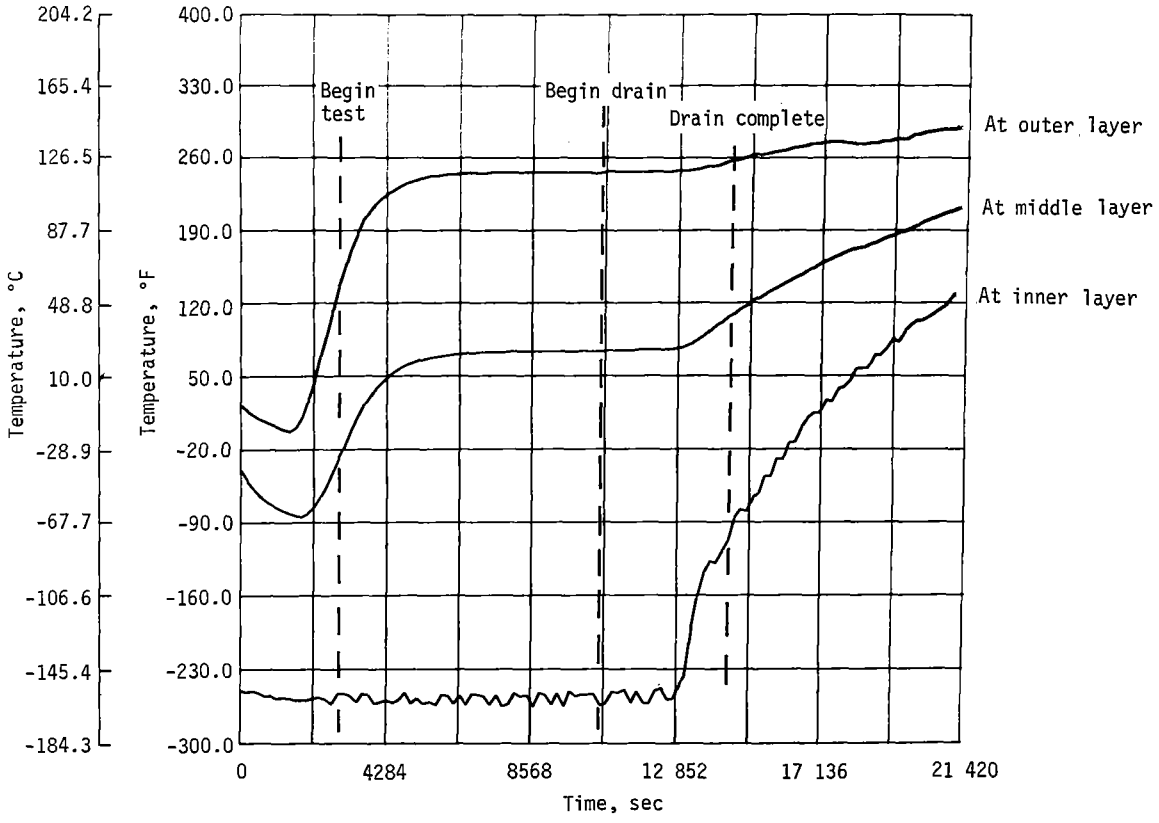

Figure 123.- Test Number 9 - Heat-Transfer Tests: Temperature of Insulation on Side of Standpipe Tank

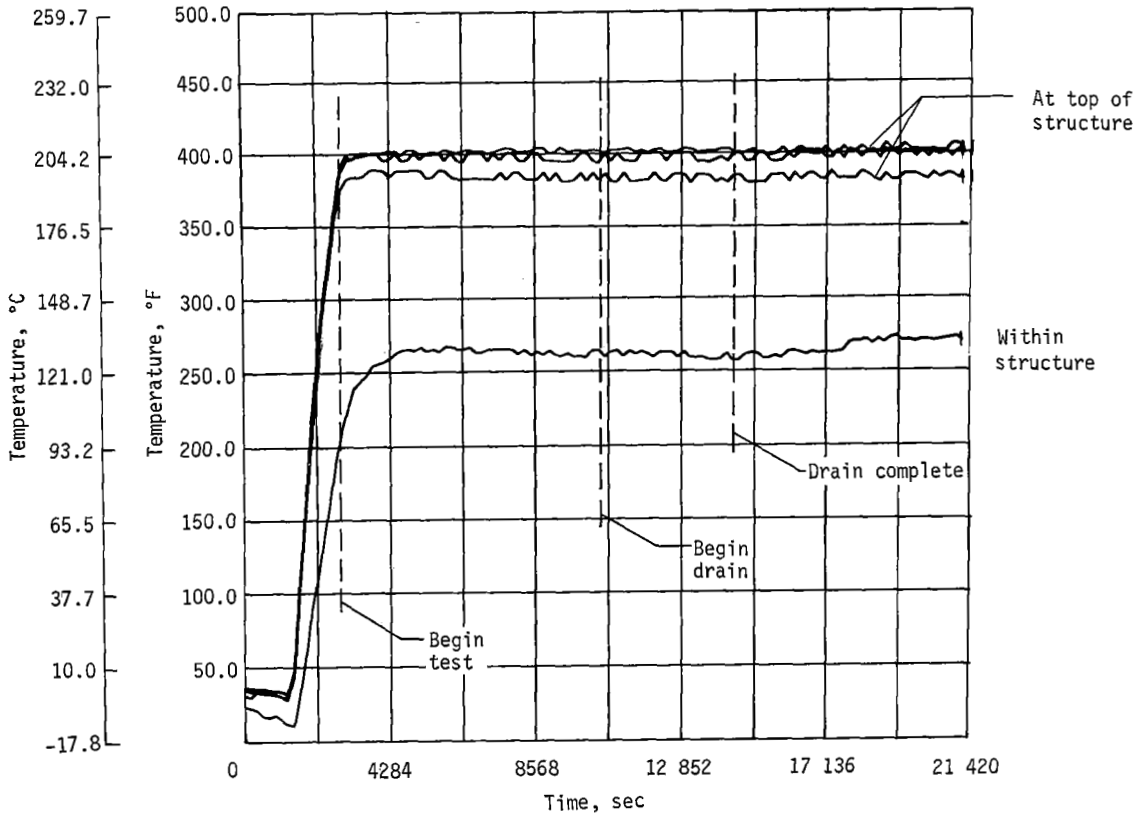

Figure 124.- Test Number 9 - Heat-Transfer Tests: Temperature of Wing Structure

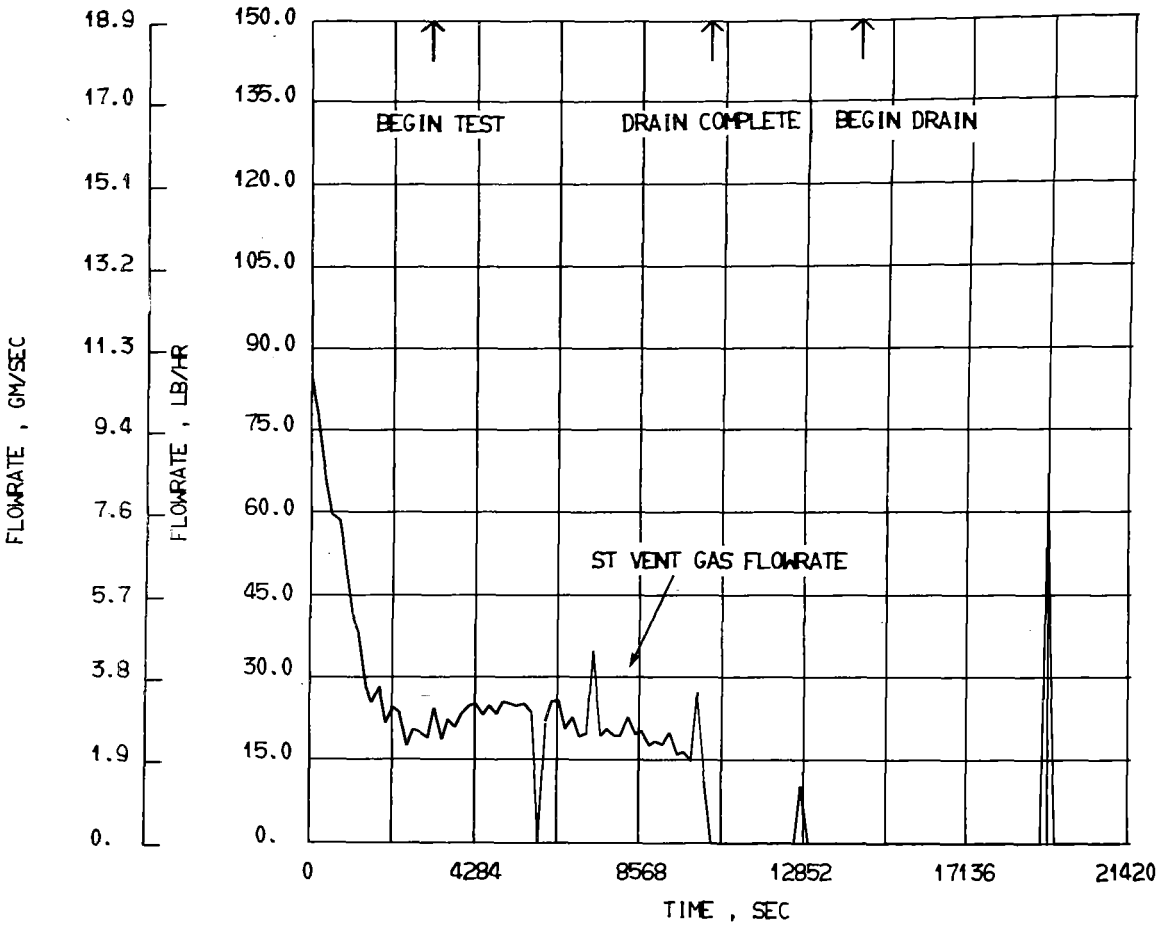

Figure 125.- Test Number 9 - Heat-Transfer Tests: Flowrate of Standpipe Tank Vent Gas

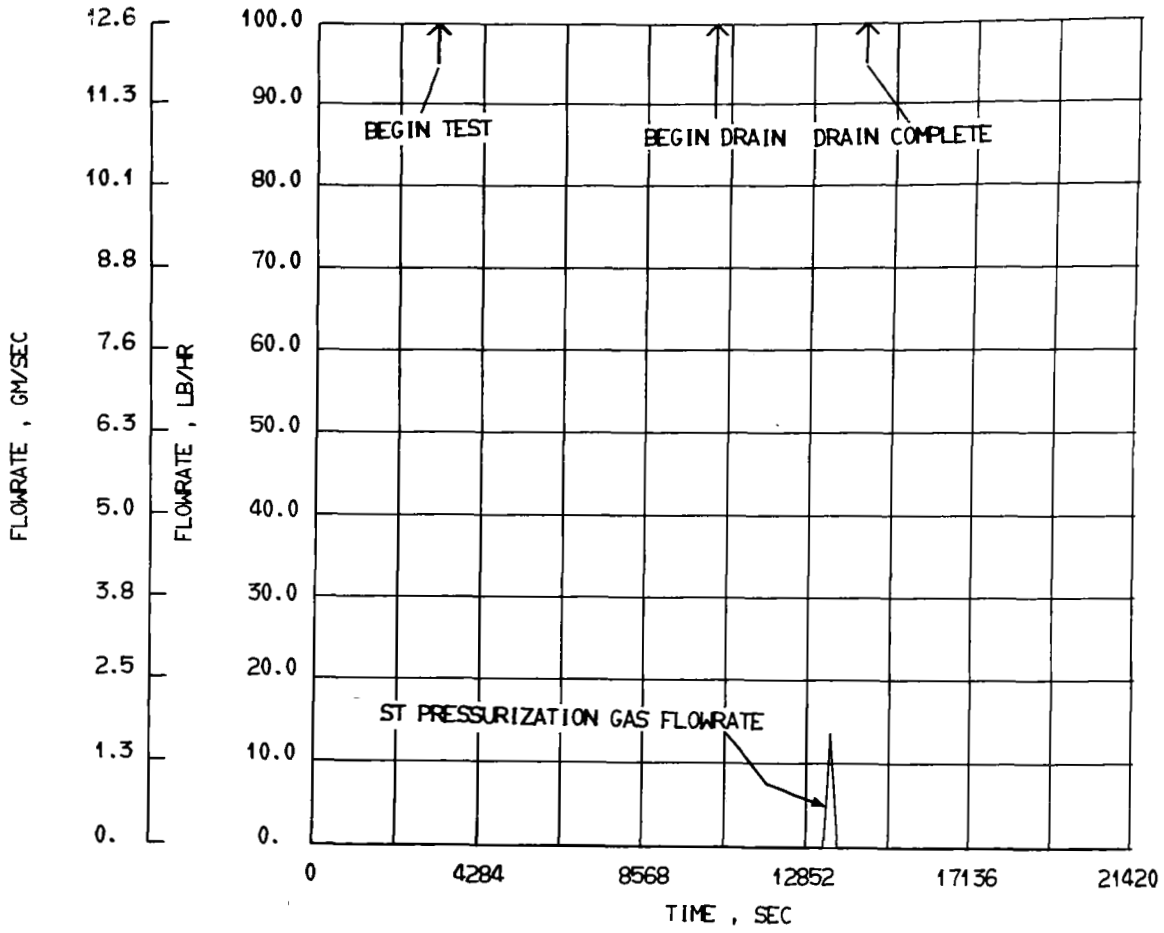

Figure 126.- Test Number 9 - Heat-Transfer Tests: Standpipe Tank Pressurization Gas

Test Number	Vent Flow Rate lb/hr	Vent Flow Rate g/sec	Average Outer Insulation Temp. °F	Average Outer Insulation Temp. °C	Average Insulation Temp. Differential °F	Average Insulation Temp. Differential °C	"Effective" Thermal Conductivity BTU/hr-ft-°F	"Effective" Thermal Conductivity Cal/sec-m-°C
9	21.02	2.68	262	127.8	522	290	0.0189	0.78
10	29.95	3.78	272	133.3	532	296	0.0253	1.04
20	18.8	2.38	280	137.8	540	300	0.0183	0.75
21	16.8	2.12	277	136.1	530	294	0.0167	0.69
30	18.8	2.38	267	130.6	527	293	0.0185	0.76
31	20.8	2.62	271	132.8	531	295	0.0204	0.84

TABLE 8 HEAT TRANSFER TEST RESULTS

value indicates that insulation system conductivity is nearly the same as the conductivity of the basic material. In other words tank supports, fill lines, vent lines, etc. do not appreciably degradate the insulation performance.

D. FUEL-TRANSFER TESTS

The objective of this test series was to provide information on the tank-to-tank pumping of liquid methane. The pump was mounted outside the tanks and wing section as shown by Figure 3. In each test, pumping was from the low-pressure tank to the high-pressure tank through an external plumbing loop. With the exception of the pump housing, the external piping system was insulated with polyurethane foam to minimize heat loss to the jumped fluid.

1. Test Description and Data

The test procedure involved loading each low-pressure tank to maximum, loading the high-pressure tank to 25%, and pressurizing the low-pressure tank to provide sufficient net positive suction head (NPSH) to the pump. The interconnected valves were opened to transfer pressure until the pump case temperature indicated that liquid had begun to flow. Then the pump was started. Pumping continued until the liquid reached the 96% level in the high-pressure tank.

The first pump run was made without sloshing, the second with continuous moderate sloshing, and the third with a period of violent sloshing when the level in the high-pressure tank reached 75%.

a. Standpipe tank tests. This series of tests was conducted with the standpipe tank in the low pressure tank position so that pumping was from the standpipe tank to the high-pressure tank.

1) Test 11: The liquid methane in the stanpipe was saturated at 20 psi (13.8N/cm^2) at the beginning of the test. At approximately 60 seconds before the initiation of pumping the tank was pressurized to 27 psi (18.6 N/cm^2) to provide pump NPSH. When pumping was started tank pressure had decayed to 20 psi (13.8 N/cm^2) and cavitation occurred. At the time when pumping was started the pump casing temperature had stabilized at -245°F (-153.9°C). As indicated by figure 127 shortly after pump start the tank was again pressurized and single phase liquid flow was established. With continued pressurization pumping at 25 gpm (1557 cc/sec) was maintained until the high pressure tank level was 96% full. During the pump run the high-pressure tank was vented to 20 psi (13.8 N/cm^2) and maintained at that pressure throughout the run. Figures 128 and 129 show ST and high-pressure tank liquid temperatures during the pump run.

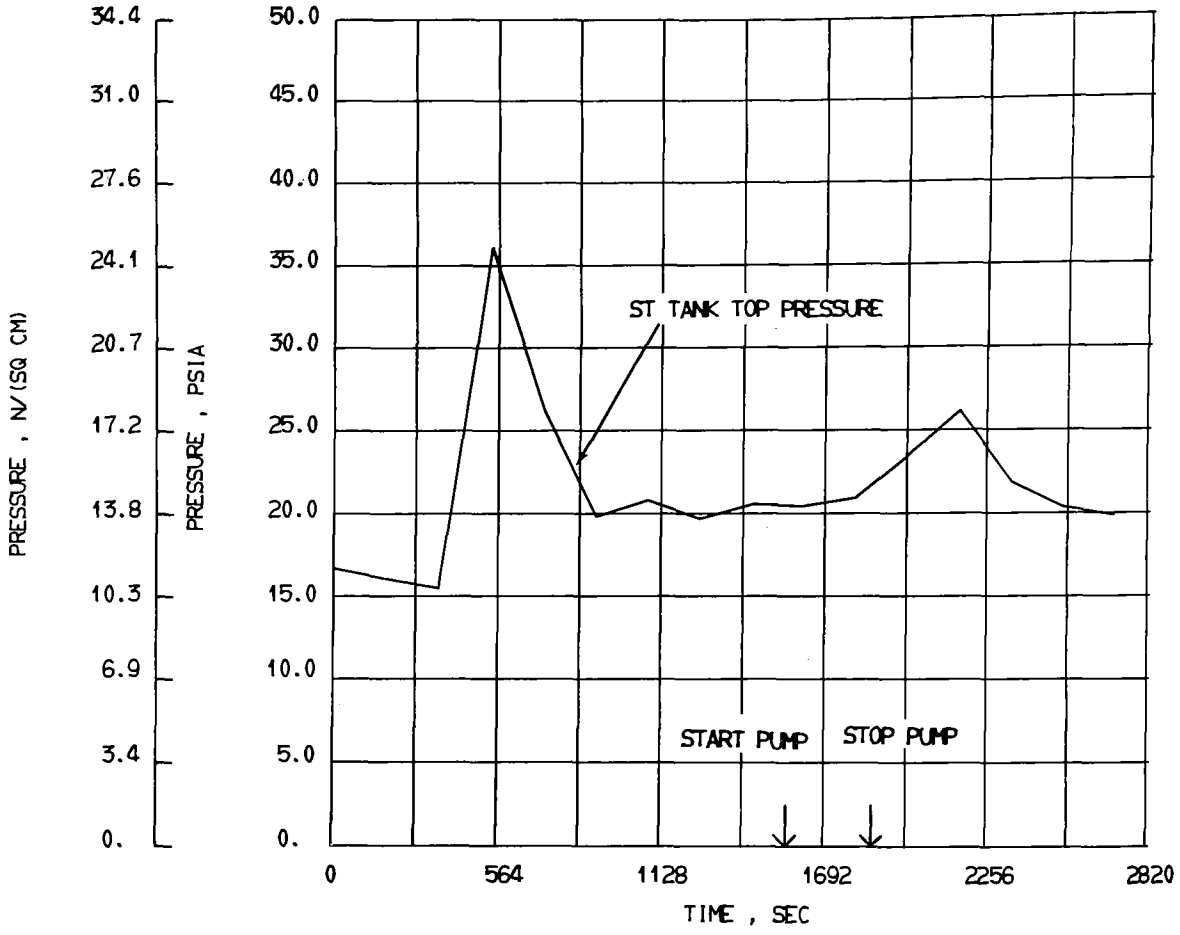

Figure 127.- Test Number II - Fuel-Transfer Tests: Pressure at Top of Standpipe Tank

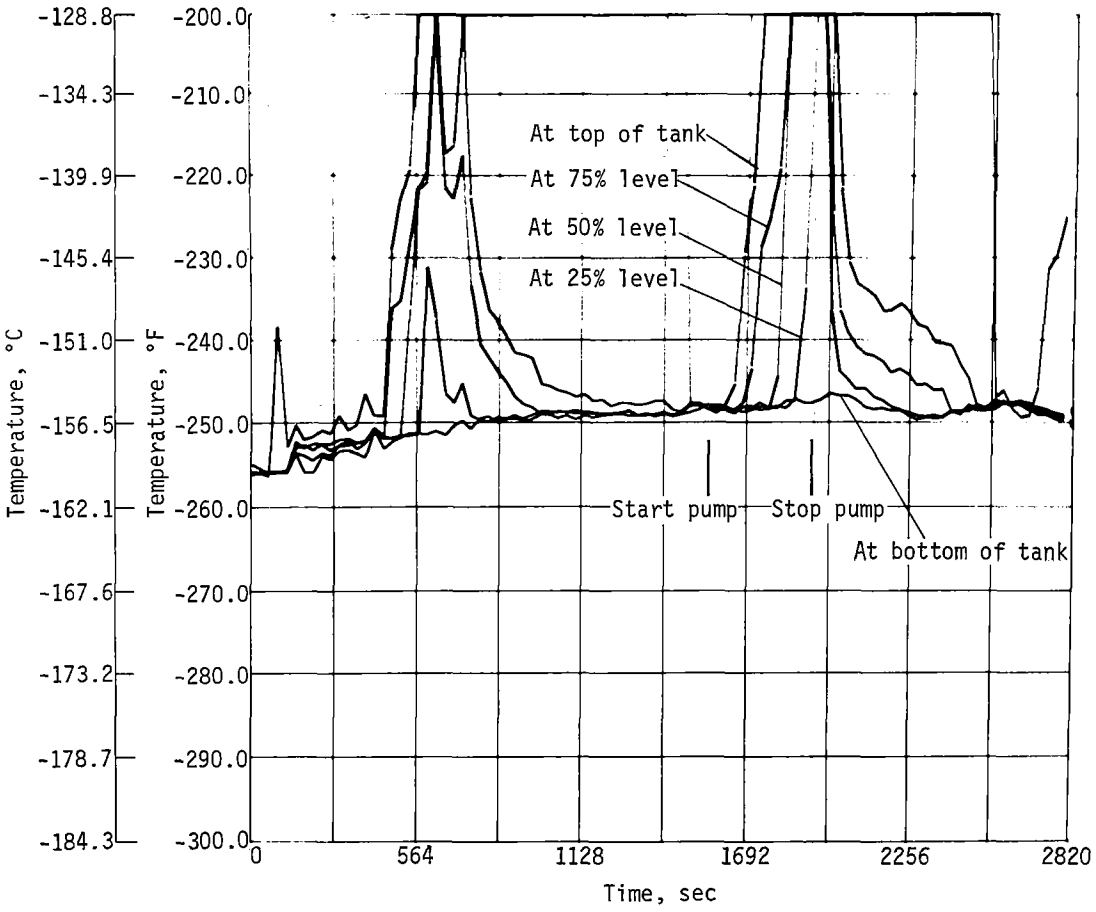

Figure 128.- Test Number 11 - Fuel-Transfer Tests: Temperature of Liquid in Standpipe Tank

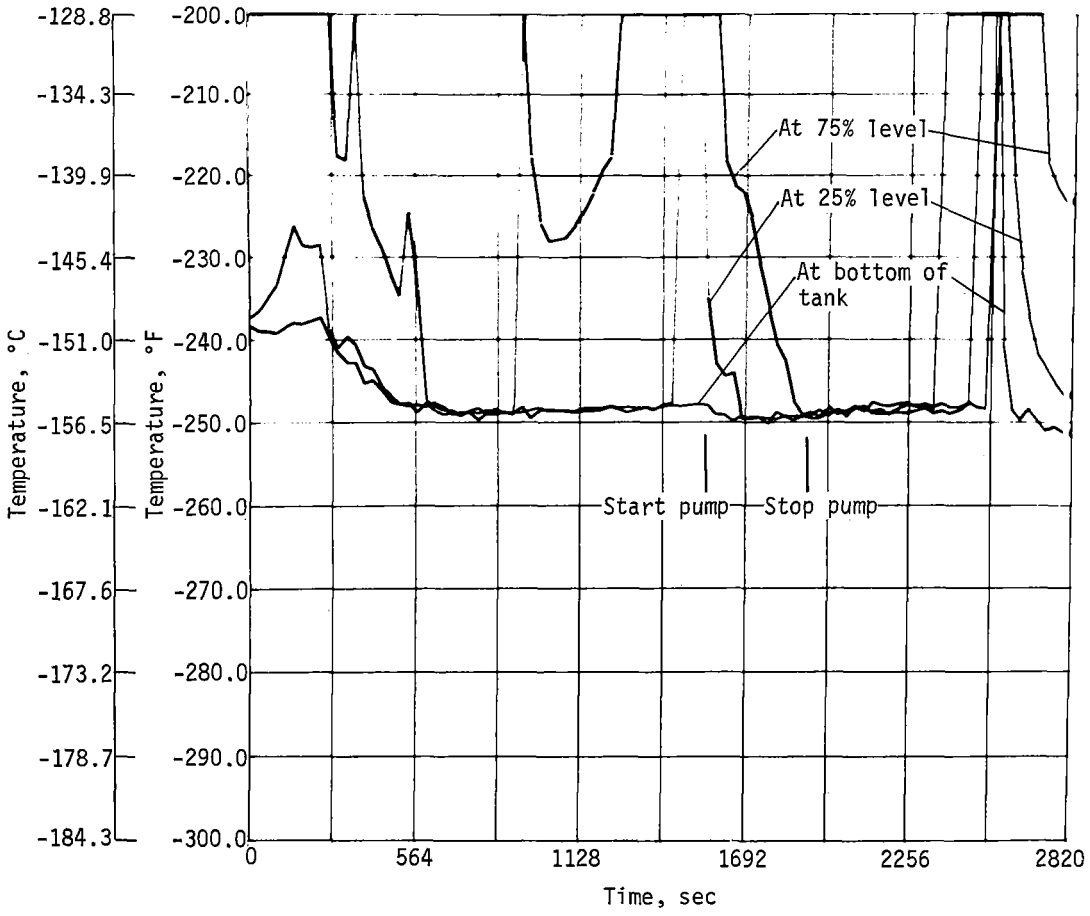

Figure 129.- Test Number II - Fuel-Transfer Tests: Temperature of Liquid in High-Pressure Tank

2) Test 12: During this pump run the tanks were exposed to continuous moderate sloshing. Initial pressure in the ST tank was 18 psia (12.4 N/cm^2). Pressurization for NPSH was to 25 psia (17.2 N/cm^2) dropping to 22 psia (15.2 N/cm^2) during the pump run. The high pressure tank was again vented during pumping as necessary and held to a pressure of 23 psia (15.9 N/cm^2) during the run. Pump rate was calculated at 67.5 gal/minute (4259 cc/sec) based upon ST tank level sensor uncoverings.

3) Test 13: Initial pressurization of the standpipe tank for this test was from 18 to 25 psia (12.4 to 17.2 N/cm^2). Pumping rate was 58 gal/minute (3659 cc/sec). Violent sloshing when the high pressure tank reached 75% full created no noticeable effect on pumping.

b. Foam-Filled tank tests. During this pumping series the faom filled tank acted as the source for pumping to the high pressure tank.

1) Test 22: Pressurization for necessary pump NPSH and to initiate pressure transfer for pump cool down was from 16 psia to 23 psia (11.0 to 15.9 N/cm^2). At pump start the tank pressure was 22 psia (15.2 N/cm^2) providing subcooling of $6F^o$ ($3.3C^o$) at the foam tank outlet to the pump. Figure 130 shows the tank pressure profile during the run. Figure 131 shows tank liquid temperatures. The pumping rate during the run was 75 gal/minute (4732 cc/sec). The high pressure tank was vented during the run with pressures ranging from 17 to 18 psia (11.7 to 12.4 N/cm^2) during pumping.

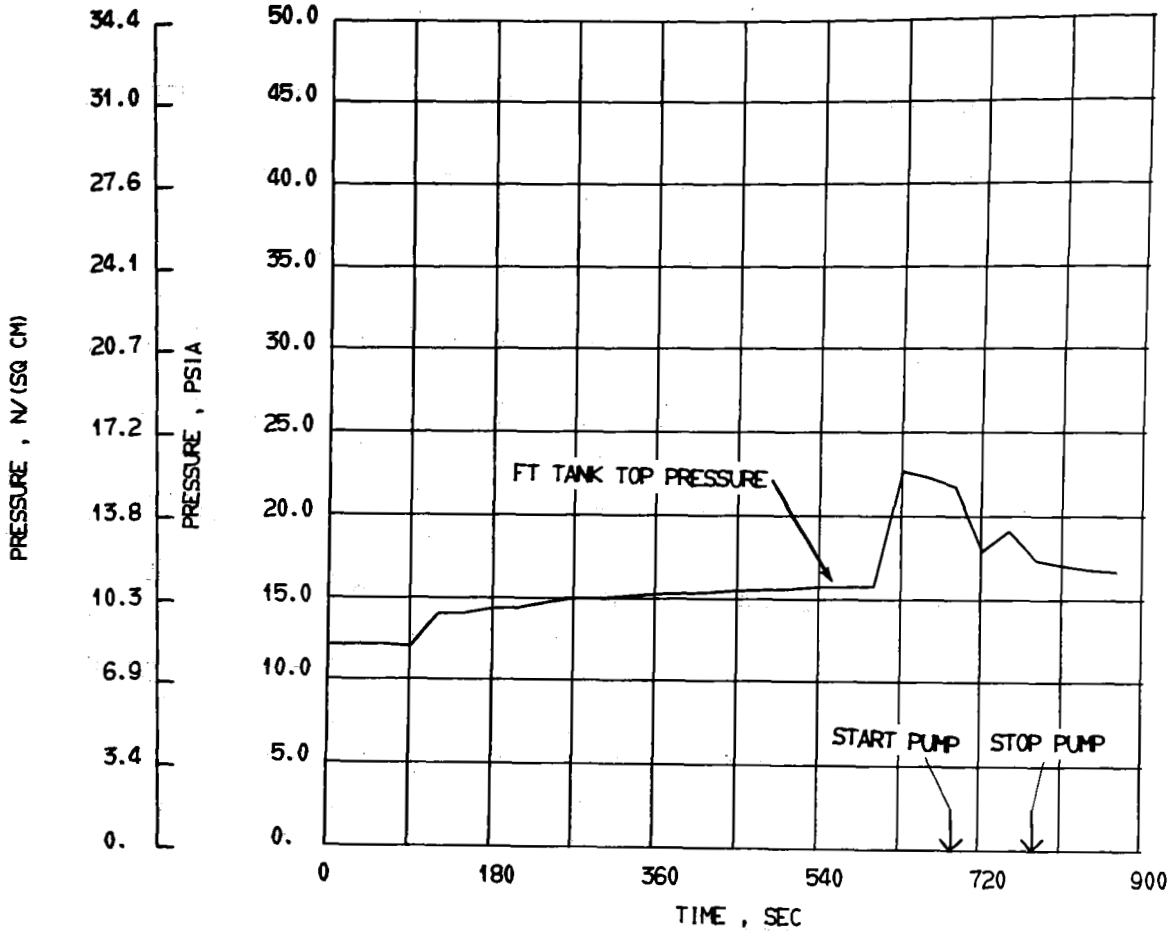

Figure 130.- Test Number 22 - Fuel-Transfer Tests: Pressure at Top of Foam-Filled Tank

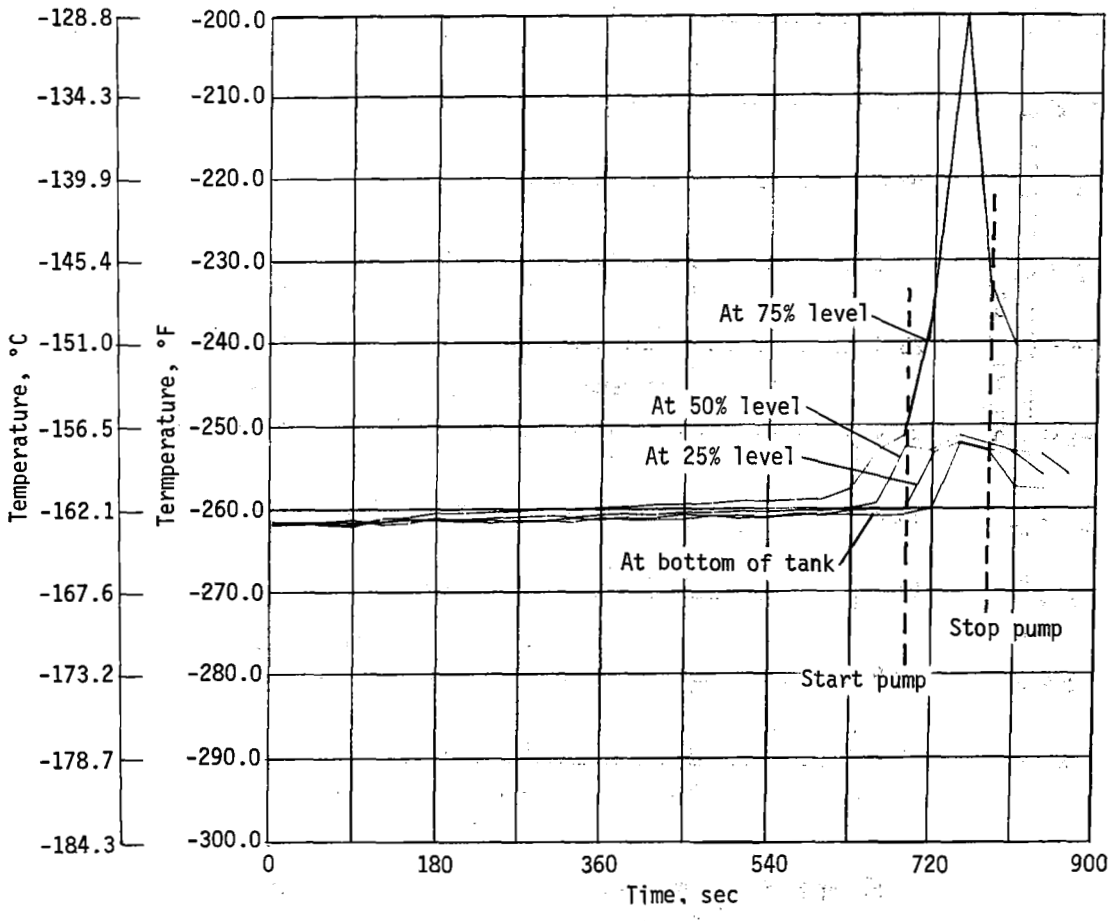

Figure 131.- Test Number 22 - Fuel-Transfer Tests:
Temperature of Liquid in Foam-Filled Tank

2) Test 23: During this test with continuous moderate sloshing, pressurization before pumping was from 16 to 18 psia (11.0 to 12.4 N/cm^2). A computed pumping rate of 94 gal/min. (5930 cc/sec.) was attained during this run. Sloshing produced no noted effect on pumping or tank liquid temperatures.

3) Test 24: This test, with a period of violent slosh when the 75% level was reached in the high pressure tank, was similar to Test 23 except that a pump rate of only 28 gal/minute (1767 cc/sec) was indicated. Some variation in actual flowrates was probably caused by variation in sensor response and the short pumping times involved. No effect on pumping by the violent sloshing was indicated by the data.

c. Baffle tank tests. During this test series the baffle tank was used as the liquid supply to the pump inlet.

1) Test 32: Pressurization for pump NPSH during this test was from 12 to 25 psia (8.3 to 17.2 N/cm^2). Tank liquid temperature at the beginning of pumping was -262°F (163.3°C) and rose to -250°F (-156.7°C) during the run. Figures 132 and 133 show baffle tank pressures and liquid temperatures during the test. With this tank configuration a combination of pressure transfer and pumping must be used due to the internal configuration of the tank. Figure 132 shows that the pump end compartment must be supplied liquid by pressure transfer in order to supply liquid to the pump inlet.

Figures 134 and 135 show high pressure tank pressure and liquid temperature lustories during the run. Prior to pumping the high pressure tank pressure was allowed to build up to 37 psia (25.5 N/cm^2). During pumping the tank was vented to provide a better pumping rate.

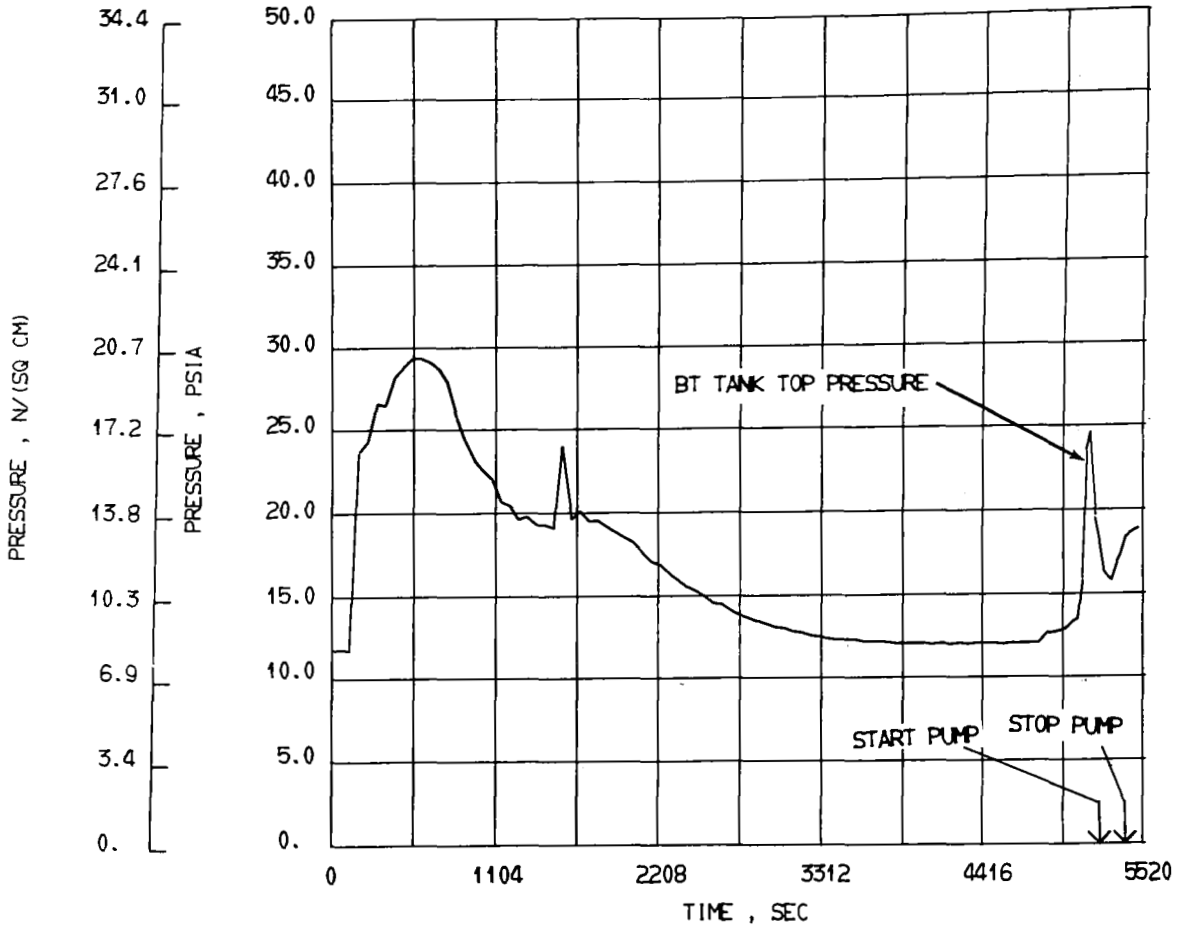

Figure 132.- Test Number 32 - Fuel-Transfer Tests: Pressure at Top of Baffled Tank

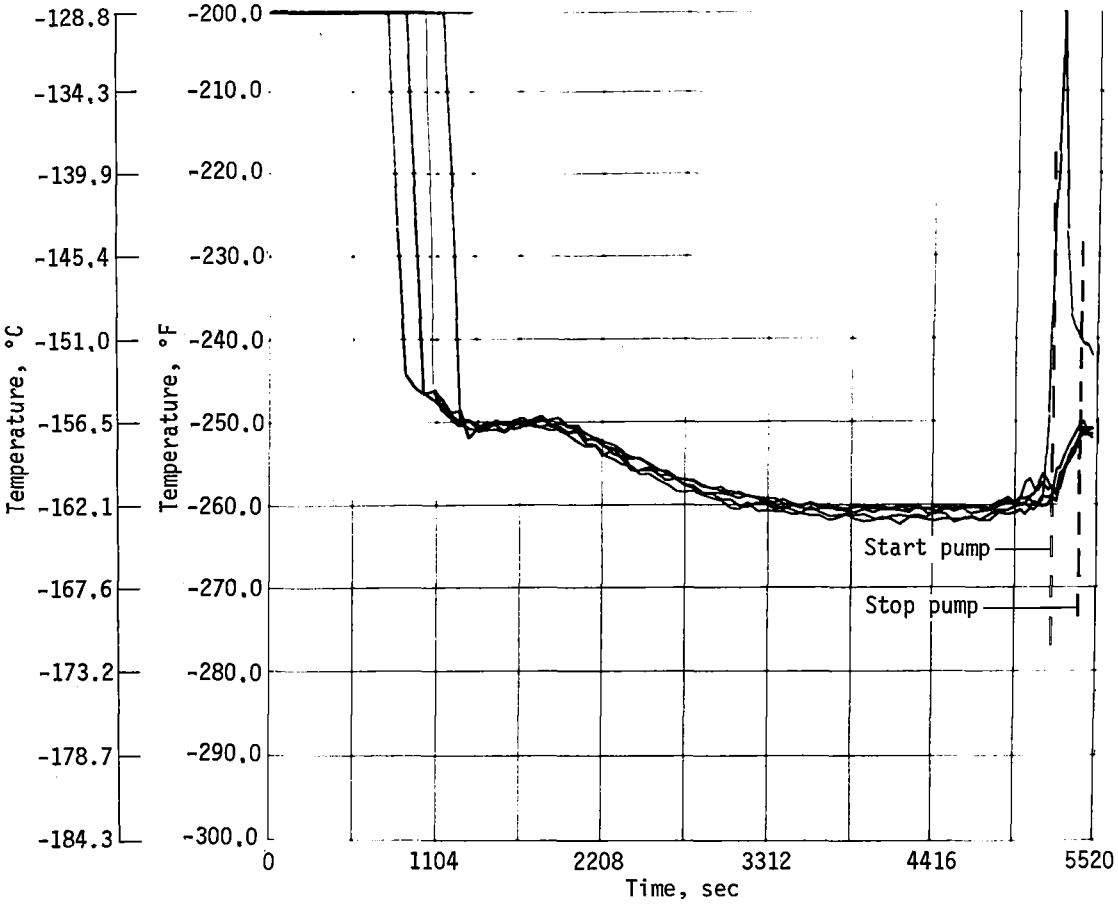

Figure 133.- Test Number 32 - Fuel-Transfer Tests:
Temperature of Liquid in Last Compartment of Baffled Tank

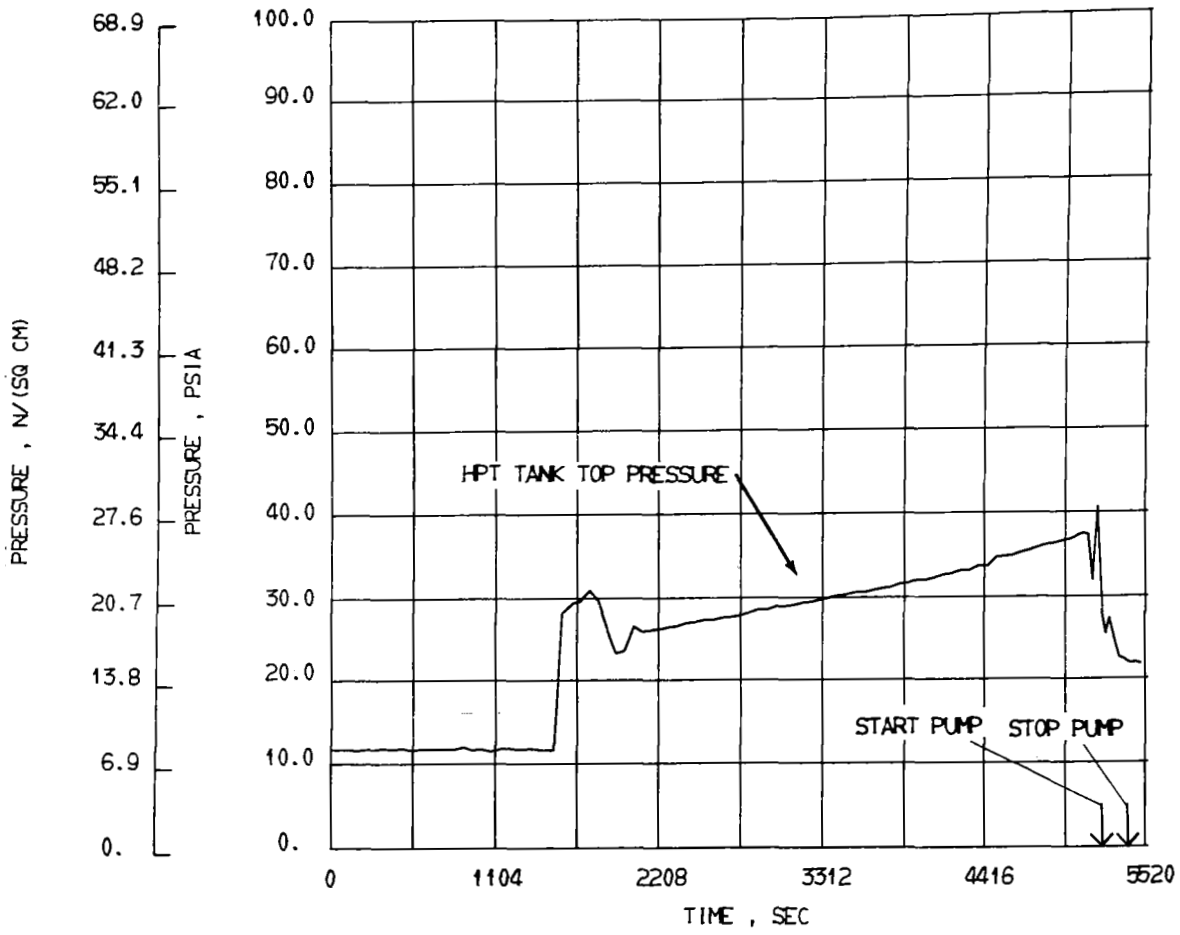

Figure 134.- Test Number 32 - Fuel-Transfer Tests: Pressure at Top of High-Pressure Tank

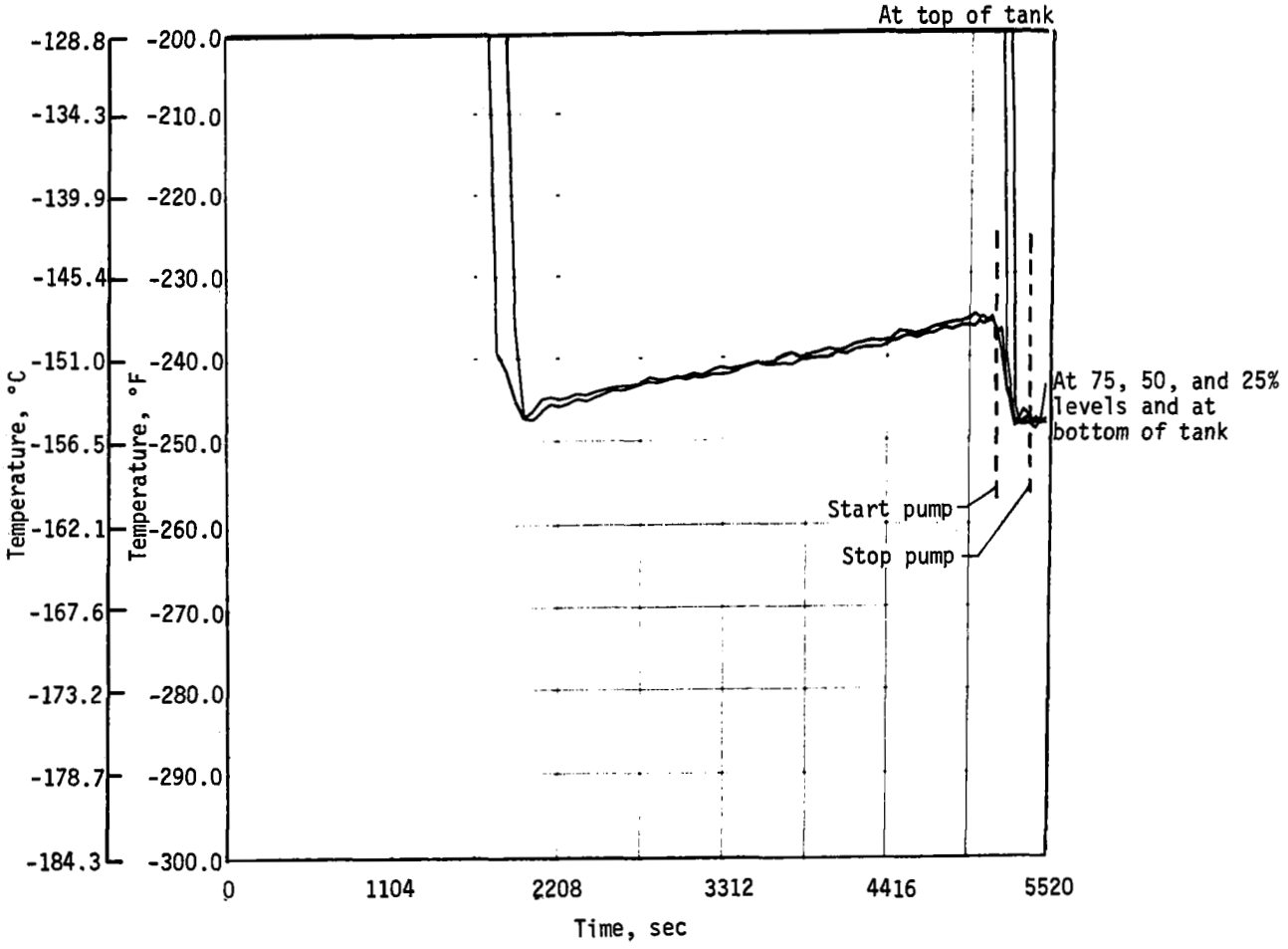

Figure 135.- Test Number 32 - Fuel-Transfer Tests: Temperature of Liquid in High-Pressure Tank

2) Test 33: This test was similar to Test 32 except that moderate sloshing was used during the pump run. No difference in results were evident as a result of the sloshing.

3) Test 34: During this test violent sloshing was started when the high pressure tank reached 75% full. As indicated by the BT tank pressure and the BT and high-pressure tank liquid temperatures of figures 136 - 138, no effect from sloshing on the pump run could be detected.

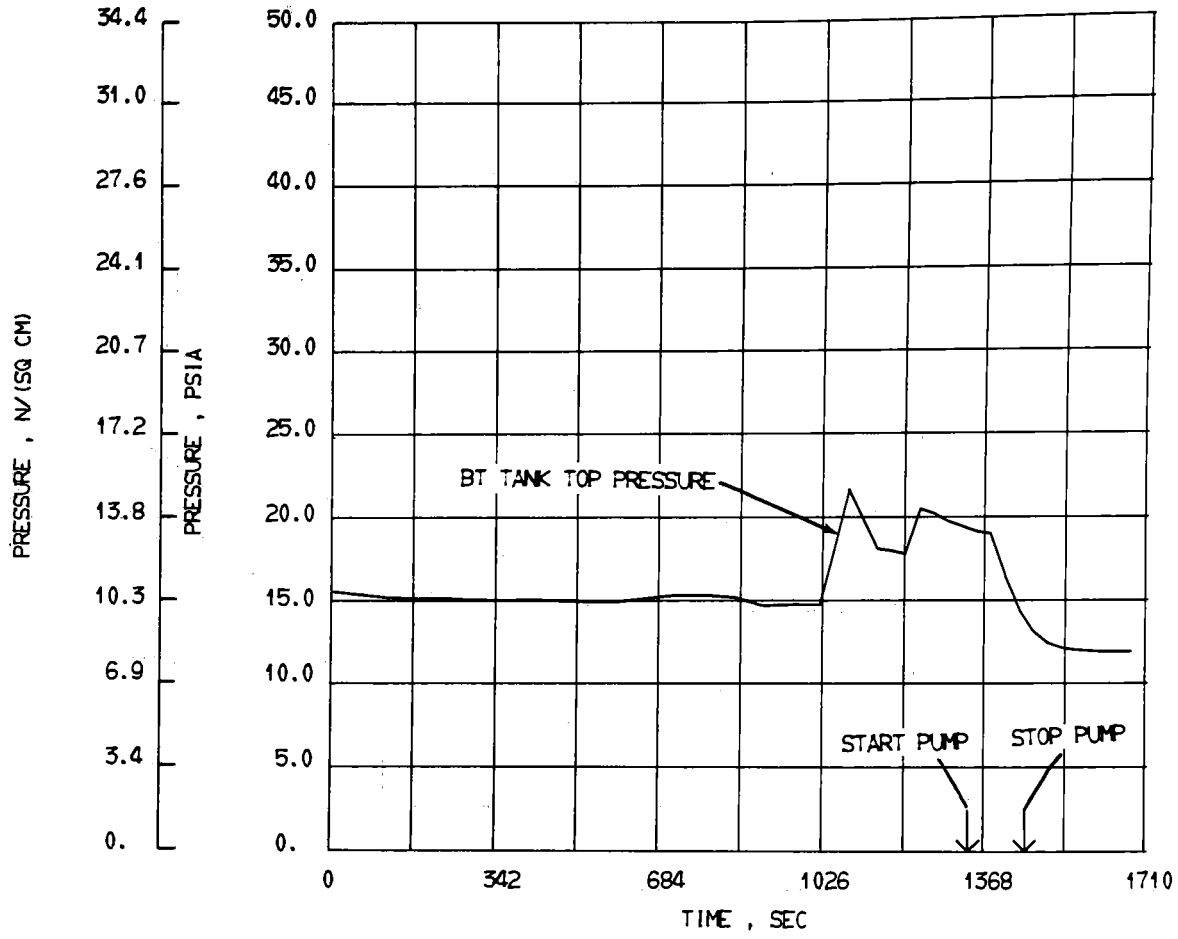

Figure 136.- Test Number 34 - Fuel-Transfer Tests: Pressure at Top of Baffled Tank

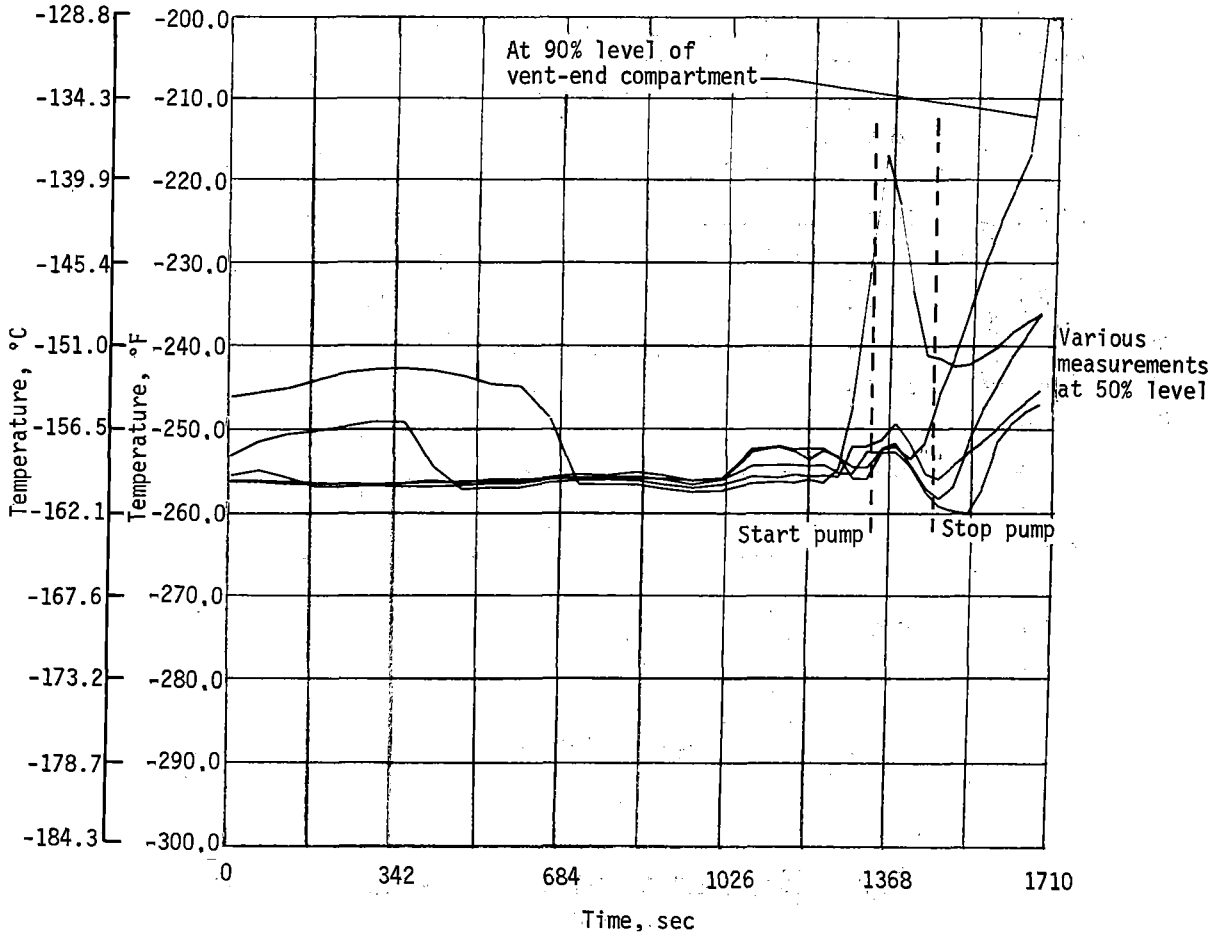

Figure 137.- Test Number 34 - Fuel-Transfer Tests:
Temperature of Liquid in Baffled Tank

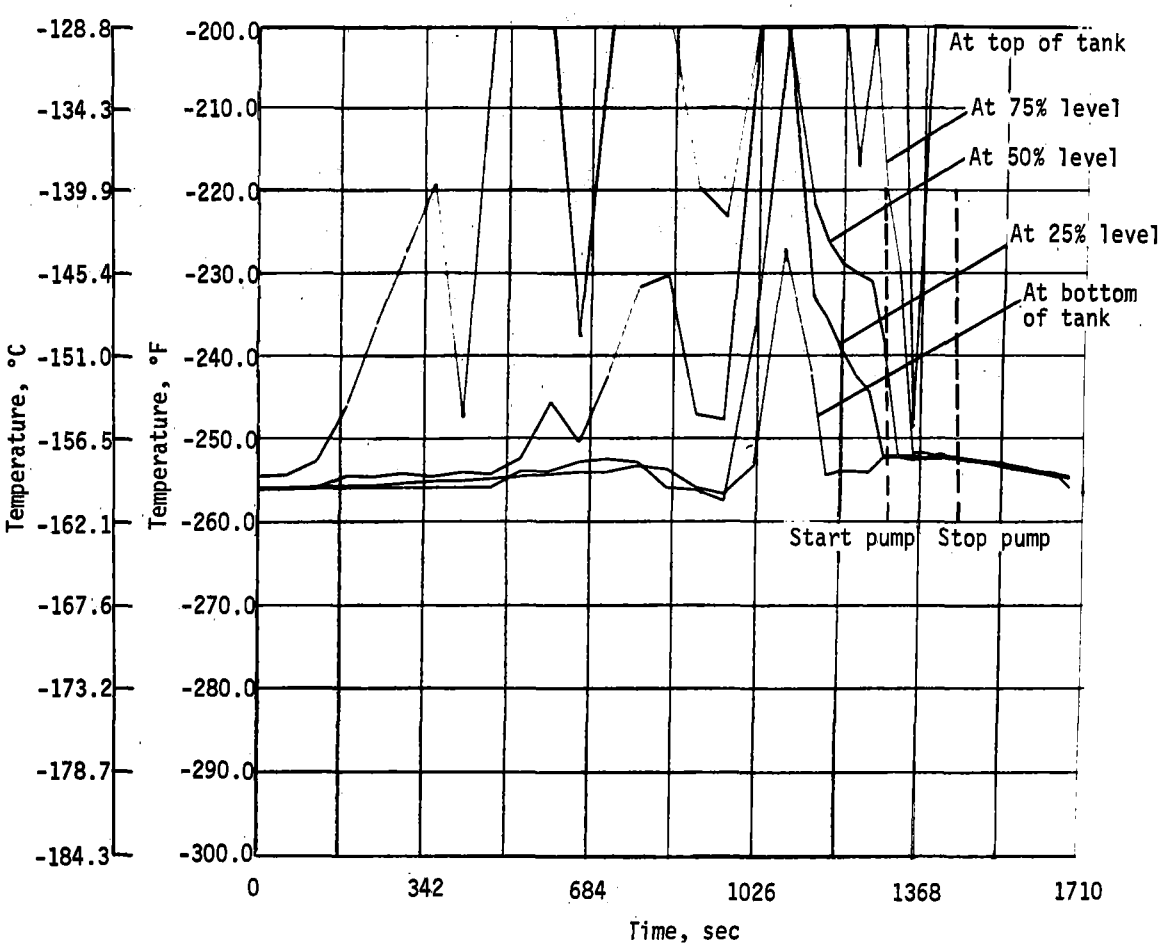

Figure 138.- Test Number 34 - Fuel-Transfer Tests: Temperature of Liquid in High-Pressure Tank

2. Test Summary

Data from pumping using each of the three low-pressure tank configurations was similar. In each case pressure in the low-pressure tank was raised from 2 to 13 psi (1.4 to 9.0 N/cm^2) above the pressure in the high-pressure tank to provide pump NPSH. The standpipe tank required the lowest pressure rise of 2 to 3 psi (1.4 to 2.1 N/cm^2) while the baffle tank required 10 to 13 psi (6.9 to 9.0 N/cm^2) in order to prevent pump cavitation. A liquid temperature rise of 2 to $3F^o$ (1.1 to $1.7C^o$) was noted in the pump loop, i.e., from the source tank outlet to the receiver tank inlet. Sloshing had no noticeable effect on pumping or on bulk liquid temperatures in the tanks during test. Pump NPSH required was 4.5 feet (1.38m) of water or about 2 psi (1.4 N/cm^2). Flow and heat losses in the systems made up the difference in tank pressure requirements over that required by the pump.

E. SIMULATED FLIGHT TEST

This series of tests was conducted to determine the response on the tank system to variations in conditions created by supersonic flight. These variations consisted of pressure changes caused by ascent to and descent from an operating altitude and wing skin heating due to supersonic flight. To simulate a flight altitude profile the pressure in the test tank was varied according to the profile shown by Figure 139. Wing skin heating was provided by banks of quartz lamps above and below the wing section. Power input to the lamps was programmed over a time span similar to that use for the altitude profile.

1. Test Description and Data, Initial Test Series

During these tests each of the low-pressure tank configurations was tested under similar conditions. The tests had four phases: a 25-minute climb to altitude, a period of tank offloading to simulate fuel usage, and a 20-minute descent. The wing skin temperature was programmed to increase ambient to 400°F (204.4°C) during ascent, to hold at 400°F (204.4°C) during the offloading period, and to decrease toward ambient during the descent.

Each of the three low-pressure tank configurations was run through the flight profile for three cases -- no sloshing, continuous moderate sloshing, and periodic violent sloshing.

a. Standpipe tank tests. - During this series of tests the standpipe tank was in the low-pressure tank position.

Tests 14, 15 and 16 varied only in the sloshing conditions imposed for each test. No effect due to sloshing could be detected so a representative run of the three was selected for presentation.

Figure 140 shows standpipe tank pressure during Test 16. The pressure increase between the ascent and descent phases indicates the 50% drainback. During this run, there were two periods of violent sloshing.

Figure 141 shows the temperatures in the standpipe tank during Test 16. During the ascent, the decreasing pressure caused bulk boiling of the liquid, which destroyed any liquid stratification. Consequently all the liquid-level probes read together.

The tank-top probe appeared to be reading the ullage temperature just above the surface of the liquid at the start of the run. Then, as the ascent began and the cold vapors cooled down the ullage, the temperature at the top of the tank dipped briefly to the temperature of the liquid. Finally, as more liquid boiled and the liquid surface dropped, the temperature at the top of the tank began to rise again.

Before the descent, the temperature of the liquid at the 50% level behaved similarly. After the drainback, this probe was uncovered, but it was just above the surface. After the draining was complete, the tank was vented in preparation for the descent. During venting, the liquid at the 50% level cooled with the ullage, and then warmed once the vent was closed and the ullage warmed.

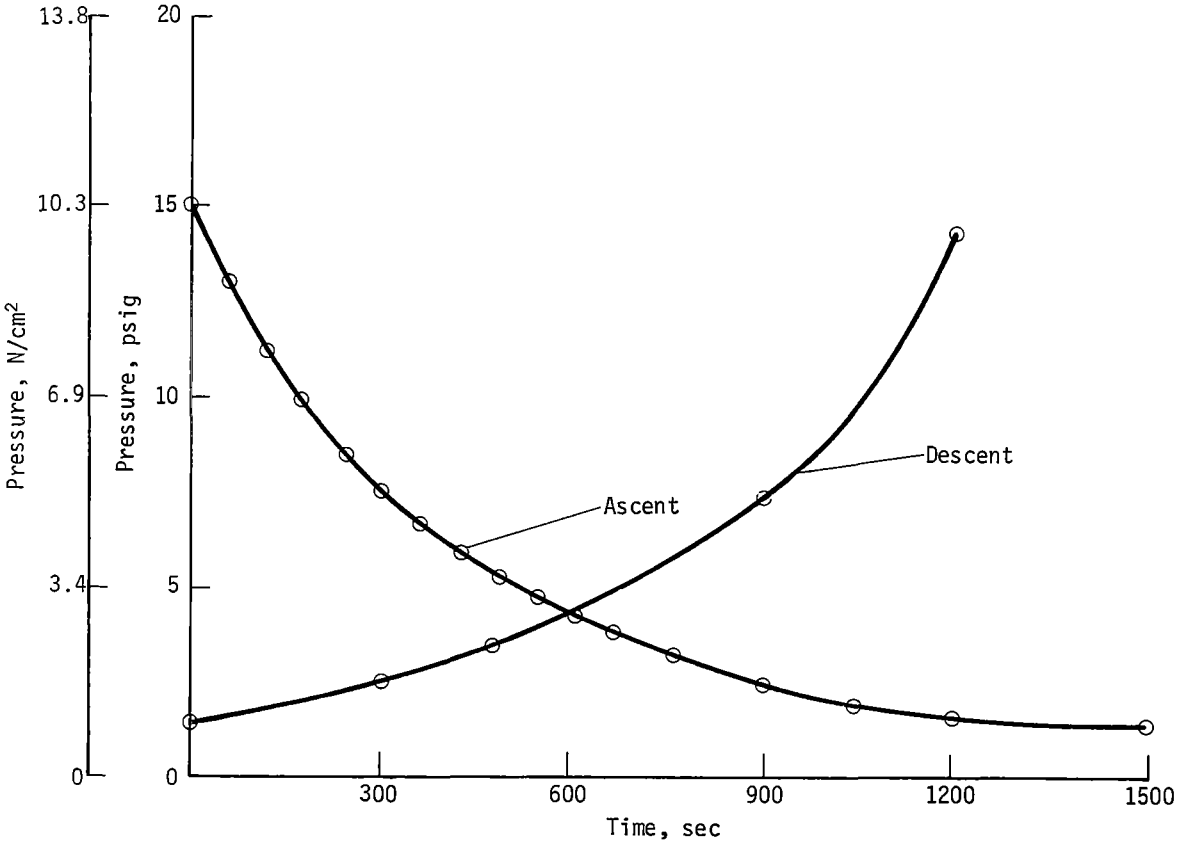

Figure 139.- Simulated Aircraft Ascent and Descent Pressure Profile

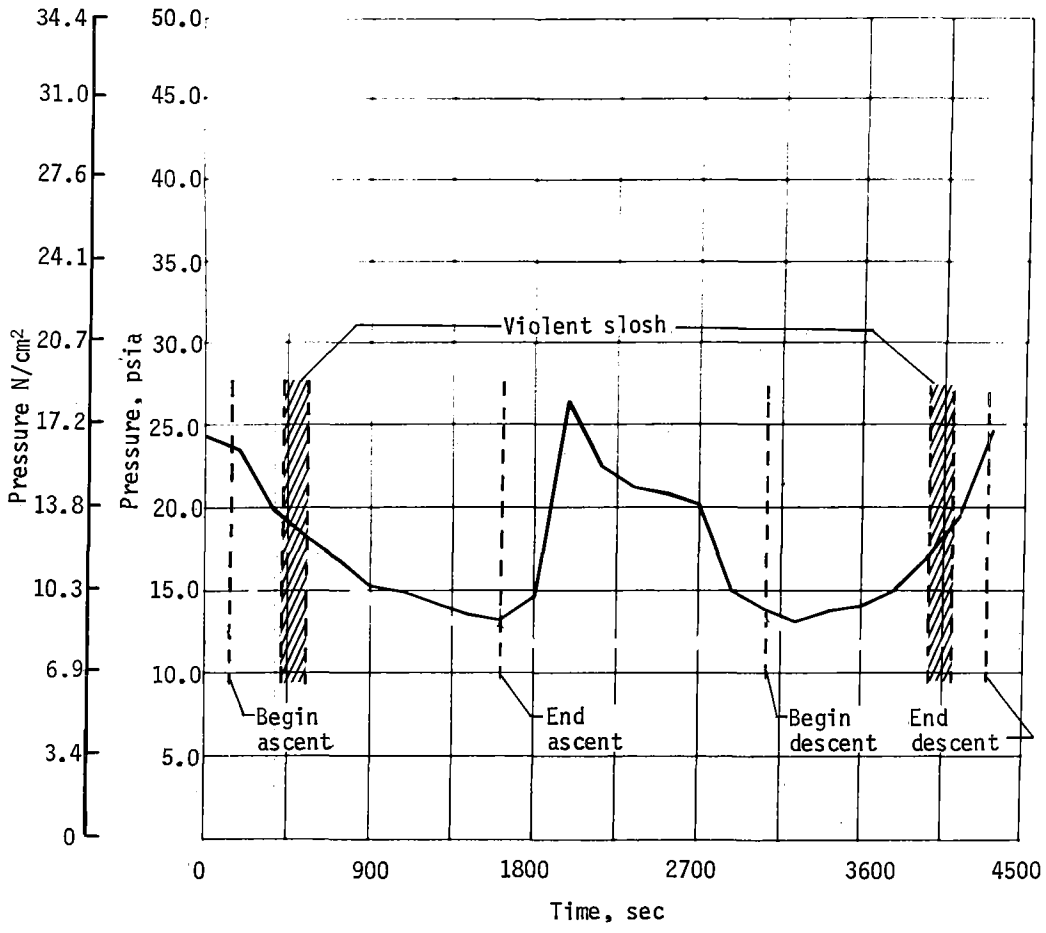

Figure 140. - Test Number 16 - Simulated Flight Test: Pressure at Top of Standpipe Tank

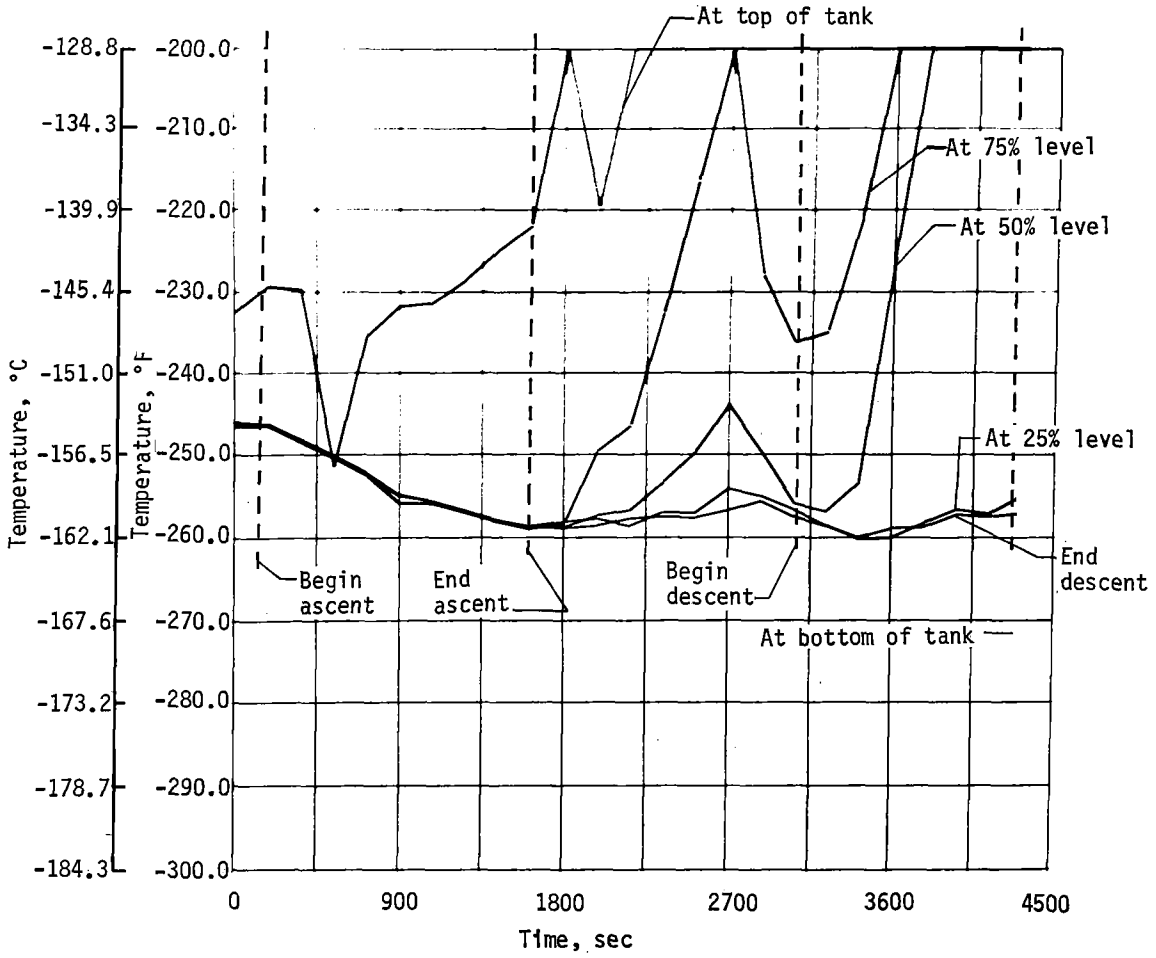

Figure 141.- Test Number 16 - Simulated Flight Test: Temperature of Liquid in Standpipe Tank

During the descent, stratification was established throughout the liquid. The condensation of the ambient pressurant gas warmed the top layer of liquid, but not enough heat leaked to the tank to warm the bulk liquid to equilibrium.

By the end of the descent, the temperature at the 25% level was -255°F (-159.4°C), or subcooled by 7F° (3.9C°), and there was about 2F° (1.1C°) of stratification from the tank bottom to the 25% level.

Figure 142 shows the temperature of the liquid at various levels in the standpipe.

Figure 143 and 144 shows the vent gas flowrates throughout Test 16 for the standpipe tank and high-pressure tank. The amount of gas vented during the ascent in Test 16 was 29.4 lb (13.3 Kg), based on the integrated flowrate curve.* Liquid subcooling at the start of the simulated ascent was negligible. The pressurization gas required during the descent could not be determined because the short pressurizing cycles (usually less than 5 sec) could not be consistently picked up with a data sampling rate of one sample each 180 sec. This problem was eliminated in Tests 42 thru 47 by using continuous data sampling.

Figure 145 shows the performance of the wing heating system. The upper wing structure reached 400°F (204.4°C) just at the end of the ascent and held there throughout the simulated cruise and fuel outflow. At the beginning of descent, the power was cut to the heat lamps, and the upper wing structure cooled to 280°F (137.8°C) by the end of the descent.

Figure 146 and 147 show how the temperature of the insulation was affected by having wing heating on one side of the tank and cryogenic temperatures on the other.

b. Foam-Filled tank tests. - These tests were similar to Test 14, 15, and 16, except that the foam-filled tank was in the test position instead of the standpipe tank. The three tests differed only in terms of the sloshing: the first test was run without sloshing, the second with continuous moderate sloshing, and the third with periodic violent sloshing. Once again, the sloshing had no noticeable effect on pressure or temperature.

The tank pressure during Test 26 is shown in Figure 148. So that the liquid would be subcooled for the ascent, the tank was vented before being pressurized (Figure 148).

In Tests 26 and 27, the bulk liquid was subcooled 11F° (6.1C°) at the start of the ascent. About 12.3 lb (5.4 Kg) of vapor was lost during each test. The temperature of the liquid during Test 26 is shown in Figure 149. As in the standpipe tank tests, there was little tendency for the liquid to

*Test 14 was similar to Test 16 with little or no subcooling before ascent. Approximately 30.1 lb (-13.6 Kg) of gas was vented. In Test 15 (continuous moderate sloshing), there was 5.5F° (3.1C°) of subcooling, and only 19.2 lb (8.7 Kg) of vapor was lost.

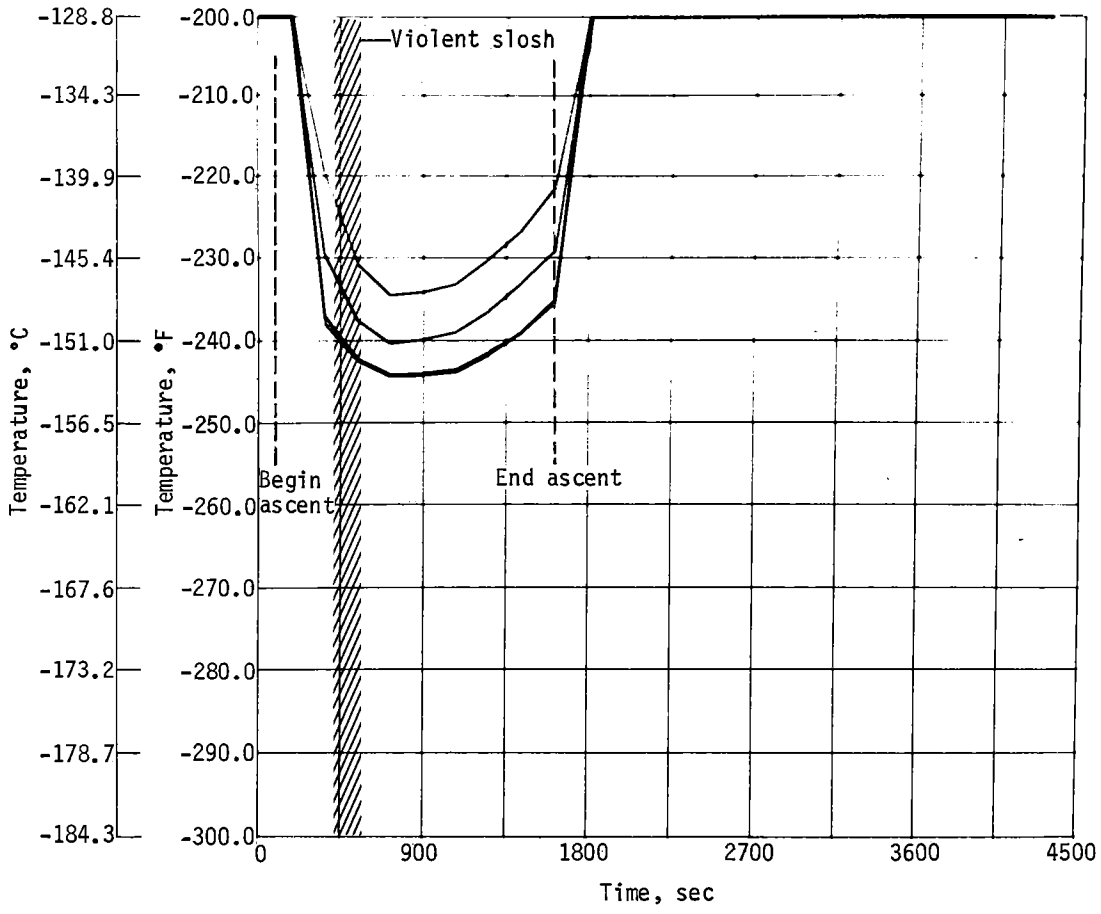

Figure 142.- Test Number 15 - Simulated Flight Test: Temperature of Liquid in Standpipe

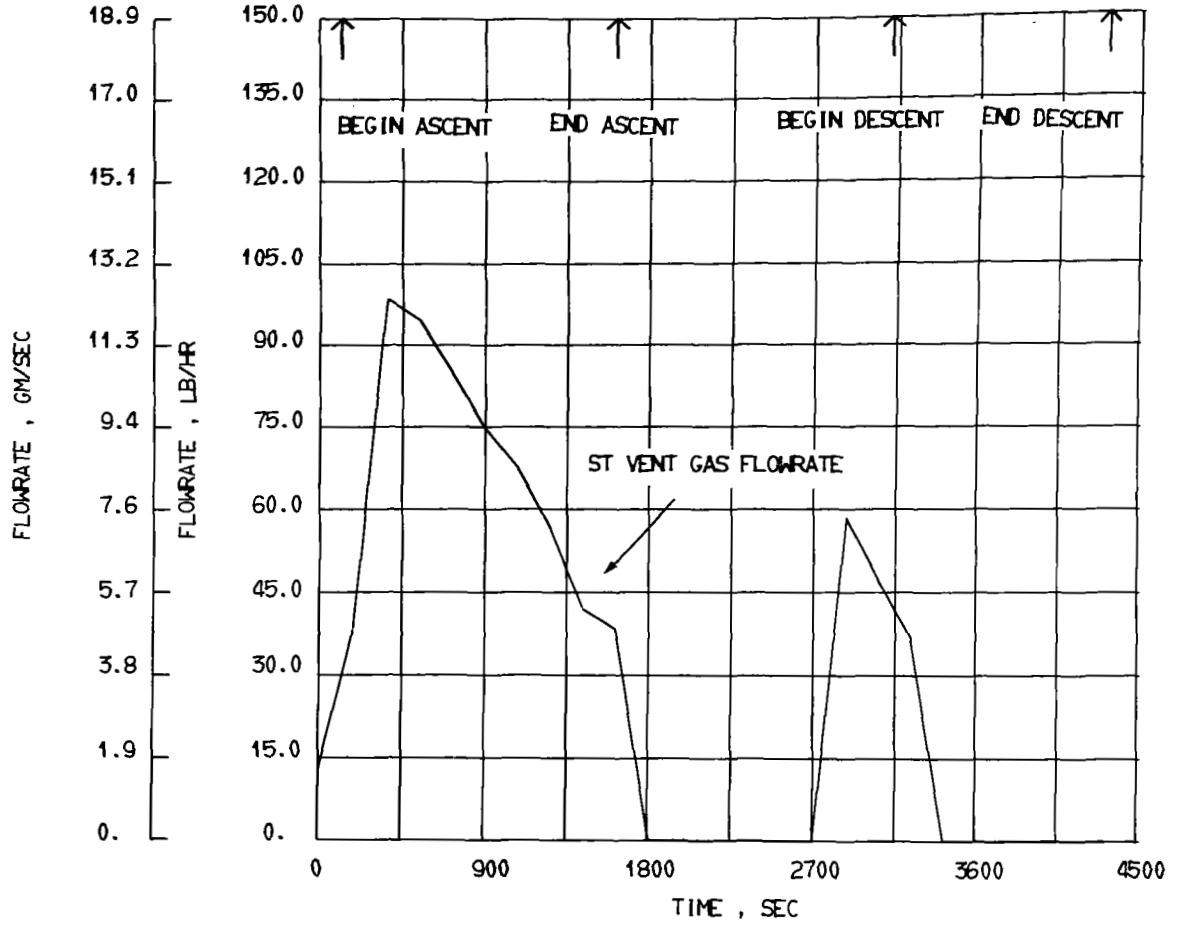

Figure 143.- Test Number 16 - Simulated Flight Test: Flowrate of Standpipe Tank Vent Gas

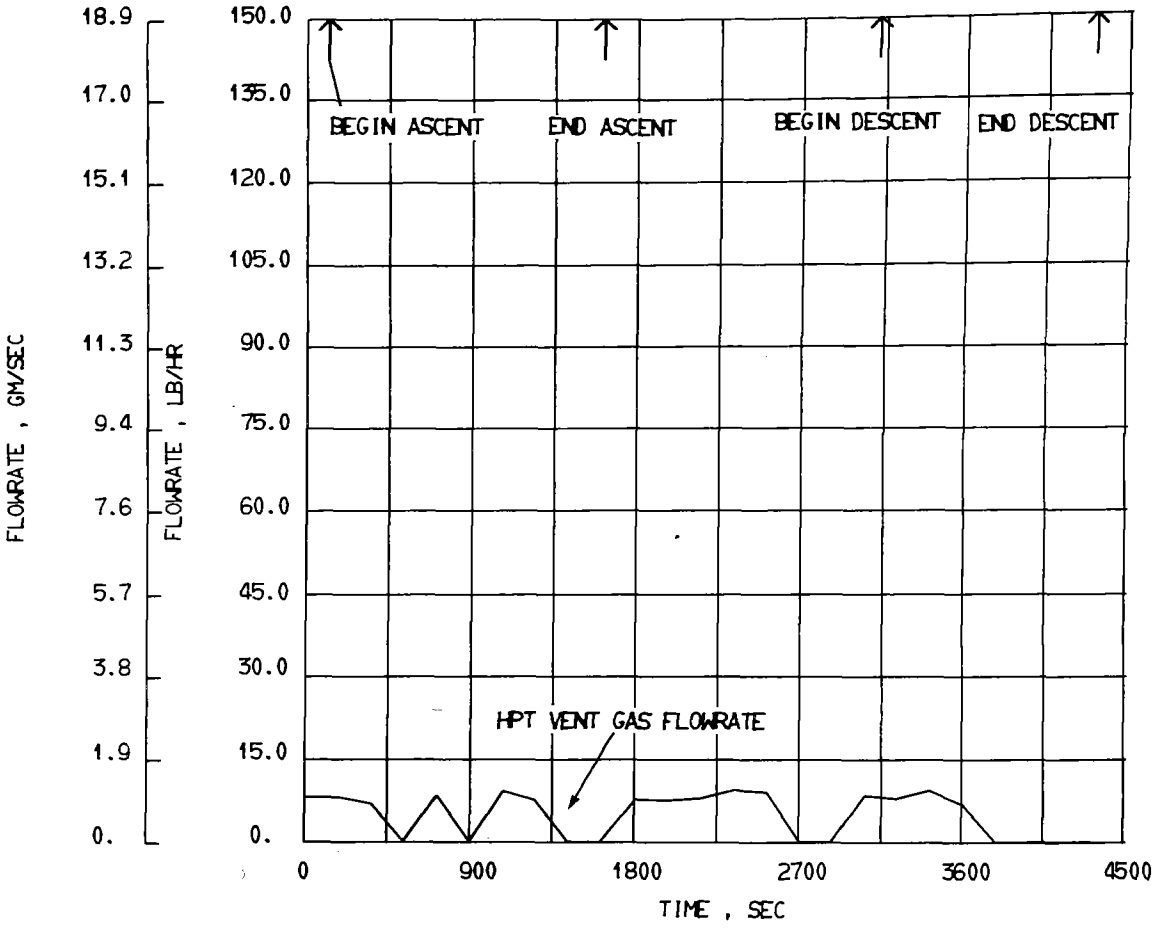

Figure 144.- Test Number 16 - Simulated Flight Test: Flowrate of High-Pressure Tank Vent Gas

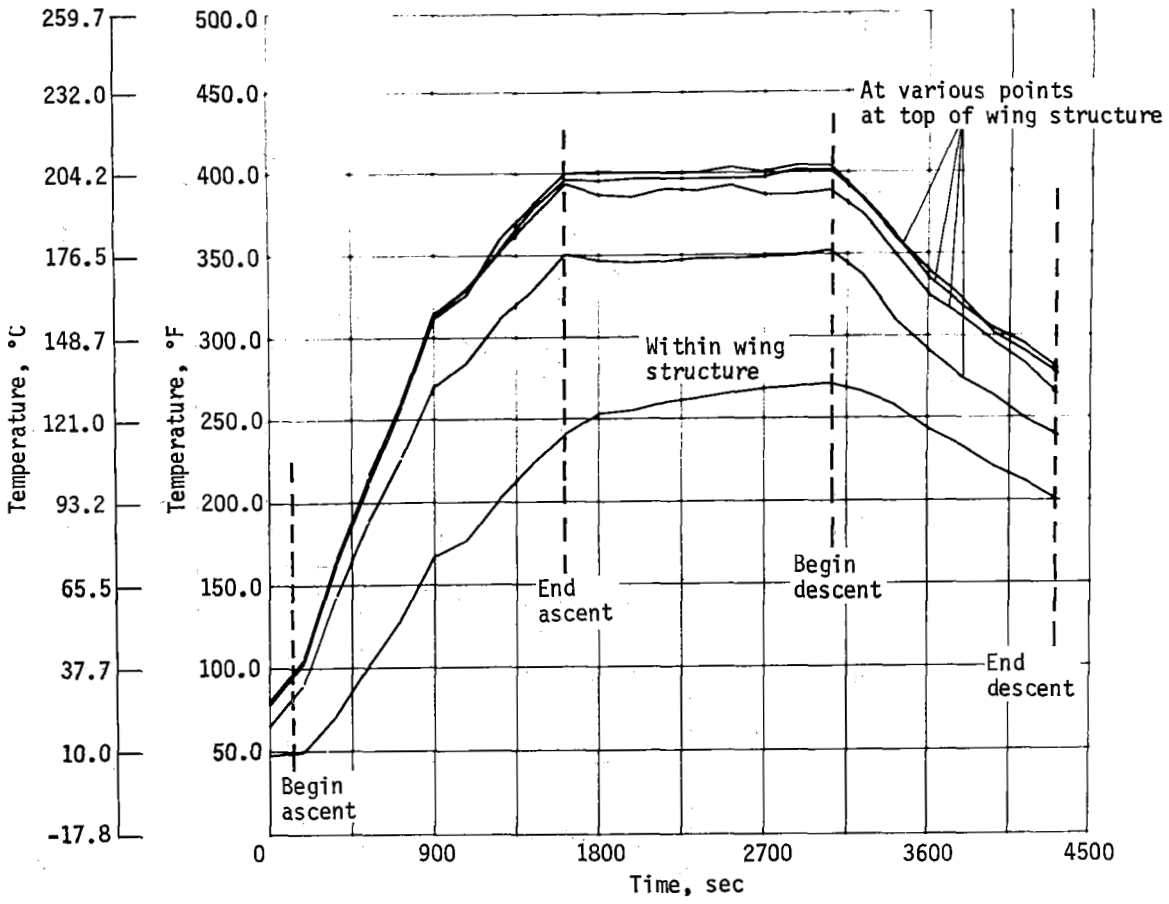

Figure 145.- Test Number 16 - Simulated Flight Test:
Temperature of Wing Structure

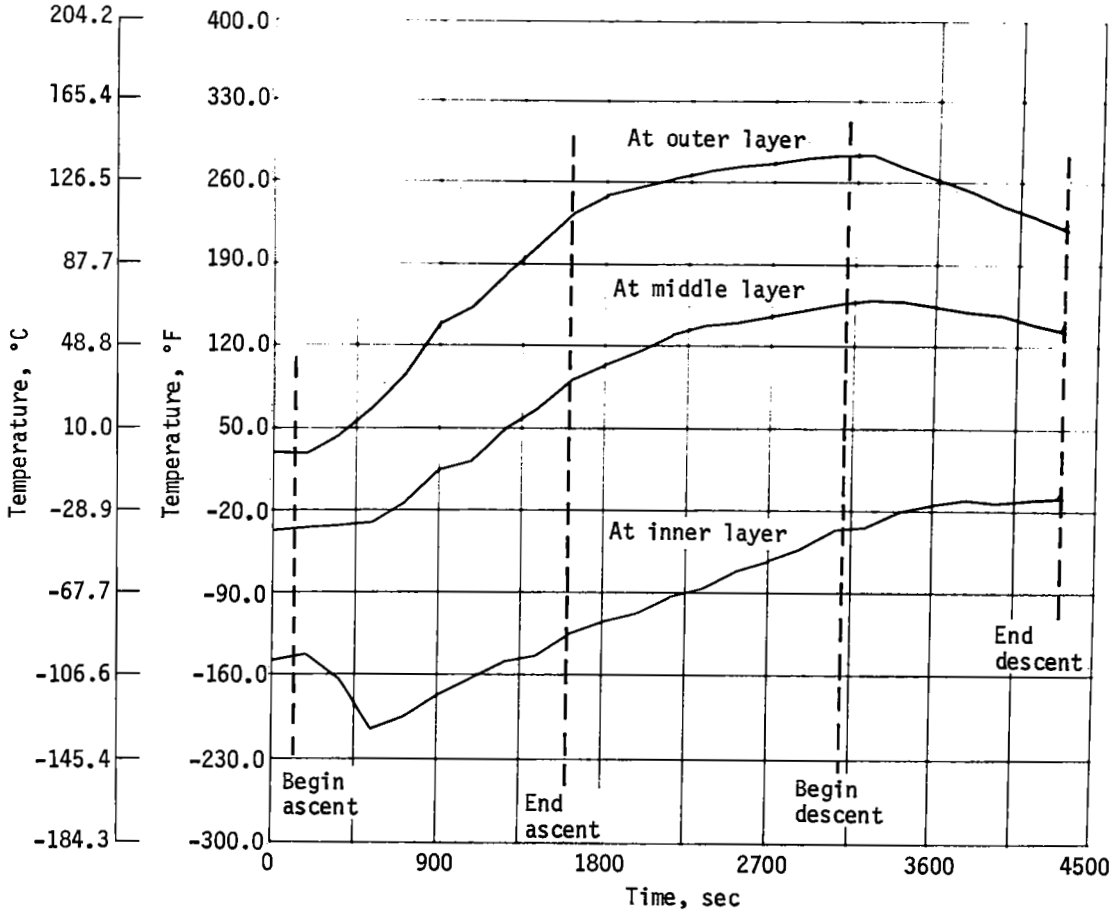

Figure 146.- Test Number 16 - Simulated Flight Test: Temperature of Insulation at Top of Standpipe Tank

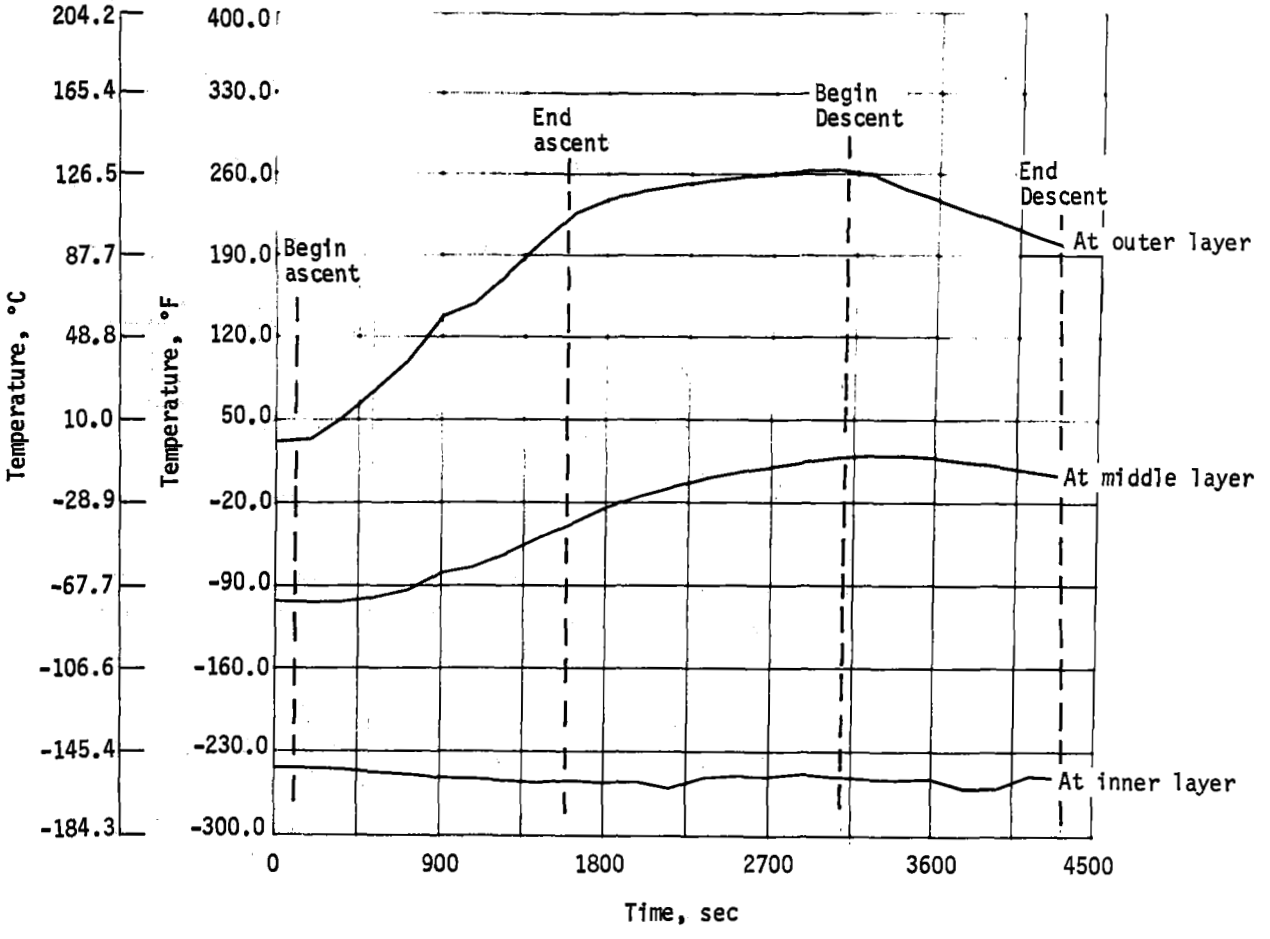

Figure 147.- Test Number 16 - Simulated Flight Test: Temperature of Insulation on Bottom of Standpipe Tank

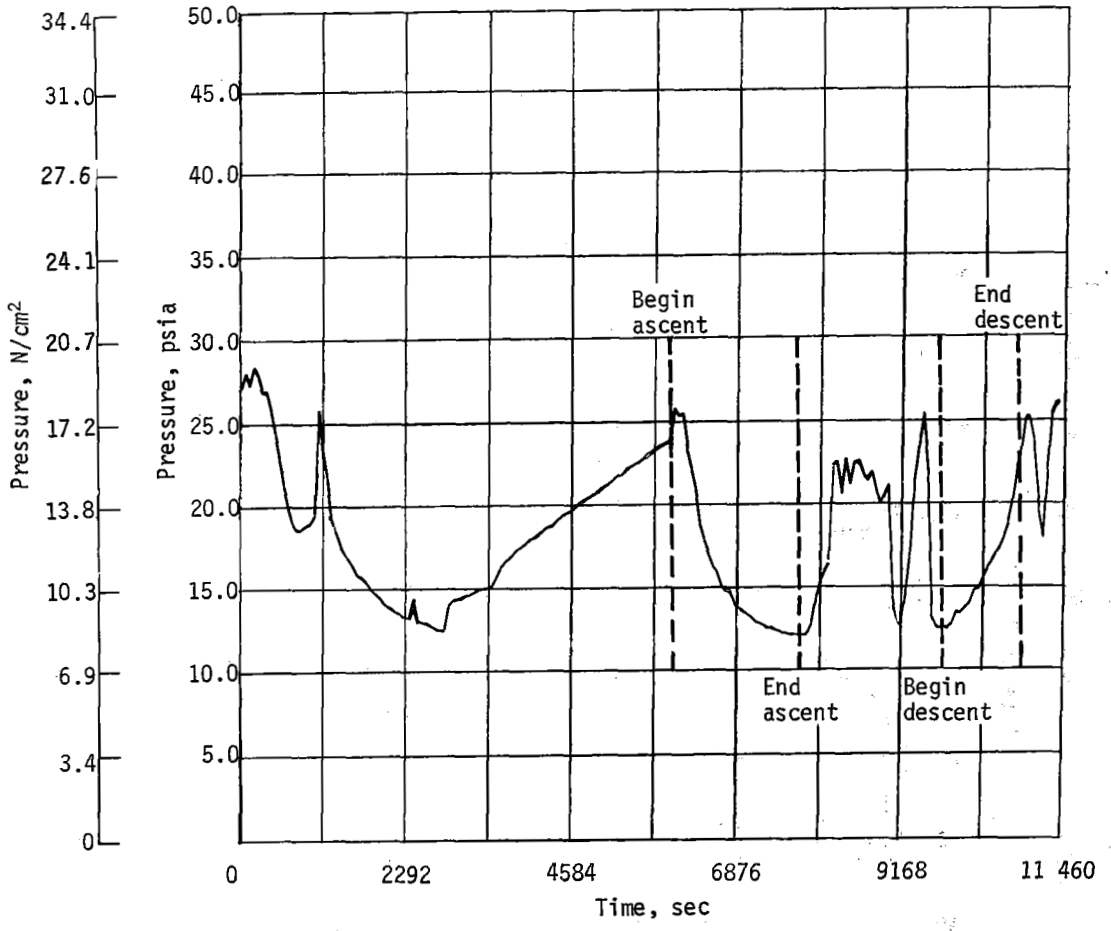

Figure 148. - Test Number 26 - Simulated Flight Test: Pressure at Top of Foam-Filled Tank

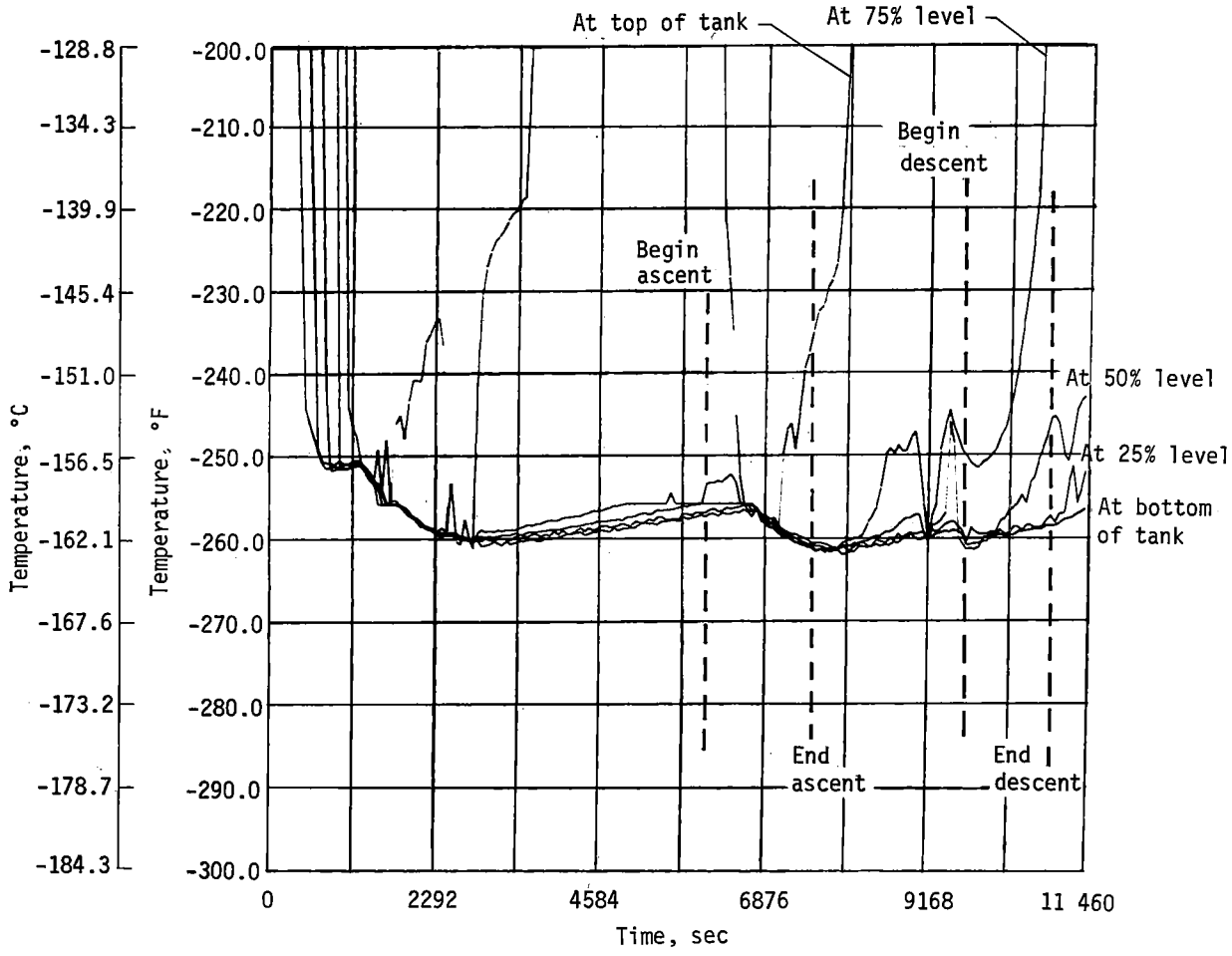

Figure 149.- Test Number 26 - Simulated Flight Test: Temperature of Liquid in Foam-Filled Tank

stratify during ascent, but considerable stratification during descent. The bulk liquid was stratified 11F° (6.1C°) by the end of the descent.

The temperatures of the insulation and wing structure were similar to those measured in the standpipe tank flight simulation tests. Figure 150 shows the temperature of the insulation on top of the foam-filled tank in Test 26.

Vent and pressurization gas flow rates for the foam tank during Test 26 are shown by Figures 151 and 152. High-pressure tank vent gas rate is shown by Figure 153.

c. Baffle tank tests. - These tests were similar to previous flight simulation tests, except that the baffled tank was used as the test tank. All three tests in this series involved sloshing as the only variable. Again, it had no noticeable effect on pressure or temperature.

Figure 154 shows the tank pressure in Test 36. No attempt was made to subcool the liquid prior to the start of the ascent during any of these three tests, so more liquid was lost during the ascent than during the tests on the foam-filled tank.

The temperature of the liquid in the baffled tank during Test 36 is plotted in Figures 155 and 156 as a function of test time and baffle compartment. Platinum temperature probes at the 50% level of each of the five compartments and at the 90% level of the first and last compartments were used for these measurements. During both ascent and descent, the baffles tended to promote stratification between compartments. The bulk boiling caused mixing in each compartment, but not between compartments.

Because there was no subcooling before the simulated ascent, a relatively large amount 31.5 lb (14.3 Kg) of vapor was boiled off during Test 36, and 34.2 lb (15.5 Kg) was lost during Test 37. In Test 35, the bulk liquid was subcooled approximately 2F° (1.1C°) before ascent and the boiloff mass was only 21.8 lb (9.9 Kg).

After the descent, the bulk liquid was subcooled by 9.0, 12.5, and 11.0F° (5.6, 6.9, and 6.1C°), respectively, in Tests 35, 36, and 37.

The temperatures of the insulation and wing structure were similar to those recorded in previous flight simulation tests.

Vent and pressurant gas flow rates for Test 36 are shown in Figures 157 and 158 for the baffle tank and the vent flow rate for the high-pressure tank is shown by Figure 159.

2. Test Description and Data - Complete Flight Profile Series

This series consisted of six additional simulated flight tests that were proposed after reviewing the test data from the original flight simulation tests. In the first three tests, the pressurant was methane gas; in the last three, it was nitrogen gas. The latter group of tests also had an added goal of measuring the solubility of nitrogen in methane. This was done by taking ten samples at various times during the pressurization cycle.

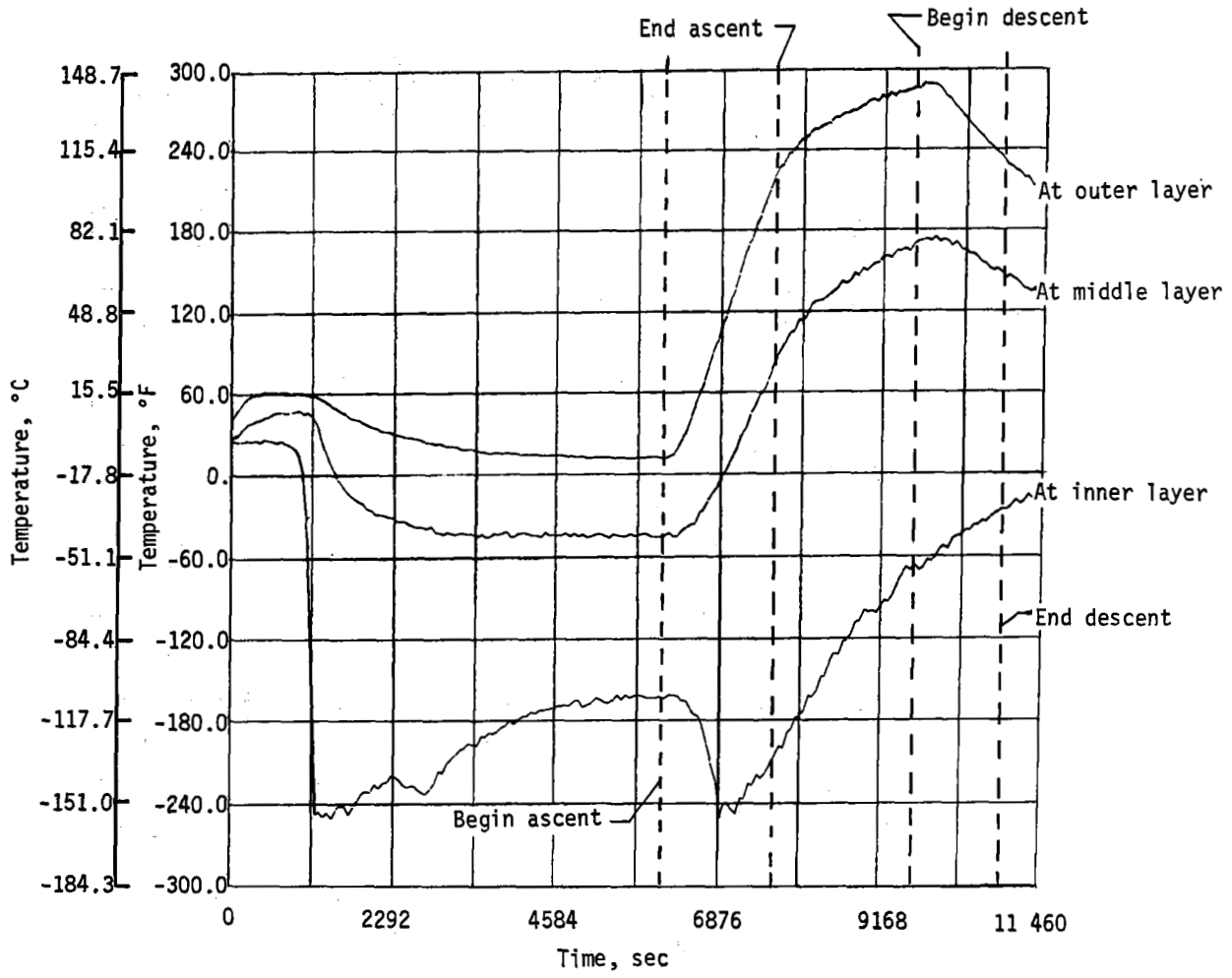

Figure 150.- Test Number 26 - Simulated Flight Test:
Temperature of Insulation at Top of Foam-Filled Tank

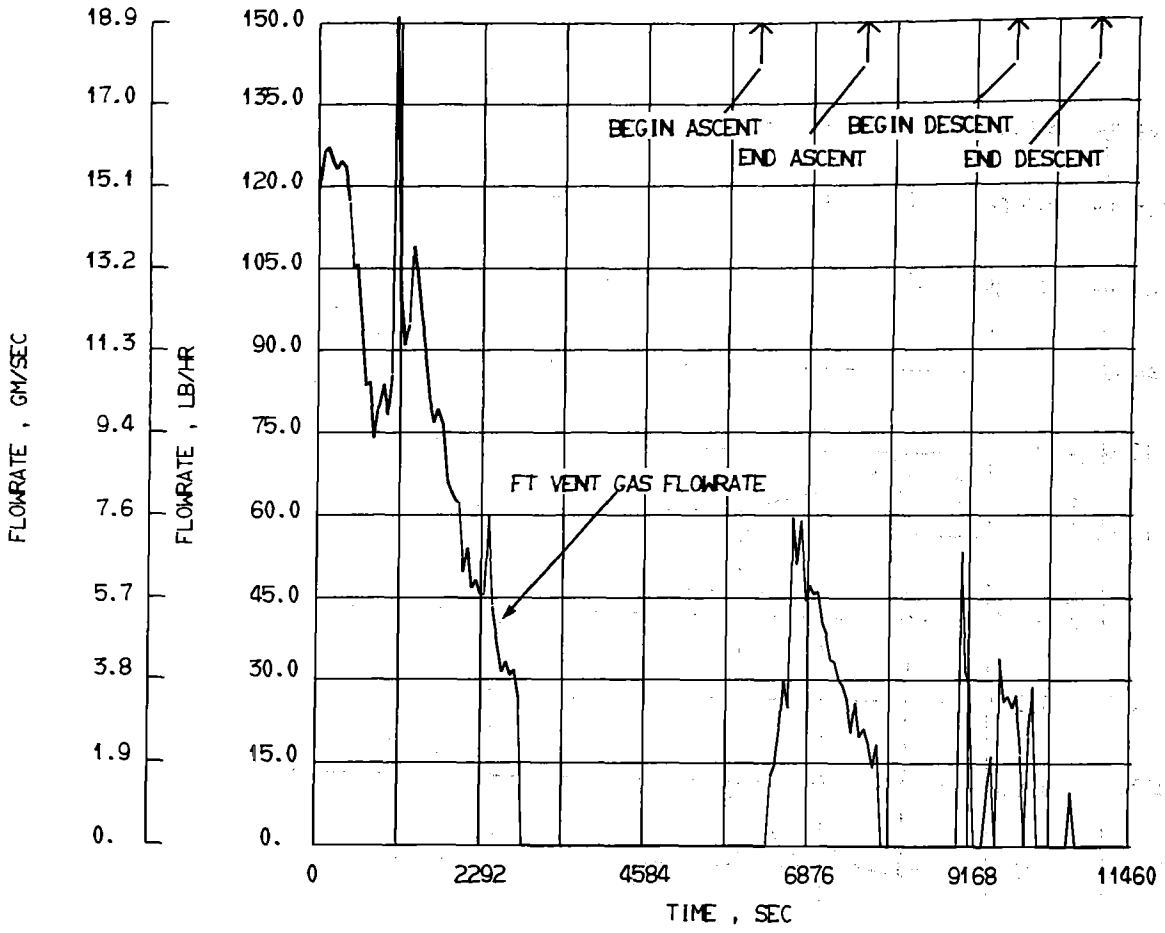

Figure 151.- Test Number 26 - Simulated Flight Test: Flowrate of Foam-Filled Tank Vent Gas

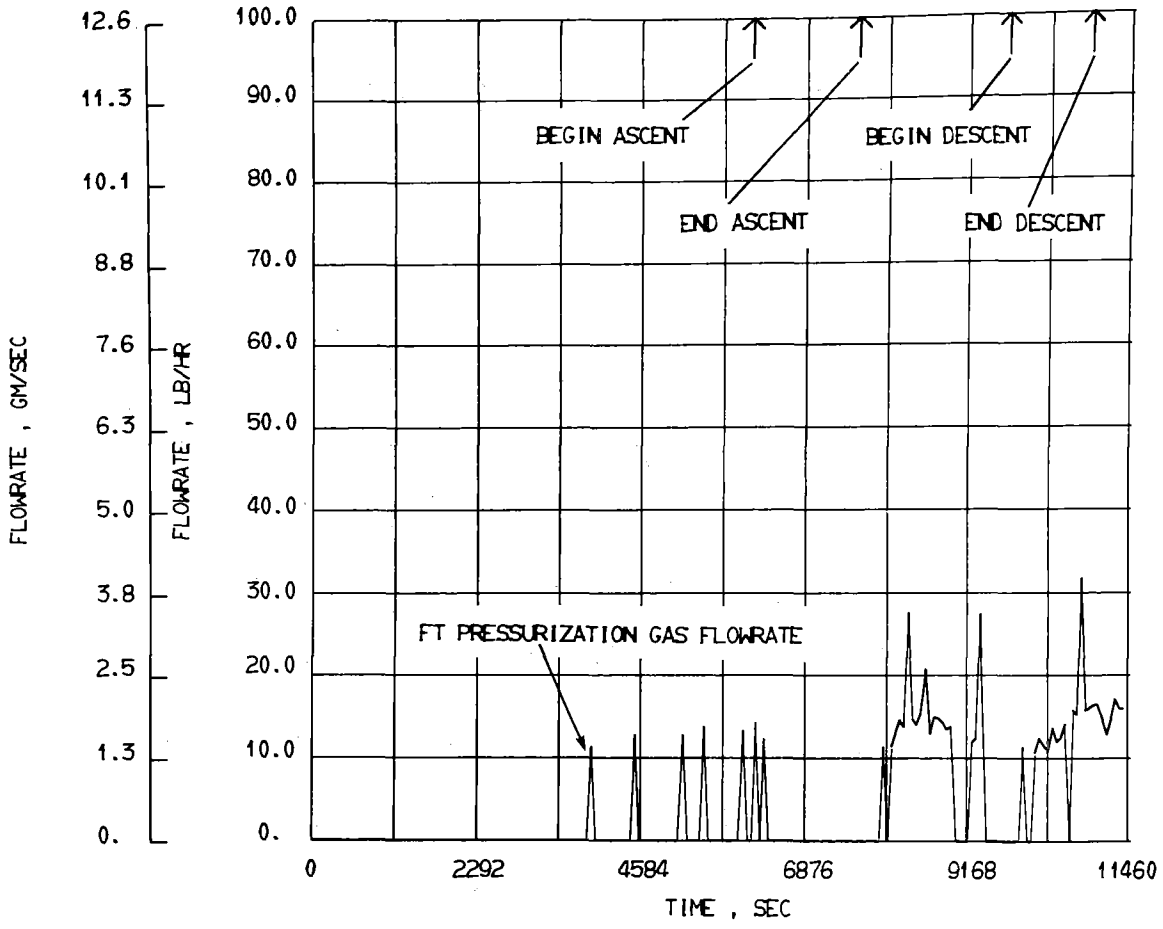

Figure 152.- Test Number 26 - Simulated Flight Test: Foam-Filled Tank Pressurization Gas

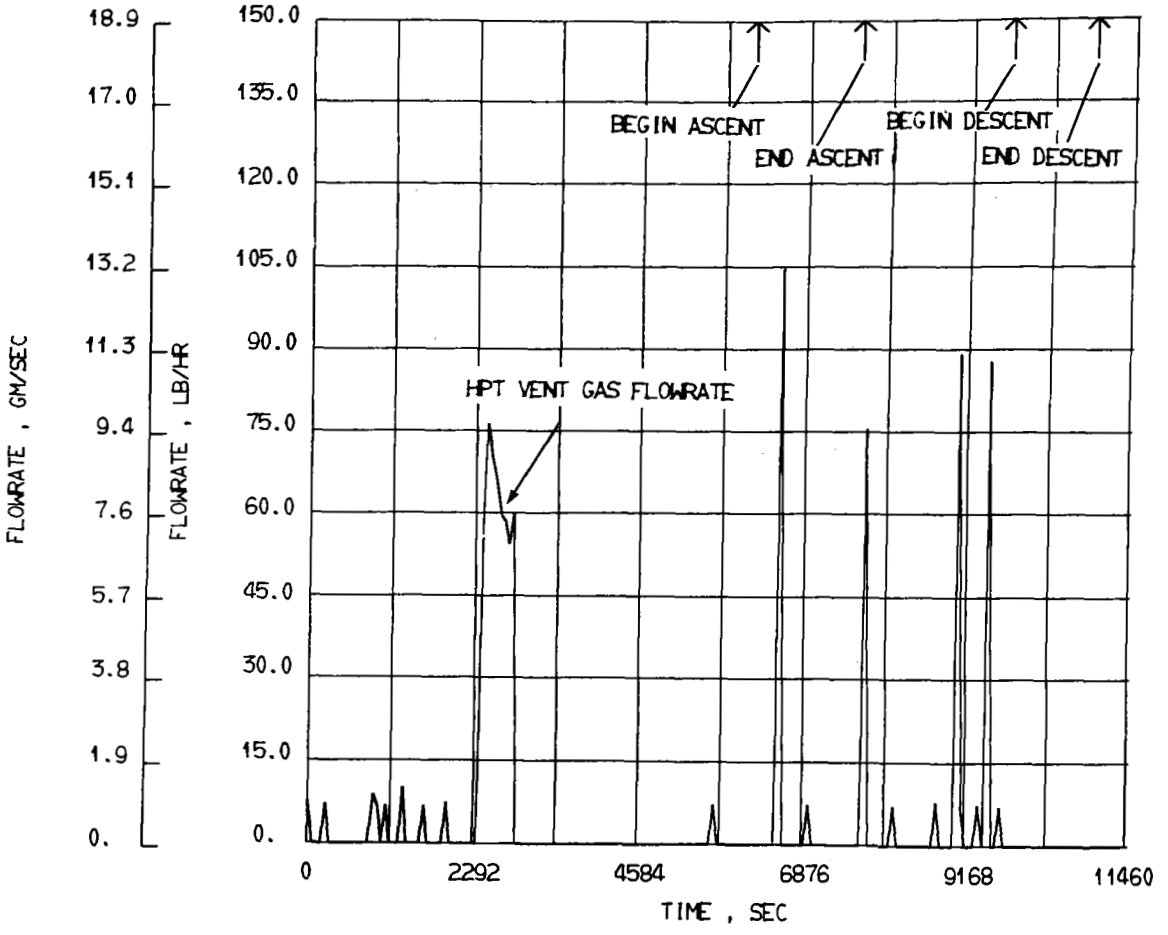

Figure 153. - Test Number 26 - Simulated Flight Test: High-Pressure Tank Vent Gas

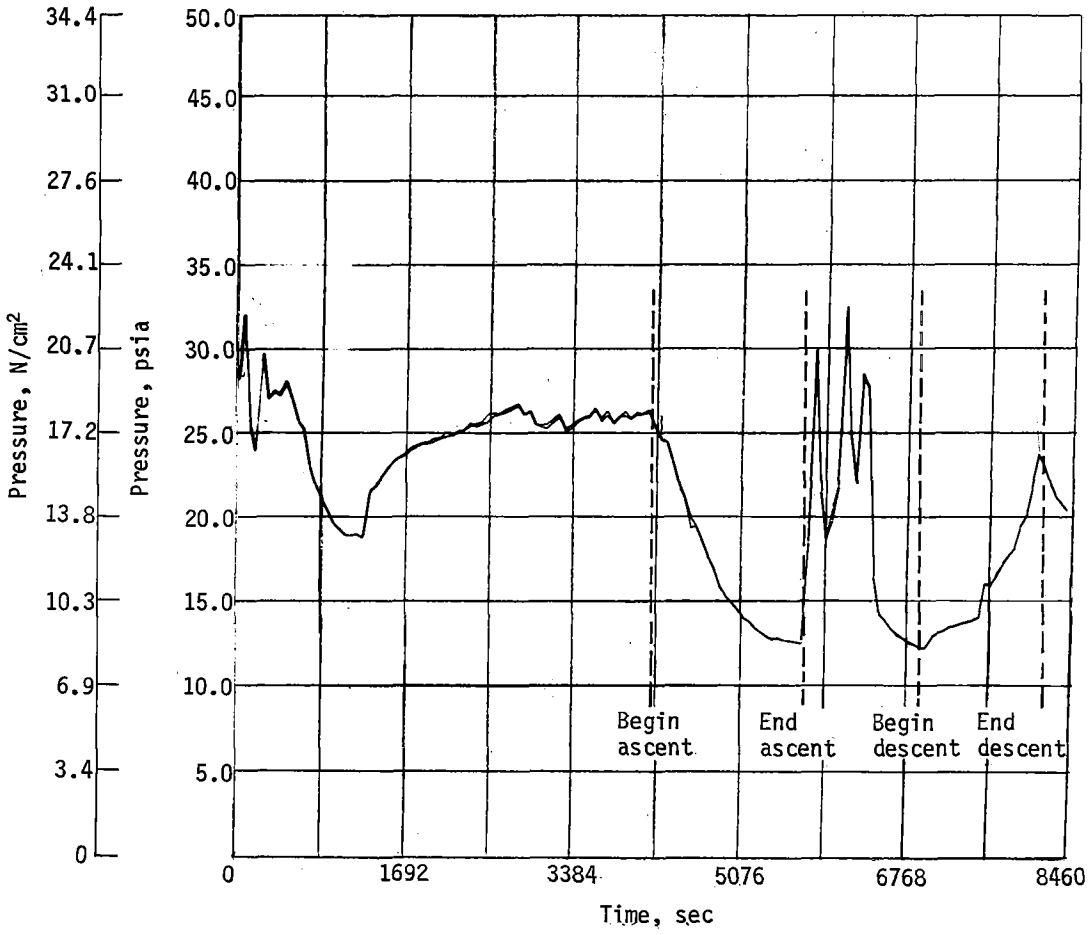

Figure 154. - Test Number 36 - Simulated Flight Test: Pressure at Top of Baffled Tank

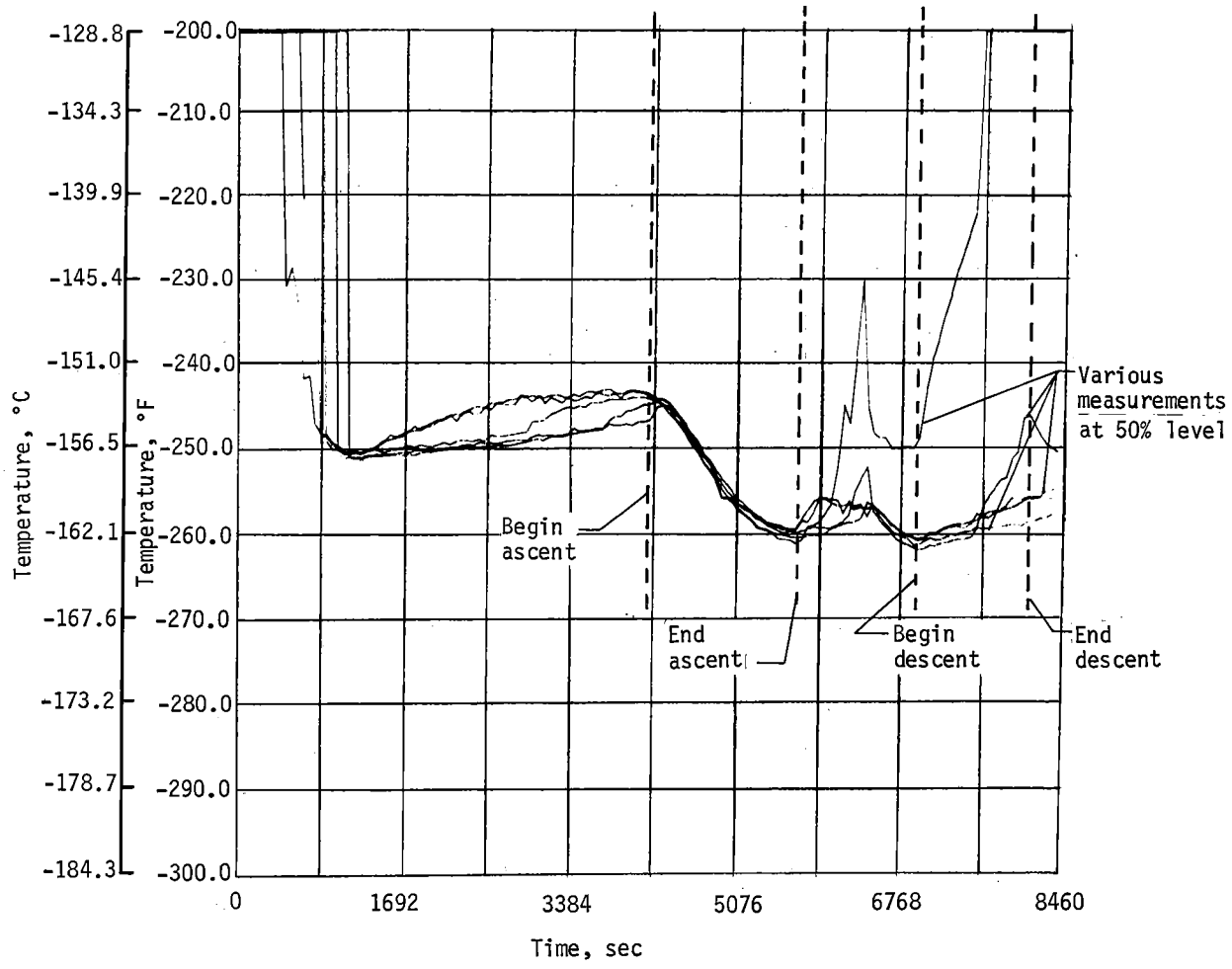

Figure 155.- Test Number 36 - Simulated Flight Test: Temperature of Liquid in First Four Compartments of Baffled Tank

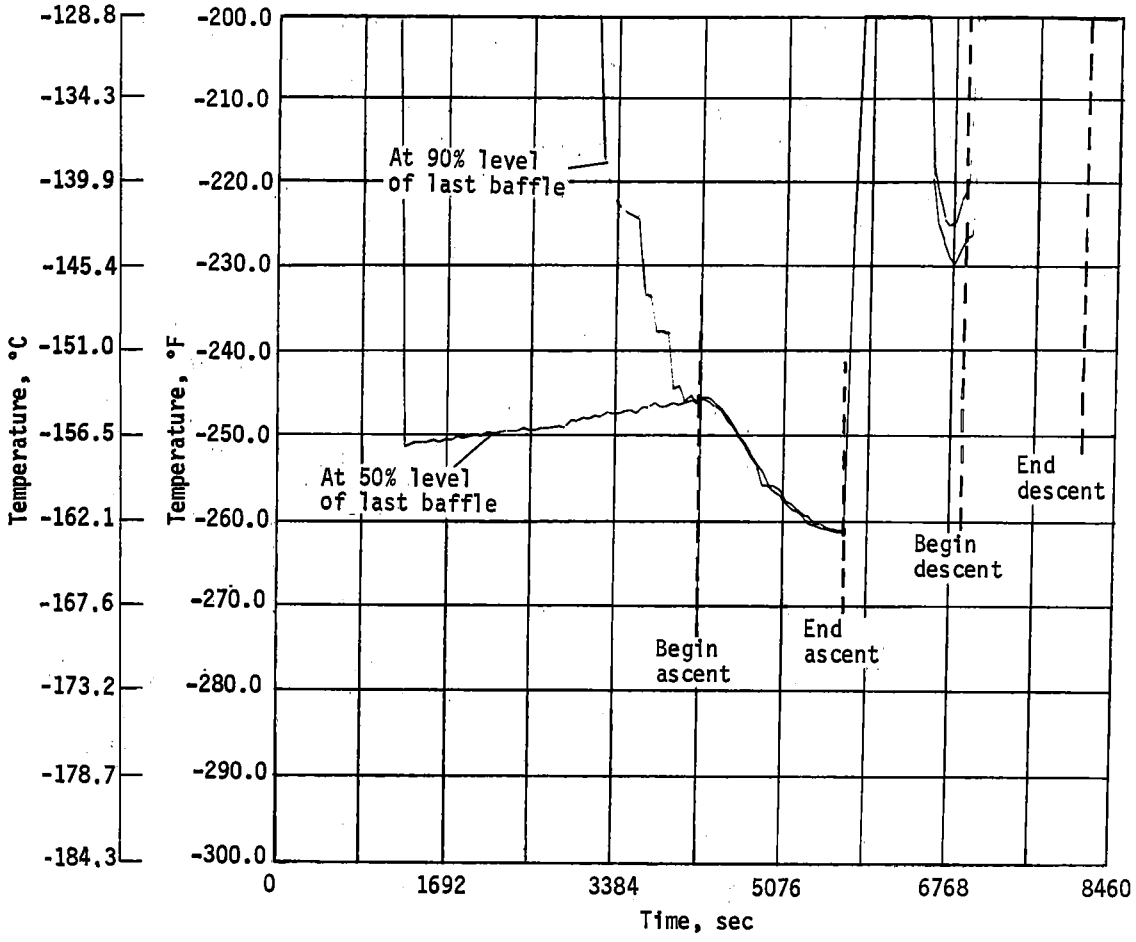

Figure 156.- Test Number 36 - Simulated Flight Test: Temperature of Liquid in Last Compartment of Baffled Tank

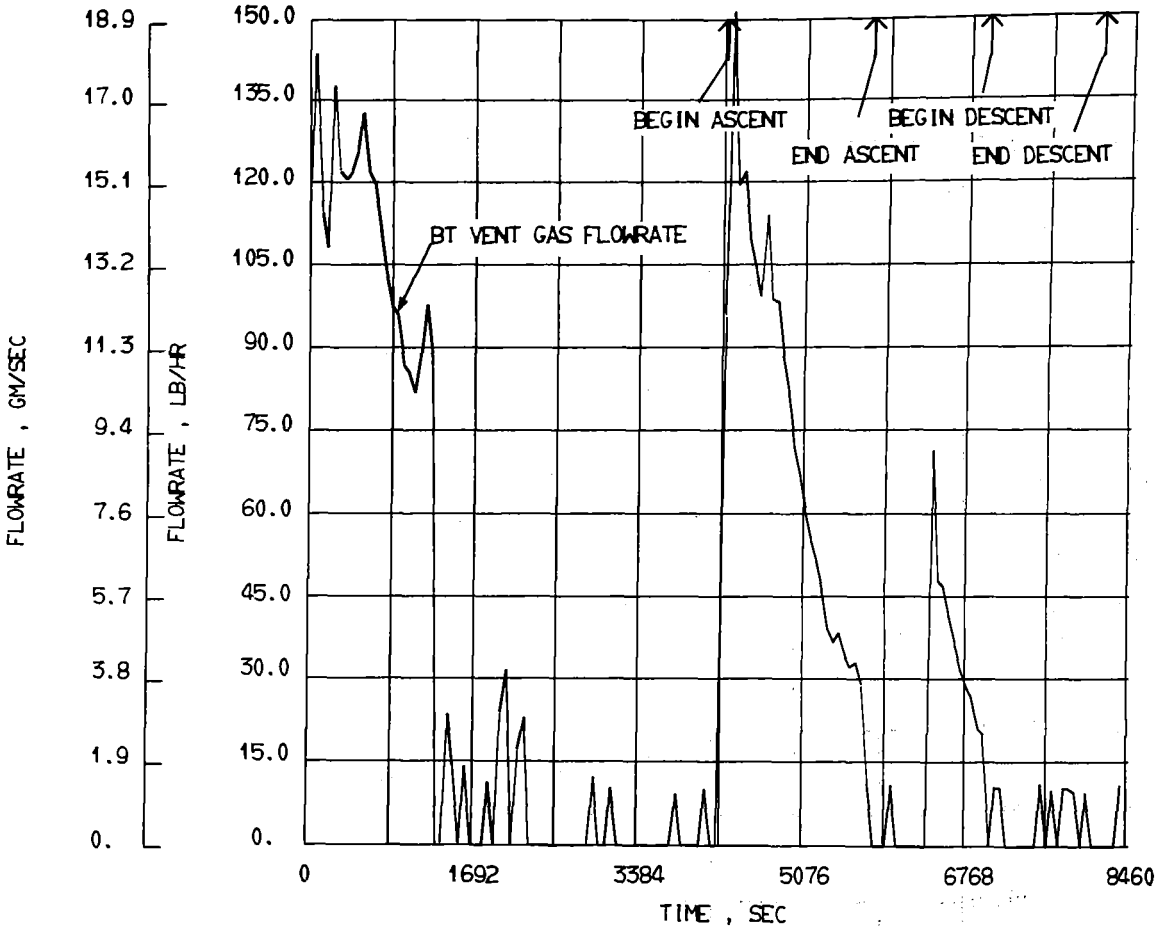

Figure 157.- Test Number 36 - Simulated Flight Test: Flowrate of Baffled Tank Vent Gas

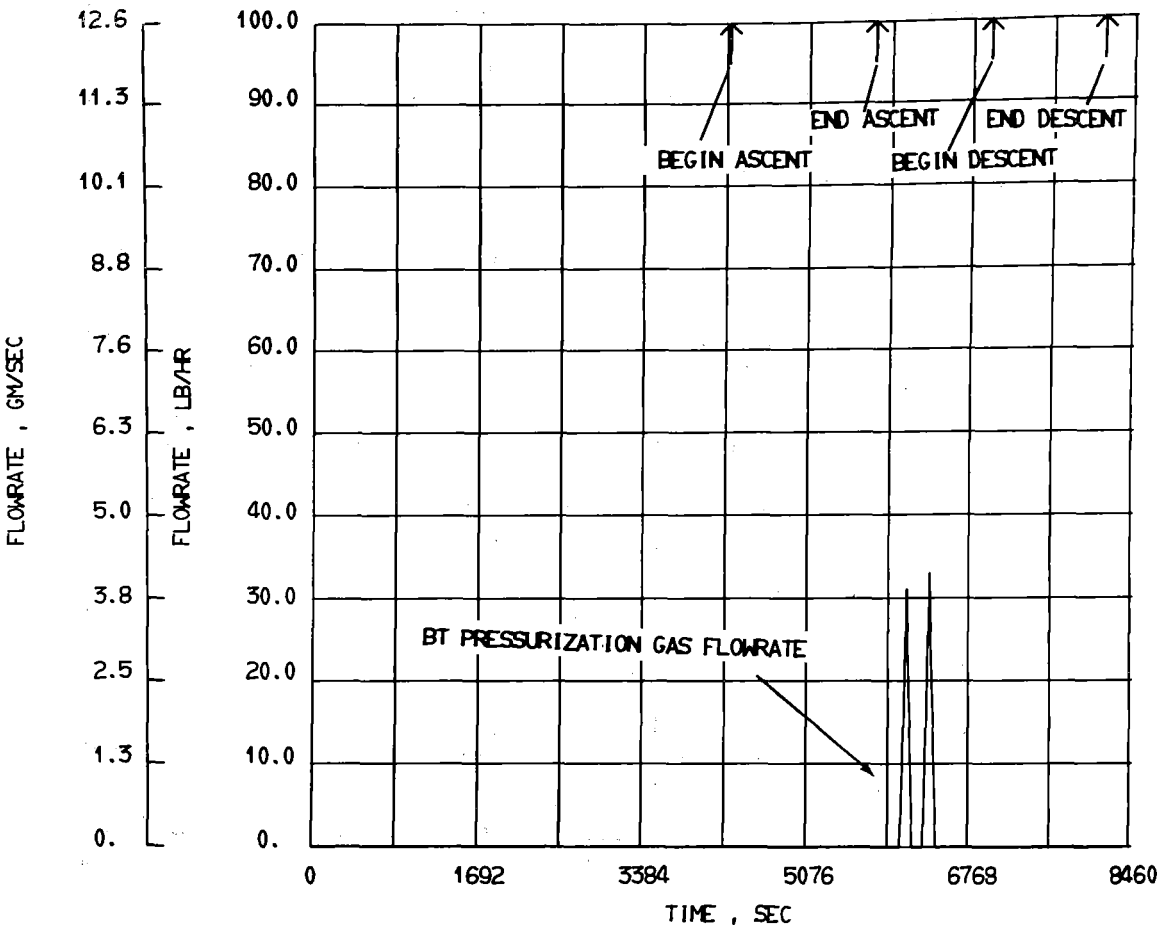

Figure 158.- Test Number 36 - Simulated Flight Test: Baffled Tank Pressurization Gas

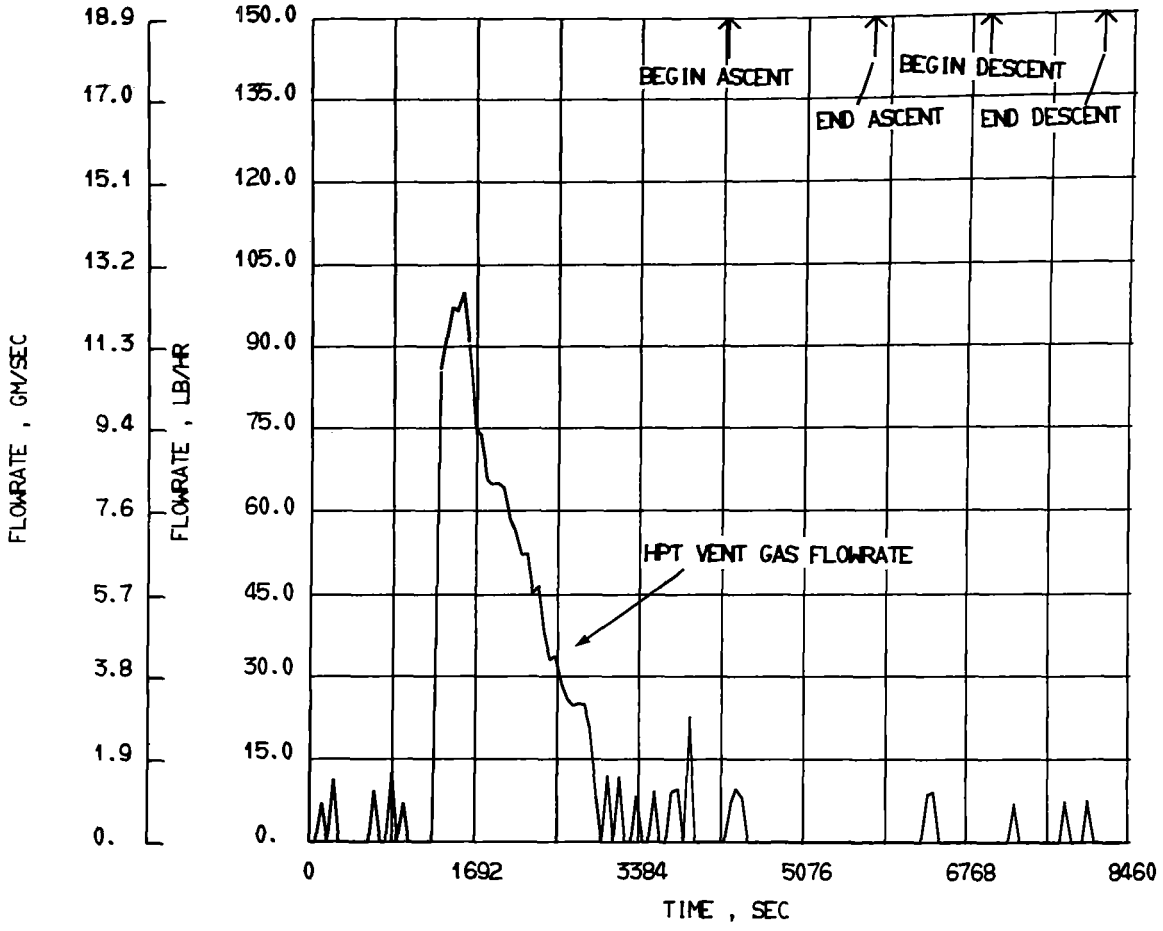

Figure 159.- Test Number 36 - Simulated Flight Test: High-Pressure Tank Vent Gas

The test procedure differed from that used in the original tests in that all phases of the flight were to be simulated in a single test. The series standpipe tank loading was followed by a taxi period (simulated by continuous moderate sloshing). Next came the simulated ascent, which consisted of the same tank pressure profile and wing structure temperature profile used in the original test series, accompanied by continuous moderate sloshing that continued throughout the simulated descent. Then came a cruise, which consisted of maintaining the tank pressures at "altitude" and simulating wing heating until draining the standpipe tank back to the 50% level. (The pressure in the standpipe tank was increased for the drainback and then decreased again to "altitude" long enough before beginning the descent for the liquid in the tank to reach thermal equilibrium.) Last came the simulated descent and unloading. The descent pressure profile was the same as that used in the original test series. The power was turned off to the wing heaters at the start of the descent, and the wing was allowed to cool throughout the remainder of the test.

a. Standpipe tank tests. - During this test series only the standpipe tank configuration was used in the low-pressure tank position.

1) Tests 42, 43, and 44: These three tests were run with liquid methane pressurized with methane vapors and followed the same test procedure. The results were very similar. Test 42 is representative of the series and is described in detail.

Figure 160 shows the pressure in the standpipe tank during the run. The large pressure rises recorded during the series loading resulted when a warm tank was first being filled and the vent rate of the flashing liquid was not large enough to maintain the desired pressure. Since the tank being filled was in series with the standpipe tank, pressure fluctuations were recorded in both tanks.

The temperature of the liquid in the standpipe tank is shown in Figure 161. At the start of the ascent, the bulk liquid (50% probe temperature) was subcooled 6.5F^{o} (3.6C^{o}) with respect to the tank pressure; the liquid at the top of the tank was about 3F^{o} (1.7C^{o}) warmer than the bulk liquid, but was still subcooled. This indicates that the upper layer of liquid was saturated and above the probe at the tank top. At about 1000 sec into the ascent, this probe uncovered, indicating that the liquid above it had vaporized and been vented.

At approximately 7700 sec into the test, all platinum probes appeared to uncover. This is the same kind of data dropout discussed earlier. The standpipe tank thermocouples supplied the necessary temperatures in these dropout areas. However, since the thermocouples are not as accurate as the platinum probes, a technique illustrated in Figure 162 was used to determine the thermocouple biases. Figure 162 is a plot of a platinum probe and thermocouple at the same level in the tank, shown on a scale that covers the dropout area.

The amount of fuel lost during the ascent was 23.1 lb (10.4 Kg), as determined by integrating the vent flowrate curve (Figure 163) during ascent. As in previous ascent tests, this corresponded to 6.5F^{o} (3.6C^{o}) of subcooling. By integrating the pressurization flowrate during the descent (Figure 164), the amount of methane gas used was determined to be 5.4 lb (2.4 Kg). The bulk liquid was subcooled 14F^{o} (7.8C^{o}) after the descent.

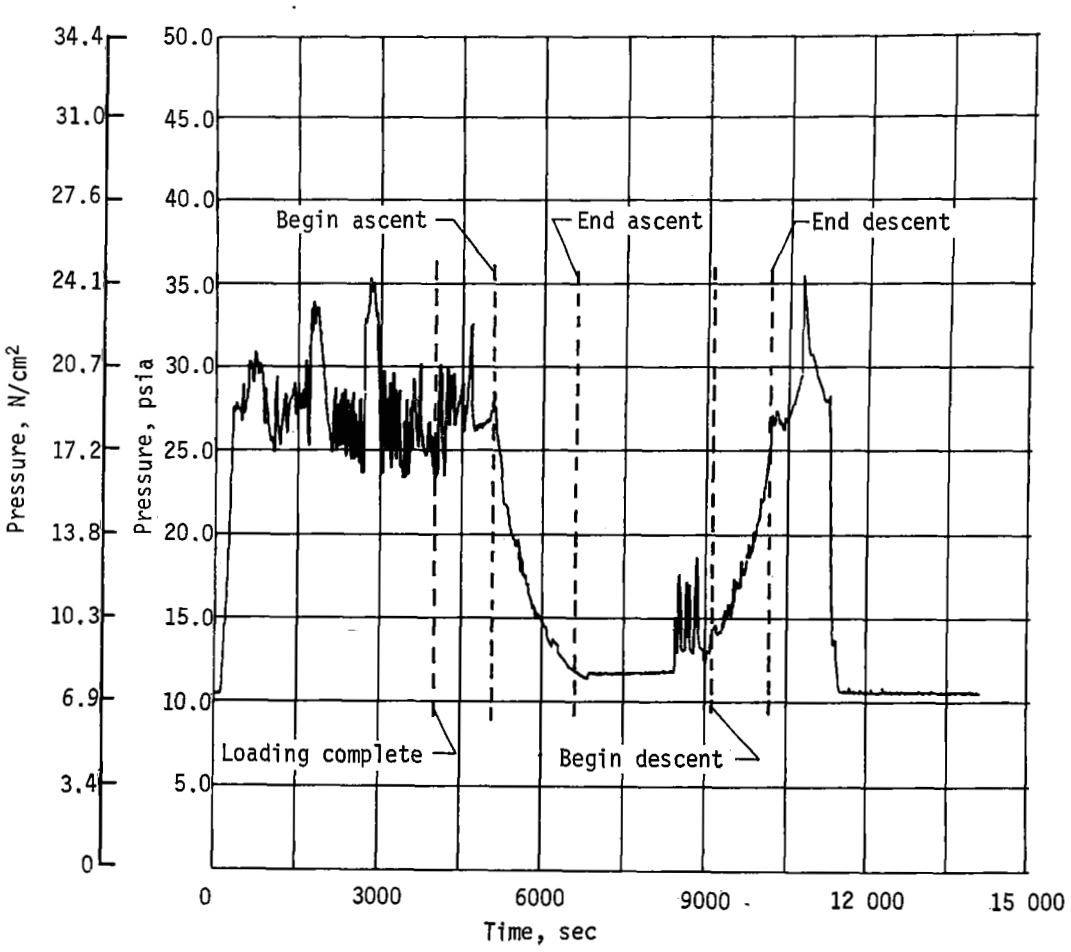

Figure 160.- Test Number 42 - Flight Simulation Test: Pressure at Top of Standpipe Tank

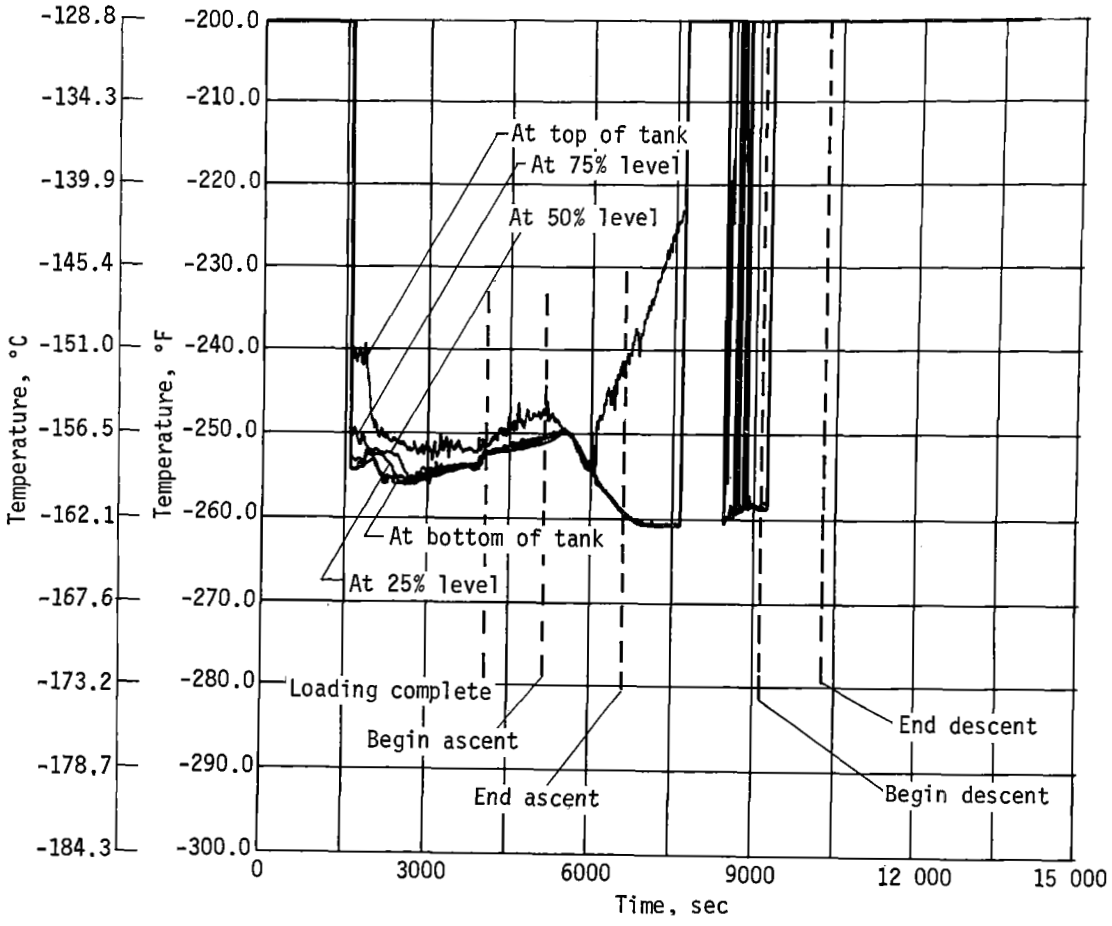

Figure 161.- Test Number 42 - Flight Simulation Test
Temperature of Liquid in Standpipe Tank

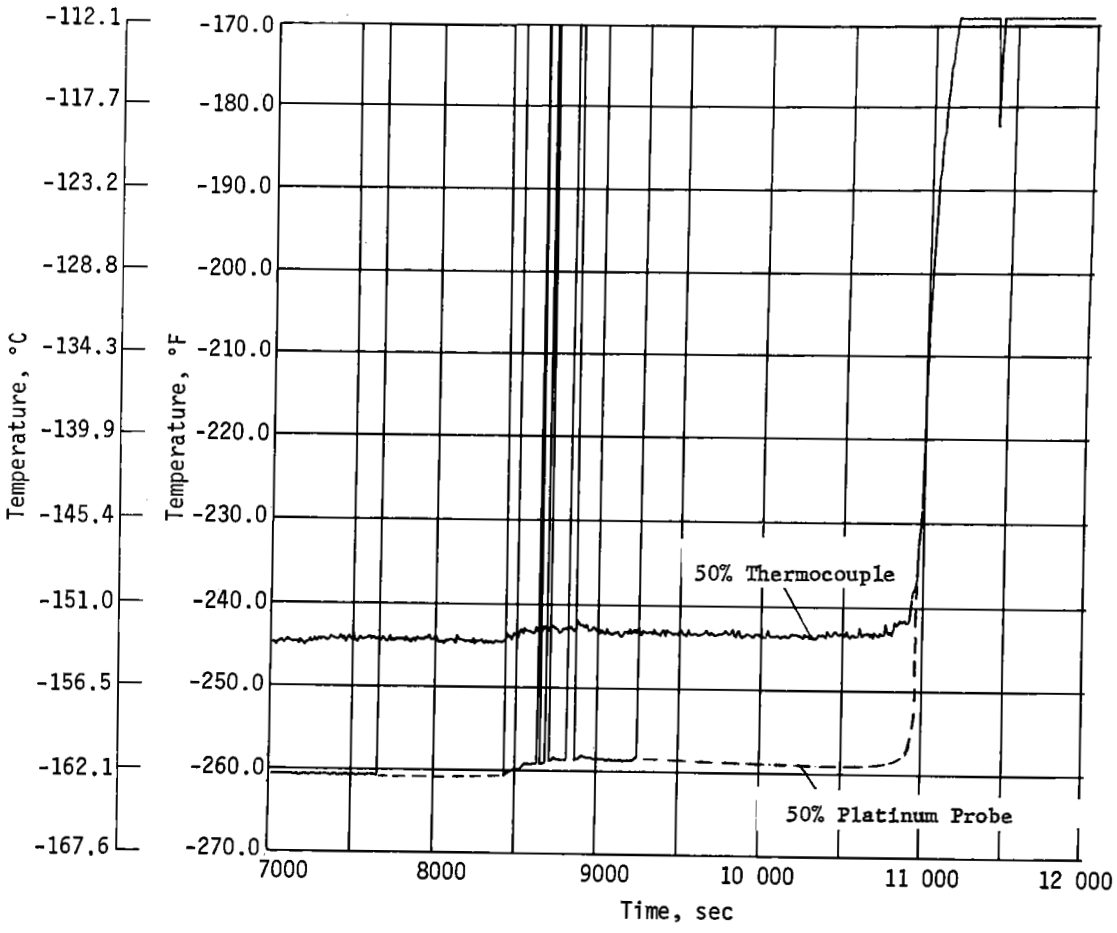

Figure 162.- Test Number 42 - Flight Simulation Test: Comparison of Platinum Probe and Thermocouple Temperature in Standpipe Tank

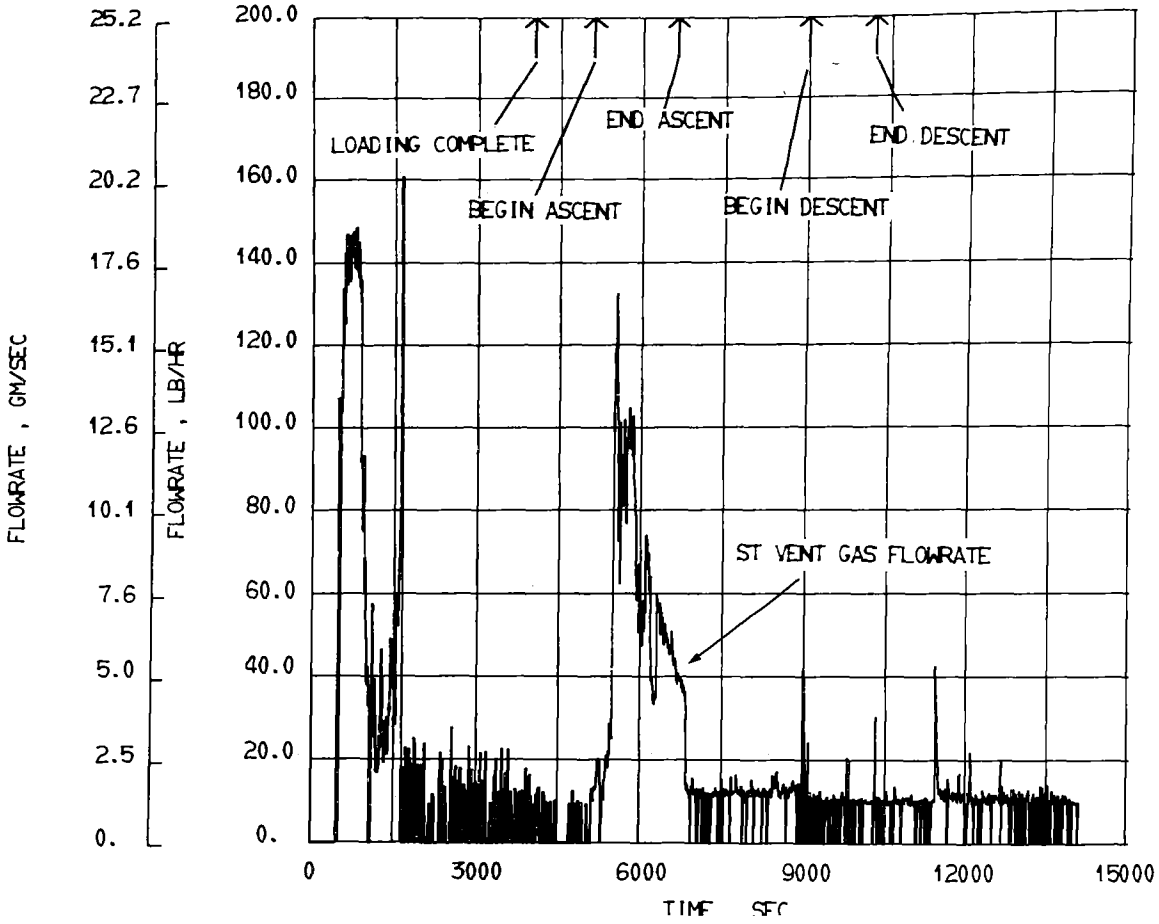

Figure 163.- Test Number 42 - Flight Simulation Test: Flowrate of Standpipe Tank Vent Gas

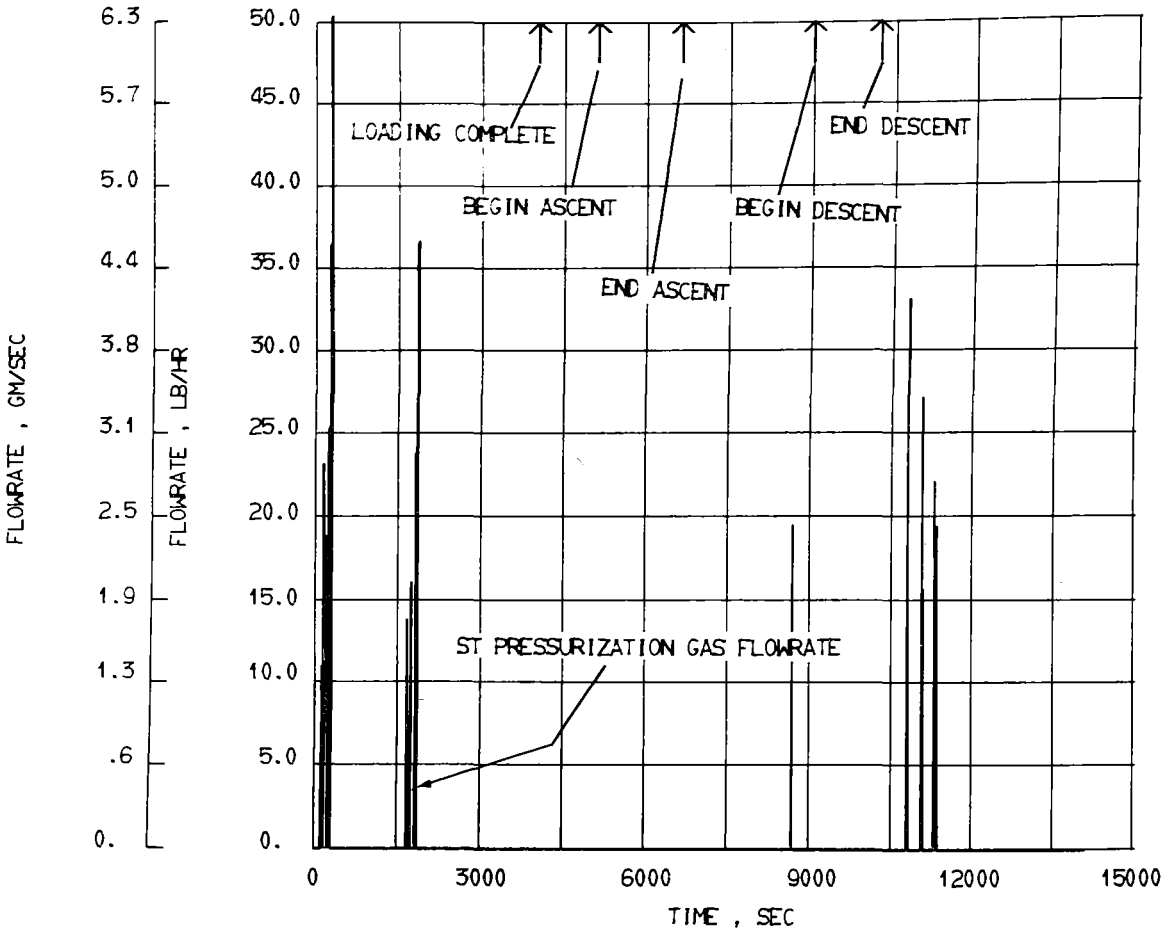

Figure 164.- Test Number 42 - Flight Simulation Test: Flowrate of Standpipe Tank Pressurization Gas

The temperature at various points on the wing structure is shown in Figure 165. As in previous flight simulation tests, the target temperature was 400°F (204.4°C). Figure 166 shows the response of the insulation temperatures on top of the standpipe tank.

2) Tests 45, 46, and 47: This series of tests was run with liquid methane pressurized with gaseous nitrogen, and included a series of samples taken throughout the pressurization portion to determine the solubility of nitrogen in liquid methane. Test 46 is typical of the series and will be presented in detail.

Figure 167 shows the pressure in the standpipe tank during Test 46. The pressure rise for drainback at around 7000 sec marked the first addition of nitrogen pressurant. The times of the samples, as well as the percentages of nitrogen in each, are shown in Table 8. All solubility values in the table are well below the equilibrium value of approximately 15% calculated with Henry's law. These values also represent the weight concentration at a point less than 1½ in. (3.87 cm) beneath the surface of the liquid and represent an upper bound for the concentration in the remainder of the liquid.

The temperature of the liquid at various levels in the standpipe is shown in Figure 168. At the start of the simulated ascent, the bulk liquid was subcooled only about 2F° (1.1C°). By integrating the vent flowrate curve during the ascent, the amount of methane lost was found to be 15.0 lb (6.8 Kg). The descent maneuver required 5.8 lb (2.6 Kg) of nitrogen, and ended with the bulk liquid subcooled 14F° (7.8C°). Pressurant and vent gas flowrates are shown by Figures 169 and 170.

The temperature at various points on the wing structure is shown in Figure 171. Figure 172 shows the response of the different layers of insulation on the side of the standpipe tank.

3. Test Summary

During the initial series of tests, i.e., through Test 37, the simulated flight tests were initiated with the ascent portion of the flight. Each of the three low-pressure tank configurations was subjected to three tests, each with a different slosh schedule. One test was run with no slosh, one with continuous moderate slosh and one with violent slosh during ascent and descent when the tank pressure was 19.4 psia (13.4 N/cm^2). There was no indication of pressure change due to slosh in any of the above tests.

The maximum possible subcooling in these tests was 16F° (8.9C°). The amount of subcooling achieved varied from 0F° (0C°) to 11F° (6.1C°). The foam-filled tank consistently exhibited much more stratification than the other tanks. The amount of stratification significantly influenced the amount of boil-off during ascent. Figure 173 shows the actual boil-off during ascent for each test as compared to the theoretical value.

The second series of tests were run only on the standpipe tank configuration and used a considerably different procedure. The profiles covered all events normally expected for a complete flight including loading, ground hold and taxi, ascent, flight usage and descent. The tanks were continuously sloshed at a moderate level. Again the slosh had no apparent effect on tank pressure.

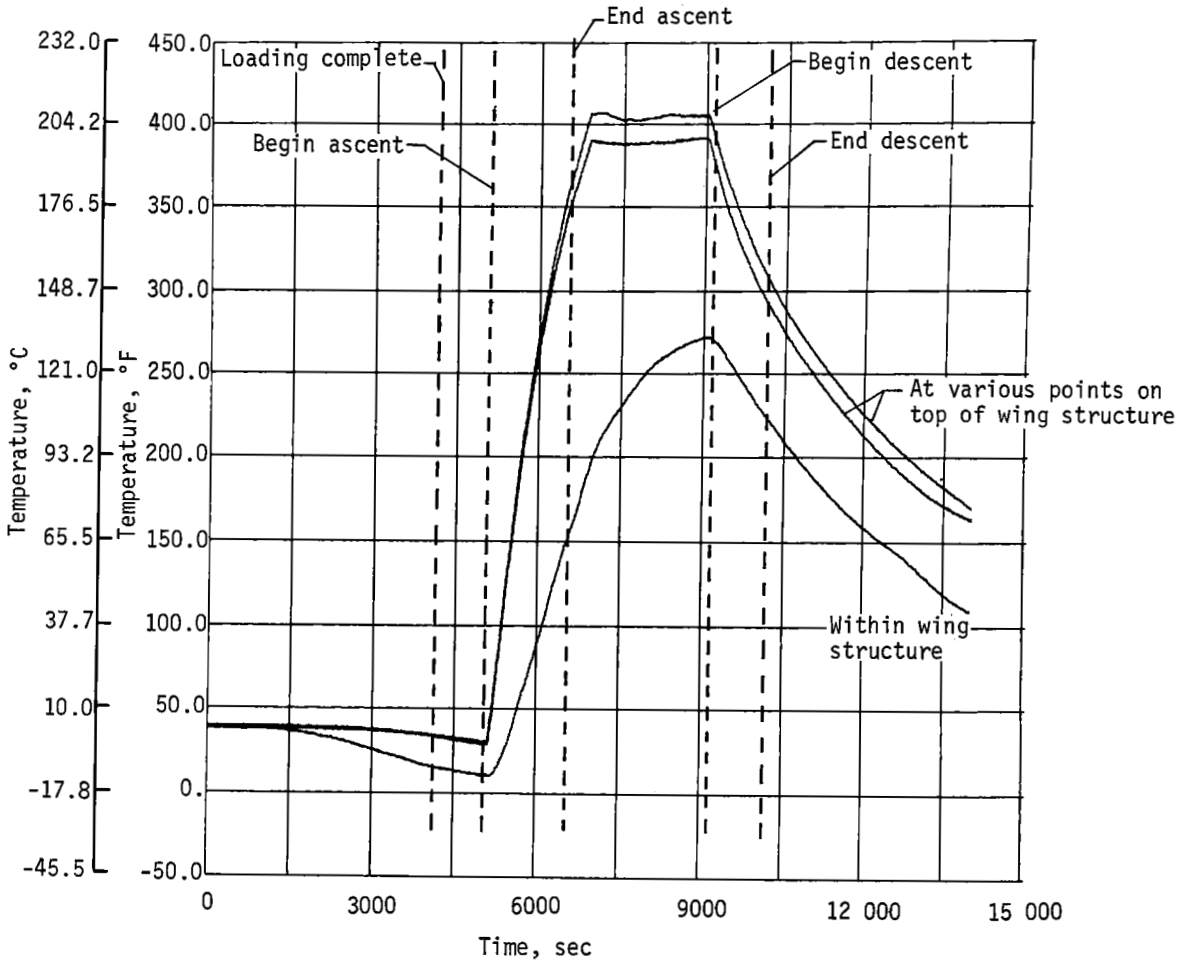

Figure 165.- Test Number 42 - Flight Simulation Test: Temperature of Wing Structure

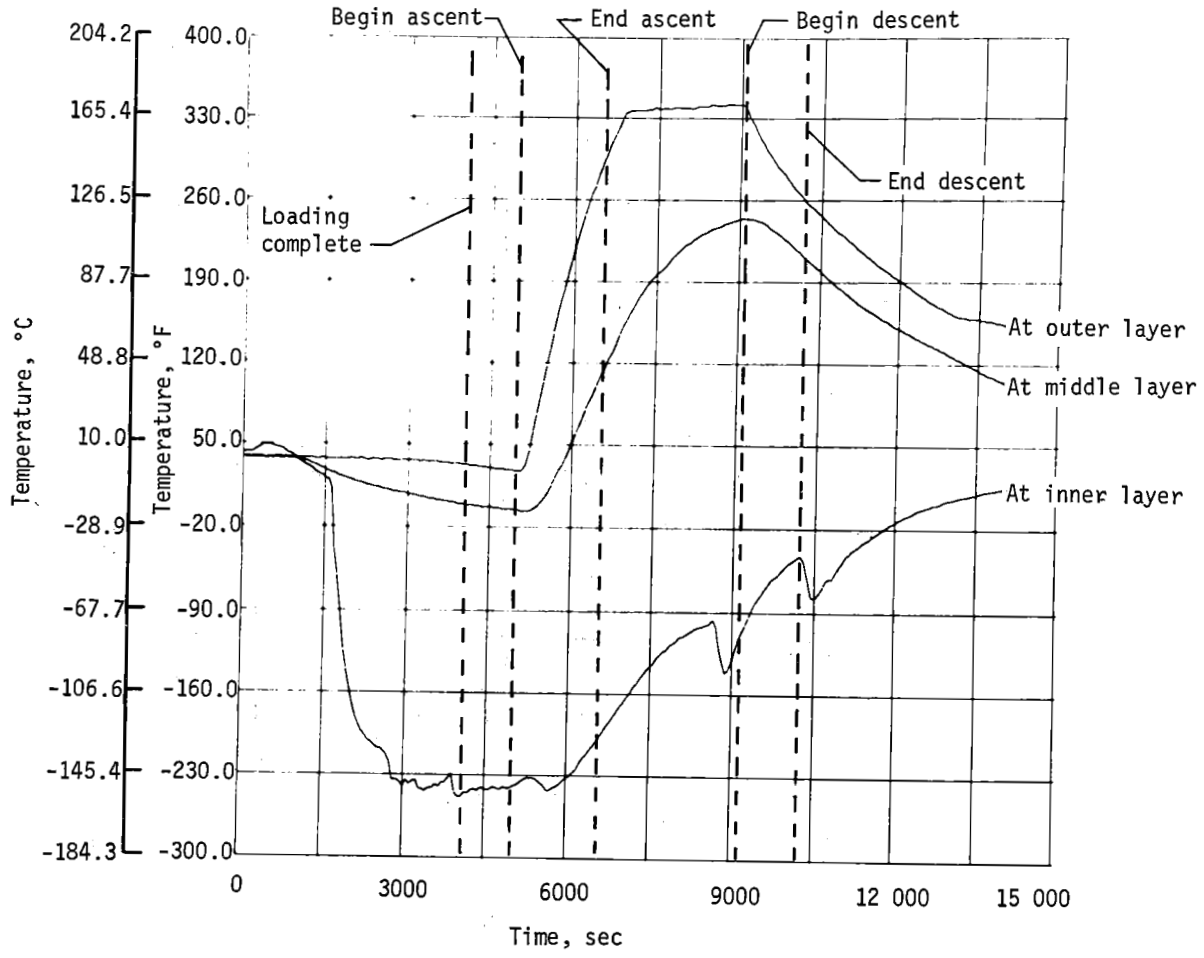

Figure 166.- Test Number 42 - Flight Simulation Test: Temperature of Insulation at Top of Standpipe Tank

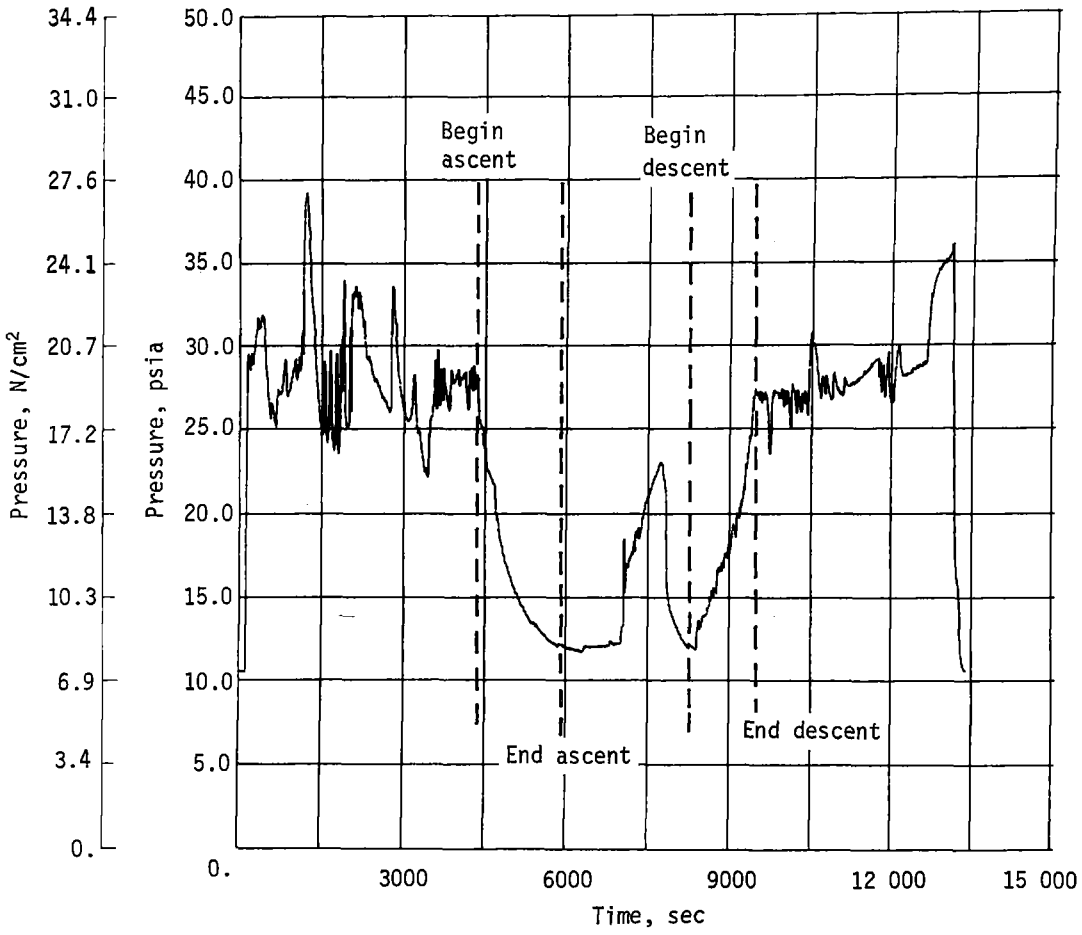

Figure 167.- Test Number 46 - Flight Simulation Test: Pressure at Top of Standpipe Tank

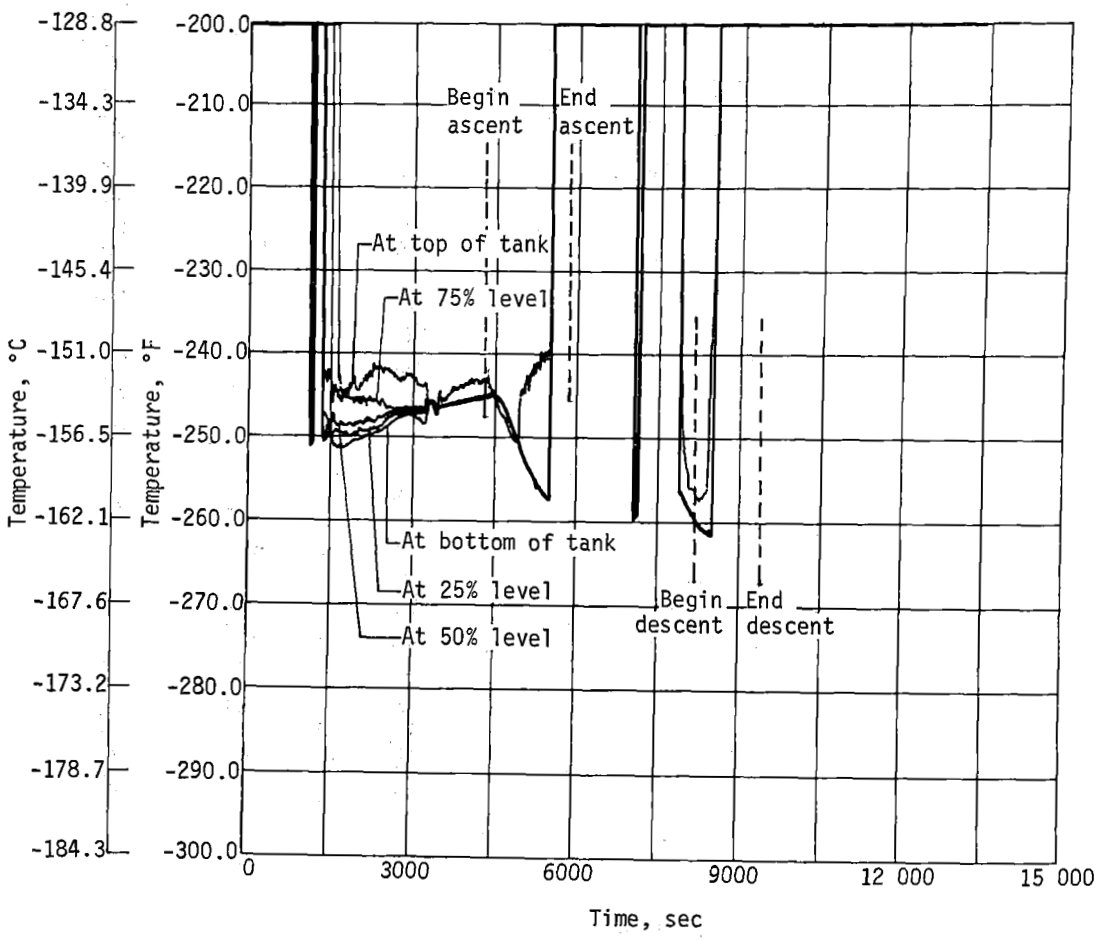

Figure 168.- Test Number 46 - Flight Simulation Test: Temperature of Liquid in Standpipe Tank

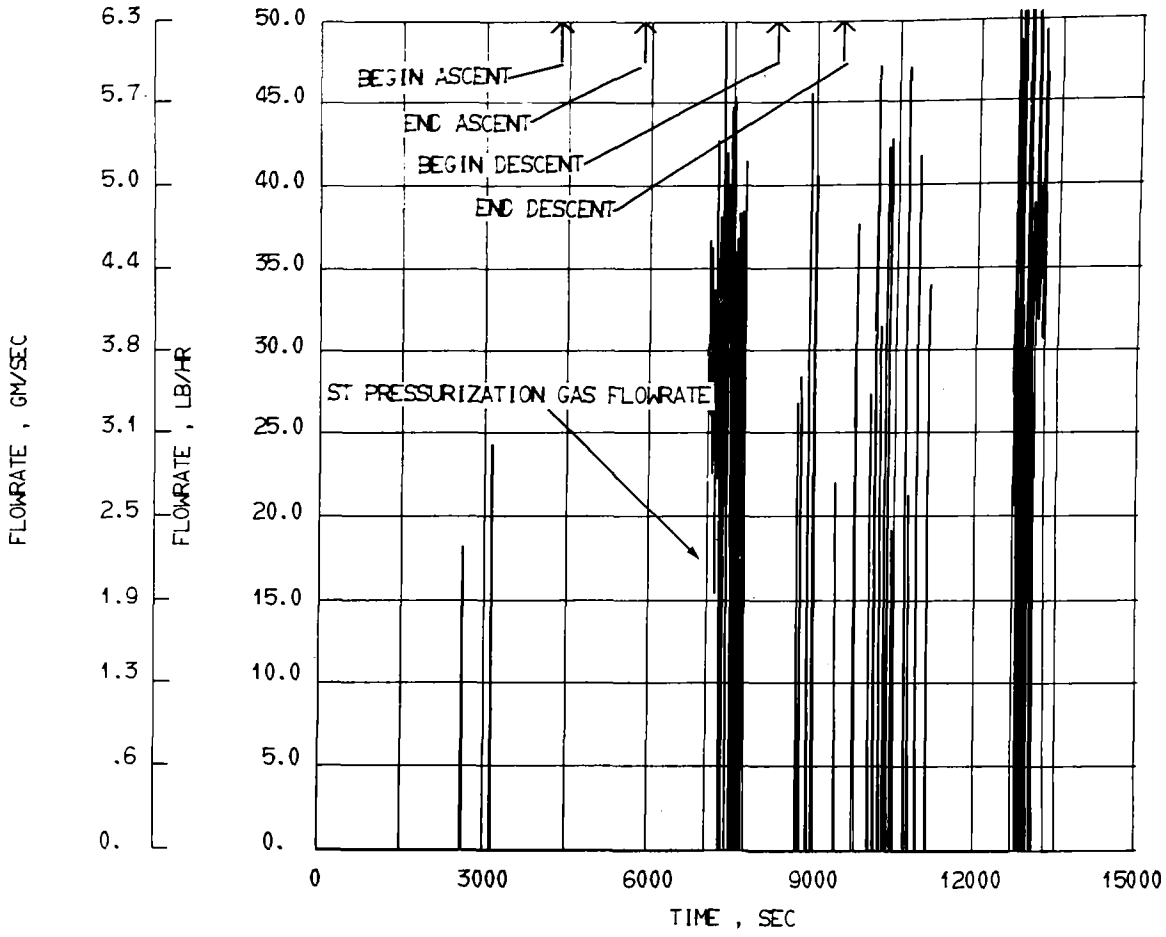

Figure 169.- Test Number 46 - Flight Simulation Test: Flowrate of Standpipe Tank Pressurization Gas

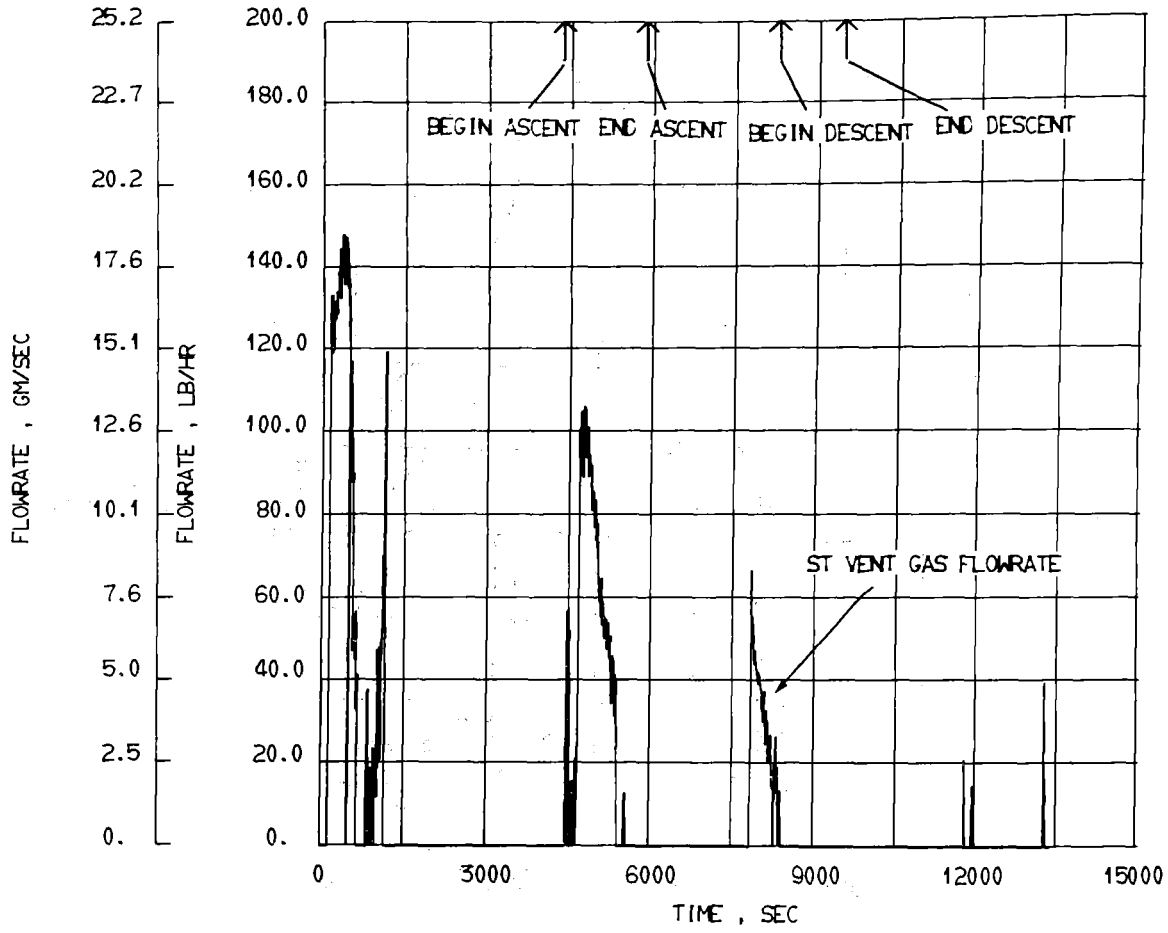

Figure 170.- Test Number 46 - Flight Simulation Test: Flowrate of Standpipe Tank Vent Gas

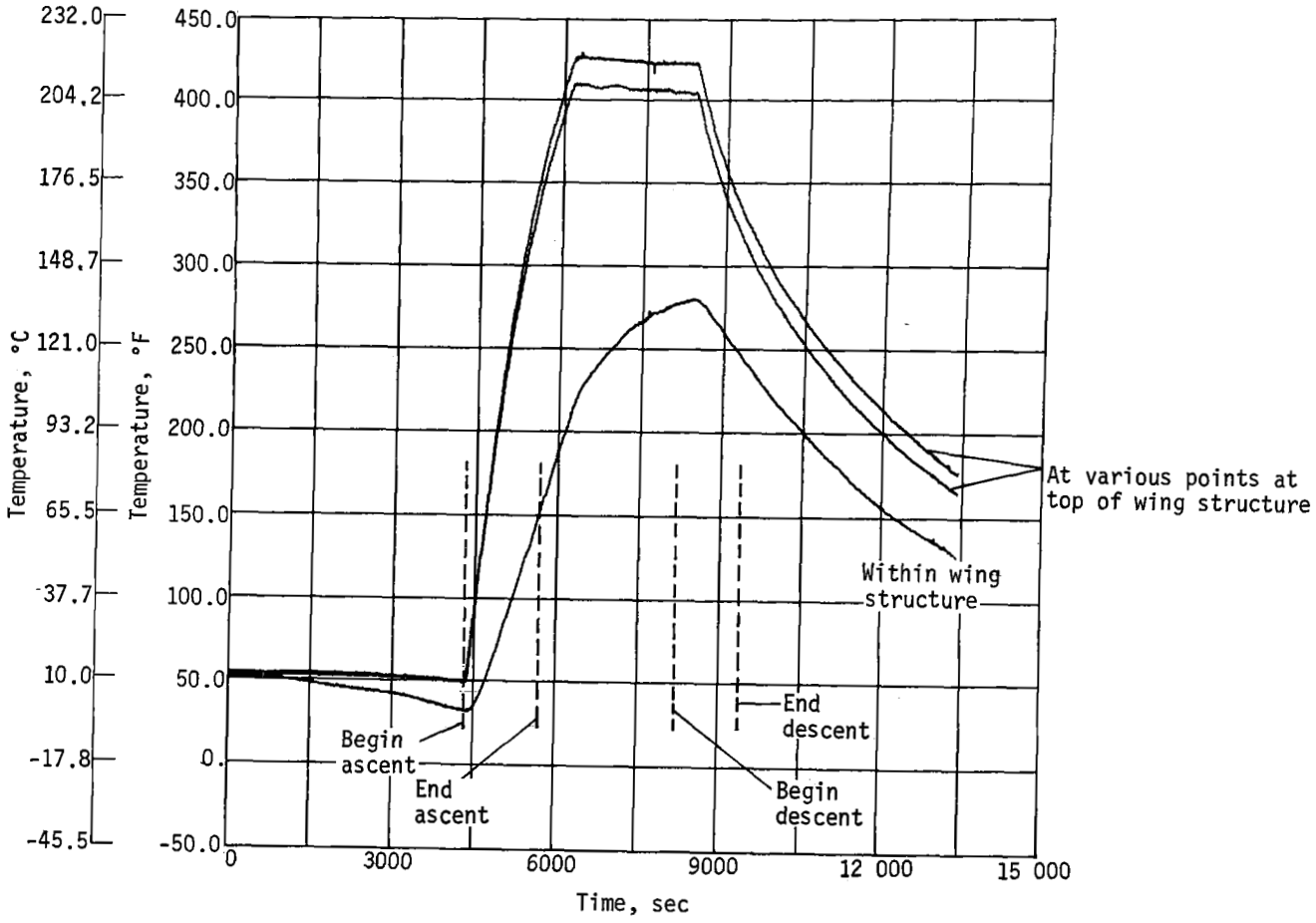

Figure 171.- Test Number 46 - Flight Simulation Test: Temperature of Wing Structure

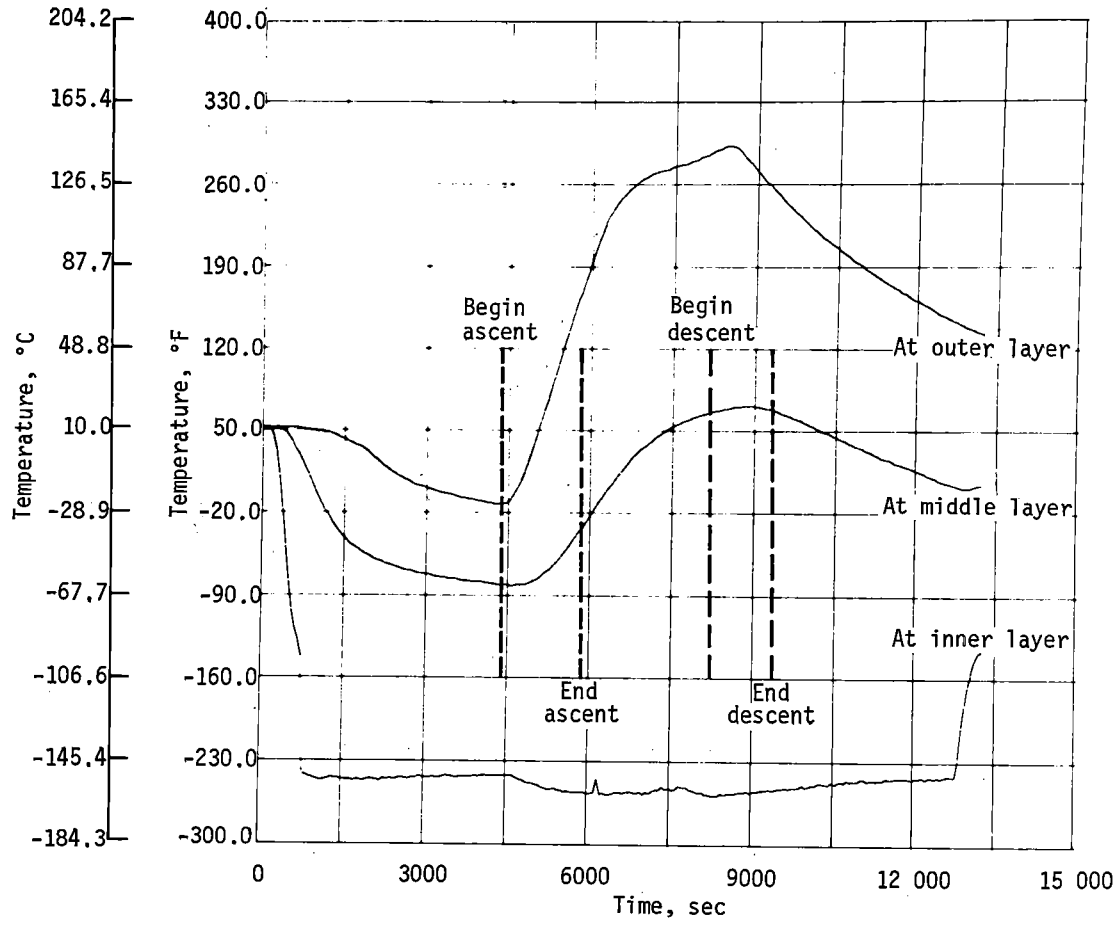

Figure 172.- Test Number 46 - Flight Simulation Test:
Temperature of Insulation on Side of Standpipe Tank

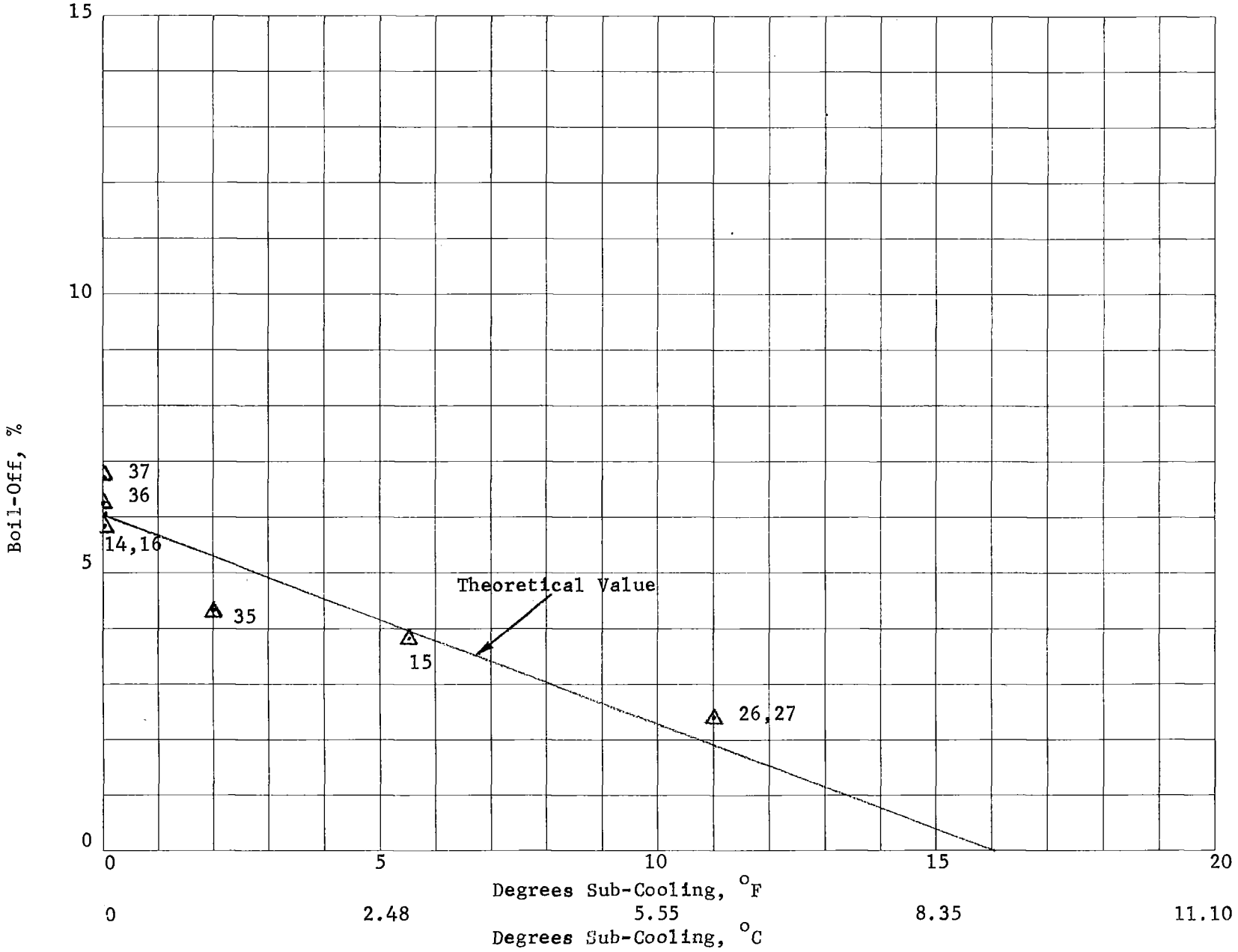

Figure 173.- Liquid Boil-off During Simulated Ascent

Three of the six test series were run using nitrogen gas as a pressurant for the liquid methane. During one of the tests a liquid sample was taken near the surface in the tank at ten test times as indicated in Table 8. Measured solubility was less than the equilibrium value predicted by Henry's law (15%) and since samples were taken near the liquid surface they should constitute an upper limit in the level.

During descent at the specified rate shown by Figure 139 pressurization was required in order to prevent tank negative pressure.

TABLE 9.- NITROGEN SOLUBILITY RESULTS

Sample no.	Time from start of test, sec	Nitrogen, % wt.
1	7 080	4.54
2	7 785	1.74
3	8 280	3.40
4	8 520	2.40
5	8 760	0.00*
6	9 000	3.00
7	9 240	0.60
8	9 480	0.38
9	10 080	0.44
10	12 600	1.12

* Inadequate Sample

VI. CONCLUSIONS AND RECOMMENDATIONS

The results of each series of tests were presented and discussed earlier. A series of overall general conclusion will be presented here and recommendations for future studies will be made.

In the series of tests which were conducted over a period of several months standard cryogenic liquid handling procedures were used and no particular difficulties were encountered. The general conclusion reached by operating personnel is that liquid methane is safer and easier to handle than liquid hydrogen or liquid oxygen and flows much easier than liquid nitrogen.

Several different methods of loading subcooled liquid methane were attempted and reasonable success was obtained with all methods. It was found that venting was required for all loading tests even when the bulk of the liquid in the fuel tanks was subcooled. Therefore, no pressurization system is required for the loading operation. No tendency for tanks pressure collapse was observed, thus tank implosion due to negative pressure across the tank wall is of no concern in loading subcooled liquid.

The standpipe tank concept was never actually tested because zero ullage was never accomplished, even though considerable effort was expended in a number of attempts to achieve it.

In order to achieve maximum subcooling of the loaded fuel, precise and constant tank pressure control is required during loading.

Generally speaking, slosh had little effort on tank pressure or the liquid temperature profile. In some cases of violent slosh with the high pressure tank a modest pressure reduction was observed, but liquid temperature patterns were uneffected. It can, therefore, be concluded that for the slosh levels tested, pressure control in flight fuel tanks can easily and reliably be maintained with a relatively simple pressure control system.

Analytical predictions of heat transfer rates into the fuel tanks were in close agreement with measured data.

Pumping and transfer of liquid methane proved to be simple and straightforward and completely within conventional engineering.

As was anticipated, the boiloff loss of fuel during ascent depressurization of the three low pressure tanks depended upon the liquid stratification profile. The foam-filled tank consistantly exhibited the greatest degree of liquid stratification. With proper design and care boiloff loss can be limited to a small percentage of the tank volume during ascent.

Tank pressure was always maintained during loading, taxi and hold, and ascent and cruise by venting only. Pressurization was required only during descent to land. Tests with nitrogen pressurization indicated that only very limited nitrogen absorption in the fuel occurred during the short descent time period. Thus it can be concluded that repressurization of the fuel tank during descent can be accomplished with either methane or nitrogen gas with negligible effect on overall propulsion efficiency.

The foam filled tank performed better than the other configurations in terms of limiting liquid mixing during filling. The weight of the foam ($1.5\#/ft^3$) adds a significant penalty to the overall fuel storage system. Attempts should be made to retain the advantages of the foam filled configuration while reducing overall weight. Lighter foam and partial foam filling should be investigated. Loading tests should be conducted with the foam-filled configurations, and very precise tank venting control.

Slosh tests should be conducted with other tanks configurations, and with other modes of slosh motion.

APPENDIX A

I. AERODYNAMIC HEATING ANALYSIS

A crossection showing the geometrical relationship between the insulated tanks and the wing section is shown below. Both the inside of the simulated wing and the exterior of the tank insulation system were painted black. This results in the best thermal coupling between the wing and the tanks and is, therefore, a worst case thermal condition. This black paint also does not appreciably degrade during test and, therefore, provides for maximum repeatability over the duration of the tests.

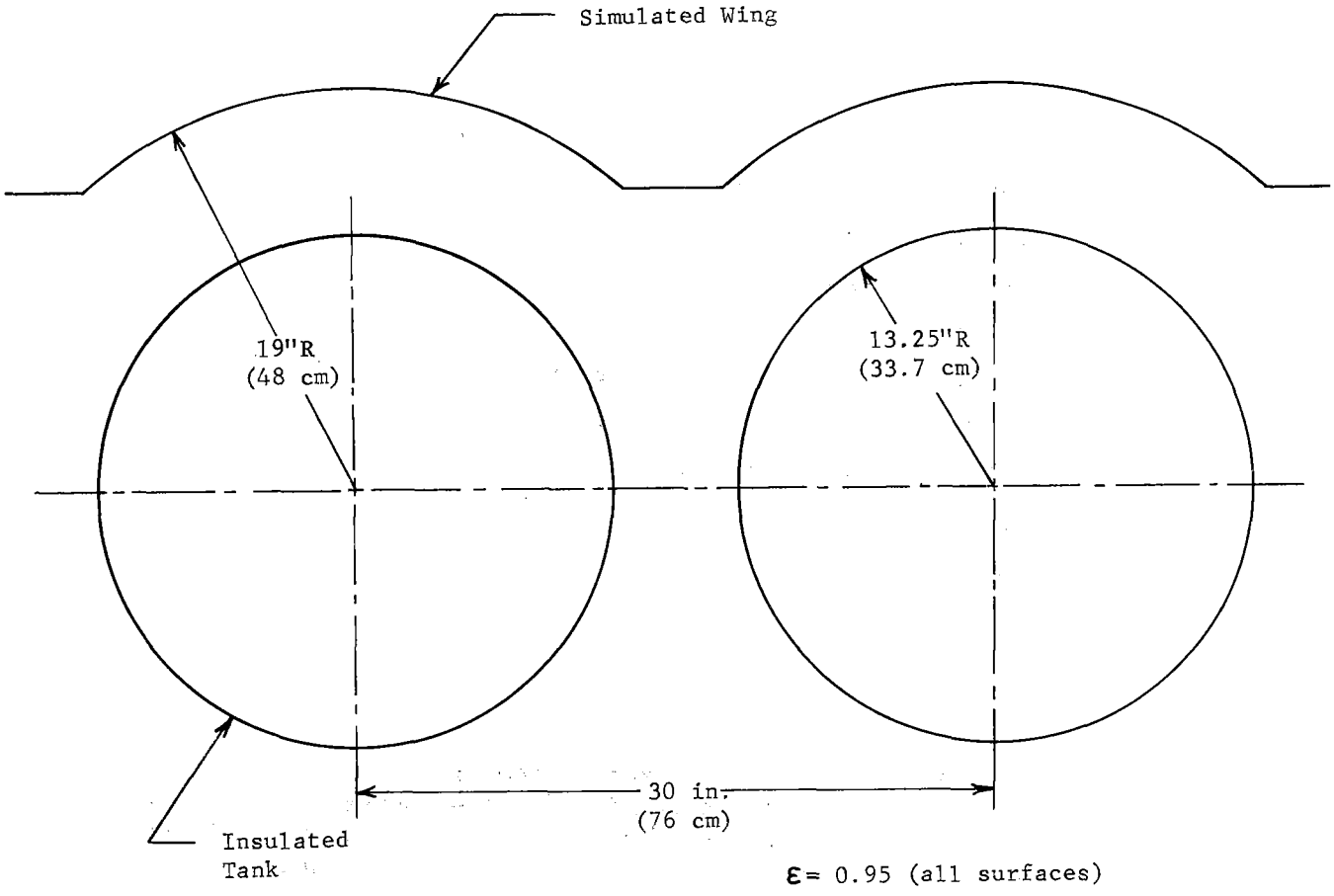

Wing Section Configuration

The thermal network describing heat flow from the simulated wing to the liquid in a full tank is shown below:

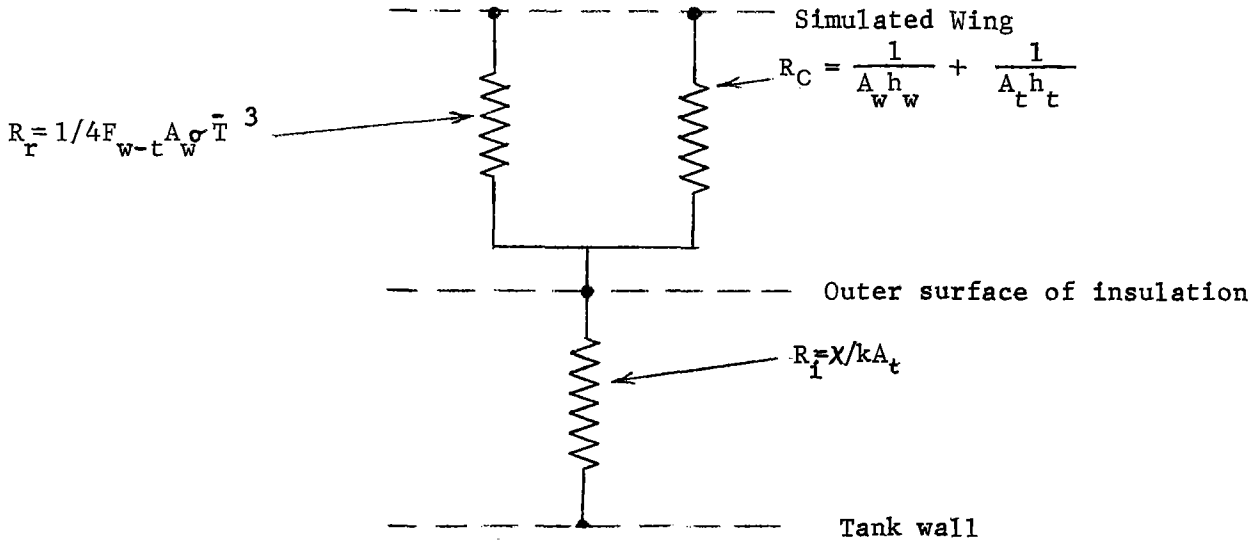

where: R = Thermal resistance, hr-^{o}R/BTU (hr-^{o}K/kcal)

F = Geometric view factor

A = Area, ft^2 (m^2)

σ = Stefan Boltzmann's constant

T = Temperature, ^{o}R (^{o}K)

h = Convection heat transfer coefficient, BTU/hr-ft^2-^{o}R (kcal/hr-m-^{o}K)

k = Insulation thermal conductivity, BTU/hr-ft-^{o}R (kcal/hr-m-^{o}K)

x = Insulation thickness, ft (m)

subscripts: w = wing

t = tank

r = radiation

c = convection

i = insulation

The insulation and convection resistances are shown as commonly defined with the convection resistance accounting for the boundry layer on the wing and on tank. The radiation resistance has been linearized in the following manner. In standard notation the heat flow from the wing to the tank is written:

$$Q = F_{w-t} A_w \sigma (T_w^4 - T_t^4)$$

Factoring the temperature difference term:

$$Q = F_{w-t} A_w \sigma (T_w^2 + T_t^2)(T_w + T_t)(T_w - T_t)$$

In terms of an average temperature:

$$Q = 4F_{w-t}A_w\sigma\bar{T}^3(T_w - T_t)$$

This averaging is appropriate if $T_w \approx T_t$ which will be shown to be true later. Therefore, the linearized radiation resistance is:

$$R_r = 1/4\ F_{w-t}A_w\sigma\bar{T}^3$$

The actual simulated wing area is about 170 ft^2 (15.8 m^2). The total tank surface area is 176 ft^2 (16.4 m^2). The geometrical view factor from the wing to the tanks is 0.84 as determined in a finite difference computer analysis. The insulation thickness was 1.25 in. (3.18 cm) and had a thermal conductivity of 0.0186 BTU/hr-ft-^oR (0.0277 kcal/hr-m-^oK). It is difficult to calculate the actual natural convection coefficients for the complicated geometry, however, for air at the temperatures of interest it is safe to assume $0.05 \leq h \leq 1.0$ BTU/hr-ft^2-^oR ($0.24 \leq h \leq 4.88$ kcal/hr-m^2-^oK). For this analysis it was assumed to be 0.75 BTU/hr-ft^2-^oR (3.66 kcal/hr-m^2-^oK) as it has little effect on the resulting temperature. Using the above parameters, the following values for resistances were calculated:

R_r = 0.00196 hr-^oR/BTU (0.00432 hr-^oK/kcal)

R_c = 0.0232 hr-^oR/BTU (0.0511 hr-^oK/kcal)

R_i = 0.0319 hr-^oR/BTU (0.0703 hr-^oK/kcal)

Since the convection resistance is nearly an order of magnitude larger than the radiation resistance, the assumption on the heat transfer coefficient was not important.

Upon combining the parallel convection and radiation resistance it is found that the thermal resistance between the wing and tank is 0.0018 hr-^oR/BTU (0.0040 hr-^oK/kcal) and the resistance through the insulation is 0.0319 hr-^oR/BTU (0.0703 hr-^oK/kcal). Assuming the wing temperature to be 400^oF (477.6^oK) and the liquid temperature to be -260^oF (110.9^oK) the outside insulation temperature can be determined by the equality:

$$\frac{400-T_i}{0.0018} = \frac{T_i - (-260)}{0.0319}$$

or, solving for T_i = 364^oF (457.6^oK).

As expected the radiation component of heat transfer between the tank and the wing is so large that there is very little temperature drop between the wing and the tank insulation.

The temperature at the top, bottom and sides of the tank during a typical heating test is shown below:

Top = 305^oF (425^oK)
Bottom = 260^oF (400^oK)
Side 1 = 245^oF (391^oK)
Side 2 = 250^oF (394^oK)

As can be seen, the temperatures are considerably below the predictions and the tank is much warmer on top than on the bottom. This is attributed to natural circulation of air within the wing, or "chimney" effect. This appears to be a significant effect and one which would exist to some extent in an airplane wing.

II. ENERGY BALANCES

In general, the heat added during a test (external heat leak) plus the initial heat of the system (tank, liquid and gas) must equal the final heat of the system. The system, in this case, is the tank wall plus any vented gas as it passes the venturi. This can be expressed in equation form as,

$$Q_E + m_T C_T T_{Ti} + m_{Li} h_{Li} + m_{Gi} h_{Gi} = m_T C_T T_{Tf} + m_{Lf} h_{Lf} + m_{Gf} h_{Gf} + m_V h_V.$$

Or, rewriting,

$$Q_E + m_T C_T (T_i - T_f)_T + m_{Li} h_{Li} - m_{Lf} h_{Lf} + m_{Gi} h_{Gi} - m_{Gf} h_{Gf} - m_V h_V = 0$$

where: Q_E = external heat leak, BTU (cal)
m = mass, lb (kg)
C = specific heat, BTU/lb-^{o}R (cal/g-^{o}K)
h = enthalpy, BTU/lb (cal/g)
T = temperature, ^{o}R (^{o}K)

and subscripts: T = tank
L = liquid
G = gas
V = vented gas
i = initial
f = final

This equation was the starting point for the energy balances presented in the following sections. In the case of the heat transfer test, several terms are zero because the test was run at steady state conditions, thus the energy balance equation is simplified.

A. HEAT TRANSFER TEST (TEST 9)

1. Theoretical Thermal Conductance

The total heat leak to the tank is composed of the heat leaks through the insulation, tank supports, and the fill and vent lines.

a. Insulation.- From calorimeter tests, the insulation was found to have a conductivity of 0.0186 BTU/hr-ft-^{o}R (0.0277 kcal/hr-m-^{o}K) under simulated tank conditions. With a surface area of 44 ft^2 (4.09 m^2) for the main tank and 4.3 ft^2 (0.40 m^2) for the standpipe, and an insulation thickness of 1.25 in. (3.18 cm),

$$q\,(\text{insulation}) = \frac{KA}{L}\Delta T = \frac{0.0186}{\frac{(1.25)}{12}}\ (48.3)\ \Delta T = 8.64\,\Delta T.$$

Hence, for an outside temperature of 400^{o}F (478^{o}K) and an inside temperature of -260^{o}F (111^{o}K),

$$q\,(\text{insulation}) = 8.64\ \left[\overline{400 - (-260)}\right] = 5702\ \text{BTU/hr}\ (1437\ \text{kcal/hr}).$$

b. Tank supports.- The tank was supported by 8 stainless steel tubes of the following approximate geometry:

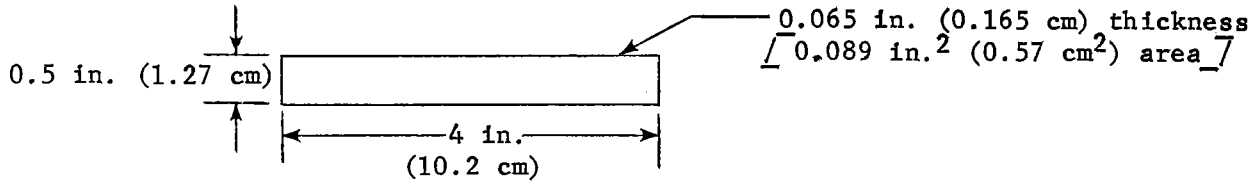

Therefore, the heat conduction through an insulated support is

$$q \text{ (tank support)} = \frac{KA}{L} \Delta T = \frac{(10)(\frac{0.089}{144})}{(\frac{4}{12})} (660) = 12.24 \text{ BTU/hr (3.08 kcal/hr).}$$

Or, for 8 supports,

$$q \text{ (tank support)} = (12.24)\ (8) = 98 \text{ BTU/hr (25 kcal/hr).}$$

c. Fill and vent lines.- The insulated fill line is 2.5 in. (6.35 cm) in diameter with a wall thickness of 0.1 in. (0.25 cm). This results in a cross-sectional conduction area of 0.79 in.^{2} (5.10 cm^2). Therefore, for the geometry and temperatures shown below, the heat conduction through the fill line is given by:

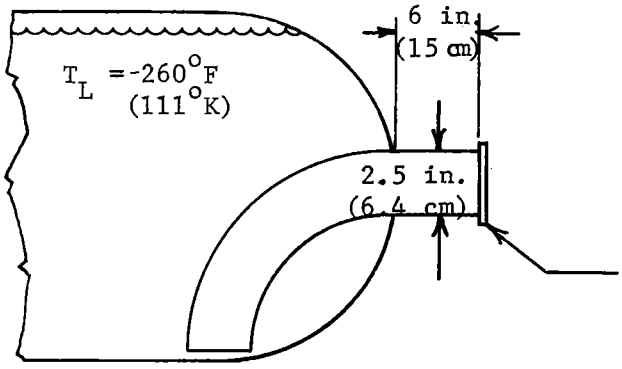

$$q \text{ (fill line)} = \frac{KA}{L} \Delta T = \frac{(10)(\frac{.79}{144})}{(\frac{6}{12})} (200 + 260)$$

$$= 50.5 \text{ BTU/hr (12.7 kcal/hr)}$$

An outer flange temperature of 200°F was assumed for this calculation. It would definitely be less than the 400°F for the outer insulation temperature in this analysis. This value seems reasonable for use with a 400°F outer insulation temperature. Due to the relatively small heat leak through the fill line, any variation in the flange temperature would effect the overall thermal performance very little.

Assuming black body radiation, the heat transfer by radiation in the fill line is:

$$q \text{ (fill line)} = \sigma A (T_1^4 - T_2^4)$$

$$= (.1714 \times 10^{-8})(\frac{\pi}{4} D^2)(660^4 - 200^4)$$

$$= 11 \text{ BTU/hr (2.8 kcal/hr)}$$

Thus, the total heat leak through the fill line is only 61.5 BTU/hr (15.5 kcal/hr). Since the vent line is only 1 in. (2.5 cm) in diameter and insulated over its 3 ft (0.9 m) length, the heat leak through it was considered negligible.

d. Effective thermal conductance.- The total heat leak into the tank is the sum of the above terms, or:

$$q\ (\text{total}) = q\ (\text{insulation}) + q\ (\text{tank supports}) + q\ (\text{fill line})$$

$$= 5702 + 98 + 61.5$$

$$= 5861.5\ \text{BTU/hr}\ (1477\ \text{kcal/hr})$$

In order to figure an overall system conductivity,

$$q\ (\text{total}) = \frac{K_{eff} A}{L}\ \Delta T$$

or

$$K_{eff} = \frac{L\, q\ (\text{total})}{A\ \Delta T} = \frac{(0.104)(5861.5)}{(48.3)(660)}$$

$$K_{eff} = 0.0191\ \text{BTU/hr-ft-}^{\circ}\text{R}\ (0.284\ \text{kcal/hr-m-}^{\circ}\text{K})$$

The small delta between the effective thermal conductivity (K_{eff}) and the thermal conductivity of the basic insulation material (K) indicates a good thermal design.

2. EMPIRICAL THERMAL CONDUCTANCE

An actual K_{eff} can be calculated from actual test data by means of an energy balance. During the heat transfer tests, the test tank was vented throughout the test, resulting in constant tank pressure and liquid and tank temperatures. Using this and the fact that mass of the ullage gas is small enough to neglect heat content, the general energy equation reduces to:

$$Q_E + h_L(m_i - m_f)_L - m_{vent} h_{vent} = 0$$

Or, since

$$(m_i - m_f) = m_{vent} \text{ and } (h_{vent} - h_L) = H_V$$

where H_V is the heat of vaporization, finally,

$$Q_E - m_{vent} H_V = 0$$

or,

$$q_E = \dot{m}_{vent} H_V$$

In solving for K_{eff}, this reduces to $K_{eff} = \frac{L\dot{m}_{vent} H_V}{A\ \Delta T}$

On test number 9, the steady state vent flowrate was 21.0 lb/hr (9.5 kg/hr) and the outside insulation temperatures were as follows:

$$\left.\begin{aligned} \text{Top} &= 295^{\circ}\text{F}\ (419^{\circ}\text{K}) \\ \text{Near side} &= 245^{\circ}\text{F}\ (391^{\circ}\text{K}) \\ \text{Bottom} &= 260^{\circ}\text{F}\ (400^{\circ}\text{K}) \\ \text{Far side} &= 250^{\circ}\text{F}\ (394^{\circ}\text{K}) \end{aligned}\right\} \quad \text{Average} = 263^{\circ}\text{F}\ (401^{\circ}\text{K})$$

Hence,

$$K_{eff} = \frac{(0.104)(21.0)(219)}{(48.3)(523)} = 0.0189 \text{ BTU/hr-ft-}^{\circ}\text{F } (0.0281 \text{ kcal/hr-m-}^{\circ}\text{K})$$

This test and all other heat transfer tests except one compare very favorably with the theoretically determined value. The results of all other tests were presented in section V-C of the final report.

B. WARM TANK LOADING (TEST 1)

As previously shown, the general energy balance equation is:

$$Q_E + m_T C_T (T_i - T_f)_T + m_{Li} h_{Li} - m_{Lf} h_{Lf} + m_{Gi} h_{Gi} - m_{Gf} h_{Gf} - m_{vent} h_{vent} = 0$$

1. Heat Leak

During loading the time averaged outside insulation temperatures were as follows:

Top temperature = 43°F (279°K)
Near side temperature = 39°F (277°K)
Bottom temperature = 35°F (275°K)
Far side temperature = 35°F (275°K)

This results in an average outside temperature of 38°F (276°K). During this same time period the average inside insulation temperatures were as follows:

Top temperature = 22°F (268°K)
Near side temperature = -146°F (174°K)
Bottom temperature = -180°F (155°K)
Far side temperature = -120°F (189°K)

The average inside temperature was -106°F (196°K). Hence,

$$(T_i - T_f)_T = 38 - (-106) = 144\ F^{\circ}\ (80K^{\circ})$$

and $$Q_E = \frac{K_{eff} A}{L} \Delta T\, \Delta\theta$$

Where: K_{eff} = 0.0197 BTU/hr-ft-$^{\circ}$R (0.0293 kcal/hr-m-$^{\circ}$K) from the heat transfer test
A = 48.3 ft^2 (4.5 m^2)
L = 1.25/12 = 0.104 ft (3.17 cm)
$\Delta\theta$ = Test duration = 1260/3600 = 0.35 hr

ΔT = The average temperature difference across the insulation during the test.

Therefore,

$$Q_E = \frac{(0.0197)(48.3)}{0.104} \quad (144)(0.35)$$

= 461 BTU (116 kcal)

2. Tank Wall Heat Capacity

The following is a summary of the tank skin temperatures prior to and after loading:

	Top	Near Side	Bottom	Far Side
Initial tank temp.	52°F (284°K)	50°F (283°K)	48°F (282°K)	46°F (281°K)
Final tank temp.	-116°F (191°K)	-244°F (120°K)	-245°F (119°K)	-243°F (120°K)

The average initial tank temperature was 49°F (283°K). Since the tank was filled to approximately 96% full, the tank top probe reading of -116°F (191°K) reflected the ullage temperature more than the top one-fourth of the tank skin. Thus, in determining the average tank temperature after loading, the top probe reading was weighted only 4%. This results in a final tank temperature of -239°F (123°K). Therefore, the change in tank energy content was:

$$m_T C_T (T_i - T_f)_T = 160\ (0.11)\ (49 + 239)$$

= 5069 BTU (1277 kcal)

3. Liquid Enthalpy

The liquid supply temperature during loading averaged -251.8°F (115.5°K). Figure A1 shows the temperature profile in the liquid. With the finite number of probes the exact shape cannot be fixed, however, based on this figure it seems reasonable to use the 50% level probe to represent the average liquid temperature. The time averaged liquid temperature during loading was -246.2°F (118.6°K). The corresponding liquid enthalpies are:

h_{Li} = 24.0 BTU/lb (13.3 cal/g)

h_{Lf} = 28.6 BTU/lb (15.9 cal/g)

The tank was filled approximately to the 96% level. In addition to this liquid, there was 30.9 lb (14.0 kg) of vapor vented during filling. Therefore,

$$m_{Lf} = V_L \rho_L = (0.96)\ (19.9)\ (25.9)$$

= 495 lb (224.5 kg)

$$m_{Li} = m_{Lf} + m_{vent} = 495 + 30.9$$

= 525.9 lb (238.5 kg)

and,

$m_{Li} h_{Li}$ = (525.9) (24.0) = 12622 BTU (3181 kcal)

$m_{Lf} h_{Lf}$ = (495) (28.6) = 14157 BTU (3568 kcal)

Figure A1 - Typical Liquid Temperature Profile After Loading

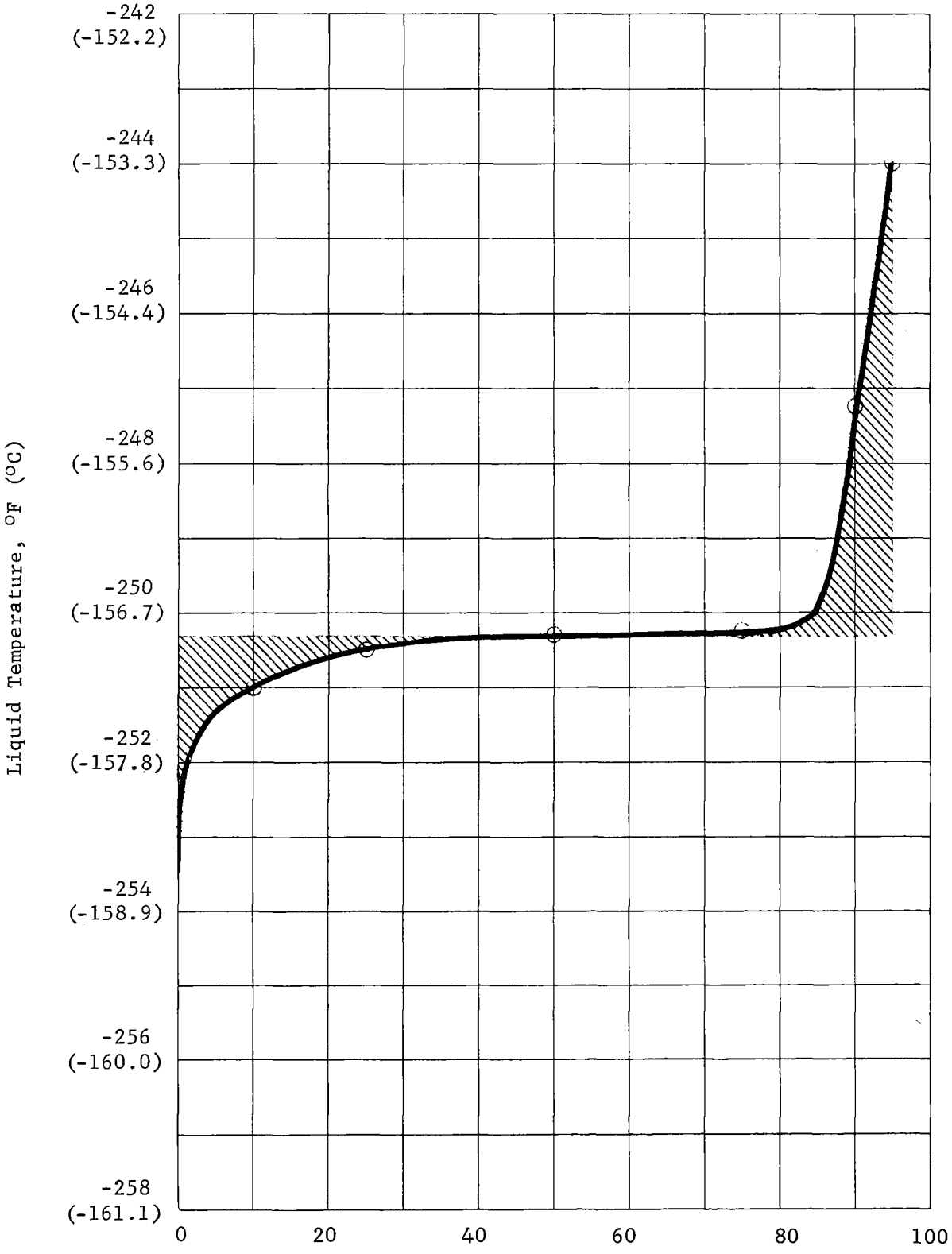

4. Ullage Gas Enthalpy

The initial and final mass of gas in the tank were:

$$m_{Gi} = \frac{P_i V_i}{R T_i} = \frac{(35)(144)(19.9)}{(96.4)(510)} = 2.04 \text{ lb } (0.93 \text{ kg})$$

$$m_{Gf} = \frac{P_f V_f}{R T_f} = \frac{(35)(144)(19.9)(0.04)}{(96.4)(222)} = 0.141 \text{ lb } (0.064 \text{ kg})$$

The initial and final gas enthalpies are 397 and 248 BTU/lb (221 and 138 cal/g). Thus,

$$m_{Gi} h_{Gi} = (2.04)(397) = 810 \text{ BTU } (204 \text{ kcal})$$

and

$$m_{Gf} h_{Gf} = (0.141)(248) = 35 \text{ BTU } (8.8 \text{ kcal})$$

5. Vent Gas Enthalpy

The average enthalpy of the 30.9 lb (14.0 kg) of vented gas is 242.5 BTU/lb (134.7 cal/g), or

$$m_{vent} h_{vent} = (30.9)(242.5) = 7493 \text{ BTU } (1888 \text{ kcal})$$

6. Heat Balance

Summing each of the terms gives:

$$461 + 5069 + 12622 - 14157 + 810 - 35 - 7493 \stackrel{?}{=} 0$$

$$18962 - 21685 \stackrel{?}{=} 0$$

$$-2723 \stackrel{?}{=} 0$$

C. COLD TANK LOADING (TEST 5)

As shown previously, the general energy balance equation is:

$$Q_E + m_T C_T (T_i - T_f)_T + m_{Li} h_{Li} - m_{Lf} h_{Lf} + m_{Gi} h_{Gi} - m_{Gf} h_{Gf} - m_{vent} h_{vent} = 0$$

1. Heat Leak

The time averaged outside insulation temperatures during loading were as follows:

Top temperature = $-17^{\circ}F$ ($246^{\circ}K$)

Near side temperature = $-6^{\circ}F$ ($252^{\circ}K$)

Bottom temperature = $-6^{\circ}F$ ($252^{\circ}K$)

Far side temeprature = $-7^{\circ}F$ ($251^{\circ}K$)

Therefore, the average outside temperature = $-9^{\circ}F$ ($250^{\circ}K$). Using the time averaged 50% liquid level probe reading of $-250^{\circ}F$ ($-116.5^{\circ}K$) as representative of the bulk liquid temperature during loading, the temperature difference across the insulation was:

$$\Delta T = -9 - (-250) = 241\ F^{o}\ (134\ K^{o})$$

or
$$q = \frac{K_{eff} A}{L} \Delta T = \frac{(0.0197)(48.3)}{0.104} \qquad (241)$$

$$= 2205\ \text{BTU/hr}\ (555\ \text{kcal/hr})$$

Since the loading procedure took 840 seconds,

$$Q_E = (\frac{840}{3600})(2205) = 514\ \text{BTU}\ (130\ \text{kcal})$$

2. Tank Wall Heat Capacity

The following is a summary of tank skin temperatures for Test 5:

	Top	Near Side	Bottom	Far Side
Initial tank temp.	$-117^{o}F$ ($190^{o}K$)	$-179^{o}F$ ($160^{o}K$)	$-250^{o}F$ ($116.5^{o}K$)	$-175^{o}F$ ($158^{o}K$)
Final tank temp.	$-115^{o}F$ ($191.5^{o}K$)	$-247^{o}F$ ($118^{o}K$)	$-250^{o}F$ ($116.5^{o}K$)	$-247^{o}F$ ($118^{o}K$)

It appears that the tank bottom still had a small quantity of liquid covering it and did not necessarily represent the entire bottom fourth of the tank. In view of this, the bottom probe reading was weighted only 10% while the three remaining readings were equally weighted. This gives an average initial tank temperature of $-166^{o}F$ ($163^{o}K$). After the tank was loaded to approximately 96% full, the tank top probe read $-115^{o}F$ ($191.5^{o}K$), reflecting the ullage temperature rather than the top one-fourth of the tank skin. Thus, the top probe was weighted only 4% in determining the final tank temperature of $-243^{o}F$ ($120^{o}K$). This results in a tank temperature change of:

$$(T_i - T_f)_T = -166 - (-243) = 77\ F^{o}\ (43\ K^{o})$$

or
$$m_T C_T (T_i - T_f)_T = (160)(0.11)(77) = 1355\ \text{BTU}\ (341\ \text{kcal})$$

3. Liquid Enthalpy

During loading the liquid temperature at the tank inlet was $-254^{o}F$ ($114^{o}K$). After loading the bulk temperature (50% level probe) was $-251.25^{o}F$ ($115.79^{o}K$). The corresponding enthalpies are:

$$h_{Li} = 21.8\ \text{BTU/lb}\ (12.1\ \text{cal/g})$$

$$h_{Lf} = 24.5\ \text{BTU/lb}\ (13.6\ \text{cal/g})$$

The tank was filled approximately to the 96% level, while 8.4 lb (3.8 kg) of vapor were vented during filling. Therefore,

$$m_{Lf} = (0.96)(19.9\ ft^3)(26.1\ \text{lb/ft}^3) = 499\ \text{lb}\ (226\ \text{kg})$$

and,
$$m_{Li} = m_{Lf} + m_{vent} = 499 + 8.4 = 507.4\ \text{lb}\ (230.2\ \text{kg})$$

This leads to:

$$m_{Li} h_{Li} = (507.4)(21.8) = 11061\ \text{BTU}\ (2787\ \text{kcal})$$

$$m_{Lf} h_{Lf} = (499)(24.5) = 12226\ \text{BTU}\ (3081\ \text{kcal})$$

4. Ullage Gas Enthalpy

The initial mass of gas in the empty tank was:

$$m_{Gi} = \frac{PV}{RT} = \frac{(22)(144)(19.9)}{(96.4)(280)} = 2.34 \text{ lb } (1.06 \text{ kg})$$

The initial ullage gas enthalpy was 278 BTU/lb (154 cal/g) or:

$$m_{Gi}h_{Gi} = (2.34)(278) = 651 \text{ BTU } (164 \text{ kcal})$$

The final mass of gas in the "filled" tank was:

$$m_{Gf} = \frac{(30)\ (144)\ (19.9)\ (0.04)}{(96.4)\ (210)} = 0.127 \text{ lb } (0.058 \text{ kg})$$

with a corresponding enthalpy of 242 BTU/lb (134 cal/g). Thus,

$$m_{Gf}h_{Gf} = (0.127)(242) = 31 \text{ BTU } (7.8 \text{ kcal})$$

5. Vent Gas Enthalpy

As stated, the quantity of vented gas during loading was 8.4 lb (3.8 kg), while the average enthalpy corresponding to the vaporization temepratures of the liquid is 242 BTU/lb (134 cal/g). Therefore, the energy lost through the vent was:

$$m_{vent}h_{vent} = (8.4)(242) = 2033 \text{ BTU } (512 \text{ kcal})$$

6. Heat Balance

Summing the above terms and equating to zero as indicated in the general energy balance equation results in the following inequality:

$$514 + 1355 + 11061 - 12226 + 651 - 31 - 2033 \stackrel{?}{=} 0$$

$$13581 - 14290 \stackrel{?}{=} 0$$

$$-709 \stackrel{?}{=} 0$$

This residual value of -709 BTU (-185 kcal) represents only about 5% of the total number of BTU's in either the positive or negative sums of the energy balance.

D. SIMULATED ASCENT TEST (TEST 42)

$$Q_E + m_T C_T (T_i - T_f)_T + m_{Li}h_{Li} - m_{Lf}h_{Lf} + m_{Gi}h_{Gi} - m_{Gf}h_{Gf} - m_{vent}\ h_{vent} = 0$$

1. Heat Leak

The heat leak is described by the following expression: $q_E = \frac{K_{eff}A}{L} \Delta T$

The following table shows the outer insulation temperatures used to determine an average overall outer tank temperature:

	Top	Near Side	Bottom	Far Side
Temperature at start of ascent	$30^{\circ}F$ ($272^{\circ}K$)	$-30^{\circ}F$ ($239^{\circ}K$)	$0^{\circ}F$ ($255^{\circ}K$)	$-5^{\circ}F$ ($253^{\circ}K$)
Temperature at end of ascent	$295^{\circ}F$ ($419^{\circ}K$)	$150^{\circ}F$ ($339^{\circ}K$)	$165^{\circ}F$ ($347^{\circ}K$)	$115^{\circ}F$ ($319^{\circ}K$)
Average temperature	$162.5^{\circ}F$ ($346^{\circ}K$)	$60^{\circ}F$ ($289^{\circ}K$)	$82.5^{\circ}F$ ($301^{\circ}K$)	$55^{\circ}F$ ($286^{\circ}K$)
Overall tank average temperature	$90^{\circ}F$ ($305\ ^{\circ}K$)			

Using the 50% level platinum probe to determine inside tank temperature, the integrated time averaged liquid temperature during ascent was $-252.5^{\circ}F$ ($115.1\ ^{\circ}K$). Hence, $\Delta T = 90 - (-252.5) = 342.5\ F^{\circ}$ ($190.3\ K^{\circ}$)

$$q_E = \frac{0.0197}{0.104}(48.3)(342.5) = 3134 \text{ BTU/hr (790 kcal/hr)}$$

or, during the 25 minute ascent,

$$Q_E = \frac{25}{60}(3134) = 1306 \text{ BTU (329 kcal)}$$

2. Tank Heat Capacity

The initial and final tank temperatures (assuming the tank wall temperature is equal to the liquid temperature) are -250.3 and $-259.2^{\circ}F$ (116.3 and $111.4\ K^{\circ}$) respectively. Hence, $(T_i - T_f)_T = 8.9\ F^{\circ}$ ($4.9\ K^{\circ}$) and for

$m_T = 160$ lbs (72.6 kg) and $C_T = 0.11$ BTU/lb $-^{\circ}F$ (0.11 cal/g-$^{\circ}K$)

$$m_T C_T (T_i - T_f)_T = (160)(0.11)(8.9) = 157 \text{ BTU (40 kcal)}$$

3. Liquid Enthalpy

Assume the tank was initially 96% full, thus the liquid mass is:

$$m_{Li} = (0.96)(19.9)(26.5) = 506 \text{ lb (229.5 kg)}$$

For

$T_{Li} = 250.3^{\circ}F$ ($116.3^{\circ}K$), $h_{Li} = 24$ BTU/lb (13.3 cal/g)

$$m_{Li} h_{Li} = 506\ (24) = 12144 \text{ BTU (3060 kcal)}$$

Since the boiloff during ascent was 23.1 lb (10.5 kg), the final liquid mass is 483 lb (219 kg). For $T_{Lf} = -259.2^{\circ}F$ ($111.4^{\circ}K$), $h_{Lf} = 17$ BTU/lb (9.4 cal/g)

$$m_{Lf} h_{Lf} = (483)(17) = 8211 \text{ BTU (2069 kcal)}$$

4. Ullage Gas Enthalpy

Assuming linear stratification in the ullage, the average temperature of gas in the standpipe tank can be determined from the average of the liquid surface and the top tank skin temperature as follows:

	Start ascent	End Ascent
Top tank skin	$-240^{\circ}F$ ($122.0^{\circ}K$)	$-201^{\circ}F$ ($143.7^{\circ}K$)
Liquid surface	$-248^{\circ}F$ ($117.6^{\circ}K$)	$-259^{\circ}F$ ($111.5^{\circ}K$)
Average temp.	$-244^{\circ}F$ ($119.8^{\circ}K$)	$-230^{\circ}F$ ($127.6^{\circ}K$)

Initial ullage volume was 4%, or

$(0.04)(19.9) = 1.0\ ft^3\ (0.028\ m^3)$

$$m_{Gi} = \frac{P_i V_i}{R\ T_i} = \frac{(144)(27)(1.0)}{(96.4)\ (216)} = 0.187\ lb\ (0.085\ kg)$$

$$m_{Gi} h_{Gi} = (0.187)(245) = 46\ BTU\ (11.6\ kcal)$$

Final ullage volume was:

$$V_i + \frac{m_{vent}}{\rho_L} = 1.0 + \frac{23.1}{26.5} = 1.87\ ft^3\ (0.053\ m^3)$$

$$m_{Gf} = \frac{P_f V_f}{R\ T_f} = \frac{(144)(13)(1.87)}{(96.4)(230)} = 0.158\ lb\ (0.072\ kg)$$

and

$$m_{Gf} h_{Gf} = (0.158)(251) = 40\ BTU\ (10.1\ kcal)$$

5. Vent Gas Enthalpy

The mass of the vented gas was 23.1 lb (10.5 kg), while the average temperature and enthalpy over the vent period were $-180^{\circ}F$ ($155.4^{\circ}K$) and 278 BTU/lb (154 cal/g) respectively. Thus,

$$m_{vent} h_{vent} = (23.1)(278)$$
$$= 6422\ BTU\ (1618\ kcal)$$

6. Heat Balance

Summing the above terms and equating to zero as indicated in the general energy balance equation results in the following inequality:

$$1306 + 157 + 12144 - 8211 + 46 - 40 - 6422 \stackrel{?}{=} 0$$
$$13653 - 14673 \stackrel{?}{=} 0$$
$$-1020 \stackrel{?}{=} 0$$

These results indicate less than a 7.5% variance in the energy balance.

DISTRIBUTION LIST

ADDRESSEE			NO. OF COPIES
NASA-Lewis Research Center 21000 Brookpark Road Cleveland, Ohio 44135			
Attention:	Report Control Office	MS 5-5	1
	Technology Utilization Office	MS 3-19	1
	Library	MS 60-3	2
	Fluid System Components Div.	MS 5-3	1
	W. L. Stewart	MS 77-2	1
	J. Howard Childs	MS 60-4	1
	Len Schopen	MS 77-3	1
	J. M. Ladd	MS 60-6	25
	J. B Esgar	MS 60-4	1
	R. H. Kemp	MS 49-1	1
	R. R. Hibbard	MS 3-5	1
	F. S. Stepka	MS 60-6	1
	R. Cahmbellan	MS 60-4	2
	E. Pleban	MS 60-4	1
	S. Lieblein	MS 100-1	1
NASA Scientific & Technical Information Facility P. O. Box 33 College Park, Maryland 20740 Attention: NASA Representative RQT-2448			6
NASA Headquarters 600 Independence Avenue, S.W. Washington, D. C. 20546 Attention: N. F. Rekos (RAP)			1
Department of the Army U. S. Army Aviation Material Laboratory Fort Eustis, Virginia 23604 Attention: John White			1
Wright-Patterson AFB, Ohio 45433			
Attention:	J. Richens AFAFL (AFIC)		1
	A. Wennerstrom (ARF)		1
	A. V. Churchill AFAPL (APFF)		1
	W. H. Goesch, Air Force Flight Dynamics Laboratory		1
	L. R. Phillips, Air Force Flight Dynamics Laboratory		1
Air Force Office of Scientific Research Propulsion Research Division USAF Washington, D. C. 20025			1
Department of the Navy Bureau of Naval Weapons Washington, D. C. 20025 Attention: Robert Brown, RAPP14			1

ADDRESSEE	NO. OF COPIES
Department of the Navy Bureau of Ships Washington, D. C. 20360 Attention: G. L. Graves	1
NASA-Langley Research Center Langley Station Technical Library Hampton, Virginia 23365 Attention: Mark R. Nichols John V. Becker	1 1
Naval Air Propulsion Test Center (AE) Naval Base Philadelphia, Pennsylvania 19112 Attention: J. R. Pichtedberger	1
United Aircraft Corporation Pratt & Whitney Aircraft Division Florida Research & Development Center P. O. Box 2691 West Palm Beach, Florida 33402 Attention: R. A. Schmidtke F. H. Daley	1 1
United Aircraft Library UAC Research Bldg. 400 Main Street East Hartford, Connecticut 06108 Attention: G. Andreini John Goncar	2 2
Northern Research & Engineering Corporation 219 Vassar Street Cambridge, Massachusetts 02139 Attention: K. Ginwala	1
General Electric Company Aircraft Engines Group Cincinnati, Ohio 45215 Attention: E. N. Bumberger M-88 J. P. Smith, Jr.	1 1
General Electric Company - Flight Propulsion Division 930-1000 Western Avenue West Lynn, Massachusetts 01905 Attention: Dr. C. W. Smith - Library Bldg. 2-40M	1

ADDRESSEE	NO. OF COPIES
AiResearch Manufacturing Company Garrett Corporation 9851 Sepulveda Boulevard Los Angeles, California 90009 Attention: Mr. R. D. Meuller	1
AVCO Corporation Lycoming Division 550 South Main Street Stratford, Connecticut 06497 Attention: C. W. Bolton	1
Continental Aviation & Engineering Corporation 12700 Kercheval Avenue Detroit, Michigan 48215 Attention: Eli H. Benstein Howard C. Welch	1 1
International Harvester Company, Solar 2200 Pacific Highway San Diego, California 92112 Attention: P. A. Pitt Mrs. L. Walper	1 1
Phillips Petroleum Company Phillips Petroleum Center Bartlesville, Oklahoma 74003 Attention: H. E. Alquist	1
Goodyear Atomic Corporation Box 268 Piketon, Ohio 45861 Attention: Department No. 423 for: C. O. Longebrake	1
George Deriderian AIR 53622 B Department of Navy Bureau of Navy Washington, D. C. 20360	1
The Boeing Company Commercial Airplane Division P. O. Box 3707 Seattle, Washington 98124 Attention: G. J. Schott M.S. 80-66	1
The Boeing Company Missille and Information Systems Division 224 N. Wilkinson Street Dayton, Ohio 45402 Attention: Warren K. Thorson	1

ADDRESSEE	NO. OF COPIES
The Boeing Company Supersonic Transport Div. P. O. Box 3733 Seattle, Washington 98124 Attention: George Hays	1
Lockheed California Company P. O. Box 551 Burbank California 91503 Attention: E. F. Versaw	1
McDonnald Douglas Aircraft Co. 3855 Lakewood Blvd. Long Beach, California 90801 Attention: Technical Information Center, CL-250 for J. E. Merriman W. B. King	 1 1
General Motors Corporation Allison Division P. O. Box 24013 Indianapolis, Indiana 46206 Attention: J. N. Barney G. E. Holbrook Library H. E. Helms	 1 1 1
Engineering Library TRW Inc. 23555 Euclid Avenue Cleveland, Ohio 44117 Attention: Elizabeth Barrett, Librarian J. Edward Taylor, Director Product Development Jet and Ordinance Division	 1 1
Westinghouse Electric Corporation Small Steam and Gas Turbine Engineering B-4 Lester Branch P. O. Box 9175 Philadelphia, Pennsylvania 19113 Attention: S. M. DeCorso J. J. Watt	 1 1
Esso Research and Engineering Center P. O. Box 61 Linden, New Jersey 07036 Attention: W. G. Hukek L. Goldstein	 1 1

ADDRESSEE	NO. OF COPIES
General Dynamics Fort Worth Division P. O. Box 748 Fort Worth, Texas 76101 Attention: P. R. deTonnancour MZ-2246	1
Dynamic Science 1800 West Deer Valey Drive Phoenix, Arizona 85027 Attention: L. M. Shaw	1
Institute of Gas Technology 3424 S. State Street Chicago, Illinois 60616	1
The Gillette Company Prudential Tower Bldg. Boston, Massachusetts 02199 Attention: J. V. Rajunas	1
General Dynamics/Convair Division P. O. Box 1128 San Diego, California 92112 Attention: Glen Yates	1